S. Nakanishi
R. Kageyama
D. Watanabe
Editors

Systems Biology

The Challenge of Complexity

The Uehara Memorial Foundation Symposium-2008

Springer

Systems Biology

Shigetada Nakanishi · Ryoichiro Kageyama
Dai Watanabe
Editors

Systems Biology

The Challenge of Complexity

Springer

Editors
Shigetada Nakanishi, M.D., Ph.D.
Director
Osaka Bioscience Institute
Osaka 565-0874
Japan

Ryoichiro Kageyama, M.D., Ph.D.
Director, Professor
Institute for Virus Research
Kyoto University
Kyoto 606-8507
Japan

Dai Watanabe, M.D., Ph.D.
Professor
Department of Biological Sciences
Faculty of Medicine, and Department
of Molecular and System Biology
Graduate School of Biostudies
Kyoto University
Kyoto 606-8501
Japan

ISBN: 978-4-431-87703-5 Springer Tokyo Berlin Heidelberg New York
e-ISBN: 978-4-431-87704-2
DOI: 10.1007/978-4-431-87704-2

Library of Congress Control Number: 2009922675

Preface

Biological signaling pathways dynamically interact with one another to form complex information networks intracellularly, intercellularly, and eventually at the level of the organism. Biology and medicine have conventionally focused on identification and characterization of functional elements in biological signaling pathways. Recently, research in this field has been pursuing a new approach, systems biology, to understand the dynamics, complexity, and physiological functions of the biological signaling networks. Instead of reductionistic analyses or large-scale studies of biomolecules piece by piece, systems biology emphasizes the need for interdisciplinary methods and analysis of the regulation and operation of information networks at the systems level.

The Uehara Memorial Symposium 2008, entitled "Systems Biology: The Challenge of Complexity," was convened in Tokyo from June 30 to July 2, 2008. The aim of the symposium was to bring together leading scientists in the field of systems biology to discuss the latest research on function and dysfunction of biological networks. The following are the main topics addressed in the symposium:

1. Dynamics and complexity of intercellular networks
2. Integrative mechanism of intracellular information networks
3. Dysfunction of information networks and related diseases

An explicit aim of the symposium was to contribute to an understanding of the complexity and dynamics of biological systems and to direct our efforts toward the development of novel strategies for disease control.

We are very pleased to be able to publish the proceedings of this exciting symposium.

Osaka, Japan — Shigetada Nakanishi, Editor

Contents

Contributors

Kentaro Abe
Department of Biological Sciences, Faculty of Medicine, and Department of Molecular and System Biology, Graduate School of Biostudies, Kyoto University, Yoshida, Sakyo-ku, Kyoto, Japan

George J. Augustine
Department of Neurobiology, Duke Medical Center, Durham, NC, USA

Eshel Ben-Jacob
School of Physics and Astronomy, Raymond and Beverly Sackler Faculty of Exact Sciences, Tel-Aviv University, Tel-Aviv, Israel

Upinder S. Bhalla
National Centre for Biological Sciences, TIFR, Bellary Road, Bangalore, India

Toshiya Endo
Department of Chemistry, Graduate School of Science, Nagoya University, Nagoya, Japan

Hisataka Fujimoto
Department of Biological Sciences, Faculty of Medicine, and Department of Molecular and System Biology, Graduate School of Biostudies, Kyoto University, Yoshida, Sakyo-ku, Kyoto, Japan

Susumu Goyama
Department of Hematology and Oncology, Graduate School of Medicine, University of Tokyo, The University of Tokyo Hospital, Bunkyo-ku, Tokyo, Japan

Sten Grillner
Nobel Institute for Neurophysiology, Department of Neuroscience, Karolinska Insititutet, Stockholm, Sweden

Taku Hasegawa
Department of Biological Sciences, Faculty of Medicine, and Department of Molecular and System Biology, Graduate School of Biostudies, Kyoto University, Yoshida, Sakyo-ku, Kyoto, Japan

Chiharu Higashida
Department of Pharmacology, Kyoto University Faculty of Medicine, Sakyo-ku, Kyoto, Japan

Russell Hill
Computational Biology and Neurocomputing, School of Computer Science and Communication, Royal Institute of Technology, Stockholm, Sweden

Motoshi Ichikawa
Department of Hematology and Oncology, Graduate School of Medicine, University of Tokyo, The University of Tokyo Hospital, Bunkyo-ku, Tokyo, Japan

Kentaro Ito
Division of Oncology, The Institute of Medical Science, The University of Tokyo, Minato-ku, Tokyo, Japan

Hideo Iwasaki
Department of Electrical Engineering & Bioscience, Waseda University, and PRESTO, Japan Science & Technology Agency (JST), Shinjuku-ku, Tokyo, Japan

Kevin A. Janes
Koch Institute for Integrative Cancer Research, Center for Cell Decision Processes, Department of Biology, and Department of Biological Engineering, Massachusetts Institute of Technology, Cambridge, MA, USA; Department of Cell Biology, Harvard Medical School, Boston, MA, USA

Ryoichiro Kageyama
Institute for Virus Research, Kyoto University, Kyoto, Japan, and Japan Science and Technology Agency, CREST, Kyoto, Japan

Hideki Katagiri
Division of Advanced Therapeutics for Metabolic Diseases, Center for Translational and Advanced Animal Research, Tohoku University Graduate School of Medicine, Aoba-ku, Sendai, Japan

Mitsuo Kawato
ATR Computational Neuroscience Laboratories, Seika, Kyoto, Japan

Shigeru Kondo
Division of Biological Science, Graduate School of Science, Nagoya University, Chikusa-ku, Nagoya, Aichi, Japan

Ryo Kunimoto
Department of PharmacoInformatics, Graduate School of Pharmaceutical Sciences, Kyoto University, Kyoto, Japan

Shinya Kuroda
Department of Biophysics and Biochemistry, Graduate School of Science, The University of Tokyo, and CREST, Japan Science and Technology Agency, Bunkyo-ku, Tokyo, Japan

Mineo Kurokawa
Department of Hematology and Oncology, Graduate School of Medicine, University of Tokyo, The University of Tokyo Hospital, Bunkyo-ku, Tokyo, Japan

Jens Looser
University of Wuerzburg, Wuerzburg, Germany

Ryosuke Matsui
Department of Biological Sciences, Faculty of Medicine, and Department of Molecular and System Biology, Graduate School of Biostudies, Kyoto University, Sakyo-ku, Kyoto, Japan

Masahiro Morita
Division of Oncology, The Institute of Medical Science, The University of Tokyo, Minato-ku, Tokyo, Japan

Georg Nagel
University of Wuerzburg, Wuerzburg, Germany

Masahiro Nakagawa
Department of Hematology and Oncology, Graduate School of Medicine, University of Tokyo, The University of Tokyo Hospital, Bunkyo-ku, Tokyo, Japan

Shigetada Nakanishi
Osaka Bioscience Institute, Osaka, Japan

Atsushi Nambu
Division of System Neurophysiology, National Institute for Physiological Sciences, and Department of Physiological Sciences, Graduate University for Advanced Studies, Myodaiji, Okazaki, Aichi, Japan

Takeshi Nitta
Division of Experimental Immunology, Institute for Genome Research, University of Tokushima, Tokushima, Japan

Yasutaka Niwa
Institute for Virus Research, Kyoto University, Kyoto, Japan and Japan Science and Technology Agency, CREST, Kyoto, Japan

Hideaki Ogasawara
National Institute of Information and Communications Technology, Seika, Kyoto, Japan, and ATR Computational Neuroscience Laboratories, Seika, Kyoto, Japan

Yasushi Okuno
Department of PharmacoInformatics, Graduate School of Pharmaceutical Sciences, Kyoto University, Kyoto, Japan

Yu-ichi Ozaki
Department of Biophysics and Biochemistry, Graduate School of Science, University of Tokyo, and CREST, Japan Science and Technology Agency, Bunkyo-ku, Tokyo, Japan

H. Christian Reinhardt
Koch Institute for Integrative Cancer Research, Center for Cell Decision Processes, Department of Biology, and Department of Biological Engineering, Massachusetts Institute of Technology, Cambridge, MA, USA

Kazuki Saito
Chiba University, Graduate School of Pharmaceutical Sciences, Inage-ku, Chiba, Japan, and RIKEN Plant Science Center, Tsurumi-ku, Yokohama, Japan

Fumiaki Sato
Department of Nanobio Drug Discovery, Graduate School of Pharmaceutical Sciences, Kyoto University, Kyoto, Japan

Kazuharu Shimizu
Department of Nanobio Drug Discovery, Graduate School of Pharmaceutical Sciences, Kyoto University, Kyoto, Japan

Hiromi Shimojo
Institute for Virus Research, Kyoto University, Kyoto, Japan, and Japan Science and Technology Agency, CREST, Kyoto, Japan

Toru Suzuki
Division of Oncology, The Institute of Medical Science, The University of Tokyo, Minato-ku, Tokyo, Japan

Yousuke Takahama
Division of Experimental Immunology, Institute for Genome Research, University of Tokushima, Tokushima, Japan

Keiko Tanaka
Department of Biophysics and Biochemistry, Graduate School of Science, University of Tokyo, Tokyo, Japan, and PRESTO, Japan Science and Technology Agency, Tokyo, Japan

Kazuya Terasawa
Department of Genomic Drug Discovery Science, Kyoto University, Sakyo-ku, Kyoto, Japan

Soken Tsuchiya
Department of Nanobio Drug Discovery, Graduate School of Pharmaceutical Sciences, Kyoto University, Kyoto, Japan

Gozoh Tsujimoto
Department of Genomic Drug Discovery Science, Kyoto University, Sakyo-ku, Kyoto, Japan

Shinsuke Uda
Department of Biophysics and Biochemistry, Graduate School of Science, University of Tokyo, CREST, Japan Science and Technology Agency, Bunkyo-ku, Tokyo, Japan

Hiroki R. Ueda
Laboratory for Systems Biology and Functional Genomics Unit, Center for Developmental Biology, RIKEN, Chuo-ku, Kobe, Hyogo, Japan

Peter Wallén
Computational Biology and Neurocomputing, School of Computer Science and Communication, Royal Institute of Technology, Stockholm, Sweden

Dai Watanabe
Department of Biological Sciences, Faculty of Medicine, and Department of Molecular and System Biology, Graduate School of Biostudies, Kyoto University, Sakyo-ku, Kyoto, Japan

Naoki Watanabe
Department of Pharmacology, Kyoto University Faculty of Medicine, Sakyo-ku, Kyoto, Japan

Cornelis J. Weijer
Division of Cell and Developmental Biology, School of Life Sciences, University of Dundee, Wellcome Trust Biocentre, Dundee, UK

Michael B. Yaffe
Koch Institute for Integrative Cancer Research, Center for Cell Decision Processes, Department of Biology, and Department of Biological Engineering, Massachusetts Institute of Technology, Cambridge, MA, USA

Tadashi Yamamoto
Division of Oncology, The Institute of Medical Science, The University of Tokyo, Minato-ku, Tokyo, Japan

Shinya Yamanaka
Center for iPS Cell Research & Application (CiRA) / Institute for Frontier Medical Sciences, Kyoto University, Kyoto, Japan

Integrative Synaptic Mechanisms of the Neural Network

Shigetada Nakanishi

Introduction

The cerebellum is a key neural substrate for motor coordination and motor learning [1,2]. The main neural circuitry of the cerebellum consists of two excitatory glutamatergic pathways: the pons–mossy fiber–granule cell–parallel fibers and the inferior olive–climbing fibers [1]. The inputs of mossy fibers and climbing fibers converge on Purkinje cells in the cerebellar cortex and deep cerebellar nuclei [1]. Besides this main circuitry, Golgi cells receive excitatory parallel fiber input and suppress granule cell transmission via the inhibitory gamma-aminobutyric acid (GABA) transmitter. The cerebellar network has been well characterized by electrophysiology and morphology, and its input/output relationship is also relatively well quantitatively assessed by both electrophysiological and behavioral analysis. Our investigations have been concerned with the regulatory mechanisms of integrative synaptic transmission, which is responsible for motor learning and motor coordination in the cerebellar circuitry.

Neural Circuits for Conditioned Eyeblink Motor Learning

The cerebellum is critically implicated in motor learning [2,3]. The conditioned eyeblink response is a typical cerebellum-dependent motor learning event [2–5]. When a conditioned sensory stimulus such as a tone is paired with an unconditioned periorbital electrical stimulus, the trained animal shows a tone-dependent eyeblink response in the absence of unconditioned stimulation (Fig. 1). Information about the conditioned stimulus is transmitted through the pons, mossy fibers, granule cells, and parallel fibers, whereas information about the unconditioned

S. Nakanishi
Osaka Bioscience Institute, 6-2-4 Furuedai, Suita, Osaka 565-0874, Japan

S. Nakanishi et al. (eds.), *Systems Biology*,
DOI:10.1007/978-4-431-87704-2_1,

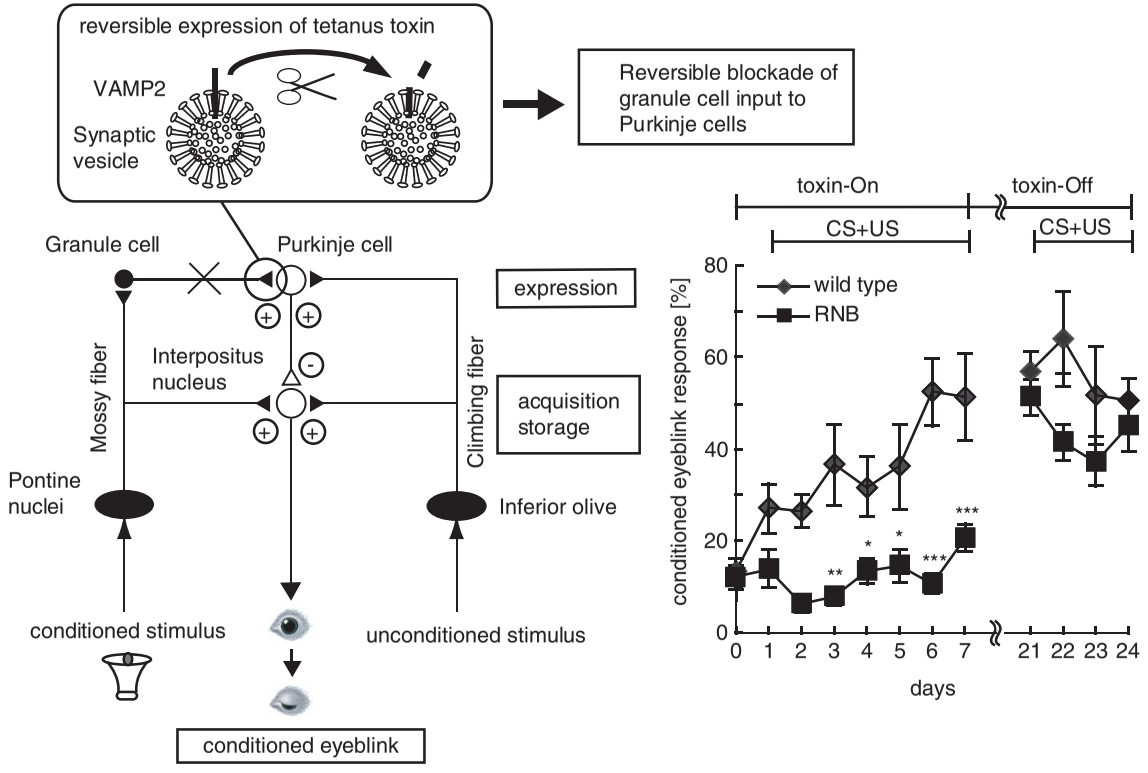

Fig. 1 Mechanistic analysis of conditioned eyeblink motor learning by reversible neurotransmission blocking techniques. *Left:* The neural circuitry responsible for conditioned eyeblink motor learning. In this circuitry, granule cell input to Purkinje cells was selectively and reversibly blocked by the tetracycline derivative DOX-dependent expression of tetanus toxin in granule cells. *Right:* Conditioned eyeblink responses in wild-type mice and reversible neurotransmission blocking (RNB) mice. In RNB mice, granule cell transmission was blocked and reversibly recovered by DOX-dependent expression of tetanus toxin. *CS*, conditioned stimulus; *US*, unconditioned stimulus

stimulus is transmitted through the inferior olive and climbing fibers (Fig. 1). Importantly, this information converges on both Purkinje cells and deep cerebellar nuclei, namely, the interpositus nucleus. However, the relative importance and the underlying mechanism of cerebellum-dependent eyeblink motor learning have remained largely unclear.

To address the neural circuits and mechanisms underlying the conditioned eyeblink response, we developed a novel technique termed reversible neurotransmission blocking (RNB) [6] (Fig. 1). With the RNB technology, we generated two lines of transgenic mice. One line of transgenic mice selectively expressed the tetracycline-activating transcription factor in granule cells under the control of the $GABA_A$ $\alpha 6$ promoter. In the second line of transgenic mice, the fusion protein of tetanus toxin and green fluorescent protein (GFP) was controlled by this transcription factor. Tetanus toxin is a bacterial toxin that specifically cleaves the synaptic vesicle VAMP2 and in turn blocks transmitter release from the synaptic vesicles [7]. When these two lines of transgenic mice were mated, the tetracycline derivative doxycycline (DOX)-dependent expression of tetanus toxin was specifically observed in granule cells. Consequently, VAMP2 was selectively and reversibly cleaved in granule cells, depending on the administration and omission of DOX [6]. The RNB mice were used to explore the mechanism underlying conditioned eyeblink motor learning with the following rationale (Fig. 1). When granule cell input to Purkinje cells is selectively blocked, the conditioned signal is not transmitted to the Purkinje cells, but this information is still conveyed to the interpositus nucleus. Therefore, the reversible blockade of granule cell transmission can delineate the role of the two information pathways in the conditioned eyeblink response.

We performed electrophysiology and behavioral experiments on conditioned eyeblink motor learning [8]. We confirmed the reversibility of blockade of granule cell transmission to Purkinje cells by extracellular recording of Purkinje cells in awake animals. This blockade, however, had no influence on climbing fiber transmission. We therefore succeeded in manipulating the reversible blocking of granule cell transmission to Purkinje cells without any impairment of response to the climbing fiber input. We then tested the conditioned eyeblink response in this model animal (Fig. 1). In RNB mice, the conditioned eyeblink response disappeared during the administration of DOX and was recovered by the omission of DOX. Importantly, when granule cell transmission was recovered by the withdrawal of DOX, the normal conditioned response was immediately induced at the beginning of the second conditioning session of the pretrained RNB mice (Fig. 1). This finding explicitly demonstrates that although the conditioned response is not expressed during DOX treatment, this memory is acquired and stored in RNB mice during DOX treatment. We further confirmed that a bilateral lesion of the interpositus nucleus completely abolished memory acquisition and storage in DOX-withdrawn RNB mice [8].

These results demonstrate that information of the conditioned signal to Purkinje cells is necessary for the expression of the conditioned response, but the memory is acquired and stored despite the absence of the conditioned signal to Purkinje cells

(Fig. 1). The most plausible interpretation of our study is that the blockade of granule cell transmission relieves tonic Purkinje cell inhibition [9,10], and that the interpositus nucleus induces latent neural plasticity in response to paired conditioned and unconditioned signals. This neural plasticity should be critical for memory acquisition and storage and would allow prompt expression of the conditioned response once the expression process is restored by the recovery of granule cell transmission [8]. We are currently investigating whether and how neural plasticity is induced at the interpositus nucleus during DOX treatment in RNB mice.

The Regulatory Role of Golgi Cells

In the cerebellar circuitry, Golgi cells also receive excitatory parallel fiber input and in turn suppress granule cell excitation through the inhibitory GABA transmitter [11,12] (Fig. 2). Golgi cell-mediated feedback inhibition is thought to be important for filtering mossy fiber input before distributing this input to the Purkinje cells.

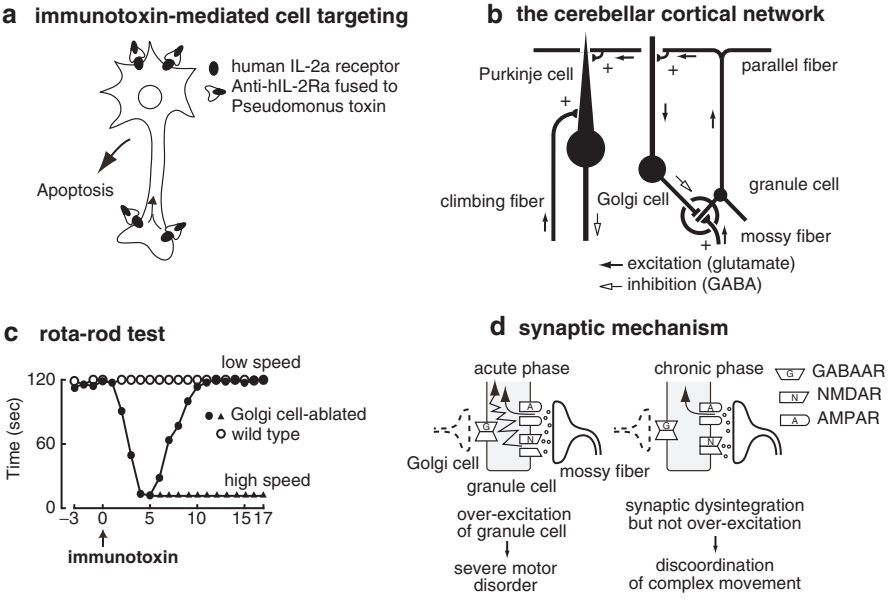

Fig. 2 Integrative mechanisms of neurotransmission at the Golgi cell–mossy fiber–granule cell synapse. **a** Principle of the immunotoxin-mediated cell targeting technology. **b** Neural circuitry of the cerebellar cortex. **c** Ability of wild-type and Golgi cell-eliminated transgenic mice to stay on a slowly rotating and a rapidly rotating rota-rod. **d** A model for synaptic mechanisms underlying motor disorders in the acute phase and the functional compensation of motor disorders in the chronic phase after Golgi cell elimination

However, Golgi cells represent less than 1% of the cerebellar cell population, and the functional role of Golgi cells in the cerebellar circuitry remains to be determined.

To address the functional role of Golgi cells in the cerebellar circuitry, we developed another technique termed immunotoxin-mediated cell targeting (IMCT) as a collaborative work with Ira Pastan in the National Institutes of Health (NIH) [13] (Fig. 2). In this technology, we generated transgenic mice that expressed the human interleukin (IL)-2 receptor under the control of a neuron-specific promoter. We then injected the recombinant immunotoxin that is composed of the human IL-2 receptor monoclonal antibody fused to *Pseudomonas* exotoxin. The immunotoxin binds to the membrane human IL-2 receptor, and this complex is internalized and then kills target cells, thereby leading to elimination of specific neuronal cells.

We constructed a transgene that contained the metabotropic glutamate receptor 2 (mGluR2) promoter, followed by the human IL-2 receptor fused to GFP. In the cerebellum of transgenic mice, the fluorescence of the GFP–IL-2 receptor complex was specifically observed in mGluR2-immunoreactive Golgi cells. Intrathecal injection of immunotoxin eliminated Golgi cells in transgenic mice but not in wild-type mice. Importantly, granule cells, Purkinje cells, and basket and stellate cells all remained intact after immunotoxin injection.

Immunotoxin-injected transgenic mice showed severe acute ataxia. When the rota-rod test was conducted at a low speed, Golgi cell-eliminated transgenic mice failed this task acutely after immunotoxin injection, but the motor disorders gradually recovered thereafter (Fig. 2). However, these mice still failed to stay on the more rapidly rotating rod. The movement disorder was never observed in immunotoxin-treated wild-type mice.

We addressed how synaptic transmission is severely perturbed in the acute phase of Golgi cell elimination and how this perturbation is at least partly compensated in the chronic phase. We performed a series of electrophysiological and optical recordings of cerebellar slices of wild-type mice and Golgi cell-eliminated transgenic mice [13]. These experiments indicated a novel mechanism for synaptic integration at mossy fiber–granule cell–Golgi cell synapses [13,14] (Fig. 2). Under normal circumstances, GABA inhibition and *N*-methyl-D-aspartic acid (NMDA) receptors play an important role in synaptic integration responsible for complex motor coordination. When Golgi cells are eliminated, GABA is depleted, and this depletion results in overexcitation of NMDA receptors and causes severe acute motor disorders. In the chronic phase, NMDA receptors are adaptively downregulated, thus relieving overexcitation of granule cells. Importantly, AMPA receptors remain unchanged before and after Golgi cell elimination, and these AMPA receptors allow animals to manage simple motor movement. However, NMDA receptors are attenuated, thus causing functional deficits in directing more complex motor coordination. Our studies demonstrate that the cooperative actions of excitatory and inhibitory receptors are important not only for integrative brain functioning but also for the compensation of brain dysfunction.

Regulatory Mechanism of Golgi Cell Inhibition

Golgi cell-mediated feedback inhibition is also known to be so strong that well-defined control of this feedback inhibition is necessary [15,16]. Otherwise, the strong inhibition would block information transmission of mossy fiber input to Purkinje cells. For example, strong facial stimulation has been shown to evoke spike discharges and then induce long silencing of putative Golgi cells in rats [17]. This silencing of Golgi cells is assumed to be important for information transmission of the strong tactile stimuli to Purkinje cells. To address how Golgi cell inhibition is properly controlled, we focused on abundantly expressing, postsynaptic mGluR2 in Golgi cells [18], because mGluR2 is often coupled to the inhibitory signaling cascade [19,20].

We performed a series of whole-cell recordings of GFP-positive Golgi cells after electrical stimulation of parallel fibers in cerebellar slices of wild-type and mGluR2 knockout mice [18] (Fig. 3). These experiments indicated that mGluR2 activates the G protein-coupled inwardly rectifying K^+ channel (GIRK) and suppresses Golgi cell excitability. Furthermore, immunostaining characterization revealed that Kir 3.2 of the GIRK K^+ channel is involved in mGluR2-mediated Golgi cell suppression.

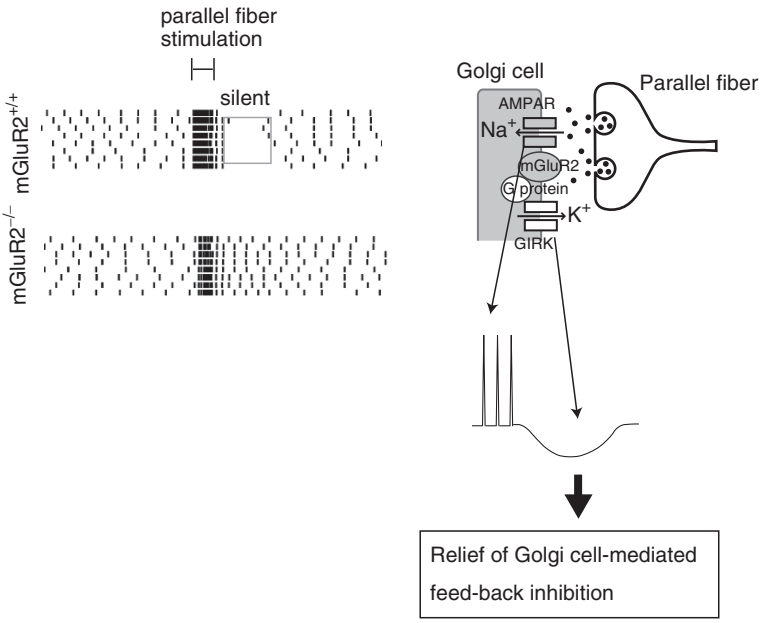

Fig. 3 Input-dependent, metabotropic glutamate receptor 2 (*mGluR2*)-mediated suppression of Golgi cell inhibition. *Left:* Spike raster plots of $mGluR2^{+/+}$ and $mGluR2^{-/-}$ Golgi cells recorded in cerebellar slices before and after strong parallel fiber stimulation. Strong parallel fiber stimulation induced spike discharges in both $mGluR2^{+/+}$ and $mGluR2^{-/-}$, and a long-lasting silent phase followed in $mGluR2^{+/+}$ but not in $mGluR2^{-/-}$. *Right:* A model of mGluR2-mediated suppression following AMPA receptor-mediated excitation of the Golgi cell

We then investigated how the postsynaptic mGluR2 senses different extents of granule cell input at Golgi cells [18]. These results explicitly indicated that when Golgi cells receive glutamatergic input from parallel fibers, AMPA receptors first excite Golgi cells and mGluR2 then suppresses Golgi cell excitability in a stimulus strength-dependent manner (Fig. 3). Therefore, the postsynaptic mGluR2 is capable of sensing the strength of presynaptic granule cell input and relieving Golgi cell-mediated feedback inhibition in a stimulus strength-dependent manner [18]. Consequently, this mechanism enables transmission of strong mossy fiber input to Purkinje cells. Furthermore, because Golgi cells project divergent axon terminals on multiple granule cells, the control by postsynaptic mGluR2 is capable of influencing a regional population of granule cells and plays an important role in spatiotemporal regulation of the cerebellar circuitry.

Concluding Remarks

The cerebellar network is organized in an orderly manner, and synaptic transmission in the cerebellar circuitry is regulated dynamically by specialized mechanisms. Our investigation of eyeblink conditioning has revealed that different local circuits in the cerebellar network participate in distinct processes of cerebellum-dependent eyeblink motor learning. In the mechanism of Golgi cell-mediated feedback inhibition, GABA inhibition and glutamate excitation by different types of glutamate receptors cooperatively and differentially regulate synaptic transmission in mossy fiber–granule cell synapses and play an important role in integrative and adaptive mechanisms for motor coordination. Moreover, the dual regulation by ionotropic and metabotropic glutamate receptors is crucial in sensing and properly transmitting different strengths of glutamate-mediated neural information in the cerebellar circuitry. Neural information is thus hierarchically processed and integrated at different levels of the neural network.

References

1. Llinas RR, Walton KD. Cerebellum. In: Shepherd GM (ed) The Synaptic Organization of the Brain. Oxford: Oxford University Press, 1998:255–288.
2. Ito M. Cerebellar long-term depression: characterization, signal transduction, and functional roles. Physiol Rev 2001;81(3):1143–95.
3. Christian KM, Thompson RF. Neural substrates of eyeblink conditioning: acquisition and retention. Learn Mem 2003;10(6):427–55.
4. Mauk MD. Roles of cerebellar cortex and nuclei in motor learning: contradictions or clues? Neuron 1997;18(3):343–6.
5. De Zeeuw CI, Yeo CH. Time and tide in cerebellar memory formation. Curr Opin Neurobiol 2005;15(6):667–74.
6. Yamamoto M, Wada N, Kitabatake Y, Watanabe D, Anzai M, Yokoyama M, Teranishi Y, Nakanishi S. Reversible suppression of glutamatergic neurotransmission of cerebellar granule cells in vivo by genetically manipulated expression of tetanus neurotoxin light chain. J Neurosci 2003;23(17):6759–67.

7. Schiavo G, Benfenati F, Poulain B, Rossetto O, Polverino de Laureto P, DasGupta BR, Montecucco C. Tetanus and botulinum-B neurotoxins block neurotransmitter release by proteolytic cleavage of synaptobrevin. Nature (Lond) 1992;359(6398):832–5.
8. Wada N, Kishimoto Y, Watanabe D, Kano M, Hirano T, Funabiki K, Nakanishi S. Conditioned eyeblink learning is formed and stored without cerebellar granule cell transmission. Proc Natl Acad Sci U S A 2007;104(42):16690–5.
9. Ito M. Long-term depression. Annu Rev Neurosci 1989;12:85–102.
10. Linden DJ. Neuroscience. From molecules to memory in the cerebellum. Science 2003;301(5640):1682–5.
11. Gabbiani F, Midtgaard J, Knopfel T. Synaptic integration in a model of cerebellar granule cells. J Neurophysiol 1994;72(2):999–1009.
12. Singer W. Neurophysiology: the changing face of inhibition. Curr Biol 1996;6(4):395–7.
13. Watanabe D, Inokawa H, Hashimoto K, Suzuki N, Kano M, Shigemoto R, Hirano T, Toyama K, Kaneko S, Yokoi M, Moriyoshi K, Suzuki M, Kobayashi K, Nagatsu T, Kreitman RJ, Pastan I, Nakanishi S. Ablation of cerebellar Golgi cells disrupts synaptic integration involving GABA inhibition and NMDA receptor activation in motor coordination. Cell 1998;95(1):17–27.
14. Nakanishi S. Synaptic mechanisms of the cerebellar cortical network. Trends Neurosci 2005;28(2):93–100.
15. Brickley SG, Cull-Candy SG, Farrant M. Development of a tonic form of synaptic inhibition in rat cerebellar granule cells resulting from persistent activation of GABAA receptors. J Physiol 1996;497(pt 3):753–9.
16. Wall MJ, Usowicz MM. Development of action potential-dependent and independent spontaneous GABAA receptor-mediated currents in granule cells of postnatal rat cerebellum. Eur J Neurosci 1997;9(3):533–48.
17. De Schutter E, Bjaalie JG. Coding in the granular layer of the cerebellum. Prog Brain Res 2001;130:279–96.
18. Watanabe D, Nakanishi S. mGluR2 postsynaptically senses granule cell inputs at Golgi cell synapses. Neuron 2003;39(5):821–9.
19. Nakanishi S. Molecular diversity of glutamate receptors and implications for brain function. Science 1992;258(5082):597–603.
20. Yokoi M, Kobayashi K, Manabe T, Takahashi T, Sakaguchi I, Katsuura G, Shigemoto R, Ohishi H, Nomura S, Nakamura K, Nakao K, Katsuki M, Nakanishi S. Impairment of hippocampal mossy fiber LTD in mice lacking mGluR2. Science 1996;273(5275):645–7.

The Molecular and Cellular Design of Networks in Motion

Sten Grillner, Peter Wallén, and Russell Hill

Introduction

In this chapter, we review the extensive knowledge gained on the lamprey nervous system through an interactive process between experiments and modeling [1–3]. The organization of the locomotor system is to a large extent conserved through vertebrate phylogeny, and it is therefore also pertinent to explore to what extent this knowledge can be applied to the more complex mammalian nervous system. The overall aim is to account for this complex set of behaviors, based on an understanding of the intrinsic cellular mechanisms determining the operation of the different neuronal networks.

The different subsystems involved in the control of locomotion can be represented as follows (Fig. 1).

- A neural system responsible for selection of the appropriate behavior, in this case locomotion. Striatum, the input layer of the basal ganglia, has an important role in this context. Striatum receives phasic input from pallium (cortex) and thalamus and a modulatory input from the dopamine system. The GABAergic striatal neurons have a high threshold for activation. When activated they can indirectly release specific motor programs by inhibiting the GABAergic output neurons of the basal ganglia (pallidum) that at rest provide tonic inhibition of the different motor programs [4] (Grillner 2006).
- A command system that, when released from basal ganglia inhibition, can elicit locomotion by activating the pattern generating circuits in the spinal cord. Two command systems for locomotion, the mesencephalic locomotor region (MLR)

S. Grillner
Nobel Institute for Neurophysiology, Department of Neuroscience, Karolinska Insititutet, Retzius väg 8, SE-171 77 Stockholm, Sweden

S. Nakanishi et al. (eds.), *Systems Biology*,
DOI:10.1007/978-4-431-87704-2_2, © Springer 2009

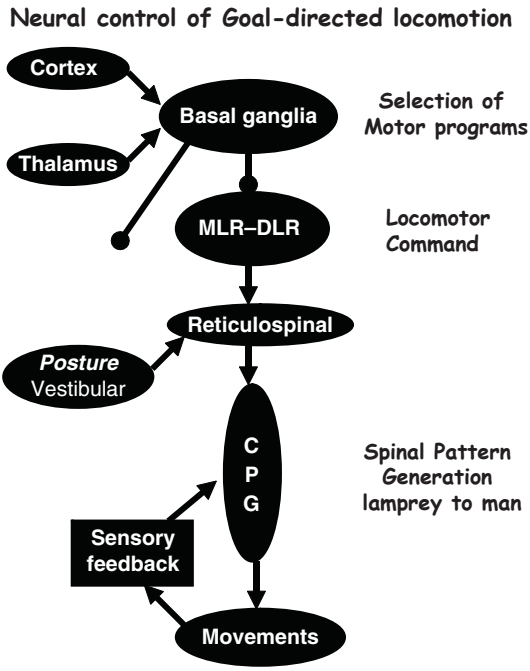

Fig. 1 Subsystems involved in the control of motor behavior, such as locomotion. Selection of a certain motor program is performed in the basal ganglia, which receive inputs from cortex (pallium) and thalamus. The basal ganglia activate indirectly command centers in the diencephalic locomotor region (*DLR*) and the mesencephalic locomotor region (*MLR*) through disinhibition. They activate the spinal central pattern generators (*CPG*) for locomotion via the reticulospinal (RS) neurons. In the brainstem, information is further integrated based on visual, sensory, and vestibular inputs to control both steering and posture. As in higher vertebrates, the spinal cord CPG neurons are modulated by local sensory feedback

and the diencephalic locomotor region (DLR), have been defined. They act via a symmetrical activation of reticulospinal neurons that turn on the spinal circuits.

- Segmental and intersegmental networks (central pattern generators, CPGs) located at the spinal level. The CPGs contain the necessary timing information to activate the different motoneurons in the appropriate sequence to produce the propulsive movements.
- The segmental burst-generating network in the lamprey contains excitatory interneurons that within the pool of interneurons provide excitation. The alternating pattern between the left and right side is provided by reciprocal inhibitory connections between pools of excitatory interneurons.
- A sensory control system, sensing the locomotor movements, helps to compenate for external perturbations by a feedback action on the spinal CPGs.

- A control system for steering the body toward different goals. The steering commands are superimposed on the basic locomotor activity and will bias the control signals so as to steer the movements to the left or right side or in other orientations [5].
- During locomotion the body moves with the dorsal side up, regardless of perturbations. This "postural" control system for orientation of the body in the gravity field depends on bilateral vestibular input that detects any deviation from the appropriate orientation of the head, whether tilt to the left or right or changes in pitch angle during locomotion. These vestibular effects are mediated via brainstem interneurons to reticulospinal neurons on the left or right side, respectively, that can elicit compensatory movements that restore the body orientation [6].

Basic Mechanisms of Burst Generation

One major problem when studying vertebrate pattern generation has been the intrinsic function of the networks controlling behaviors such as respiration and locomotion. In the case of lower vertebrates such as the lamprey and the frog embryo, the locomotor networks are comparatively well understood. At the segmental level, recurring locomotor bursts can be generated even in a hemisegment, provided that the excitability is high enough [7,8]. The burst generation is primarily dependent on a pool of excitatory interneurons (EINs). Within this pool EINs excite other EINs (AMPA and NMDA receptors), although mutual excitation between individual EINs has not been observed (Figs. 2, 3) [9]. These pools of EINs form burst-generating kernels within the CPG. The excitatory drive to the EIN kernel is provided by the locomotor command regions via glutamate reticulospinal neurons, whereas the burst generation primarily results from the intrinsic synaptic and membrane properties of the EINs. Although there are inhibitory premotor interneurons [10] that can be active during locomotion, they are not essential for burst generation, because they can be blocked without any effects on burst frequency [7].

The EINs have overshooting action potentials and a fast and a slow AHP similar to that of motoneurons [11,12]. Although they, for reason of their small size, have been studied in lesser detail than the larger spinal neurons, their properties appear very similar.

Each hemisegment is estimated to have around 30 EINs. In addition to the segmental EIN interaction, EINs have brief ascending (three segments) and longer descending (six to eight segments) axonal branches [11,13]. Each EIN will thus receive excitation not only from segmental EINs but also from EINs located both rostrally and caudally to itself. The connectivity ratio within the pool of EINs is estimated to be approximately 10%.

If a pool of model or real EINs is activated from the brainstem or experimentally by a bath applying glutamate agonists, burst activity will be produced, the rate of which depends on the excitatory drive. The initial depolarization of EINs will make the EINs with the lowest threshold start firing, and they will in turn activate other

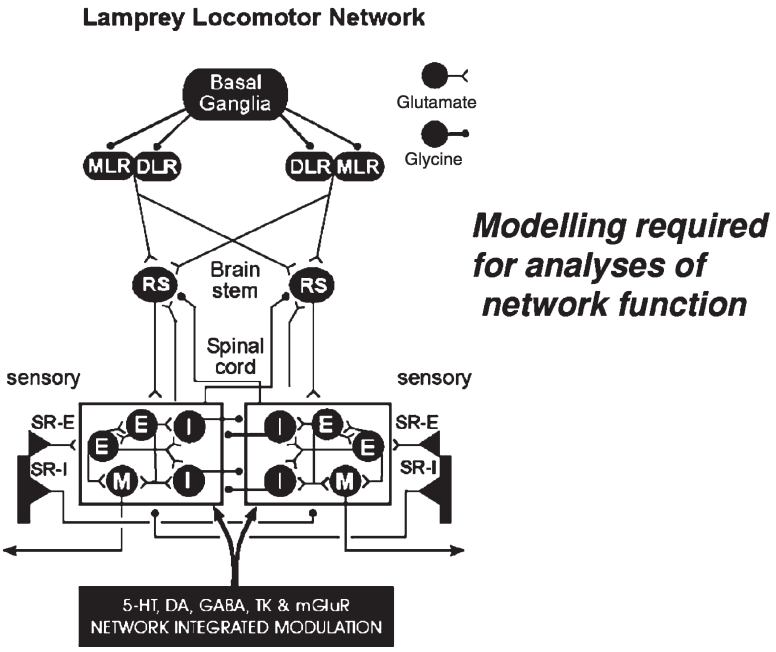

Fig. 2 Locomotor network of the lamprey. Schematic representation of the forebrain, brainstem, and spinal components of the neural circuitry that generates rhythmic locomotor activity. All neuron symbols denote populations rather than single cells. The reticulospinal (*RS*), glutamatergic neurons excite all classes of spinal interneurons and motoneurons. The excitatory interneurons (*E*) excite all types of spinal neurons, i.e., the inhibitory glycinergic interneurons (*I*) that cross the midline to inhibit all neuron types on the contralateral side and motoneurons (*M*). The stretch receptor neurons are of two types: one excitatory (*SR-E*), which excites ipsilateral neurons, and one inhibitory (*SR-I*), which crosses the midline to inhibit contralateral neurons. RS neurons receive excitatory synaptic input from the diencephalic and the mesencephalic locomotor regions (*DLR* and *MLR*), which in turn receive input from the basal ganglia as well as visual and olfactory input. In addition, metabotropic receptors are also activated during locomotion and are an integral part of the network (*5-HT*, 5-hydroxytryptamine; *DA*, dopamine; *GABA*, gamma-aminobutyric acid; *TK*, tachykinin; and *mGluR*, metabotropic glutamate receptor)

EINs synaptically. When the EINs are depolarized, the membrane depolarization can be boosted by the opening of both voltage-dependent NMDA receptors and low-voltage-activated Ca^{2+} channels. This process will be responsible for the initiation of the burst (Fig. 4). During the ongoing burst activity, Ca^{2+} will enter through several different channels including both NMDA channels and a variety of voltage-dependent Ca^{2+} channels. The Ca^{2+} levels will in turn activate Ca^{2+}-dependent K^+ channels (K_{Ca}) that will pull the membrane potential downward and close voltage-dependent channels (e.g., NMDA), and thereby terminate the burst. In addition to K_{Ca} channels, K_{Na} channels also contribute to the hyperpolarization [14,15]. Following the termination of the burst the Ca^{2+} levels will be enhanced, which will lead to a hyperpolarization caused by K_{Ca} activation that will gradually decline as

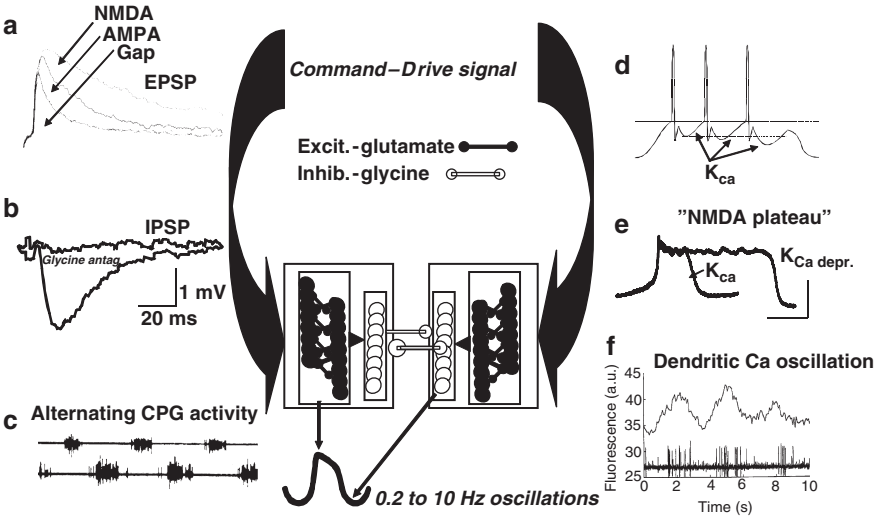

Fig. 3 Schematic representation of the spinal networks for locomotion. The spinal networks that coordinate locomotion are located at the segmental level and consist of a pool of excitatory glutamatergic interneurons, which provide excitation within the pool of interneurons (*filled symbols* = glutamatergic). They are activated from the locomotor command centers in mesencephalon and diencephalon via reticulospinal glutamatergic axons. The descending axons provide an excitatory postsynaptic potential (*EPSP*), which has three components: AMPA, NMDA, and gap junctions (**a**). The glutamatergic interneurons in turn activate glycinergic interneurons (*open symbols*) with axons that inhibit neurons at the contralateral side (**b**). (*IPSP*, inhibitory postsynaptic potential.) Excitatory interneurons project to ipsilateral interneurons that receive out-of-phase inhibition from the contralateral side; this results in alternating efferent activity between the left and right side (**c**). One feature of major importance for terminating burst activity is a calcium (*Ca*) entry in soma and dendrites (**f**) during activity, which results in the activation of calcium-dependent potassium channels (K_{Ca}). The action potential is followed by a slow after-hyperpolarization (sAHP) caused by K_{Ca}. The summation of the sAHPs lead to frequency adaptation (**d**), and the K_{Ca} also contributes to the termination of the plateau potentials (**e**). Time and voltage calibrations as indicated in the figures except for **e**

the cells reduce cytoplasmic Ca^{2+} levels by uptake. When the EIN population has recovered from the K_{Ca} activation, a new burst will be initiated by the background excitatory drive.

Generation of Alternating Activity

The generation of alternating activity between two pairs of antagonists, such as the left and right side of a segment, is a standard element in many networks. The burst-generating kernels on each side in the lamprey segment can produce recurring burst activity by themselves. By connecting them through reciprocal inhibition, alternating

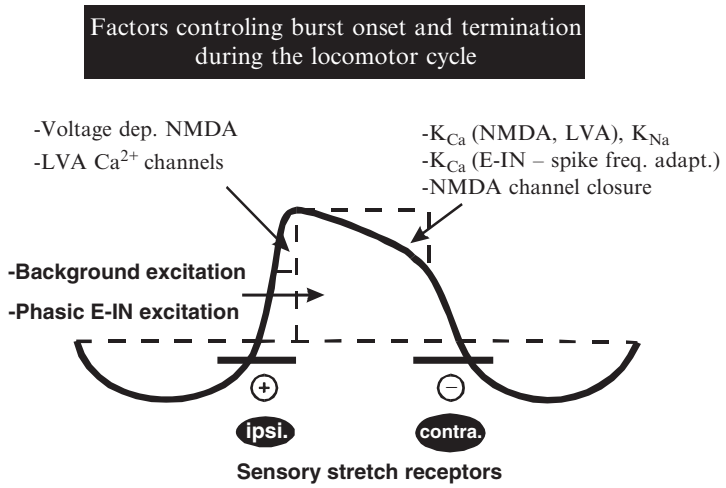

Fig. 4 Factors controlling burst onset and termination. Several different factors contribute to the initiation of the depolarizing phase, its maintenance, and its termination. In addition to conventional synaptic receptor activation, voltage-dependent NMDA receptors, low-voltage activated Ca^{2+} channels (LVA-CA), and Na^{+} channels may be activated. Ca^{2+} and Na^{+} will enter the cell through these channels, cause activation of K_{Ca}, and thereby a progressive hyperpolarization leading to closure of the NMDA channels. The initiation of the depolarizing phase is facilitated by activation of ipsilateral (*ipsi.*) excitatory stretch receptor neurons, whereas the termination of the depolarized phase is partially a result of activation of contralateral (*contra.*) inhibitory stretch receptor neurons. E-IN, excitatory interneurone

activity will occur (Figs. 2, 3). The EINs drive, in addition to ipsilateral motoneurons, also inhibitory commissural interneurons that provide inhibition of the different neurons on the contralateral side [12,16,17]. Thus, when one side is bursting the contralateral side will be inhibited, and as the burst is terminated the ipsilateral side will initiate an excitatory burst from the background excitatory drive [18]. This side will then in turn inhibit the first side and so forth.

Intersegmental Network

The lamprey swims normally by producing an undulatory wave propagated from head to tail (Fig. 5). The faster the wave is propagated backward along the body, the faster the animal will move forward through the water [19–21]. The delay between the activation of each segment is around 1% of the cycle duration regardless of whether the cycle duration is 2 s or 0.10 s. As the lamprey has about 100 segments, this means that the delay from head to tail fin will be constant around one full cycle whether the lamprey swims fast or slowly. This rostrocaudal propagation

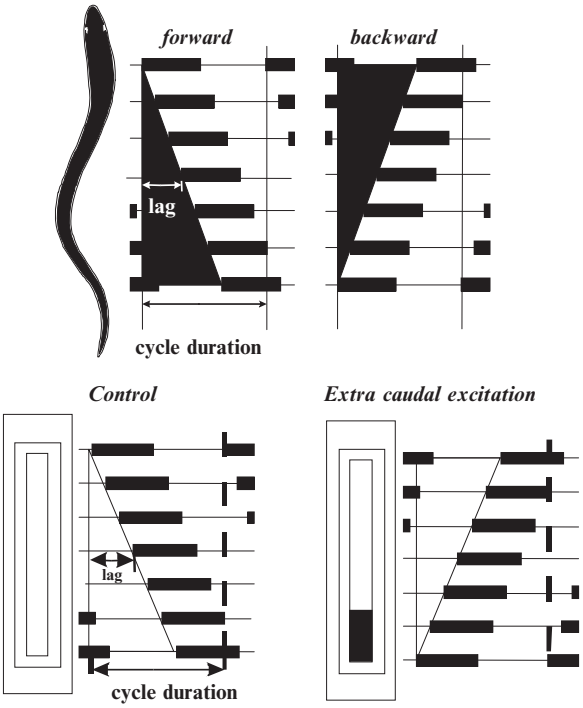

Fig. 5 Lamprey spinal cord intersegmental coordination. During swimming, a mechanical wave is transmitted along the body by sequential activation of the muscle segments. When the animal moves forward, there is a lag between consecutive segments in the spinal cord. This lag is always a certain proportion of the cycle duration (i.e., a constant phase lag). It can be reversed into a wave that is propagated from tail to head, as during backward swimming. In the isolated spinal cord preparation, a rostral to caudal lag is also seen. This pattern can be reversed if, for example, extra excitation is added to the caudal spinal cord. The caudal segments then receive a higher inherent frequency and can then entrain the more rostral segmental networks

of the wave also occurs during locomotor activity in the isolated spinal cord (Fig. 5) and is thus basically part of the standard spinal pattern generation.

If caught in a corner, the lamprey can also swim backward [22] by reversing the direction of the mechanical wave (Fig. 5). A reversed-phase coupling can be produced in the isolated spinal cord if the caudal part of the spinal cord has higher excitability than more rostral segments [23]. Essentially, the segments with the highest excitability will lead the activity and those with lower excitability will follow with a delay.

The EINs extend over an area of around 3 segments rostral to the cell body and 8 segments caudally [13]. This pattern applies to all EINs along the spinal cord, and they thus form a continuous network that is not separated by segmental boundaries. Such a hemicord network, only including the EIN connectivity, can generate not only bursting but also an intersegmental rostrocaudal lag. The rostrocaudal phase

lag can be generated in a simulation with 100 segments and 3000 EINs. This number of neurons and connectivity approaches that which is found biologically. If the relative excitability along the cord is modified so that the rostral part has lower excitability then the caudal one, the phase lag is reversed, as found experimentally. The phase lag remains constant along the spinal cord with both a forward and a backward coordination. This finding thus shows that a segmental coupling of exclusively excitatory interneurons with appropriate cellular and intersegmental connectivity can produce an appropriate phase coupling for forward and backward swimming.

The hemicord coordination is of interest from the analytical point of view, but physiologically there is always a reciprocal activity at the left and the right side, resulting in the propulsive locomotor movements. Segmentally, the EINs also activate commissural inhibitory interneurons that ensure that the activity is alternating in each segment. The intersegmental coordination has also been modeled with a more theoretical approach [24].

Steering

What we have considered so far is the neural basis of symmetrical locomotor movements. To make the movements behaviorally meaningful, we need in addition to steer them. Steering movements to the left or right side are achieved through an asymmetrical activation of reticulospinal neurons on the left and right side, particularly involving the middle and posterior rhombencephalic reticular nuclei [5,25,26]. This activation results in longer and more intense bursts on the side toward which a turning response occurs (Fig. 6B). Reproducible steering responses to the left or right side can be elicited in a reduced brainstem–spinal cord in vitro preparation by trigeminal stimuli that, via lower brainstem interneurons, impinge on the reticulospinal neurons [27]. The basic brainstem circuitry for turning is thus comparatively simple (Fig. 6A). The reticulospinal neurons impinge on both the EINs and the commissural inhibitory interneurons and will thereby excite to provide longer bursts on the same side and concurrently also a longer inhibition of the contralateral side. These results have been analyzed both experimentally and through modeling [28].

The foregoing results illustrate the basic neural machinery for turning, but this does not unravel the mechanisms by which the animal itself will elicit goal-directed steering toward a particular object or prey. Tectum (superior colliculus) is an important structure in this context. It receives input from the eye that is organized in a retinotopic fashion. It provides thus a sensory map that is aligned to a motor map, which can elicit eye movements to a target and also orientation movements of the body and finally locomotion [29], seemingly toward an object that gave rise to activation of the retina (Fig. 6C). The tectal circuitry in interaction with the basal ganglia presumably is responsible for this action; however, this is outside the scope of this brief review.

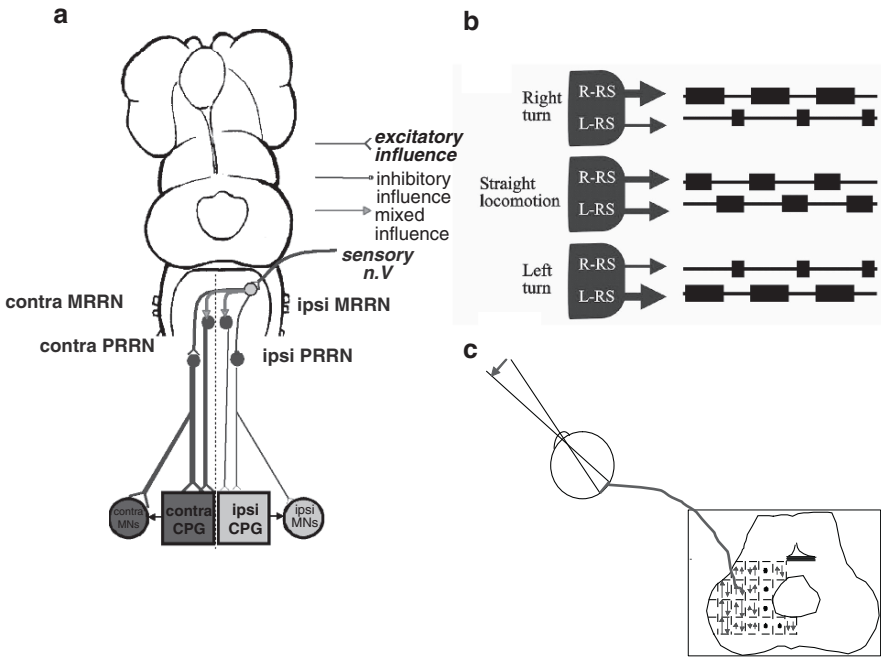

Fig. 6 Exploration of the mechanisms controlling steering in the lamprey. **a** During experimental conditions, steering signals can be produced by trigeminal sensory inputs (*sensory n. V*) that via interneurons activate preferentially contralateral medial and posterior rhombencephalic reticulospinal neurons (*MRRN* and *PRRN*) that project to the spinal cord [26]. *Black*, excitation; *gray*, inhibition. The descending signals affect both the CPG and the motoneurons (*MNs*) directly. **b** An asymmetrical activation of *RS* neurons results in a steering movement toward the more strongly activated side. Behaviorally, this will allow the animal to escape, or swim away from, the original stimulus (compare **a**). **c** In **a** and **b,** the turning machinery itself is illustrated: goal-directed steering toward a certain object requires sensory processing. The tectum receives input from the eye in a retinotopic fashion, thus forming a motor map, which can elicit both appropriate eye and orientation movements toward a given target [29], which will result in steering if the animal is swimming

Network Properties Can Be Radically Modified via G Protein-Coupled Receptors

We have discussed the network operation in terms of fast synaptic interaction on the millisecond level acting via ionotropic glutamate, glycine, and GABA receptors ($GABA_A$). At all levels of the central nervous system (CNS) there are also slower forms of synaptic transmission mediated by metabotropic receptors acting at second, minute, or hour time scales. These transmitter systems not only influence mood and attention but also fine tune a variety of sensory and motor functions. These systems include peptidergic, aminergic (5-HT, noradrenaline, dopamine), endocannabinoid, nitric oxide, metabotropic glutamate ($mGluR_{1-7}$), and GABA

receptors ($GABA_B$). Each of these receptors may change the properties of a network by modifying the action of specific cellular and synaptic targets, for instance, by phosphorylating a specific ion channel subtype. Practically all networks analyzed, whether vertebrate or invertebrate, are subject to many forms of modulation that can fundamentally modify cellular and network properties. The functional significance of this type of modulation is presumably to be able to adapt and optimize the function of a network to varying behavioral demands. A wealth of information has emerged from different vertebrate and invertebrate model systems, but for reasons of space we illustrate here general principles using three examples from the lamprey system (Table 1).

Table 1 Metabotropic amino acid, aminergic, and peptidergic G protein-mediated modulation of ion channel, synaptic, cellular, and network activity in the lamprey spinal cord

Modulation: ion channels → network activity

	Presyn. gating	$Ca_v1.3$ (LVA)	$Ca_v2.1$-2.2 (HVANP/Q)	IP3	SK1-K_{Ca}	K_{Na}	K^+	NMDA	Network (frequency)
$GABA_B$	*Inh*	↘	↘		(↘)	*0*			↘
$mGluR_1$	*0*	*0*	*0*			*0*	↘	↗	↗
$mGluR_5$	*0*	*0*	*0*	Ca^{2+} *osc* ↗		*0*			↘
$mGluR_{II-III}$	*Inh*		*0*			*0*			↘
$5\text{-}HT_{1A}$	*Inh*	↘	↘		(↘)	*0*			↘
D2	*Inh*	↘			(↘)	*0*			↘
TK	*Facil.*				↘		↘	↗	↗
NPY	*Inh*								*0*
SOM		*0*	*0*		*0*		↗		↘
NT		*0*	*0*		*0*				↗

The table summarizes the results of a number of studies (see text). The effects of different transmitters and receptors on different targets are listed in the columns on the right. Gray backgrounds indicate receptors known to be activated endogenously during fictive locomotion. The presynaptic actions can be targeted to sensory afferents, excitatory or inhibitory interneurons and descending reticulospinal axons. Different transmitters have selective actions on different cellular targets (Inh indicates presynaptic inhibition and Facil facilitation). The locomotor network phasically modulates, in each cycle, the synaptic transmission from sensory afferents and interneurons. The modulation of HVA_{Ca}, LVA_{Ca}, K_{Ca} and K^+ and NMDA channels is indicated with a downward arrow for depression and an upward arrow for facilitation. Again, the effects may be specific to particular cell types. Finally, the effects on the network level have been studied on the background of locomotor activity (arrows relate to locomotion burst frequency), and in related modeling experiments. 5-HT, 5-hydroxytryptamine (serotonin) receptor; D_2, type 2 dopamine receptor; HVA, high voltage activated; mGluR, metabotropic glutamate receptor; NPY, neuropeptide Y; SOM, somatostatin; NT, neurotensin; TK, tachykinin

The lamprey CPG is embedded in a number of modulatory systems [3,30], some of which are activated as soon as the network starts to operate. Neurons of the spinal 5-HT system are located in the midline where they form a dense plexus, from which 5-HT is released in a paracrine fashion onto the dendrites of network interneurons [31]. 5-HT reduces the current carried through N-type Ca^{2+} channels [32], which in turn results in a reduction of the amplitude of the slow K_{ca}-dependent after hyperpolarization (sAHP) [33,34]. In addition, 5-HT has presynaptic inhibitory effects on excitatory synapses [32]. The 5-HT-mediated reduction of the K_{Ca} current results not only in a reduction of the sAHPs but also in a higher frequency of action potentials and a reduced spike frequency adaptation. The net effect at the network level is a reduced burst frequency, with longer and more intense bursts and a more regular burst pattern. The 5-HT system thus contributes to the operation of the CPG by modifying the properties of the network interneurons and the transmitter they release at their synapses. 5-HT appears to be involved in the control of most vertebrate locomotor networks. Indeed, in mammals as in the lamprey, the raphe-spinal and parapyramidal 5-HT neurons are turned on as locomotion begins [35,36].

Metabotropic glutamate receptors [37] are activated as soon as glutamatergic neurons become active during locomotion. One subtype, $mGluR_1$ [38], is activated during locomotor activity and acts to speed up locomotor activity through several distinct cellular mechanisms, mediated in part by phospholipase C–protein kinase C and IP_3 pathways. $MGluR_1$ activation enhances the NMDA receptor current, reduces a leak conductance, and triggers the release of endocannabinoids, which in turn reduces glycinergic synaptic current from contralateral neurons via a presynaptic action. These three cellular mechanisms are convergent and produce net excitatory and stabilizing effects on the network.

Tachykinins (including substance P) are released during activity in the locomotor network and exert an excitatory effect to induce a more regular burst pattern [39,40]. When the action of tachykinins is blocked by receptor-specific antagonists, burst frequency is reduced. Similarly to $mGluR_1$, the tachykinins act via a protein kinase C-mediated facilitation of NMDA currents. The tachykinins also modify the activity-dependent synaptic plasticity in crossed inhibitory synapses; although the first IPSP in a spike train may be unchanged, the subsequent IPSPs decline in amplitude much faster than under control conditions, thus enhancing burst frequency [41]. If tachykinins are applied in high concentrations, their action may last over 24 h.

Although fast synaptic actions determine motor pattern in a given instant, the response pattern of the neurons and the efficacy of their synapses are, to a large extent, determined by the actions of these modulatory systems, which help the network adapt to different behavioral challenges. In the lamprey (Table 1), the molecular targets of several modulators have been identified. Because intrinsic network function and behavior is also well understood, it is possible to estimate the effect of modulation of a target gene on the actual motor behavior and thus bridge the gap from gene to behavior [3].

Concluding Remarks

The aim of this brief review is to serve as an introduction to the lamprey model system in the study of the cellular and molecular bases of vertebrate motor behavior and in particular the intrinsic function of these neuronal networks.

Acknowledgments We hereby acknowledge the support of the European Commission (Neurobotics, SG, Spinal Cord Repair, Lampetra) and The Swedish Research Council (S.G., J.).

References

1. Grillner, S. Neuronal networks in motion from ion channels to behaviour. An R Acad Nac Med (Madr) 2006;123(2):297–8.
2. Grillner, S., et al. Neural bases of goal-directed locomotion in vertebrates: an overview. Brain Res Rev 2008;57(1):2–12.
3. Grillner, S. The motor infrastructure: from ion channels to neuronal networks. Nat Rev Neurosci 2003;4(7):573–86.
4. Grillner, S. Biological pattern generation: the cellular and computational logic of networks in motion. Neuron 2006;52(5): 751–66.
5. Wannier, T., et al. Differential effects of the reticulospinal system on locomotion in lamprey. J Neurophysiol 1998;80(1):103–12.
6. Deliagina, T.G., et al. Vestibular control of swimming in lamprey. III. Activity of vestibular afferents: convergence of vestibular inputs on reticulospinal neurons. Exp Brain Res 1992;90(3):499–507.
7. Cangiano, L. and S. Grillner. Mechanisms of rhythm generation in a spinal locomotor network deprived of crossed connections: the lamprey hemicord. J Neurosci 2005;25(4):923–35.
8. Cangiano, L. and S. Grillner. Fast and slow locomotor burst generation in the hemispinal cord of the lamprey. J Neurophysiol 2003;89(6):2931–42.
9. Parker, D. and S. Grillner. The activity-dependent plasticity of segmental and intersegmental synaptic connections in the lamprey spinal cord. Eur J Neurosci 2000;12(6):2135–46.
10. Buchanan, J.T. and S. Grillner. A new class of small inhibitory interneurones in the lamprey spinal cord. Brain Res 1988;438(1-2):404–7.
11. Buchanan, J.T., et al. Identification of excitatory interneurons contributing to generation of locomotion in lamprey: structure, pharmacology, and function. J Neurophysiol 1989;62(1):59–69.
12. Biro, Z., R.H. Hill, and S. Grillner. 5-HT modulation of identified segmental premotor interneurons in the lamprey spinal cord. J Neurophysiol 2006;96:931–5.
13. Dale, N. Excitatory synaptic drive for swimming mediated by amino acid receptors in the lamprey. J Neurosci 1986;6(9):2662–75.
14. Hill, R., et al. Apamin blocks the slow AHP in lamprey and delays termination of locomotor bursts. Neuroreport 1992;3(10):943–5.
15. Wallen, P., et al. Sodium-dependent potassium channels of a Slack-like subtype contribute to the slow afterhyperpolarization in lamprey spinal neurons. J Physiol 2007;585(Pt 1):75–90.
16. Buchanan, J.T. Identification of interneurons with contralateral, caudal axons in the lamprey spinal cord: synaptic interactions and morphology. J Neurophysiol 1982;47(5):961–75.
17. Ohta, Y. and S. Grillner. Monosynaptic excitatory amino acid transmission from the posterior rhombencephalic reticular nucleus to spinal neurons involved in the control of locomotion in lamprey. J Neurophysiol 1989;62(5):1079–89.
18. Hellgren, J., S. Grillner, and A. Lansner. Computer simulation of the segmental neural network generating locomotion in lamprey by using populations of network interneurons. Biol Cybern 1992;68(1):1–13.

19. Wallen, P. and T.L. Williams. Fictive locomotion in the lamprey spinal cord in vitro compared with swimming in the intact and spinal animal. J Physiol (Lond) 1984;347:225–39.
20. Williams, T., et al. Locomotion in lamprey and trout: the relative timing of activation and movement. J Exp Biol 1989;143:559–66.
21. Grillner, S. On the generation of locomotion in the spinal dogfish. Exp Brain Res 1974;20(5):459–70.
22. Islam, S.S., et al. Pattern of motor coordination underlying backward swimming in the lamprey. J Neurophysiol 2006;96(1):451–60.
23. Matsushima, T. and S. Grillner. Neural mechanisms of intersegmental coordination in lamprey: local excitability changes modify the phase coupling along the spinal cord. J Neurophysiol 1992;67(2):373–88.
24. Cohen, A.H., et al. Modelling of intersegmental coordination in the lamprey central pattern generator for locomotion. Trends Neurosci 1992;15(11): 434–8.
25. Deliagina, T.G., P.V. Zelenin, and G.N. Orlovsky. Encoding and decoding of reticulospinal commands. Brain Res Brain Res Rev 2002;40(1-3):166–77.
26. Deliagina, T.G., et al. Activity of reticulospinal neurons during locomotion in the freely behaving lamprey. J Neurophysiol 2000;83(2):853–63.
27. Fagerstedt, P., et al. Lateral turns in the lamprey. II. Activity of reticulospinal neurons during the generation of fictive turns. J Neurophysiol 2001;86(5):2257–65.
28. Kozlov, A.K., et al. Modeling postural control in the lamprey. Biol Cybern 2001;84(5):323–30.
29. Saitoh, K., A. Ménard, and S. Grillner. Coordination of eye and locomotor movement elicited from the lamprey tectum. In: SFN Annual Meeting 2004, San Diego.
30. El Manira, A. and P. Wallen. Mechanisms of modulation of a neural network. News Physiol Sci 2000;15:186–191.
31. Christenson, J.P., et al. 5-Hydroxytryptamine depresses reticulospinal excitatory postsynaptic potentials in motoneurones of the lamprey. In: Fuxe L.F.A.K. (ed) Volume Transmission in the Brain: Novel Mechanisms for Neural Transmission. Raven Press, New York: 1991:159–70.
32. Hill, R.H., et al. 5-HT inhibits N-type but not L-type $Ca(2^{+})$ channels via 5-HT1A receptors in lamprey spinal neurons. Eur J Neurosci 2003;18(11):2919–24.
33. Wallen, P., et al. Effects of 5-hydroxytryptamine on the afterhyperpolarization, spike frequency regulation, and oscillatory membrane properties in lamprey spinal cord neurons. J Neurophysiol 1989;61(4):759–68.
34. Biro, Z., R.H. Hill, and S. Grillner. 5-HT modulation of identified segmental premotor interneurons in the lamprey spinal cord. J Neurophysiol 2006;96(2):931–5.
35. Jacobs, B.L. and C.A. Fornal. Serotonin and motor activity. Curr Opin Neurobiol 1997;7(6):820–5.
36. Liu, J. and L.M. Jordan. Stimulation of the parapyramidal region of the neonatal rat brain stem produces locomotor-like activity involving spinal 5-HT7 and 5-HT2A receptors. J Neurophysiol 2005;94(2):1392–404.
37. El Manira, A., et al. Metabotropic glutamate receptors provide intrinsic modulation of the lamprey locomotor network. Brain Res Brain Res Rev 2002;40(1-3):9–18.
38. Kettunen, P., et al. Neuromodulation via conditional release of endocannabinoids in the spinal locomotor network. Neuron 2005;45(1):95–104.
39. Parker, D., W. Zhang, and S. Grillner. Substance P modulates NMDA responses and causes long-term protein synthesis-dependent modulation of the lamprey locomotor network. J Neurosci 1998;18(12):4800–13.
40. Perez, C.T., R.H. Hill, and S. Grillner. Endogenous tachykinin release contributes to the locomotor activity in lamprey. J Neurophysiol 2007;97(5):3331–9.
41. Parker, D. and S. Grillner. Activity-dependent metaplasticity of inhibitory and excitatory synaptic transmission in the lamprey spinal cord locomotor network. J Neurosci 1999;19(5):1647–56.

Bacterial Complexity: More Is Different on All Levels

Eshel Ben-Jacob

Introduction

This chapter presents new clues, drawn from the morphogenesis of bacterial colonies, for the challenges of complexity posed in the integrative study of biological systems (systemic or systems biology). Some exciting observations of complex cooperative behavior of bacteria in colonies are presented, guided by the assumption that they might shed new light on the foundations and evolution of biocomplexity in general. The chapter is aimed at researchers of different disciplines—microbiology, biology, chemistry, physics, mathematics, and computer science—so, to make it comprehensible to all, I have avoided the use of specialized terminology and limited the presented details.

Bacteria are not the simple, solitary creatures of limited capabilities they were long believed to be. The impression that bacteria act as unsophisticated, solitary creatures stems from years of laboratory experiments in which they were grown under artificial conditions. However, under the harsh conditions in the wild, or in the laboratory under growth conditions that mimic natural environments, these versatile organisms work as a team and employ chemical communication to form highly complex colonies of 10^9–10^{12} bacteria each [1–11]. Such colonies behave much like a multicellular organism with cell differentiation, distribution of tasks, and, in some cases, even modules that act like reproductive organs.

One aspect of these behaviors has to do with collective engineering of complex spatial organization of the colony, with the bacteria forming different patterns to better cope with the environment [8–11]. To form such multicellular superorganisms, new functional features appear at every level from the internal cellular gel and genome states to the growth of the colony as a whole, thus facilitating a high level of functional complexity. Bacteria cannot store genetically all the relevant information required for creating colonial patterns. In a new scenario that I propose they need not do so, because the respective units (the individual bacteria) assume newly co-generated

E. Ben-Jacob
School of Physics and Astronomy, Raymond and Beverly Sackler Faculty of Exact Sciences, Tel-Aviv University, 69978 Tel-Aviv, Israel

S. Nakanishi et al. (eds.), *Systems Biology*,
DOI:10.1007/978-4-431-87704-2_3, © Springer 2009

traits and faculties that are not explicitly stored in the genetic information of the individuals [8–13]. The required contextual information is cooperatively generated by using internally stored information, as well as new information extracted from the environment. Thus, these bacteria only require genetically stored information on how to produce perceptive faculties and how these capabilities, along with the guidelines for using them, may be employed to generate new knowledge as required [8–13].

Engineered Complexity of the *Paenibacillus dendritiformis* Bacteria

To study the mechanisms and principles by which the bacteria regulate (engineer) the complexity of colonial patterns, we developed a new strain of lubricating bacteria, *Paenibacillus dendritiformis* [8]. The patterns shown in Fig. 1 are generated during colony development of these bacteria in response to growth on nutrient-poor and hard surfaces. To cope with this situation, the bacteria collectively produce a lubricating layer of fluid that allows them to swim on the hard surface. The engineering capabilities of the bacteria are reflected by their ability to perform collective sensing of the level of nutrients and the hardness of the surface. Consequently, they regulate the genome level to adjust the secretion of lubrication and its viscosity to generate colonies whose structure matches the growth conditions.

Chemotactic Signaling

To achieve even greater engineering efficiency, bacteria employ the mechanisms of chemotactic signaling. Chemotaxis is cell movement in response to gradients in the concentration of a chemical agent [8–11]. The movement can be biased either toward higher concentrations (attractive) or away from high concentrations (repulsive). Bacteria are too short to detect chemical gradients, yet swimming bacteria found a smart solution to detect gradients and bias their movement accordingly. For attractive (repulsive) bias, they detect the concentration as they swim, and if the concentration increases (decreases) they delay their tumbling. We emphasize that this process involves sensing (of the chemical level), memory (of the measured concentration), and information processing—evaluation of the change in concentration between measurements.

The most familiar case of chemotaxis is attraction to an external chemical such as a nutrient. There is evidence that such chemotaxis occurs in these colonies and is responsible for an increased expansion rate and colony “bushiness” at intermediate values of the nutrient concentration (Fig. 1e). At relatively higher nutrient levels, additional bacterial density variations are visible within the branches (Fig. 1d). Model simulations can be used to test the idea that the patterns result from bacterial

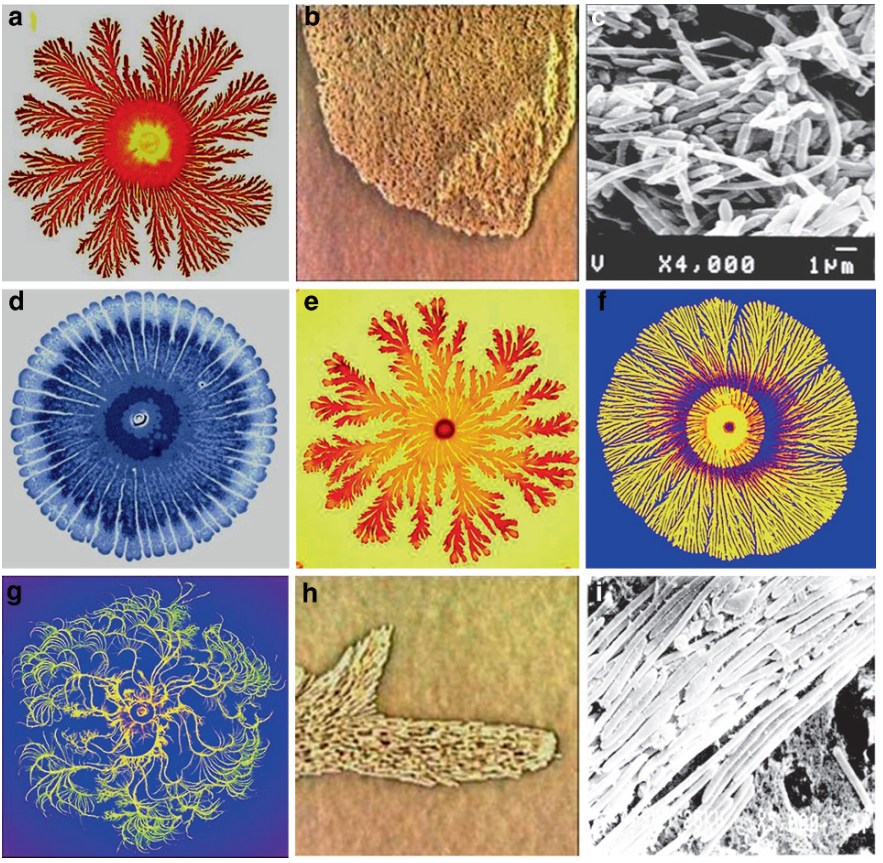

Fig. 1 Colonial morphogenesis of the *Paenibacillus dendritiformis* bacteria when grown on hard and food-depleted substrate. The colony starts from a droplet (5 µl) inoculation at the center of the Petri dish (*darker dot*). After inoculation, the bacteria go through an "embryonic" colonial stage for several hours (presumably of assessment of the environmental conditions), and only then does the colony start to expand outward on the surface [8–11]. **a** It takes the colony about 2 days to reach the observed size of about 5 cm in diameter shown here. **b** Snapshot from a video clip taken through an optical microscope with 500× magnification. The video clip observations reveal bacteria swimming: segments of straight motion for about 1–3 s at a speed of about 1 µm/s, interrupted by bacterial tumbling terminating in a random new direction; that is why the bacterial movement is usually modeled as random walk. **c** A scanning electron micrograph. Note the variability in the individual bacteria. It is now understood that phenotypic diversity is not arbitrary but collectively regulated to afford the colony elevated group flexibility [48]. **d** Typical pattern developed at higher food levels when attractive chemotactic signaling is activated (as is concluded by comparison with model simulations). **e** Typical pattern when food chemotaxis dominates the growth at intermediate levels of food. **f** Colonial pattern at a low level of food when repulsive chemotactic signaling is assumed to be intensified. The colors are added to indicate the bacterial density. As explained in the text, the *P. dendritiformis* bacteria can perform morphotype transition from branching to a chiral pattern exhibiting the formation of curly branches (**g**). **h** Snapshot from a video clip taken through an optical microscope at 500×. The video clip observations reveal that upon elongation the cells alter their collective movement from the typical run-and-tumble of the swimming cells (**b**) to a coordinated forward-backward movement, which yields, as shown by model simulations, an organized twist of the branches with a specified handedness. To bring this about, the bacteria suppress cell division and become elongated, as observed via scanning electron microscope (**i**). Transmission electron microscope observations reveal that the cells contain several chromosomes

utilizing attractive chemotactic signaling. Very different patterns form at low nutrient levels (Fig. 1f). To explain the mechanism, we recall that part of the branch-making dynamics relies on the cells going into a nonmotile state further back from the colony front, where the nutrient level is extremely low. Based on model simulation, it was proposed that cells emit a repellent chemical as they are entering this state, leading to the observed colony pattern in this case.

Open Question

So, the picture that emerges is that the basic branching pattern is sculpted by the combined action of a variety of chemotactic strategies. As these different influences sort themselves out, changing conditions and changing bacterial strains always lead to new structures. Exactly how information from the outside is utilized to help decide which, if any, of these processes need to be turned on is still an open question. Yet there are increasing hints that these decisions are made cooperatively, much like what is known to be true regarding the collective decision making of bacteria to sporulate or the decision to share genetic information.

Reversible and Inheritable Identity Switching

A remarkable trait of the *P. dendritiformis* bacteria is their identity-switching ability; cooperatively, they can make drastic alterations of their internal genomic state, effectively transforming themselves into practically different cells [5,8]. Under conditions somewhat more favorable to motion, such as growth on a softer substrate, the bacteria engineer radically different classes of chiral colony patterns in which the branches are thinner and curl in the same direction (Fig. 1g). Accompanying the colonial structure is a designed genome change: the bacteria are now programmed to become manyfold longer and have multiple chromosomes. The morphotype transitions are both inheritable: the identity is maintained during Luria-Bertani (LB) growth and even throughout sporulation/germination. Yet the transitions are reversible; for example, the reverse transitions from chiral to ordinary branching occur on harder substrates (when higher bacteria densities are required to produce sufficient amounts of lubrication). Optical microscope observations during colony development reveal the following: upon elongation, the cells alter their collective motion from the typical run-and-tumble to a coordinated forward-backward motion with limited tumbling [*].

---

[*] Bacterial images and video clips are available from PhysicaPlus, the online magazine of the Israel Physical Society http://physicaplus.org.il and at Ben Jacob's home page http://star.tau.ac.il/~eshel/.

Complexity of the *Paenibacillus vortex* Bacteria

Some bacterial strains organize their colonies by generating modules, each consisting of many bacteria, which are used as building blocks for the colony as a whole. This behavior is observed, for example, in the lubricating bacteria *Paenibacillus vortex* shown in Fig. 2 [5,8–11]. The modules of this lubricating strain are groups of bacteria that move around a common center. Model simulation suggests that the vortices are generated by the action of attractive chemotaxis and possibly physical links between bacteria [14]. It is also suggested that the vortices are "pushed out" in response to a repulsive chemotactic agent secreted by bacteria at the center of the colony. The bacteria in each vortex have high length variability, with some of the cells being tens of micrometers long with several chromosomes. Genome sequencing results indicate that this strain (and the *P. dendritiformis*) has genes for both flagella and pili motility [15].

The Complexity Challenge of Modular Organization

Maintaining the integrity of the individual vortices while they serve as higher-order building blocks of the colony requires advanced communication: each cell has to follow far more complex dynamics, being part of both a specific vortex and the whole colony, so that it can adjust its activities accordingly. A greater challenge is

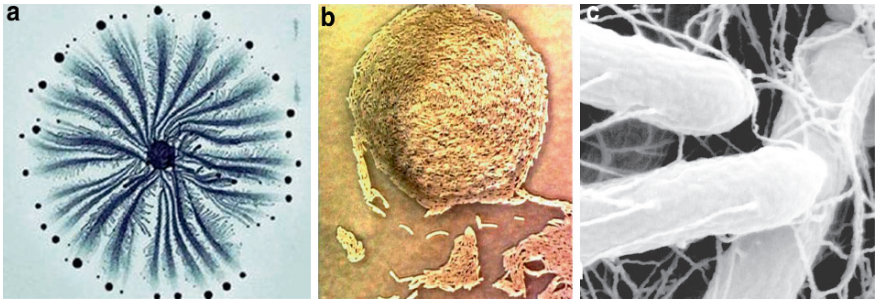

Fig. 2 Modular colonial organization of the *Paenibacillus vortex* bacteria. In (**a**) we see the colony organization. The diameter of the colony shown is about 5 cm. Each *dot* is a module or cluster of bacteria that move; hence, the term vortex. **b** Each vortex (500× picture taken from a video clip) is composed of many cells that swarm collectively around their common center at about 10 μm/s. The vortices vary in size from tens to millions of bacteria, according to their location in the colony. The cells in the vortex replicate, and the vortex expands in size and moves outward as a unit, leaving behind a trail of motile but usually nonreplicating cells, the vortex branch. The dynamics of the vortices is quite complicated and includes attraction, repulsion, merging, and splitting of vortices. Yet, from this complex, seemingly chaotic dynamics, a colony with complex but nonarbitrary organization emerges [*]. **c** Electron microscope view of the individual bacteria showing flagella and pili (courtesy of I. Colin [14])

posed by the formation of new vortices that emerge in the trail behind a vortex. Following initiation signals, the nonmotile cells in the trail start to secrete lubricating fluid and begin to move quite rapidly as a turbulent "biofluid," until an eddy forms and turns into a new vortex as the cells in the eddy generate strong coupling. The entire process appears to be under advanced communication-based cooperative control that goes hand in hand with genome-wide changes in the individual cells. For the integrity of the vortices to be maintained (as the cells replicate), the changes at the gene network level have to be inheritable. The results support the idea of "more is different on all levels" and that it afforded by epigenetic memory.

Cell Differentiation

The idea of epigenetic memory that goes together with cell differentiation is more directly supported by the observations shown in Fig. 3 even after several generations of growth, colonies started from inocula taken from the center of a colony significantly differ in pattern from those started from inocula taken from the leading vortices.

Complexity Transfer

We developed a simple experimental procedure to further test the idea of cell differentiation and task distribution. The procedure involves extension of the idea of replica plating. A large-diameter (several centimeters) cylinder made of Plexiglas covered with a thin sterile paper is used as a stamp. It is (gently) placed above a mother colony and then on another plate with fresh substrate. Figure 4 shows how the pattern of the mother colony is thus copied. In principle, the cells that are

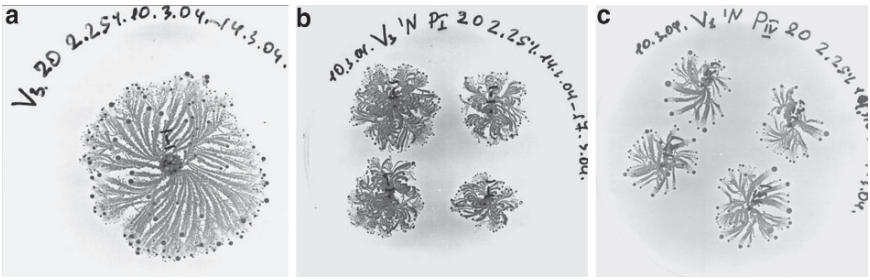

Fig. 3 Precursors of cell differentiations. **a** The mother colony from which cells were taken (by picking). The growth patterns of colonies taken from the center in **a**, the *darker area* from which the mother colony started, are shown in **b**. **c** The growth patterns of colonies started from cells taken from large vortices at the front of the mother colony

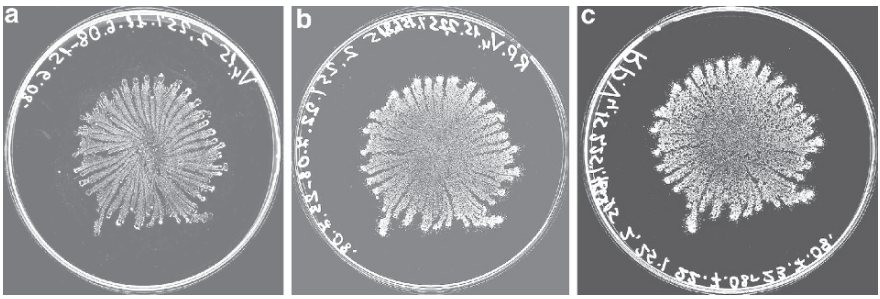

Fig. 4 Replicating colony pattern. **a** The mother colony. Negative colors are used; *white* indicates high bacteria density. **b** A colony grown from replica plating of the mother colony. **c** A colony grown from a successive stamping

transferred to the fresh dish could grow and expand in all directions. Instead, they follow quite accurately the complex pattern of the mother colony, as each cell keeps its functional role in the mother colony.

Functional Complexity and Learning from Experience

In natural habitats, bacteria are regularly exposed to nonlethal (subinhibitory) levels of antibiotic material. Previously [8], I proposed the idea of "functional complexity": the complexity of the colony organization has an important functional role as it affords the bacteria with higher adaptability to cope with environmental stresses. For example, upon encountering antibiotic stress, the bacteria re-shape the colony pattern [8,9,16], as is shown in Fig. 4. Recently it has been suggested that bacteria also possess (epigenetic) memory of the past [9,13], which enables them to keep track of how they handled previous encounters with antibiotics (Fig. 1c). Bacteria learn from past experience and can cope better upon a second encounter with the same antibiotic, as is reflected by the fact that the colony expands faster and has a more complex pattern (Fig. 5). This effect can be erased by growth in neutral conditions. One possibility is that this effect is connected with a genetic shift in the population. Another possibility involves heritable (epigenetic) effects at the genome level.

Information Processing on All Levels

As was pointed out [8–13], bacteria sense the environment and perform internal information processing (according to the internally stored information) to extract latent information embedded in the complexity of their environment. The latent

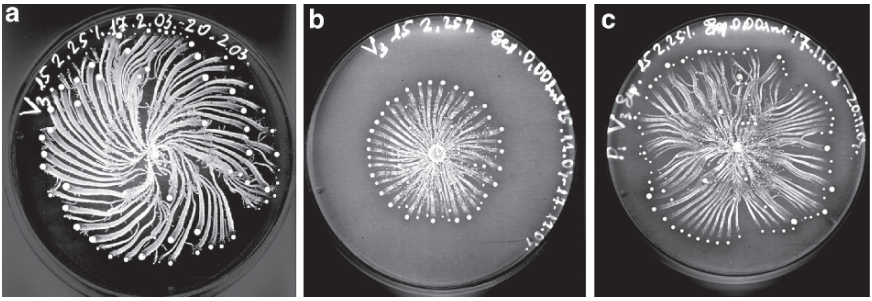

Fig. 5 Learning from experience. The observations show the response of the *Paenibacillus vortex* bacteria to nonlethal levels of Septrin. **a** Normal growth pattern in the absence of antibiotic. The effect of first exposure of the bacteria to the antibiotic is shown in **b**; the response in a second encounter is shown in **c**. Learning from experience (**c**) is manifested by the fact that upon second encounter with the antibiotic the colony expands faster and the pattern has higher complexity [9]

information is then converted into usable or "active" information that affects the bacterium activity as well as intracellular changes [12,13,17].

Although an individual bacterium can sense only a limited area between replications, a colony that is composed of billions of bacteria can sense a large area and over long time periods. Collectively, bacteria can glean relevant latent information embedded in the complex environment over larger distances and longer periods of time. To coordinate such cooperative ventures, bacteria have developed various methods of biochemical communication such as quorum sensing by using a variety of mediators, which range from simple molecules to polymers, peptides, complex proteins, genetic material, and even "cassettes of genetic information" such as plasmids and viruses [8,9,12,13,18]. The intercellular communication is afforded by the evolution of highly complex and intricate intracellular signaling mechanisms involving signal transduction networks [19] and genetic language to turn genes off and on [20]. These mechanisms exhibit functional complexity, which generates intrinsic meaning for contextual interpretations of chemical messages and for formulating appropriate complex responses.

The observations shown in Fig. 6 illustrate that bacteria exchange information extracted from the environment, process the information, and act accordingly. The *P. vortex* bacteria, while moving on M-H agar, form snakelike swarms hundreds of bacteria wide [14]. The swarms can expand very efficiently toward several nutrient sources placed on the surface. To coordinate such search strategy, the individual bacteria must respond not only to local gradients in food concentration but also to differences in concentration between remote locations. Hence, they must exchange the information they detect and compare local conditions to those detected at different locations.

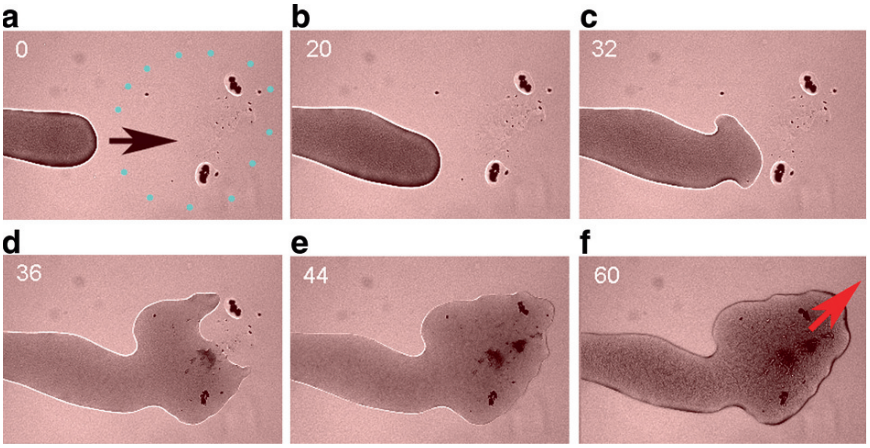

Fig. 6 Swarming intelligence of the *Paenibacillus vortex* bacteria. The pictures (×50) show a snapshot from a video clip of a branch of a colony of *P. vortex* bacteria moving on 0.3% w/v Mueller–Hinton agar (M-H agar). The branch is extending into an area where extracellular material derived from washes of swarming cells was delivered by toothpick and allowed to soak into the agar. Time of frame capture is noted in seconds. **a** Starting ($t = 0$): Area of extract outlined in *blue dots* with direction of cell mass elongation shown by the *black arrow*. **b** *Dark marks* inside the area of the extract are disturbances caused by the toothpick contacting the agar ($t == 20$). **c** Stage $t = 32$: Cell mass starts to disperse as it contacts the area of the extract. **d** Stage $t = 36$. **e** Stage $t = 44$: Cell mass has dispersed into area of extract. **f** Stage $t = 60$: Additional cells are moving into this area from further back in the colony; the cell mass is growing in volume at the tip, and extends in the direction of the *red arrow*. (Video courtesy of I. Colin [14])

Concluding Remarks and Looking Ahead

I have shown how complex colonial forms (patterns) emerge through the communication-based singular interplay between individual bacteria (the micro-level) and the colony (the macro-level). Each bacterium is, by itself, a biotic autonomous system with its own internal cellular gel that possesses informatics capabilities (storage, processing, and interpretation of information). These capabilities afford the cell a certain freedom to select its response to biochemical messages it receives, including self-alteration and broadcasting messages to initiate alterations in other bacteria. Such self-plasticity and decision-making capabilities elevate the level of bacterial cooperation during colonial self-organization.

As the individuals in a growing colony begin to respond to the colony itself (i.e., information flow from the colony to the individual), these individuals respond by regulating their movements, growth rates, the various tasks they perform, the chemical signals they send to other bacteria, and even their gene network state (phenotypic state) according to the received signals.

The essential new lesson learned from bacteria is that colonial high complexity provides the degree of plasticity and flexibility required for better durability and adaptability of the whole colony to a dynamic environment. According to this

picture, new features collectively emerge during biotic self-organization on every level, from the membranes and cytoplasm to the whole colony. The cells thus assume newly co-generated traits and abilities that are not explicitly stored in the genetic information of the individuals. For example, bacteria cannot genetically store all the information required for creating the colonial patterns. In the new picture, they do not need to do so because the required information is cooperatively generated as self-organization proceeds by bacterial communication, informatics, and self-plasticity capabilities. Thus, the bacteria need only have genetically stored the guidelines for producing these capabilities and use them to generate new information as required.

It seems that bacteria have some sort of collective memory by which they keep track of how they handled their previous encounters with antibiotics. They know how to collectively glean information from the environment, "talk" with each other, distribute tasks, generate collective memory, and turn their colony into a *cybernetic system*—a massive "brain" that can perform distributed information processing, learn from past experience, and possibly alter the genome organization or even create new genes to better cope with novel challenges [12,13,17].

Acknowledgments This chapter is a concise summary of a lecture presented in the Uehara meeting on "Systems Biology: The Challenge of Complexity" in Tokyo, 2008. I am most thankful to the Uehara Foundation and the organizers of the meeting for hospitality and support of my stay in Tokyo. I am thankful to Inna Brainis for technical assistance and to Ingham Colin for his collaboration and for providing the pictures shown in Fig. 3 and the clips shown in Fig. 6. The research presented here has been supported in part by the Maguy-Glass Chair in Physics of Complex Systems and the Tauber Fund.

References

1. Matsushita, M. and Fujikawa, H. (1990) Diffusion-limited growth in bacterial colony formation. Physica A 168:498–506
2. Ben-Jacob, E., et al. (1994) Generic modeling of cooperative growth patterns in bacterial colonies. Nature (Lond) 368:46–49
3. Cohen, I., Czirok, A. and Ben-Jacob, E. (1996) Chemotactic based adaptive self-organization during colonial development. Physica A 233:678–698.
4. Shapiro, J.A. and Dworkin, M. (1997) Bacteria as Multicellular Organisms. Oxford University Press, Oxford
5. Ben-Jacob, E. et al. (1998) Cooperative organization of bacterial colonies: from genotype to morphotype. Annu Rev Microbiol 52:779–806
6. Shapiro, J.A. (1998) Thinking about bacterial populations as multicellular organisms. Annu Rev Microbiol 52:81–104
7. Ben Jacob, E., Cohen, I. and Levine, H. (2000) Cooperative self-organization of microorganism. Adv Phys 49:395–554
8. Ben-Jacob, E. (2003) Bacterial self-organization: co-enhancement of complexification and adaptability in a dynamic environment. Philos Trans R Soc Lond A361:1283–1312
9. Ben Jacob, E. et al. (2004) Bacterial linguistic communication and social intelligence. Trends Microbiol 12(8):366–372
10. Ben Jacob, E., Aharonov, Y. and Shapira, Y. (2005) Bacteria harnessing complexity. Biofilms 1:239–263

11. Ben Jacob, E. and Levine, H. (2006) Self engineering capabilities of bacteria. J R Soc Interface 3:197–214
12. Ben-Jacob, E. and Shapira, Y. (2005) Meaning-based natural intelligence vs. information-based artificial intelligence. In: Ben-Noon C. (ed) Cradles of Creativity. Sharey Mishpat, Jerusalem
13. Ben-Jacob, E., Shapira, Y. and Tauber, A.I. (2006) Seeking the foundations of cognition in bacteria: from Schrödinger's negative entropy to latent information. Physica A 359:495–524
14. Ingham, J.C. and Ben-Jacob, E. (2008) Swarming and complex pattern formation in *Paenibacillus* vortex studied by imagine and tracking cells. BMC Microbiol 8:1–36
15. We have completed sequencing the genome of the two strains *P. dendritiformis* and *P. vortex*. The data will soon be published and posted: see http://star.tau.ac.il/~eshel/
16. Ben Jacob, E. et al. (2000) Bacterial cooperative organization under antibiotic stress, Physica A 282:247–282
17. Ben-Jacob, E. (1998) Bacterial wisdom, Gödel's theorem and creative genomic webs. Physica A 248:57–76
18. Bassler, L.B. and Losicck, R. (2006) Bacterially speaking. Cell 125:237–246
19. Ptashne, M. and Gann, A. (2002) Genes and Signals. Cold Spring Harbor Press, Cold Spring Harbor, NY
20. Searls, D.B. (2002) The language of genes. Nature (Lond) 420:211–217

How Animals Get Their Skin Patterns: Fish Pigment Pattern as a Live Turing Wave

Shigeru Kondo

Reaction-Diffusion (RD) Model

There are several theoretical mechanisms that are able to generate spatial patterns autonomously without any pre-pattern.[1,2] Among them, the most plausible in the biological system is the reaction-diffusion (RD) mechanism, which was first presented by A. Turing in 1952[3,4] and mathematically refined by mathematical biologists.[5,6] In the model, the spatial pattern is made as stationary waves generated by the interactive RD of putative chemical substances. According to the mathematical study using computer simulation, an RD system is able to generate stable and evenly spaced patterns when the whole network satisfies a condition: "local activation and long-range inhibition."[6] The spatial patterns made by the system (e.g., "RD pattern" or "Turing pattern") do not need any pre-pattern and autonomously regenerates when artificially disturbed.

However, in spite of its theoretical importance, until very recently Turing's theory was not widely accepted by experimental biologists, for two major reasons. The first is that the main concept of the theory, "the pattern is made by wave," is quite unfamiliar to many experimental biologists. The second is the difficulty of showing the existence of "wave." To prove that the RD mechanism functions in a morphogenetic event, we need to show that the pattern possesses the dynamic nature of the RD wave.

Biological Phenomena in Which the Involvement of the RD Mechanism Is Suspected

The first clear experimental support for this mechanism came in chemical experiments in the early 1990s. Castets et al. and Ouyang and Swinney succeeded in making the Turing pattern using complex chemical reactions.[7,8] Their work encouraged biologists

S. Kondo
Division of Biological Science, Graduate School of Science, Nagoya University, Furo-cho, Chikusa-ku, Nagoya City, Aichi Prefecture 464-8602, Japan

S. Nakanishi et al. (eds.), *Systems Biology*,
DOI:10.1007/978-4-431-87704-2_4,

to study the theoretical mechanism, and Kondo and Asai presented the first reliable data of the existence of the Turing pattern in biological systems in 1995.[9] They recorded the pattern change of the pigment pattern of a marine angelfish, *Pomacanthus imperator*, and suggested that the time course of the pattern change is identical to that predicted by Turing's theory. The involvement of the Turing mechanism is now seriously investigated experimentally in many morphological events: hair pattern of mammals,[10–12] feather pattern of birds,[13–15] regeneration of *Hydra*,[16–18] and right–left determination in the vertebrates.[19–21] In these cases, a candidate of the core functional molecules of pattern formation was proposed. For example, in the case of mouse hair pattern, Sick et al. suggested that the WNT and DKK proteins play the roles of the putative activator and inhibitor in the reaction-diffusion system.[12] Moreover, by artificially changing the parameters of the interactions, it is possible to induce the pattern change that is predicted from the simulation, suggesting that the RD mechanism underlies the determination of the hair distribution. However, most of these morphogenetic events are irreversible, and the patterns that we can observe are completed and fixed ones. Therefore, it is usually impossible to directly detect the existence of the "wave" in the course of the pattern-forming event.

Observation of the Characteristic Movement of the RD Wave in Animal Skin

To date, pigmentation patterns in animal skins,[1,22] feathers of birds,[13,14] and shells of snails[23] are the only examples in which we can detect the dynamic nature of Turing waves as a time course of the pattern change. Especially, the two-dimensional (2-D) skin pattern of fish is quite convenient to study because their waves are sometimes alive even when the fish has grown up into an adult.

For example, when a striped angelfish (*Pomacanthus imperator*) grows, the branching points of the stripes slide horizontally as the zip opens and add a number of stripes; eventually the spacing between the stripes remains stable (Fig. 1a).[9] In the case of the spotted catfish (*Plecostoms*), both division of the spots and insertion of the new spots occur to retain the density and size of the spots (Fig. 1b).[24] Both stripes and the spots are the most typical 2-D patterns generated by the RD mechanism, and the time course of the pattern change possesses the characteristics of the dynamics of RD waves, strongly suggesting that the RD mechanism underlies the process of pigment pattern formation of fish.

Pigment Pattern of Zebrafish Retains the Dynamic Nature of the RD Wave During the Postembryonic Stage

About two decades ago, the zebrafish, a small fish species with very clear stripes in the trunk and fins, was selected as the model animal for biological study and for the use of the genomic information and molecular genetic technologies that are available to

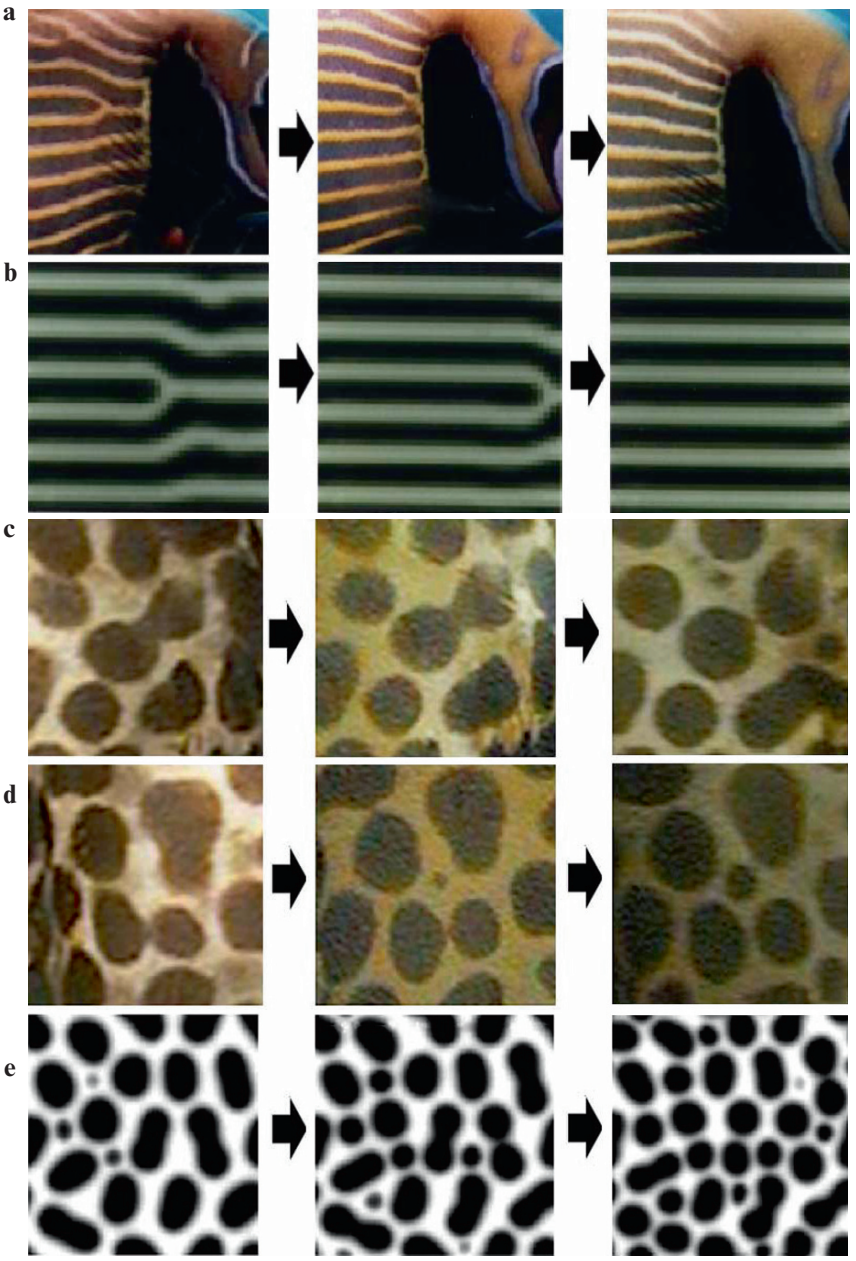

Fig. 1 Dynamic pattern change that occurred in the fish and simulation. **a** Change of stripe pattern occurred in the skin of *Pomacanthus imperator* during 90 days; the prediction made by simulation of the reaction diffusion mechanism is shown in **b**. Sliding of the branch point was observed in both systems. **c**, **d** Change of spot pattern as occurred in the skin of a catfish, *Plecostoms*, during 14 days; the simulation is shown in **e**. Division (**c**) and insertion (**d**) of the spot are observed in both real fish and the simulation based on the reaction-diffusion (RD) model. (From [9] and [24])

identify the molecular mechanism of Turing formation. The pattern of skin pigmentation in zebrafish is composed of three types of pigment cells distributed in the hypodermis: melanophores, the main component of dark stripes; xanthophores, the main component of light stripes; and iridophores.[25,26] Although differing from the stripes of *Pomacanthus imperator* in that the stripes of zebrafish do not become rearranged during normal growth, artificial disturbance of the pattern can induce the characteristic pattern change that is specific to the RD mechanism. By using a laser to kill the pigment cells in specific regions, it is possible to induce a dynamic movement of the stripes that is characteristic of the stationary wave of the RD mechanism. Yamaguchi et al.[27] continuously killed the melanophores in the dorsal two black stripes and observed that the ventral black stripe bent and moved dorsally to fill the vacant space (Fig. 2). This movement of the stripes clearly shows that the pigment pattern of the zebrafish is made and maintained dynamically by the RD, or a very similar, mechanism.

The fact that killing of the pigment cells induced the pattern change in the experiments suggests that the pigment cells do not simply make the hidden pattern visible but are the major players in the pattern formation.[27] Therefore, to uncover the mechanism, the most critical aspect should be the identification of the interactions between the two types of pigment cells (melanophores and xanthophores).

Mutants That Affect Both Development of Pigment Cells and the Resulting Pattern

The zebrafish mutants those have abnormal skin patterns are classified into two categories: those with a defect in the development of pigment cells; and those with normal development of pigment cells at the embryonic stage, but which have a disrupted pattern in the adult fish. Molecular genetic studies of the mutants in the first category have shown that *nacre*,[28] *sparse*,[29] and *rose*[30] are required for the development of melanophores, and that *panther*[31] is required for the development of xanthophores. The *nacre* gene codes a transcription factor, Mitf1, that is required by the cells to develop to the melanophore precursor; *sparse* and *panther* code the class II receptor tyrosine kinases, c-*kit* and c-*fms*, respectively; *rose* codes the endothelin receptor b1; and *sparse* fish lack the embryonic melanophores, but the adult melanophores are normally integrated in the stripes (Fig. 3). The number of embryonic melanophores in *rose* fish is normal, but a reduced number of adult melanophores compose the disturbed stripe.[32] The double mutant of these genes loses almost all the melanophores, suggesting that there are two different populations in the melanophores, and only the adult type is required for the stripe pattern formation.

Interestingly, when one of the pigment cell types fails to develop, other types of pigment cells fail to localize to their normal positions.[28–31,33,34] *nacre* fish lack all melanophores and *panther* fish lack xanthophores. In both cases, the remaining pigment cells cannot form clear stripes but disperse randomly or form aggregates of uncertain shape. However, when a pigment cell type that is lost in the mutant is introduced, clear stripes

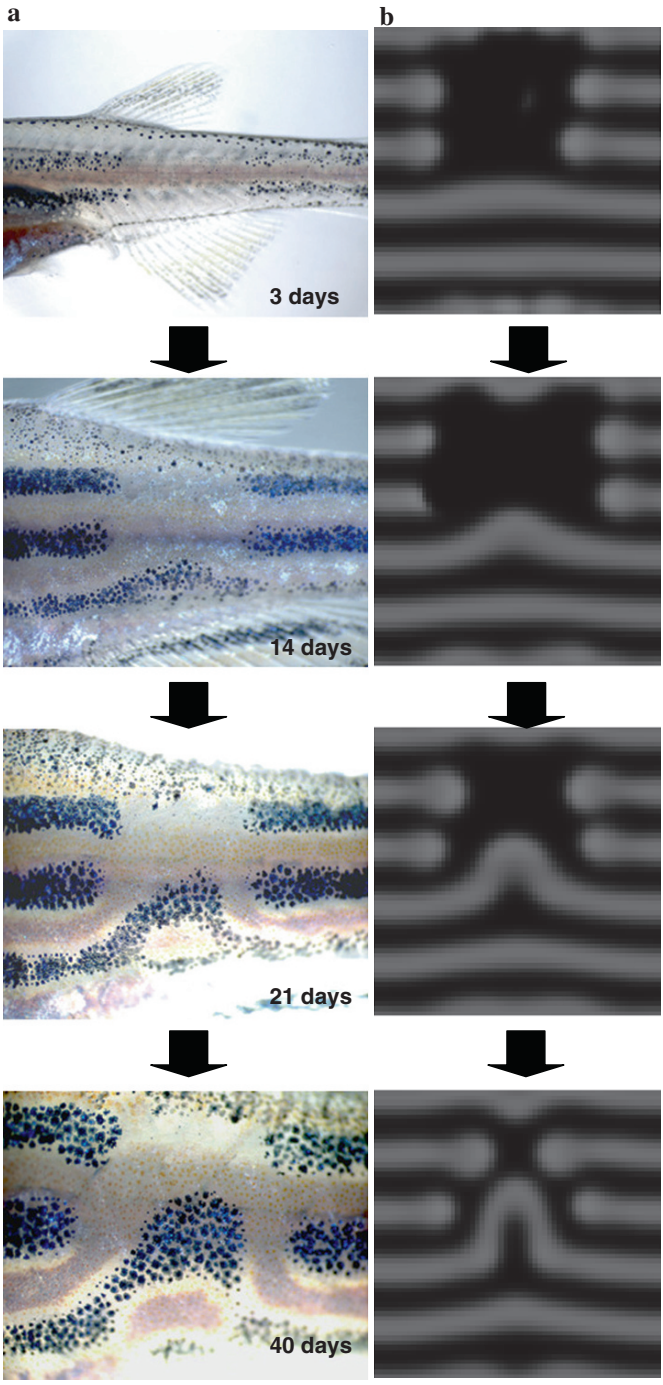

Fig. 2 Dynamic change of the zebrafish pigment pattern induced by laser experiment. **a** Time course of the pattern change. Melanophores in the upper two black stripes are killed by laser. **b** Time-lapse captured images of the regeneration process produced by simulation of the reaction-diffusion mechanism. (From [27])

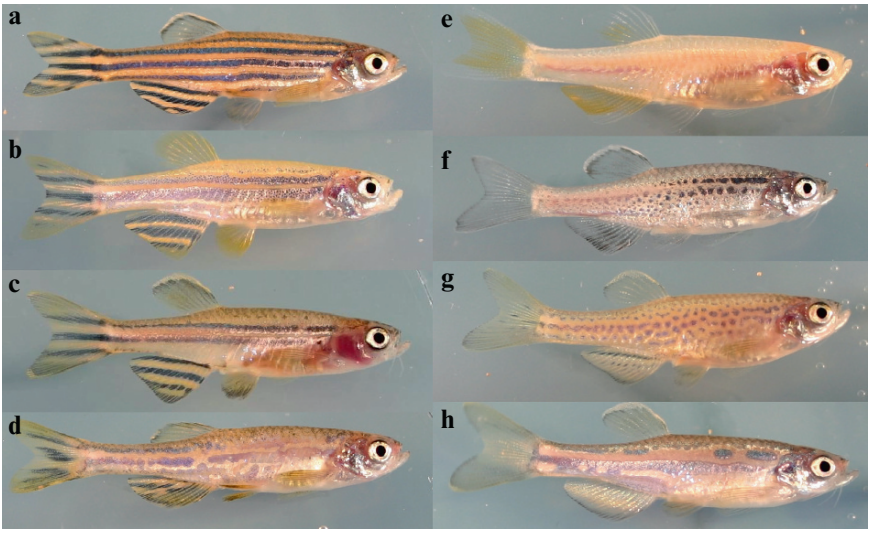

Fig. 3 Pigment patterns of zebrafish mutants: wild type (**a**), *sparse* (**b**), (c)*nacre* (**c**), *puma* (**d**), *panther* (**e**), *jaguar* (*obelix*) (**f**), and *leopard* (**g**)

are regenerated only in the region where both types of pigment cells exist. This experimental result shows that mutual interaction between melanophores and xanthophores plays a critical role in the generation of skin pigmentation pattern.[25,35–37]

Mutants That Affect the Pattern But Do Not Affect the Development of Pigment Cells

Mutants of *jaguar*/*obelix*[37] and *leopard*[37,38] belong to this second category. In these mutants, development and distribution of the pigment cells is normal in embryos and young fish (~4 weeks). In adult fish, although development of pigment cells is normal, their spatial arrangement (pattern) is changed, suggesting that these genes are specifically required for pattern formation. The jaguar mutant fish have wider stripes and the leopard fish have spotted patterns. The chimera experiment done by Maderspacher with these mutants suggested that *jaguar* (*obelix*) is required in melanophores to promote their aggregation and to control boundary integrity, and *leopard* regulates homotypic interaction within both melanophores and xanthophores, and interaction between the two, thus controlling boundary shape.[37] The positional cloning of the *jaguar* mutant revealed that this gene codes a inwardly rectifying potassium channel, Kir7.1.[39] kir channels are a group of ion channels that transfer potassium ion unidirectionally from the outside to the inside of the cell.[40–44] It is shown in the study of cultured cells that this class of channels is responsible for the stability of the membrane potential and sensitivity to the external signals.[45–47] Recently, Jantzi et al. reported that the kir channel (Kir2.2) facilitates cell-to-cell

communication that propagates the contraction signal in the hamster retractor muscle feed artery.[48] In zebrafish, the Kir7.1 gene is expressed in the melanophores,[39] suggesting that the channel controls the interaction of the melanophores. The responsible gene for the *leopard* mutant is cloned and identified to be a component of gap junction, connexin41.8.[49] Connexin41.8 is expressed in many kinds of skin cells including melanophores and xanthophores. As the expression level of the connexin41.8 gene is very low in any cell of the zebrafish skin, very little is yet known about the function and the role of the molecule in the pigment pattern formation. Johnson et al. reported recently that the other class of gap junction gene, connexin43, codes the *shortfin (sof)* gene, which controls the length of the fins of the zebrafish.[50] This fact is quite interesting because it implies that a similar mechanism could control the size of limbs and the 2-D patterns in the skin.

Future Directions

Although molecular genetic studies have been identifying the genes and molecules involved in pigment pattern formation of fish, the questions as to how they are organized and how they generate the RD wave remain largely unanswered. To understand pigment pattern formation, it is necessary to integrate all the molecular reactions and deduce how such a complex system behaves. For this purpose, the framework of RD mechanism is required. In most of the mathematical models of the RD systems, the putative molecular network is composed of chemicals that control the synthesis of the molecules and diffuse them in the field. However, it is

Table 1

Mutant	Gene	Pattern	Melanophore	Xanthophore	Iridophore
sparse	kit/receptor tyrosine kinase	Stripe, boundary is slightly ambiguous	EM absent	Present	Present
rose	ednrb1/G protein-coupled receptor	Fewer stripes, but normal in fins	LM absent	Present	Absent
puma	Not cloned	Purely formed	LM absent	Present	Present
nacre	mitf1/transcription factor	Clusters of xanthophores, but purely striped	Absent	Present	Present
panther	fms /receptor tyrosine kinase	Scattered melanophores	Fewer	Absent	Present
jaguar (*obelix*)	kir7.1/potassium channel	Wider stripes	Present	Present	Present
leopard	Connexin41.8/ gap junction	Spots	Present	Present	Present

Source: Modified from [25]

also possible to compose an equivalent network with the interaction of two types of cell (melanophores and xanthophores). Therefore, there is no theoretical difficulty in applying the model to the zebrafish pigment pattern formation.

Recent mathematical studies on the RD and the related autonomous pattern-forming system revealed that the necessary conditions for the spatial pattern (spots and stripes) formation is the combination of "local activation" and "long-range inhibition."[51] Therefore, to find the core molecules of the RD mechanism, measuring the effective distance for each signaling molecule is essential. Use of advanced live-imaging techniques will help to assess whether the functioning molecules behave as the model predicts and will also help to develop the correct molecular-level network. With the cooperation of advanced molecular genetics and mathematical modeling, the long-unsettled question of how animal skin patterns are generated will be solved in the near future.

References

1. Murray, J. D. & Oster, G. F. Generation of biological pattern and form. IMA J Math Appl Med Biol **1:**51–75 (1984).
2. Meinhardt, H. Models of Biological Pattern Formation. Academic Press, London (1982).
3. Turing, A. The chemical basis of morphogenesis. Philos Trans R Soc Lond B **237:**37–72 (1952).
4. Gierer, A. & Meinhardt, H. A theory of biological pattern formation. Kybernetik **12:**30–39 (1972).
5. Murray, J. Mathematical Biology. Springer, Berlin (2003).
6. Meinhardt, H. & Gierer, A. Pattern formation by local self-activation and lateral inhibition. Bioessays **22:**753–760 (2000).
7. Castets, V., Dulos, E., Boissonade, J. & De Kepper, P. Experimental evidence of a sustained standing Turing-type nonequilibrium chemical pattern. Phys Rev Lett **64:**2953–2956 (1990).
8. Ouyang, Q. & Swinney, H. Transition from a uniform state to hexagonal and striped Turing patterns. Nature (Lond) **352:**610–612 (1991).
9. Kondo, S. & Asai, R. A reaction-diffusion wave on the skin of the marine angelfish *Pomacanthus*. Nature (Lond) **376:**765–768 (1995).
10. Nagorcka, B. N. Evidence for a reaction-diffusion system as a mechanism controlling mammalian hair growth. Biosystems **16:**323–332 (1983).
11. Jung, H. S. et al. Local inhibitory action of BMPs and their relationships with activators in feather formation: implications for periodic patterning. Dev Biol **196:**11–23 (1998).
12. Sick, S., Reinker, S., Timmer, J. & Schlake, T. WNT and DKK determine hair follicle spacing through a reaction-diffusion mechanism. Science **314:**1447–1450 (2006).
13. Harris, M. P., Williamson, S., Fallon, J. F., Meinhardt, H. & Prum, R. O. Molecular evidence for an activator-inhibitor mechanism in development of embryonic feather branching. Proc Natl Acad Sci U S A **102:**11734–11739 (2005).
14. Prum, R. O. & Williamson, S. Reaction-diffusion models of within-feather pigmentation patterning. Proc Biol Sci **269:**781–792 (2002).
15. Jiang, T. X. et al. Integument pattern formation involves genetic and epigenetic controls: feather arrays simulated by digital hormone models. Int J Dev Biol **48:**117–135 (2004).
16. Gierer, A. et al. Regeneration of hydra from reaggregated cells. Nat New Biol **239:**98–101 (1972).
17. Bode, H. R. Head regeneration in *Hydra*. Dev Dyn **226:**225–236 (2003).

18. Technau, U. et al. Parameters of self-organization in *Hydra* aggregates. Proc Natl Acad Sci U S A **97:**12127–12131 (2000).
19. Nakamura, T. et al. Generation of robust left-right asymmetry in the mouse embryo requires a self-enhancement and lateral-inhibition system. Dev Cell **11:**495–504 (2006).
20. Hamada, H. et al. Role of asymmetric signals in left-right patterning in the mouse. Am J Med Genet **101:**324–327 (2001).
21. Hamada, H., Meno, C., Watanabe, D. & Saijoh, Y. Establishment of vertebrate left-right asymmetry. Nat Rev Genet **3:**103–113 (2002).
22. Murray, J. D., Deeming, D. C. & Ferguson, M. W. Size-dependent pigmentation-pattern formation in embryos of *Alligator mississippiensis*: time of initiation of pattern generation mechanism. Proc R Soc Lond B Biol Sci **239:**279–293 (1990).
23. Meinhardt, H. The Algorithmic Beauty of Sea Shells. Springer, Berlin (2003).
24. Asai, R., Taguchi, E., Kume, Y., Saito, M. & Kondo, S. Zebrafish leopard gene as a component of the putative reaction-diffusion system. Mech Dev **89:**87–92 (1999).
25. Kelsh, R. N. Genetics and evolution of pigment patterns in fish. Pigment Cell Res **17:**326–336 (2004).
26. Hirata, M., Nakamura, K., Kanemaru, T., Shibata, Y. & Kondo, S. Pigment cell organization in the hypodermis of zebrafish. Dev Dyn **227:**497–503 (2003).
27. Yamaguchi, M., Yoshimoto, E. & Kondo, S. Pattern regulation in the stripe of zebrafish suggests an underlying dynamic and autonomous mechanism. Proc Natl Acad Sci U S A **104:**4790–4793 (2007).
28. Lister, J. A., Robertson, C. P., Lepage, T., Johnson, S. L. & Raible, D. W. nacre encodes a zebrafish microphthalmia-related protein that regulates neural-crest-derived pigment cell fate. Development (Camb) **126**:3757–3767 (1999).
29. Parichy, D. M., Rawls, J. F., Pratt, S. J., Whitfield, T. T. & Johnson, S. L. Zebrafish sparse corresponds to an orthologue of c-kit and is required for the morphogenesis of a subpopulation of melanocytes, but is not essential for hematopoiesis or primordial germ cell development. Development (Camb) **126:**3425–3436 (1999).
30. Parichy, D. M. et al. Mutational analysis of endothelin receptor b1 (rose) during neural crest and pigment pattern development in the zebrafish *Danio rerio*. Dev Biol **227:**294–306 (2000).
31. Parichy, D. M., Ransom, D. G., Paw, B., Zon, L. I. & Johnson, S. L. An orthologue of the kit-related gene fms is required for development of neural crest-derived xanthophores and a subpopulation of adult melanocytes in the zebrafish, *Danio rerio*. Development (Camb) **127:**3031–3044 (2000).
32. Johnson, S. L., Africa, D., Walker, C. & Weston, J. A. Genetic control of adult pigment stripe development in zebrafish. Dev Biol **167:**27–33 (1995).
33. Rawls, J., EM., M. & SL., J. How the zebrafish gets its stripes. Dev Biol **240:**301–314 (2001).
34. Johnson, S. L., Africa, D., Horne, S. & Postlethwaite, J. H. Half-tetrad analysis in zebrafish: mapping the ros mutation and the centromere of linkage group I. Genetics **139:**1727–1735 (1995).
35. Parichy, D. M. & Turner, J. M. Temporal and cellular requirements for Fms signaling during zebrafish adult pigment pattern development. Development (Camb) **130:**817–833 (2003).
36. Parichy, D. M., Turner, J. M. & Parker, N. B. Essential role for puma in development of postembryonic neural crest-derived cell lineages in zebrafish. Dev Biol **256:**221–241 (2003).
37. Maderspacher, F. & Nusslein-Volhard, C. Formation of the adult pigment pattern in zebrafish requires leopard and obelix dependent cell interactions. Development (Camb) **130:**3447–3457 (2003).
38. Kirschbaum, F. Untersuchungen ueber das Farbmuster der Zebrabarbe Brachydanio rerio (Cyprinidae, Teleostei). Wilhelm Roux's Arch **177:**129–152 (1975).
39. Iwashita, M. et al. Pigment pattern in jaguar/obelix zebrafish is caused by a Kir7.1 mutation: implications for the regulation of melanosome movement. PLoS Genet **2:**e197 (2006).

40. Doring, F. et al. The epithelial inward rectifier channel Kir7.1 displays unusual K^+ permeation properties. J Neurosci **18:**8625–8636 (1998).
41. Nakamura, N., Suzuki, Y., Ikeda, Y., Notoya, M. & Hirose, S. Complex structure and regulation of expression of the rat gene for inward rectifier potassium channel Kir7.1. J Biol Chem **275:**28276–28284 (2000).
42. Kim, S. J. et al. Inwardly rectifying K^+ channels in the basolateral membrane of rat pancreatic acini. Pflugers Arch **441:**331–340 (2000).
43. Kusaka, S. et al. Functional Kir7.1 channels localized at the root of apical processes in rat retinal pigment epithelium. J Physiol **531:**27–36 (2001).
44. Shimura, M. et al. Expression and permeation properties of the K(+) channel Kir7.1 in the retinal pigment epithelium. J Physiol **531:**329–346 (2001).
45. Wischmeyer, E., Doring, F. & Karschin, A. Stable cation coordination at a single outer pore residue defines permeation properties in Kir channels. FEBS Lett **466:**115–120 (2000).
46. Suzuki, Y. et al. Expression of the K^+ channel Kir7.1 in the developing rat kidney: role in K^+ excretion. Kidney Int **63:**969–675 (2003).
47. Yasuda, K. et al. Expression and functional properties of unique inward rectifier K^+ channel Kir7.1 in the porcine iris and retinal pigment epithelium. Curr Eye Res **27:**279–287 (2003).
48. Jantzi, M. C. et al. Inward rectifying potassium channels facilitate cell-to-cell communication in hamster retractor muscle feed arteries. Am J Physiol Heart Circ Physiol **291:**H1319–H1328 (2006).
49. Watanabe, M. et al. Spot pattern of leopard *Danio* is caused by mutation in the zebrafish connexin41.8 gene. EMBO Rep **7:**893–897 (2006).
50. Iovine, M. K., Higgins, E. P., Hindes, A., Coblitz, B. & Johnson, S. L. Mutations in connexin43 (GJA1) perturb bone growth in zebrafish fins. Dev Biol **278:**208–219 (2005).
51. Meinhardt, H. & Gierer, A. Pattern formation by local self-activation and lateral inhibition [see comment]. Bioessays **22:**753–760 (2000).

Characterization and Application of Natural Light-Sensitive Proteins

Jens Looser and Georg Nagel

Introduction

Photoreceptors

Light is essential to life as the primary source of energy, but it is also sensed by many organisms to gain information about the environment. For this second purpose, several photoreceptors evolved in nature, among them the rhodopsins and the blue-light sensors. Rhodopsins are found not only in the animal kingdom but also in prokaryotes, Archaea, and green algae—so far, however, not in higher plants. The UV/blue-light-sensing photoreceptors for phototropism and photomorphogenesis in plants were found to be flavoproteins, of which homologues were found in all kingdoms. Although the signaling chains initiated by these photoreceptors in their natural cellular environment still have to be worked out, especially in plants, some of these photoreceptors could be successfully transplanted to other organisms to act as light-regulated molecular tools. Here we describe briefly the properties of and applications for type I rhodopsins and a photoactivated adenylyl cyclase (PAC), a flavoprotein from *Euglena gracilis*.

Type I Rhodopsins

Rhodopsins are proteins with seven transmembrane helices (7TM) that are light sensitive via the chromophor retinal (vitamin A). Several rhodopsins regulate, via a signaling chain, the activity of ion channels. These ion channels are sometimes called "light sensitive" although their light sensitivity is completely indirect. Animal rhodopsins belong to the large family of G protein-coupled receptors. All rhodopsins consist of a

J. Looser and G. Nagel
University Wuerzburg, JvSachs-Platz 2, 97082 Wuerzburg, Germany

S. Nakanishi et al. (eds.), *Systems Biology*,
DOI:10.1007/978-4-431-87704-2_5, © Springer 2009

protein moiety, the opsin, and a covalently linked (as Schiff base to a lysine in TM7) chromophor. The chromophor is 11-*cis* retinal in the ground state of animal rhodopsins (type II rhodopsins). Archaea, bacteria, fungi, and green algae contain similar (still 7TM) but different rhodopsins, which, however, have other functions. These type I, or microbial type, rhodopsins contain all-*trans* retinal in the ground state and are not G protein-coupled receptors but light-activated ion pumps, providing cells with a mechanism to convert light energy into chemical energy, or photoreceptors, enabling phototaxis of microbes. Bacteriorhodopsin (BR) and halorhodopsin (HR) use photons for active transport of H^+ to the outside and Cl^- to the cytoplasm, respectively, whereas the sensory rhodopsins I and II couple to their specific transducer (Schmies et al., 2001) to trigger a signaling chain to the flagellar motor.

Blue-Light Sensors

Photoreceptors for blue light (and UV-A) were first hypothesized to exist in plants where they are involved in phototropism (growth to or from the light source) and photomorphogenesis (light-dependent development of the plant). From their action spectrum it could be speculated that they are flavoproteins, i.e., that they contain a UV-A/blue-light-absorbing flavin derivative as chromophor. These derivatives are most commonly flavin mononucleotide (FMN) and flavin adenine dinucleotide (FAD), derivatives of riboflavin (vitamin B_2). Currently known light-sensing flavoproteins are divided in three groups: the FMN-using phototropins, and the FAD-using cryptochromes and BLUF proteins (BLUF, blue light using FAD, a domain on these photoreceptors). Their signaling pathways are different; however, they often involve kinase activity and autophosphorylation. PAC, a BLUF protein from *E. gracilis*, is the first and so far only known light-activated adenylyl cyclase.

Results and Discussion

Bacteriorhodopsin and Halorhodopsin

BR and HR were purified from their natural source and rigorously studied with respect to their photocycle and three-dimensional structure. For both light-driven ion pumps the structure, even of photocycle intermediates, is now known to be about 2 Å, and transport of H^+ (BR) or Cl^- (HR) through the protein is well understood. Although biochemical assays could show potential dependence of light-activated H^+ transport in BR (Michel and Oesterhelt, 1976), it was not possible to gain exact data about the voltage dependence of ion pumping, neither from the tiny Archaebacteria nor from purified (and reconstituted) protein. An alternative is heterologously expressed type I rhodopsins. The first functional heterologous expression of bacteriorhodopsin was demonstrated by Büldt and coworkers in *Schizosaccharomyces pombe* (Hildebrandt et al., 1989, 1993). As these fission

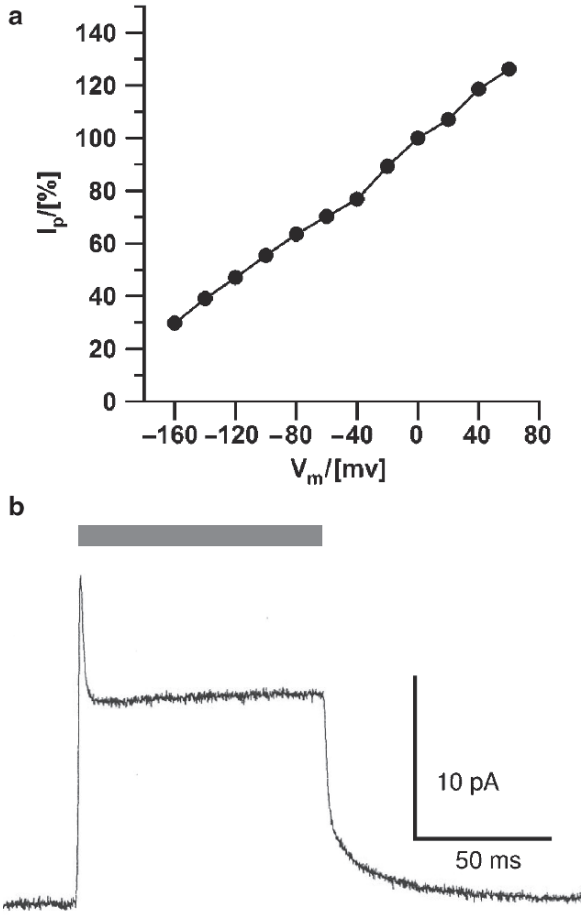

Fig. 1 Photocurrent caused by light-activated H^+ pumping of bacteriorhodopsin (BR), expressed in oocytes of *Xenopus laevis*. **a** Current–voltage relationship of stationary BR photocurrent in whole oocytes. Photocurrent is plotted as percentage of photocurrent at 0 mV. (Adapted from Nagel et al., 1998, with permission.) **b** BR photocurrent at 0 mV in giant excised inside-out membrane patch. Duration of light flash is indicated by *grey bar*

yeast cells are too small for electrophysiological analysis, we expressed BR in oocytes of *Xenopus laevis*, large cells (>1 mm diameter) that allow easy access for two-electrode voltage-clamp analysis (Nagel et al., 1995). Light-induced currents were strongly voltage dependent but always outward directed in the measured voltage range (from −160 mV to +60 mV), as expected for a H^+-exporting ion pump (Fig. 1a). The action spectrum of these photocurrents showed a maximum at 570 nm, well in accordance with the absorption maximum of 568 nm for BR (Nagel et al., 1995). For a better time resolution, we recorded from giant (20–30 µm diameter) excised inside-out oocyte membrane patches (Hilgemann, 1989; Nagel et al., 1992),

expressing BR. Upon illumination an outward current increased rapidly and desensitized to a stationary photocurrent (~70% at 0 mV) during continuous illumination, before returning to the dark current with two time constants of ~1 ms and ~15 ms (Fig. 1b). Obviously this light-activated current will hyperpolarize a non-voltage-clamped cell quickly and reversibly.

We then expressed the light-driven chloride pump halorhodopsin from *Natronomonas pharaonis* (NpHR) or from *Halobacterium salinarum* (HsHR) in oocytes. Photocurrents were again outward directed in the whole voltage range and strongly dependent on extracellular chloride (Fig. 2a). For NpHR, we deter-

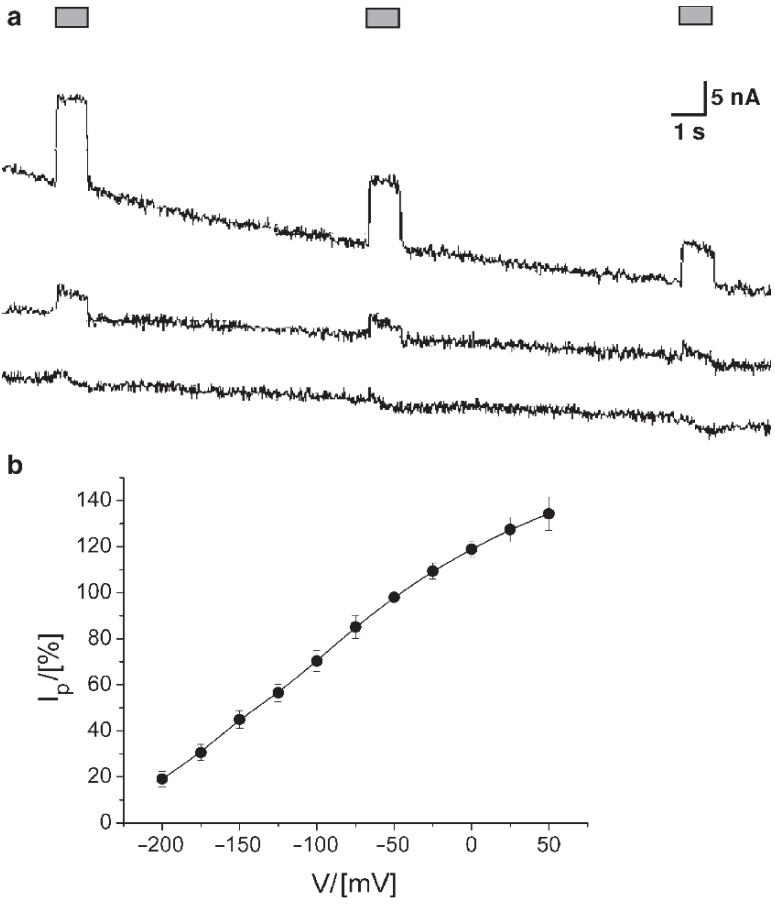

Fig. 2 Light-activated Cl^- pumping by halorhodopsin (NpHR). **a** Continuous recording from a whole oocyte during exchange of 121 mM Cl^- against D,L-aspartate (from *top to bottom*). Light flashes are indicated by *grey bars*. (From Zhang et al., 2007, with permission.) **b** Current–voltage relationship of stationary NpHR photocurrent in whole oocytes. Photocurrent is plotted as percentage of photocurrent at −50 mV. (From Zhang et al., 2007, with permission)

mined a $K_{0.5}$ of 16 mM Cl^-; chloride affinity was lower for HsHR ($K_{0.5}$ = 32 mM Cl^-) (Zhang et al., 2007). The current–voltage relationship of light-driven chloride pumping is quite similar to the I-V of BR pump currents (Fig. 2b), again allowing us to hyperpolarize a HR-expressing cell, simply by illumination. The action spectrum maximum for light-activated, hyperpolarizing current we determined to be 580 nm (Zhang et al., 2007). Our colleagues at Stanford University (Deisseroth and coworkers) and University of Frankfurt (Gottschalk and coworkers) then showed that NpHR is ideally suited to suppress action potentials in rat neurons or muscle contractions in live *Caenorhabditis elegans*, respectively, by illumination with amber light (Zhang et al., 2007).

Channelrhodopsins

Type I rhodopsins were suggested to trigger phototaxis in green algae (Foster et al., 1984) where photoreceptor currents occur with a delay of less than 30 µs after flash stimulation (Sineshchekov et al., 1990; Harz & Hegemann, 1991). This finding suggested an intimate link between photoreceptor and electrical conductance. It was not possible to clone these opsins, but recently overlapping partial cDNA sequences appeared in an EST database (Asamizu et al., 2000) of the green alga *Chlamydomonas reinhardtii* that encodes opsin-related proteins. The sequences were named channelopsins (Chop1 and Chop2) by us (Nagel et al., 2002). The core regions (about 300 N-terminal amino acid residues of more than 700) comprise seven hypothetical transmembrane segments with sequence similarity (15%–20%) to the archaeal sensory rhodopsins (SR), the ion transporters bacteriorhodopsin (BR) and halorhodopsin (HR) (Nagel et al., 2002; Sineshchekov et al., 2002; Suzuki et al., 2003). Sequence analysis suggests that K296 in Chop1 and K257 in Chop2 is the retinal-binding amino acid; 60% of the 22 amino acids that are in direct contact with the retinal in BR are identical (9 amino acids, aa) or conservatively exchanged (4 aa) in Chop1. Photocurrent measurements on *C. reinhardtii* cell populations, in which the ratio of Chop1 and its homologue Chop2 has been changed by an antisense approach, demonstrated that both functional channelrhodopsins, ChR1 and ChR2, contribute to the photoreceptor currents, but the mechanism remained obscure (Sineshchekov et al., 2002). Antibodies against Chop1 detected expression in the eye spot (Suzuki et al., 2003) where previously the tightly coupled photoreceptor–ion conductance complex was localized (Harz and Hegemann, 1991).

We expressed channelrhodopsin-1 and channelrhodopsin-2 in oocytes, either as full-length proteins of more than 700 amino acids or as the N-terminal half of 346 (ChR1-346) and 315 (ChR2-315) amino acids, comprising essentially the seven transmembrane, rhodopsin-typical helices (Nagel et al., 2002, 2003) (Fig. 3a). No differences in light-induced electrical currents were observed between full-length and shortened versions. Light-induced currents of channelrhodopsins were, however, quite different from light-induced currents of BR or HR as they showed a clear reversal potential (Fig. 3b,c). Therefore it could be concluded

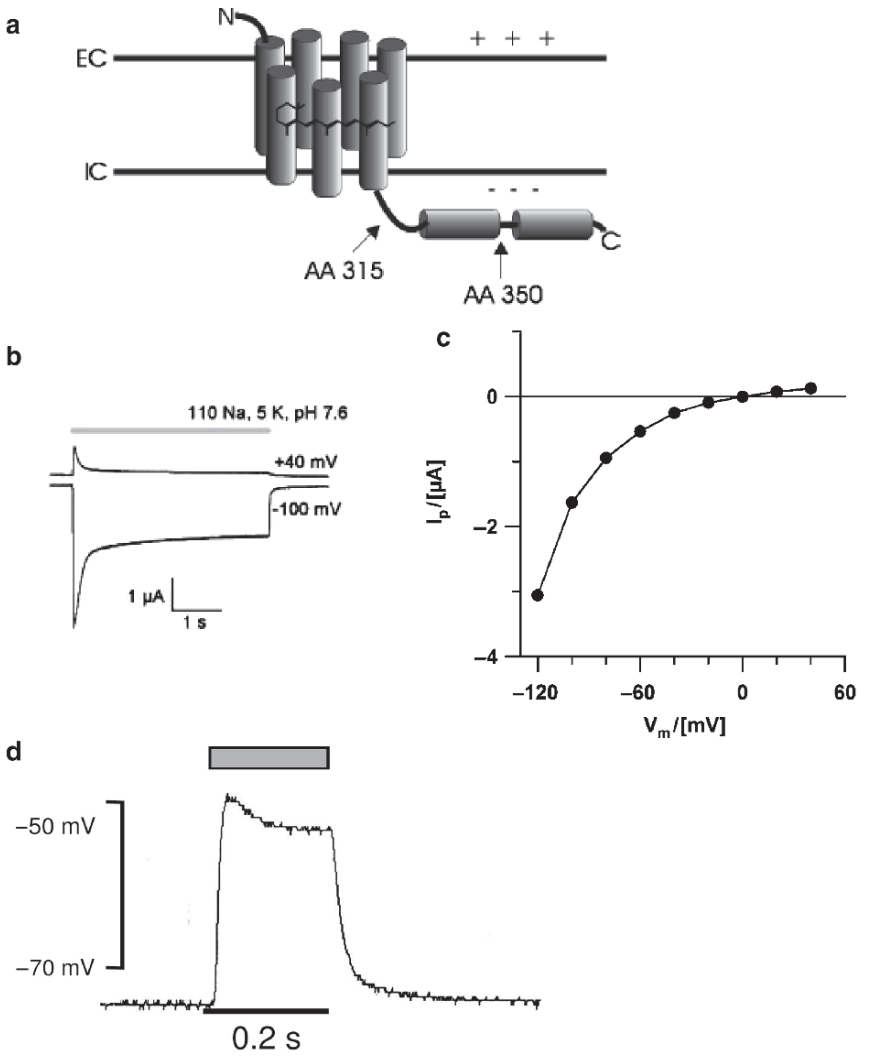

Fig. 3 Structure and function of channelrhodopsin-2 (ChR2). **a** Cartoon of the ChR2-structure comprising a 7TM segment, a rab-like domain (320–350), and a Gly-rich domain (350–737). *EC*, extracellular side; *IC*, intracellular side; *AA*, amino acids. (From Nagel et al., 2003, with permission.) **b** Light-activated current in whole oocyte, expressing ChR2-315 (first 315 amino acids of ChR2), at +40 mV and at −100 mV. Duration of light flash is indicated by *grey bar*. (From Nagel et al., 2003, with permission.) **c** Current–voltage relationship of stationary ChR2 photocurrent in whole oocytes in Na^+-containing Ringer's solution, as in **b** (pH 07.6). (Adapted from Nagel et al., 2003, with permission.) **d** Ability of ChR2 to depolarize cells by illumination with blue light. Current clamp measurement of an illuminated (*grey bar*) oocyte. (From Nagel et al., 2003, with permission)

that channelrhodopsins are directly light-gated ion channels. Further experiments with exchange of extracellular ions led to the conclusion that channelrhodopsin-1 (ChR1) is a light-gated proton channel (Nagel et al., 2002) and that channelrhodopsin-2 (ChR2) is a light-gated cation channel with permeabilities

for protons > Li^+ > Na^+ > K^+ > Ba^{2+} ≈ Ca^{2+} but no permeability to Mg^{2+} or to anions (Nagel et al., 2003). As expected from a proton channel, at neutral pH, light-activated currents of ChR1 were much smaller than of ChR2, although we recently noticed also some small cation permeability of ChR1 at pH 9, in accordance with a recent publication by Berthold et al. (2008). The I-V relation of light-induced ChR2 currents is inward rectifying with a reversal potential near 0 mV (Fig. 3c), clearly indicating that activation of ChR2 will lead to a collapse of membrane potential. Indeed, light activation of ChR2 in oocytes or mammalian cells leads to a drastic depolarization (Fig. 3d). The action spectrum of ChR2 photocurrents showed a maximum between 460 and 480 nm (Nagel et al., 2003), conveniently blue-shifted by more than 100 nm with respect to the maximum of the hyperpolarizing NpHR.

Expression of ChR2 in neurons made these light sensitive, allowing light flashes to induce action potentials at high frequency and with great reliability (Boyden et al., 2005). Expression of ChR2 in nerve or muscle cells of *C. elegans* provided a convenient way to depolarize these cells and achieve dramatic behavioral effects in live animals (Nagel et al., 2005).

Photoactivated Adenylyl Cyclases (PACα and PACβ)

Recently the photoreceptor for photophobic response of *Euglena gracilis* was shown to be a tetramer of two highly homologous BLUF flavoproteins, PACα and PACβ (Iseki et al., 2002). Watanabe and coworkers showed that the purified photoreceptor of ~400 kDa had some adenylyl cyclase activity in the dark, which was about 100 fold stimulated by illumination with UV-A or blue light. We expressed these proteins together and separately in oocytes and tested for cAMP generation with an immunoassay on oocyte extracts or by measuring electrical conductance of whole oocytes coexpressing PAC and cAMP-sensitive ion channels (Schröder-Lang et al., 2007). Surprisingly, PACα alone showed adenylyl cyclase activity, which was strongly increased by short flashes of blue light (Fig. 4a). Coexpression of PACα and PACβ made no difference to expression of PACα alone, but expression of PACβ alone showed much weaker activity, comparable to the activity of 100-fold less PACα. For very sensitive detection of cAMP we used CFTR, an anion channel that is activated by (oocyte-endogenous) cAMP-dependent protein kinase (PKA, $K_{0.5}^{cAMP} \approx 100$ nM). For fast detection of cAMP, however, we coexpressed PACα with the directly cAMP-gated cation channel CNGA2-C460W/E583M ($K_{0.5}^{cAMP} \approx 1$ μM) (Fig. 4b). As can be seen from the rapid change of electrical current, PACα responds very rapidly to light with cAMP production ($\tau < \approx 10$ ms) upon switching on the light and also must decrease its activity very rapidly in the dark, as deduced from experiments with light flashes of different duration (Schröder-Lang et al., 2007). PACα and PACβ are composed of two BLUF domains (F1, F2), binding FAD, and two cyclase domains (C1, C2), which are known to dimerize in homologous cyclases. By mutation of conserved residues in C1 or C2, we were able to completely knock down the activity of PACα. When we then coexpressed

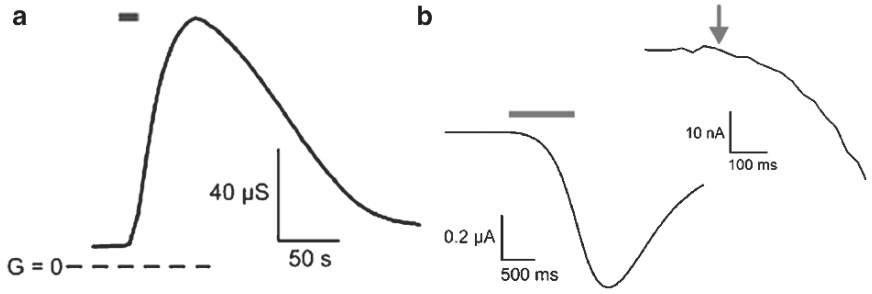

Fig. 4 Fast and reversible light-induced [cAMP] increase in oocytes via PACα, measured by cAMP-sensitive ion channels. **a** Light-induced increase of CFTR-mediated conductance by 20 s illumination (*grey bar*) of coexpressed PACα. (Adapted from Schröder-Lang et al., 2007, with permission.) **b** Light-induced (1 s; *grey bar*) current increase of CNGA2 mutant channel, coexpressed with PACα. Onset is very fast, as shown in *inset* (*arrow* indicates start of illumination). (Adapted from Schröder-Lang et al., 2007, with permission)

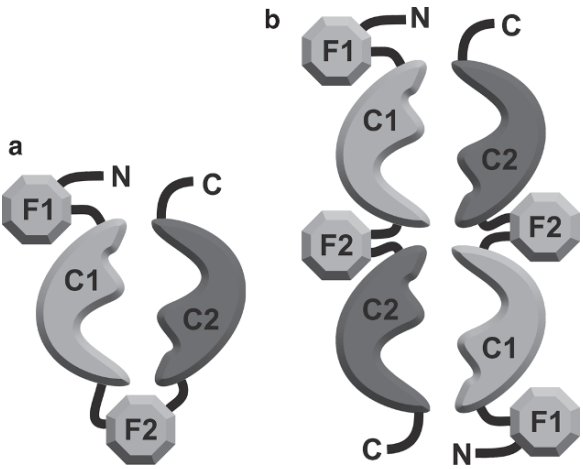

Fig. 5 Models of domain arrangement in PACα. **a** This model of a PACα monomer could explain construction of a cyclase from two C domains. **b** Dimer model of PACα, as suggested by a mixture of lethal C1 and C2 mutants that showed restored cyclase activity, whereas each mutant alone had no activity

nonfunctional C1 and C2 mutants of PACα with CFTR, we partially restored dark- and light-induced activity of PACα, which strongly suggests that PACα dimerizes to build functional intermolecular C1–C2 domains (Fig. 5).

Acknowledgments This work was supported by the German Research Association (DFG) to G.N. (NA407/6).

References

Asamizu E, et al. (2000) Generation of expressed sequence tags from low-CO_2 and high-CO_2 adapted cells of *Chlamydomonas reinhardtii*. DNA Res **7:**305–7.

Berthold P, Tsunoda SP, Ernst OP, Mages W, Gradmann D, Hegemann P (2008) Channelrhodopsin-1 initiates phototaxis and photophobic responses in *Chlamydomonas* by immediate light-induced depolarization. Plant Cell **20:**1665–77.

Boyden ES, Zhang F, Bamberg E, Nagel G, Deisseroth K (2005) Millisecond-timescale, genetically targeted optical control of neural activity. Nat Neurosci **8(9):**1263–8.

Foster KW, Saranak J, Patel N, Zarilli G, Okabe M, Kline T, Nakanishi K (1984) A rhodopsin is the functional photoreceptor for phototaxis in the unicellular eukaryote *Chlamydomonas*. Nature (Lond) **311:**756–9.

Harz H, Hegemann P (1991) Rhodopsin-regulated calcium currents in *Chlamydomonas*. Nature (Lond) **351:**489–91.

Hildebrandt V, Ramezani-Rad M, Swida U, Wrede P, Grzesiek S, Primke M, Büldt G (1989) Genetic transfer of the pigment bacteriorhodopsin into the eukaryote *Schizosaccharomyces pombe*. FEBS Lett **243:**137–40.

Hildebrandt V, Fendler K, Heberle J, Hoffmann A, Bamberg E, Büldt G (1993) Bacteriorhodopsin expressed in *Schizosaccharomyces pombe* pumps protons through the plasma membrane. Proc Natl Acad Sci U S A **90:**3578–82.

Hilgemann DW (1989) Giant excised cardiac sarcolemmal membrane patches: sodium and sodium-calcium exchange currents. Pflügers Arch. 415(2):247-9.

Holland EM, Braun FJ, Nonnengässer C, Harz H, Hegemann P (1996) The nature of rhodopsin-triggered photocurrents in *Chlamydomonas*. I. Kinetics and influence of divalent ions. Biophys J **70:**924–31.

Iseki M, Matsunaga S, Murakami A, Ohno K, Shiga K, Yoshida K, Sugai M, Takahashi T, Hori T, Watanabe M (2002) A blue-light-activated adenylyl cyclase mediates photoavoidance in *Euglena gracilis*. Nature (Lond) **415(6875):**1047–51.

Michel H, Oesterhelt D (1976) Light-induced changes of the pH gradient and the membrane potential in *H. halobium*. FEBS Lett **65:**175–8.

Nagel G, Hwang T-C, Nastiuk KL, Nairn AC, Gadsby DC (1992) The protein kinase A-regulated cardiac Cl^- channel resembles the cystic fibrosis transmembrane conductance regulator. Nature (Lond) **360:**81–4.

Nagel G, Möckel B, Büldt G, Bamberg E (1995) Functional expression of bacteriorhodopsin in oocytes allows direct measurement of voltage dependence of light induced H^+ pumping. FEBS Lett **377:**263–6.

Nagel G, Kelety B, Möckel B, Büldt G, Bamberg E (1998) Voltage dependence of proton pumping by bacteriorhodopsin is regulated by the voltage-sensitive ratio of M1 to M2. Biophys J **74:**403–12.

Nagel G, Ollig D, Fuhrmann M, Kateriya S, Musti AM, Bamberg E, Hegemann P (2002) Channelrhodopsin-1: a light-gated proton channel in green algae. Science **296:**2395–8.

Nagel G, Szellas T, Huhn W, Kateriya S, Adeishvili N, Berthold P, Ollig D, Hegemann P, Bamberg E (2003) Channelrhodopsin-2, a directly light-gated cation-selective membrane channel. Proc Natl Acad Sci U S A **100:**13940–5.

Nagel G, Brauner M, Liewald JF, Adeishvili N, Bamberg E, Gottschalk A (2005) Light-activation of Channelrhodopsin-2 in excitable cells of *Caenorhabditis elegans* triggers rapid behavioral responses. Curr Biol **15(24):**2279–84.

Schmies G, Engelhard M, Wood PG, Nagel G, Bamberg E (2001) Electrophysiological characterization of specific interactions between bacterial sensory rhodopsins and their transducers. Proc Natl Acad Sci U S A **98:**1555–9.

Schröder-Lang S, Schwärzel M, Seifert R, Strünker T, Kateriya S, Looser J, Watanabe M, Kaupp UB, Hegemann P, Nagel G (2007) Fast manipulation of cellular cAMP level by light in vivo. Nat Methods **4:**39–42.

Sineshchekov OA, Litvin FF, Keszthelyi L (1990) Two components of photoreceptor potential in phototaxis of the flagellated green alga *Haematococcus pluvialis*. Biophys J **57:**33–9.

Sineshchekov OA, Jung K-H, Spudich JL (2002) From the cover: Two rhodopsins mediate phototaxis to low- and high-intensity light in *Chlamydomonas reinhardtii*. Proc Natl Acad Sci U S A **99:**8689–4.

Suzuki T, Yamasaki K, Fujita S, Oda K, Iseki M, Yoshida K, Watanabe M, Daiyasu H, Toh H, Asamizu E, Tabata S, Miura K, Fukuzawa H, Nakamura S, Takahashi T (2003) Archaeal-type rhodopsins in *Chlamydomonas*: model structure and intracellular localization. Biochem Biophys Res Commun **301:**711–7.

Zhang F, Wang L-P, Brauner M, Liewald JF, Kay K, Watzke N, Wood PG, Bamberg E, Nagel G, Gottschalk A, Deisseroth K (2007) Multimodal fast optical interrogation of neural circuits. Nature (Lond) **446:**633–9.

Systems Biology of Mammalian Circadian Clocks

Hiroki R. Ueda

Introduction: Systems Biology as "Biology After Identification"

Recent large-scale efforts in genome sequencing, expression profiling, and functional screening have produced an embarrassment of riches for life sciences researchers, and biological data can now be accessed in quantities that are orders of magnitude greater than were available even a few years ago. The growing need for interpretation of data sets, as well as the accelerating demand for their integration to a higher-level understanding of life, has set the stage for the advent of systems biology [1,2], in which biological processes and phenomena are approached as complex and dynamic systems. Systems biology is a natural extension of molecular biology and can be defined as "biology after identification of key gene(s)." We see systems biological research as a multistage process, beginning with the comprehensive identification and quantitative analysis of individual system components and their networked interactions, and leading to the ability to control existing systems toward the desired state and design new ones based on an understanding of structure and underlying dynamical principles (Fig. 1).

The Mammalian Circadian Clock as a Model System

We have taken the mammalian circadian clock as an initial model system that exhibits system-level dynamical and structural properties to develop research strategies and technologies for the studies of complex and dynamic biological systems. The mammalian circadian clock consists of complexly integrated feed-back and feed-forward loops [3] and also exhibits well-defined dynamical properties [4],

H.R. Ueda
Laboratory for Systems Biology and Functional Genomics Unit, Center for Developmental Biology, RIKEN, 2-2-3 Minatojima-minamimachi, Chuo-ku, Kobe, Hyogo 650-0047, Japan

S. Nakanishi et al. (eds.), *Systems Biology*,
DOI:10.1007/978-4-431-87704-2_6, © Springer 2009

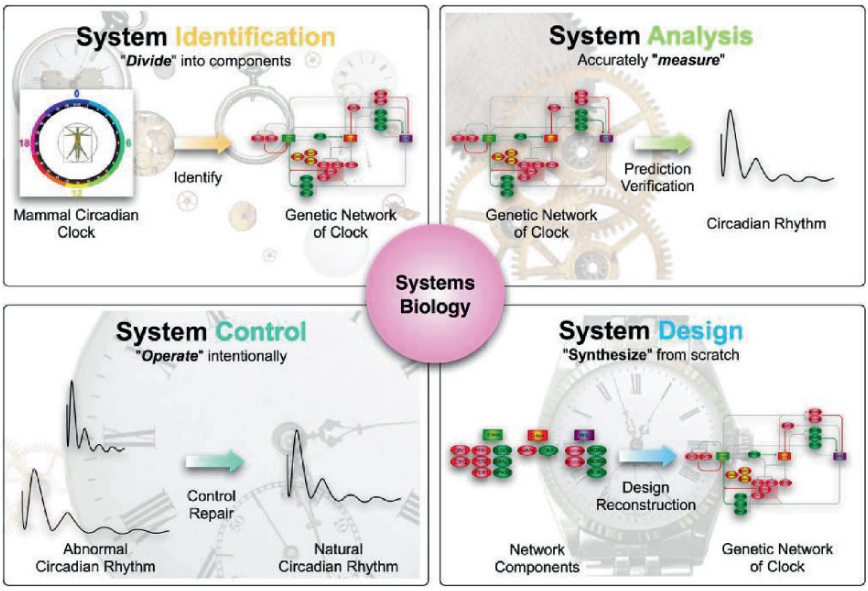

Fig. 1 Systems biology. Systems biological research starts with comprehensive identification (*upper left panel*). In this step, individual system components and their networked interactions are comprehensively identified. In the second step, to derive the design principle of a target system, the behavior of the system is predicted and validated through an accurate measurement with perturbations (*upper right panel*). An understanding of the design principle of the system is essential to derive the method of controlling the system toward the desired state (*lower left panel*). Finally, the level of understanding is confirmed by reconstruction of the system (*lower right panel*)

including (1) endogenous oscillations of an approximately 24-h period; (2) entrainment to external environmental changes (temperature and light cycle); (3) temperature compensation over a wide range of temperature; and (4) synchronization of multiple cellular clocks despite the inevitable molecular noise. All these dynamic properties would be difficult to elucidate without utilizing such system-level approaches. In addition to its advantages as a basic model system for systems biological research, the function of the circadian clock is intimately involved in the control of metabolic and physiological processes [3,5], and its dysregulation is associated with the onset and development of numerous human diseases, including sleep disorders, depression, and dementia (Fig. 2). An improved understanding at the system level promises to provide biomedical and clinical investigators with a powerful new arsenal for attacking these conditions. In the following sections, we describe in detail systems biology strategies and technologies (especially, system identification and system design) in addition to their application to the specific question of mammalian circadian clocks.

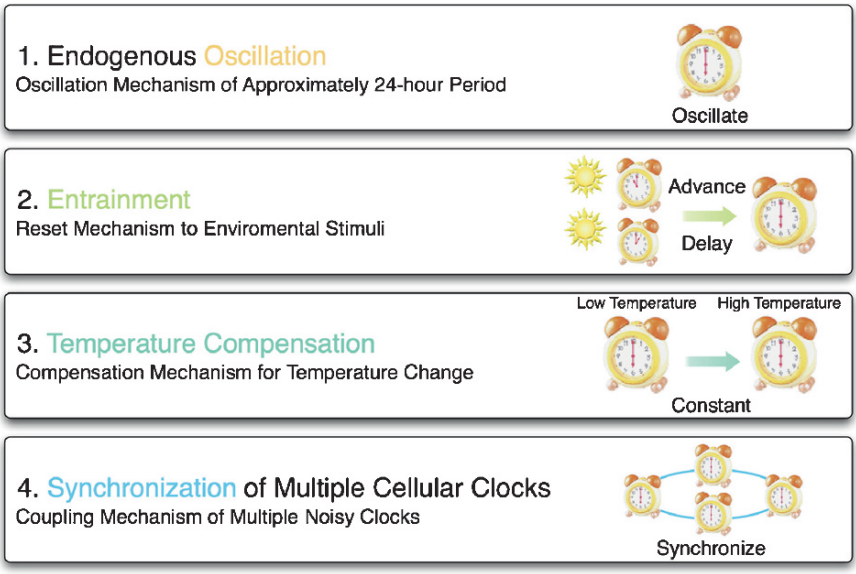

Fig. 2 Dynamic properties of mammalian circadian clocks. Although circadian clocks appear to be cell autonomous oscillators (**1**), the clock can synchronize with the environment (**2**). Period length is kept constant irrespective of temperature (**3**). In a multicell tissue such as the suprachiasmatic nucleus (SCN), the clocks synchronize with each other (**4**)

System Identification of Clocks

Following the completion of genome projects for species such as mouse and human, genome-wide resources such as siRNA or cDNA libraries have undergone considerable expansion. Development of high-throughput technologies also assists in the efficient use of these resources. These genome-wide resources and technologies as well as genome-associated information currently allow us to comprehensively identify system components of interest (system identification).

Circadian clocks of multicellular organisms consist of complexly integrated regulatory loops with positive or negative regulators known as clock genes [6–19]. The transcriptional regulation network of these genes forms a circadian clock oscillator, which is known to control output genes and affect physiological and metabolic processes [3,5]. Although some transcriptional regulations of identified clock genes have been the subject of previous studies, a system-level understanding of circadian clocks remains to be elucidated. In this section on identification of clocks, we provide results of our system identification of mammalian circadian clocks [20,21].

The mammalian circadian master clock is primarily located in the suprachiasmatic nucleus (SCN) [3]. Transcript analyses have indicated that circadian clocks are not restricted to the SCN but are found in several tissues [22], including liver

and cultured fibroblast cells such as Rat-1 [23,24] or NIH3T3 [25] cells. The mechanisms underlying circadian rhythms are also known to be conserved across species [4]. At the basic core of the clock lies a transcriptional/translational feedback loop [26–28], whose primary components are known as "clock genes" [6–19]. For example, in the mouse system, transcription factors CLOCK and BMAL1 proteins dimerize and directly and indirectly activate transcription of the *Per* and *Cry* genes through E-box elements (5'-CACGTG-3') [26,27]. The PER and CRY proteins accumulate in the cytosol, and are then translocated following phosphorylation into the nucleus, where they inhibit the activity of CLOCK and BMAL1 [3]. The turnover of the inhibitory PER and CRY proteins leads to a new cycle of activation by CLOCK and BMAL1 via E-box elements. Despite the reporting of many transcriptional regulations of each gene, however, an overview of circadian clock core network remains to be put forward.

Complicated networks cannot be elucidated without access to both (1) comprehensive identification of network circuits and (2) accurate measurement of system dynamics. In a previous attempt to comprehensively identify the circadian clock core network, we first quantitatively and comprehensively measured genome-wide gene expression using a high-density oligonucleotide probe array [29] and identified genes showing circadian oscillation with characteristic expression patterns through biostatistics (Fig. 3). The second step involved comprehensively determining the transcription start sites [30] (TSSs) and conserved noncoding regions to construct the genome-wide promoter/enhancer database. Using these data, we predicted that there was a relationship between expression patterns of identified genes and DNA regulatory elements on their promoter/enhancer regions. We found clock-controlled elements (CCEs), E-boxes (5'-CACGTG-3') [31]/E'-boxes (5'-CACGTT-3') [21,32], D-boxes (5'-TTATG[C/T]AA-3') [33], or RREs (5'-[A/T]A[A/T]NT[A/G]GGTCA-3') [34] are distributed throughout the oscillatory genes.

To determine the role of these elements in the circadian clock, we utilized an cell culture system with which we can monitor circadian rhythms in transcriptional dynamics using a destabilized luciferase (d*Luc*) reporter driven by clock-controlled

Fig. 3 (continued) peak time. Colors in descending order from *red* to *black* to *green* represent the normalized data. From the obtained data, we identified a set of genes rhythmically expressed under both LD and DD. We classified 101 genes in the SCN and 393 genes in the liver as "significantly rhythmic under both LD and DD." **c** Temporal expression profiles of transcription factors in the SCN (*upper panel*) and liver (*lower panel*) under constant darkness (DD) conditions. Relative mRNA levels under DD condition of the indicated genes were measured with a quantitative polymerase chain reaction (QPCR) assay, in which *GAPDH* expression was used as an internal control. Data were normalized so that the average copy number (QPCR) over a 12-point time course is 1.0. Circadian expression of transcription factors having functional and evolutionary conserved E-boxes (*Dbp*, *Dec1*, and *Dec2*), both of E-boxes/E'-boxes and D-boxes (*Per1*, *Per2*, *RevErbA*α, and *RevErbA*β), D-boxes (*Per3*, *Ror*α, and *Ror*β), RREs (*Bmal1*, *Clock*, *Npas2*, and *E4bp4*), both of E-boxes/E'-boxes and RREs (*Cry1* and *Ror*γ), on their noncoding regions. *Clock* and *Ror*γ were constitutively expressed in the SCN

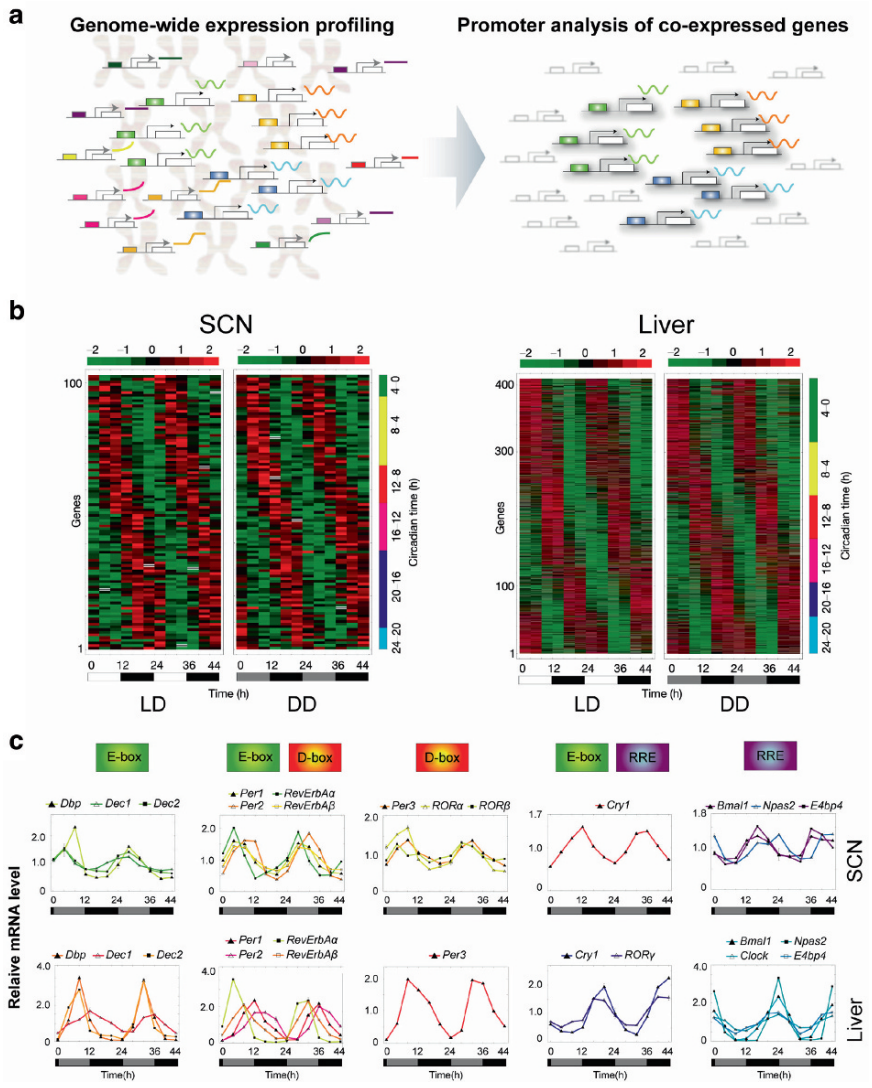

Fig. 3 **a** Strategy for identification of clock-controlled elements (CCEs). Gene expression information was obtained by performing comprehensive expression profiling (*left panel*). Through statistical analysis, genes with a special characteristic pattern of expression (circadian oscillation) were selected (*right panel*; oscillatory genes are indicated by their *color*). DNA regulatory elements for specific issue (i.e., expression timing) were predicted by combining expression pattern information and transcriptional regulatory elements information from promoter regions. **b** Genome-wide expression profiles in mouse central (*SCN; left panel*) and peripheral (*liver; right panel)* clocks. Total RNA was extracted every 4 h during light/dark cycles (LD) or constant darkness (DD) over 2 days and used to determine genome-wide gene expression profiles with the Affymetrix mouse high-density oligonucleotide probe array (GeneChip). Data were normalized so that the average signal intensity and standard deviation over 12-point time courses were 0.0 and 1.0, respectively. *Columns* represent time points, and *rows* represent genes that were organized by

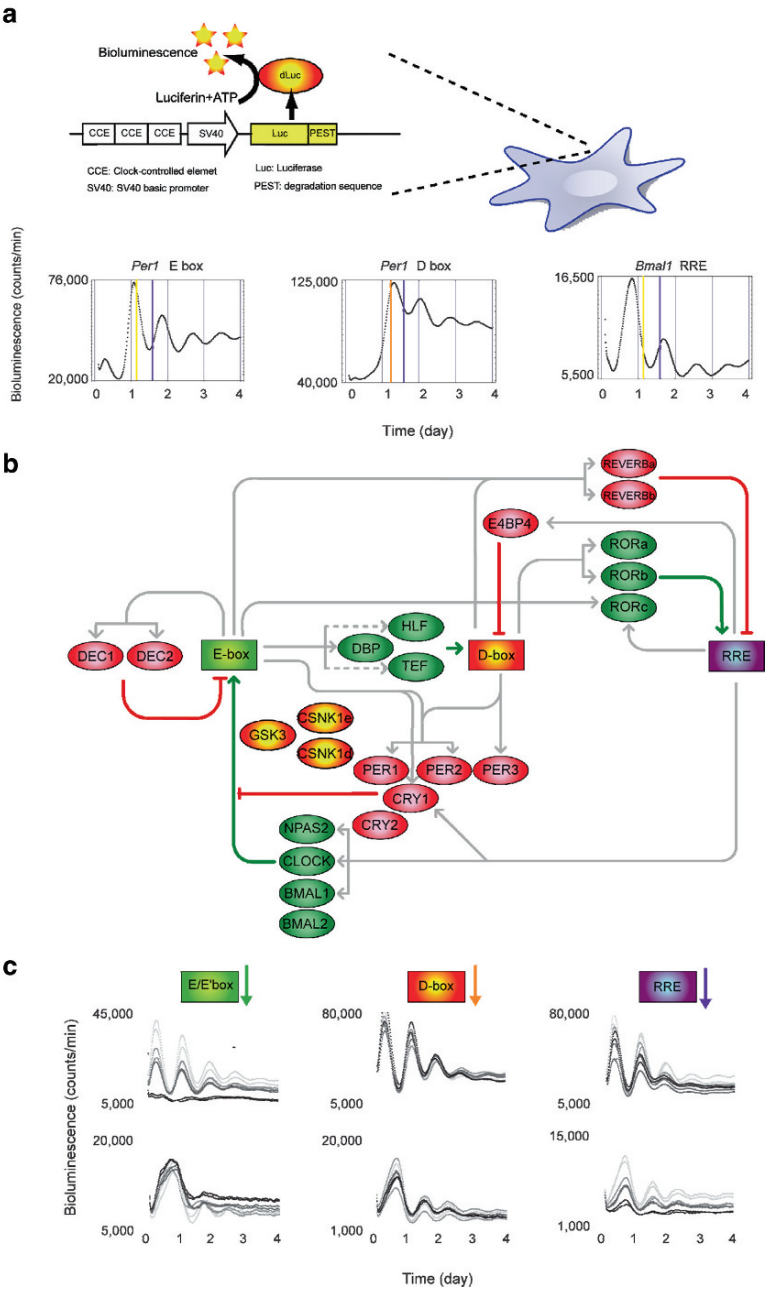

Fig. 4 **a** Schematic overview of experiment. Cultured mammalian cell (Rat-1) was transfected with d*Luc* under the regulation of CCE and SV40 basic promoter. The circadian change of the bioluminescence was monitored by a PMT detector over several days (*upper panel*). Representative circadian rhythms of bioluminescence from wild-type CCE fused to the SV40 basic promoter driving a d*Luc* reporter. The circadian bioluminescence phase from the *Per2* promoter and that of

promoters (Fig. 4A). In this cell culture system, named the "*in cellulo* cycling assay," we transiently transfected reporter constructs into cultured Rat-1 cells, stimulated with dexamethasone, and measured their bioluminescence. Dexamethasone was administrated to induce macroscopic circadian oscillations in the cultured cells. Through the genome-wide searching described above, we found CCEs on 16 clock/clock-controlled genes promoter/enhancers. Then, using the *in cellulo* cycling assay system, we were able to reveal that functionally and evolutionary conserved E/E'-boxes are located on noncoding regions of nine genes (*Per1*, *Per2*, *Cry1*, *Dbp*, *Rorγ*, *RevErbAα/Nr1d1*, *RevErbAβ/Nr1d2*, *Dec1/Bhlhb2*, and *Dec2/Bhlhb3*), D-boxes on those of seven genes (*Per1*, *Per2*, *Per3*, *RevErbAα*, *RevErbAβ*, *Rorα*, and *Rorβ*), and RREs on those of six genes (*Bmal1/Arntl*, *Clock*, *Npas2*, *Cry1*, *E4bp4/Nfil3*, and *Rorγ*}. Based on this functional and conserved transcriptional regulatory mechanism, we succeeded in drawing transcriptional circuits underlying mammalian circadian rhythms (Fig. 4B) [21].

Our analysis further suggested that regulation of E/E'-boxes is the topological vulnerability point in mammalian circadian clocks. We functionally verified this concept using *in cellulo* cycling assay systems (Fig. 4C). Overexpression of repressors of E/E'-box regulation (CRY1 [27]), RRE regulation (REVERBAα [14,20]), or D-box regulation (E4BP4 [16]) affected circadian rhythmicity in *Per2* or *BMAL1* promoter activity. The effects were different, however, between each repressor, and the severest effect was observed when the E/E'-box was attacked. Such different modes of effect cannot be explained by mere quantitative differences in the strength of these three repressors, indicating that there is some qualitative difference between E/E'-box, D-box, and RRE regulation in circadian rhythmicity [21].

Design of Clocks

We herein describe in detail the final step of systems biology, system design, reconstruction of the system using a hypothesized design principle that has been revealed through the efforts of a combination strategy of system identification, system analysis, and system control for validating the sufficiency of the system components. Three specific features of circadian oscillatory wave are the period length, the amplitude, and the peak phase. In this section, we introduce our recent study on the design principles on phase determination using an in vitro cell culture system as the "physical simulator" [35].

Fig. 4 (continued) the *Bmal1* promoter are indicated by *yellow* and *purple* lines, respectively (*bottom panels*). **b** Schematic representation of transcriptional network of mammalian circadian clock. Genes and CCEs are depicted as *ellipsoids* and *rectangles*, respectively. Transcriptional/translational activation and repression are depicted as *gray*, *green*, and *red* lines, respectively. **c** Effect of repression on each CCE. The *E/E'-boxes*, *D box*, and *RRE* are repressed by overproduction of CRY1, E4BP4, and REVERBAα, respectively. The consequences of those repressions were monitored by *Per2*-dLuc (*upper panel*) and *Bmal*1-dLuc (*lower panel*). d*Luc*, destabilized luciferase; CCE, clock-controlled elements; PMT, photomultiplier tube

Design of Circadian Circuits: Phase Determination

Although the network structure composed by clock genes and clock-controlled DNA elements (CCEs; Fig. 4) has been described comprehensively, the dynamic principles governing this transcriptional circuit remain elusive. One of the key issues concerning the logic of the mammalian circadian clock is how the circadian oscillating genes expression peaks ("phases") are determined. In attempting to elucidate this issue, we have started a project for understanding the molecular logic of phase-controlling system(s). For this purpose, we have extended our in vitro cycling assay system to the "physical simulator," with which we can implement artificial circuits of interest. We used this system to prove the sufficiency of the components we predict in natural circadian phase-controlling mechanisms.

Mammalian circadian clocks are composed of complexly integrated transcriptional regulatory loops. To reach a system-level understanding of the circadian clock controlling system, we focused on the three main transcriptional regulation elements (CCEs), E/E'-box, D-box, and RRE (Fig. 4). We first focused on the daytime transcriptional regulation mediated via the D-box. The transcriptional activator DBP activates genes expression via the D-box, whereas the transcriptional repressor E4BP4 represses expression (Fig. 5A, upper panel). *Dbp* is regulated by the E-box,

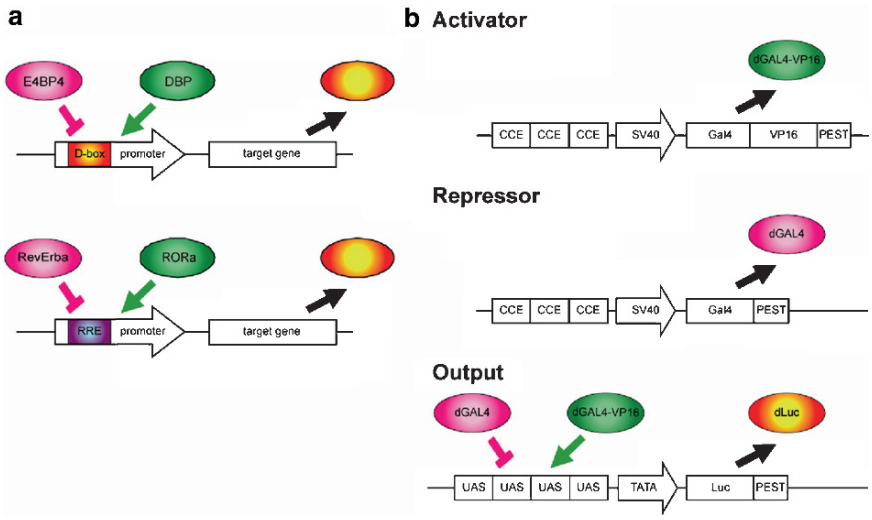

Fig. 5 Synthetic transcriptional circuit of mammalian circadian clocks. **a** Hypothetical models of daytime and nighttime output regulation. In natural circuits, *Dbp* and *E4bp4* control the expression via the D-box. Similarly, *RevErbA*α and *Ror*α participate in the regulation via the RRE. **b** The artificial transcriptional system. dGAL4-VP16 and dGAL4 were used as the activator and repressor. These transcriptional factors were expressed under the control of three tandem repeats of a CCE (E'-box of *Per2*, D-box of *Per3*, or RRE of *Bmal1*). The artificial activator and repressor competitively bind the four tandem repeats of UAS in the artificial promoter to regulate the output reporter gene *dLuc*. For observation of the dynamic behavior of this artificial circuit, NIH3T3 cells were transiently transfected with plasmids harboring the activator, repressor, or reporter, and the reporter activity was monitored under a real-time bioluminescence measuring system

the morning control element, while *E4bp4* is under the regulation of the RRE, the nighttime control element. On the basis of this transcriptional circuit information, we hypothesized that a morning activator and a nighttime repressor can determine the daytime transcriptional output mediated through the D-box. Similarly, RRE activators (e.g., *Ror*α) are expressed during the daytime under the control of the D-box, and the RRE repressors (e.g., *RevErbA*α) seem strongly influenced by the morning element (E'-box; Fig. 5A, lower panel). We have therefore also been able to make the simple hypothesis that a daytime activator and a morning repressor can specify the nighttime transcriptional output mediated through the RRE. To test these hypotheses, we adopted a synthetic approach to physically simulate an identified structure and observed the resulting dynamics using artificial transcriptional circuits.

To design and implement artificial transcriptional circuits in mouse NIH3T3 cells, which have a self-oscillating circadian clock, we developed an in vitro cycling assay system composed by the following three components: an artificial activator (a destabilized GAL4-VP16 fusion protein: dGAL4-VP16), an artificial repressor (a destabilized GAL4 protein: dGAL4), and an output reporter [a destabilized *luciferase* (*dLuc*) gene driven by a minimal TATA box fused with four tandem repeats of UAS, the GAL4-binding sequence] (Fig. 5B). In this system, the input from artificial activator and repressor competitively regulates the output and reporter gene expression through the UAS (Fig. 5B, lower panel), and the dynamics of the output could be monitored through the light intensity of the expressed dLuc protein under a real-time bioluminescence measuring system. As the artificial activator and repressor are driven by the SV40 basic promoter fused with three tandem repeats of CCEs, we could control the expression timing of these artificial regulators via the morning (E'-box), daytime (D-box), or nighttime (RRE) elements. We reasoned that if (and only if) the phases of the transcriptional activator(s) and repressor(s) are acceptable determinants of the phase of the downstream transcriptional output, then it should be possible to generate the natural phases using synthetic transcriptional regulators and promoters. If this were proved to be so, the findings would prove to be very significant, as transcription factors are regulated by various posttranscriptional mechanisms, including translation, phosphorylation, ubiquitination, sumoylation, and nuclear transportation, which are thought to contribute, at least in part, to the phase decision of the downstream transcriptional outputs.

Using the in vitro cycling assay system as a physical simulator, we first tested our hypothesis for daytime output by examining the dynamic behavior of the transcriptional output generated from the competition of an artificial morning activator controlled via E'-box and a nighttime repressor controlled via RRE. The phases of the activator and repressor in this experiment were detected at circadian time (CT) 4.0 $\pm$ 0.29 ($n = 2$), and CT17.1 $\pm$ 0.37 ($n = 2$). The transcriptional output driven by these regulators exhibited circadian oscillation with a phase at CT7.7 $\pm$ 0.85 ($n = 2$), which is very close ($\leq$1.0 h) to the corresponding natural daytime (D-box) phase, CT8.7 $\pm$ 1.13 (Fig. 6A). These results suggest that morning activation and nighttime repression are sufficient to determine the daytime transcriptional output. Importantly, we could not observe high-amplitude circadian oscillation by expressing the morning activator or nighttime repressor alone. From these, we concluded that both morning activation and nighttime repression are necessary for daytime output.

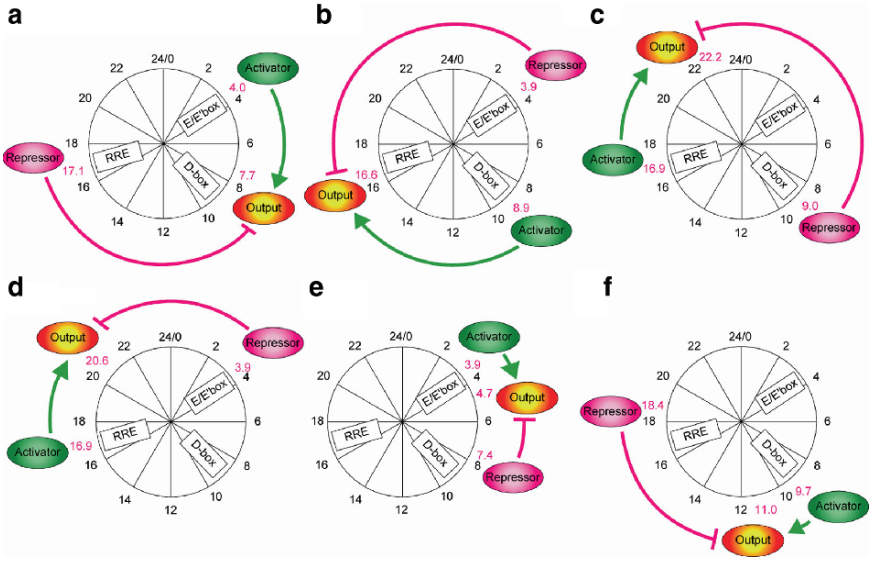

Fig. 6 Promoter activities of an activator, repressor, and output in different artificial transcriptional circuits: morning activator under E'-box control and nighttime repressor under RRE control (**a**); daytime activator under D-box control and morning repressor under E'-box control (**b**); nighttime activator under RRE control and daytime repressor under D-box control (**c**); nighttime activator and morning repressor (**d**); morning activator and daytime repressor (**e**); and daytime activator and nighttime repressor (**f**). The schemes summarize the representative promoter activities of each artificial circuit monitored by bioluminescence from NIH3T3 cells, where an activator, repressor, and output phases are indicated with their peak time indicated by circadian time (*red numbers*)

We next tested the hypothesis for nighttime output by examining another artificial circuit consisting of an artificial daytime activator under D-box control and a morning repressor under E'-box control. The phases of a transcriptional activator and repressor in this experiment were at CT8.9 ± 0.28 (n = 2) and CT3.9 ± 0.13 (n = 2). The transcriptional output driven by the regulators exhibited circadian oscillation with its phase at CT16.6 ± 1.04 (n = 2), which is very close (≤1.0 h) to the corresponding natural nighttime phase (CT17.0 ± 0.81) (Fig. 6B). These results also suggest that daytime activation and morning repression are necessary and sufficient to generate the circadian nighttime output, implying that the input phases of transcriptional regulators can determine the phases of transcriptional output. These findings led us to reason that various combinations of transcriptional regulators with CCEs for the three basic circadian phases (morning, daytime, and nighttime) might not only generate the basic phases but also other phases. Indeed, we succeeded in generating various phases though simple combinations of the transcriptional regulators of the three basic circadian phases (Fig. 6C–F).

Importantly, even if the phase of the activator was not changed, the advanced or delayed phase of the repressor led to a corresponding change in the phase of transcriptional output (Fig. 6). Similarly, a change in the activator phase also led to a

corresponding alteration in the output phase (Fig. 6). We can deduce from these findings that mammalian circadian clocks can start from three basic phases to the final, practically continuous, phases through transcriptional cascades, which have been observed in vivo in the central and peripheral clock tissues (e.g., SCN and liver). Moreover, this concept is supported by our recent observations that many transcription factors are rhythmically expressed at various phases in the liver (Fig. 3) and that some seem to be under the direct control of the circadian clock via CCEs. In addition, our in vitro findings lead to the concept that the natural transcription activator(s) and repressor(s) that bind the similar DNA elements are expected to generate additional output phases because they are expressed in different in vivo phases.

In these experiments, we showed that the transcriptional regulation of upstream transcription factors can determine the phase of the downstream output. This study presents a synthetic approach to the "proof-by-synthesis" of transcriptional logic, which provides us with a new strategy, not only to investigate the requirements for identified components and/or their interactions but also to reveal as-yet unidentified components or interactions. These results reveal design principles for elucidating continuous transcriptional outputs observed in vivo and for the logical design of artificial promoters working at novel phases. Logical synthesis of artificial circuits with defined structure and observation of their dynamics provide an alternative strategy applicable for the investigation of complex and dynamic biological systems such as mammalian circadian clocks.

Conclusion

After identification of key clock genes, there are increasing demands for higher-order understanding of design principles in mammalian circadian clocks. In this chapter, we introduced systems biological approaches, beginning with comprehensive identification (System Identification) and quantitative analysis (System Analysis) of individual clock components and their networked interactions, and leading to the ability to control existing systems toward the desired state (System Control) and to design new ones based on an understanding of structure and underlying dynamical principles (System Design). We also described the detailed examples in the application of Systems Identification and System Design for the mammalian circadian clocks. We strongly believe that it is now high time to fully integrate these systems biology approaches for the solution of various system-level questions in mammalian circadian clocks.

Acknowledgments We thank our collaborators. System Identification of clocks is a collaboration with Drs. W. Chen, A. Adachi, H. Wakamatsu, S. Hayashi, T. Takasugi, M. Nagano, K. Nakahama, Y. Suzuki, S. Sugano, M. Iino, Y. Shigeyoshi, S. Hashimoto, M. Sano, and M. Machida. System Analysis of clocks is a collaboration with Drs. T.K. Sato, R.G.. Yamada, H. Ukai, J.E. Baggs, L.J. Miraglia, T.J. Kobayashi, D.K. Welsh, S.A. Kay, and J.B. Hogenesch. System Control of clocks is the collaboration with Drs. H. Ukai, T.J. Kobayashi M. Nagano,

K. Masumoto, M. Sujino, T. Kondo, K. Yagita, and Y. Shigeyoshi. System Design of Clocks is a collaboration with Drs. M. Nakajima, M. Ishida, M. Ukai-Tadenuma, and T. Kasukawa. The molecular timetable method is a collaborative work with Drs. W. Chen, Y. Minami, S. Honma, K. Honma, M. Iino, and S. Hashimoto. The theoretical study on Synchronization of Clocks is a collaboration with K. Hirose and M. Iino. We also thank Drs. I. Nikaido, H. Ukai, R.G. Yamada, T.J. Kobayashi, M. Nakajima, Y. Minami, and A. Wada for creation of the figures and critical reading of the manuscript. This research was supported by an intramural Grant-in-Aid from CDB, Director's Fund from CDB, President's Fund from RIKEN, Grant-in-Aid for Genome-Network Project, and Scientific Research on Priority Areas "Systems Genomics" from MEXT, Japan, and a Grant-in-Aid for NEDO project from METI, Japan.

References

1. Kitano H (2002) Systems biology: a brief overview. Science 295:1662–1664
2. Kitano H (2002) Computational systems biology. Nature (Lond) 420:206–210
3. Reppert SM, Weaver DR (2002) Coordination of circadian timing in mammals. Nature (Lond) 418:935–941
4. Dunlap JC, Loros JJ, DeCoursey PJ (eds) (2004) Chronobiology: Biological Timekeeping. Sinauer Associates, Sunderland, MA
5. Panda S, Hogenesch JB, Kay SA (2002) Circadian rhythms from flies to human. Nature (Lond) 417:329–335
6. King DP, Zhao Y, Sangoram AM et al (1997) Positional cloning of the mouse circadian clock gene. Cell 89:641–653
7. Bunger MK, Wilsbacher LD, Moran SM et al (2000) Mop3 is an essential component of the master circadian pacemaker in mammals. Cell 103:1009–1017
8. Bae K, Jin X, Maywood ES et al (2001) Differential functions of mPer1, mPer2, and mPer3 in the SCN circadian clock. Neuron 30:525–536
9. Zheng B, Albrecht U, Kaasik K et al (2001) Nonredundant roles of the mPer1 and mPer2 genes in the mammalian circadian clock. Cell 105:683–694
10. van der Horst GT, Muijtjens M, Kobayashi K et al (1999) Mammalian Cry1 and Cry2 are essential for maintenance of circadian rhythms. Nature (Lond) 398:627–630
11. Vitaterna MH, Selby CP, Todo T et al (1999) Differential regulation of mammalian period genes and circadian rhythmicity by cryptochromes 1 and 2. Proc Natl Acad Sci U S A 96:12114–12119
12. Lowrey PL, Shimomura K, Antoch MP et al (2000) Positional syntenic cloning and functional characterization of the mammalian circadian mutation tau. Science 288:483–492
13. Sato TK, Panda S, Miraglia LJ et al (2004) A functional genomics strategy reveals Rora as a component of the mammalian circadian clock. Neuron 43:527–537
14. Preitner N, Damiola F, Lopez-Molina L et al (2002) The orphan nuclear receptor REV-ERB-alpha controls circadian transcription within the positive limb of the mammalian circadian oscillator. Cell 110:251–260
15. Wuarin J, Schibler U (1990) Expression of the liver-enriched transcriptional activator protein DBP follows a stringent circadian rhythm. Cell 63:1257–1266
16. Mitsui S, Yamaguchi S, Matsuo T et al (2001) Antagonistic role of E4BP4 and PAR proteins in the circadian oscillatory mechanism. Genes Dev 15:995–1006
17. Honma S, Kawamoto T, Takagi Y et al (2002) Dec1 and Dec2 are regulators of the mammalian molecular clock. Nature (Lond) 419:841–844
18. Zylka MJ, Shearman LP, Weaver DR et al (1998) Three period homologs in mammals: differential light responses in the suprachiasmatic circadian clock and oscillating transcripts outside of brain. Neuron 20:1103–1110

19. Reick M, Garcia JA, Dudley C et al (2001) NPAS2: an analog of clock operative in the mammalian forebrain. Science 293:506–509
20. Ueda HR, Chen W, Adachi A et al (2002) A transcription factor response element for gene expression during circadian night. Nature (Lond) 418:534–539
21. Ueda HR, Hayashi S, Chen W et al (2005) System-level identification of transcriptional circuits underlying mammalian circadian clocks. Nat Genet 37:187–192
22. Yamazaki S, Numano R, Abe M et al (2000) Resetting central and peripheral circadian oscillators in transgenic rats. Science 288:682–685
23. Balsalobre A, Damiola F, Schibler U (1998) A serum shock induces circadian gene expression in mammalian tissue culture cells. Cell 93:929–937
24. Yagita K, Tamanini F, van Der Horst GT et al (2001) Molecular mechanisms of the biological clock in cultured fibroblasts. Science 292:278–281
25. Akashi M, Nishida E (2000) Involvement of the MAP kinase cascade in resetting of the mammalian circadian clock. Genes Dev 14:645–649
26. Gekakis N, Staknis D, Nguyen HB et al (1998) Role of the CLOCK protein in the mammalian circadian mechanism. Science 280:1564–1569.
27. Kume K, Zylka MJ, Sriram S et al (1999) mCRY1 and mCRY2 are essential components of the negative limb of the circadian clock feedback loop. Cell 98:193–205.
28. Shearman LP, Sriram S, Weaver DR et al (2000) Interacting molecular loops in the mammalian circadian clock. Science 288:1013–1019
29. Lipshutz RJ, Fodor SP, Gingeras TR et al (1999) High density synthetic oligonucleotide arrays. Nat Genet 21:20–24
30. Suzuki Y, Taira H, Tsunoda T et al (2001) Diverse transcriptional initiation revealed by fine, large-scale mapping of mRNA start sites. EMBO Rep 2:388–393
31. Hogenesch JB, Gu YZ, Jain S et al (1998) The basic-helix-loop-helix-PAS orphan MOP3 forms transcriptionally active complexes with circadian and hypoxia factors. Proc Natl Acad Sci U S A 95:5474–5479
32. Yoo SH, Ko CH, Lowrey PL et al (2005) A noncanonical E-box enhancer drives mouse Period 2 circadian oscillations in vivo. Proc Natl Acad Sci U S A 102:2608–2613
33. Falvey E, Marcacci L, Schibler U (1996) DNA-binding specificity of PAR and C/EBP leucine zipper proteins: a single amino acid substitution in the C/EBP DNA-binding domain confers PAR-like specificity to C/EBP. Biol Chem 377:797–809
34. Harding HP, Lazar MA (1993) The orphan receptor Rev-ErbA alpha activates transcription via a novel response element. Mol Cell Biol 13:3113–3121
35. Ukai-Tadenuma M, Kasukawa T, Ueda HR (2008) Proof-by-synthesis of the transcriptional logic of mammalian circadian clocks. Nat Cell Biol 10:1154–1163

Toward Understanding How the Immune System Establishes a Diverse Yet Self-Tolerant T-Cell Repertoire: Stepwise Roles of Thymic Microenvironments

Takeshi Nitta and Yousuke Takahama

Introduction

The thymus is an organ that supports the development and repertoire formation of T lymphocytes (1). Thymic parenchyma consists of leukocytic cells called thymocytes, the majority of which belong to the T-lymphoid lineage, and various stromal cells including thymic epithelial cells (TEC) (2). Thymic stromal cells provide multiple signals to support manifold processes of thymocyte development that are essential for the supply of circulating T lymphocytes (3). In response to these signals, developing thymocytes undergo proliferation, differentiation, and relocation to generate mature T lymphocytes that carry a diverse yet self-tolerant repertoire of T-cell antigen receptors (TCR) (4). These steps of T-lymphocyte development take place in anatomically discrete regions of the thymus where a variety of specialized stromal cells are localized (5).

T lymphocytes arise from hematopoietic stem cell-derived T-lymphoid progenitor cells that migrate to the thymus (6). Most immature hematopoietic cells that have just entered the thymus lack the expression of CD4 and CD8 and therefore belong to CD4/CD8 double-negative (DN) thymocytes (7, 8). The development of DN thymocytes is associated with the dynamic relocation of the cells in thymic parenchyma; T-lymphoid progenitor cells in adult mouse thymus are mostly localized in the corticomedullary junction, the area between deep cortex and medulla (9), whereas thymocytes migrate toward the capsular region of the thymus during differentiation and develop into CD4/CD8 double-positive (DP) thymocytes (10). DP thymocytes expressing TCR on the cell surface are localized in the cortex. DP thymocytes move actively within the cortical microenvironment (11, 12), probably seeking TCR interaction with major histocompatibility complex (MHC)-encoded molecules that are associated with self-peptides. Cortical DP thymocytes that interact via their TCR with the self-peptide–MHC complex are selected for survival or death depending on the avidity of the interaction (13, 14). DP thymocytes that receive TCR signals with ligand interactions of weak avidity and nonextensive aggregation are induced to survive

T. Nitta and Y. Takahama
Division of Experimental Immunology, Institute for Genome Research,
University of Tokushima, Tokushima 770-8503, Japan

S. Nakanishi et al. (eds.), *Systems Biology*,
DOI:10.1007/978-4-431-87704-2_7, © Springer 2009

and differentiate into mature thymocytes, the process referred to as positive selection (15, 16). By contrast, DP thymocytes that receive TCR signals with ligand interactions of strong avidity and extensive aggregation are destined to die (17, 18), a process referred to as negative selection. During positive selection, the differential kinetics of TCR–ligand interactions determines cell lineage to become either $CD4^+$ $CD8^-$ or $CD4^-$ $CD8^+$ single-positive (SP) thymocytes (19). Positively selected thymocytes relocate to thymic medulla, where they further interact with self-peptides displayed in the medullary microenvironment (20). Medullary TEC (mTEC) express a diverse set of genes representing peripheral tissues (21), thereby contributing to the establishment of self-tolerance in thymic medulla. A nuclear factor called autoimmune regulator (AIRE) participates in this promiscuous gene expression in mTEC (22). Consequently, a diverse yet self-tolerant TCR repertoire is formed in the thymus, and mature T lymphocytes with such a TCR repertoire are released to the circulation. Thus, T-cell repertoire formation consists of stepwise fate determinations of thymocyte development in different thymic microenvironments. The dynamic relocation of developing thymocytes within thymic microenvironments is crucial for T-cell repertoire selection.

The aforementioned control of T-lymphocyte development in the thymus is supported in multiple thymic microenvironments that are formed by different sets of thymic stromal cells. Thymic stromal cells are composed of TEC and other stromal cells, including mesenchymal cells, endothelial cells, and hematopoietic cells, such as dendritic cells (DC) and macrophages (23). TEC consist of at least two major populations, cortical TEC (cTEC) and mTEC, which play crucial roles in the development and repertoire formation of T lymphocytes. cTEC and mTEC are derived from common progenitor cells that are generated from the endoderm of the third pharyngeal pouch (24–26). The development of TEC is dependent on many transcription factors, including Tbx1, Hoxa3, Pax1, and Foxn1 (27–30). Thymic mesenchymal cells are also crucial for supporting thymus generation and T-lymphocyte development (31, 32). It is also fascinating to note that thymic stromal cells that support T-lymphocyte development are supported, in turn, by developing thymocytes. The bidirectional signal exchanges between thymocytes and thymic stromal cells are appreciated as “thymic crosstalk” (33–35).

To understand how T lymphocytes are selected to establish a diverse yet self-tolerant repertoire in the thymus, we performed genome-wide screening for genes that are expressed in the thymus and that affect thymus development. We find that β5t-containing thymoproteasomes specifically expressed by cTEC play a pivotal role in the positive selection of CD8 SP thymocytes. We also find that positively selected thymocytes begin expressing CCR7, a chemokine receptor, and thereby relocate to thymic medulla where mTEC produce CCR7 ligands. Furthermore, we find that tumor necrosis factor (TNF) superfamily (TNFSF) ligands, including RANKL and CD40L, are produced by positively selected thymocytes and pivotally regulate mTEC development and thymic medulla formation. Thus, our study shows that sequential encounter of developing thymocytes with a unique set of self-molecules in the cortical microenvironment and another set of self-molecules in the medullary microenvironment is essential for the generation of a diverse yet self-tolerant repertoire of T lymphocytes.

Positive Selection in Thymic Cortex and β5t-Containing Thymoproteasomes

A number of studies support the notion that low-affinity self-peptides present in thymic cortex are responsible for the positive selection of developing thymocytes. However, the nature of positively selecting peptides and positively selecting antigen-presenting cells remains elusive (36). A single MHC–peptide complex expressed by cTEC can produce a diverse repertoire of T lymphocytes (37), suggesting that any peptide that causes low-avidity TCR engagement might be capable of triggering positive selection of thymocytes. It was also suggested that, rather than initial positive selection, subsequent negative selection establishes repertoire formation of T lymphocytes (38). Furthermore, it was shown that the experimental capability of inducing positive selection is not limited to cTEC but can be detected in fibroblasts and DC (39–41). It was also shown that developing thymocytes and thymus-reentering T lymphocytes can induce positive selection of thymocytes (42–45). Thus, the possibility that cTEC, or any other cells in the thymic cortex, have any specialized capability to induce positive selection seemed unlikely until recently.

Our recent discovery of a novel subunit of the 20S proteasome, β5t, has revealed a unique capability of cTEC to support the positive selection of thymocytes (46). Proteasomes are multicatalytic protease complexes that are responsible for regulated proteolysis in eukaryotic cells and for the generation of antigenic peptides presented by class I MHC molecules (47, 48). The 20S proteasome is responsible for the proteolytic activity of the proteasome and is composed of 28 subunits (two α-rings with α1 to α7 subunits and two β-rings with β1 to β7 subunits). Among these subunits, β1, β2, and β5 are responsible for caspase-like, trypsin-like, and chymotrypsin-like catalytic activities, respectively (49, 50). Interferon-γ induces the production of a new set of catalytic subunits, β1i, β2i, and β5i, to replace their constitutive counterparts, β1, β2, and β5, thereby forming immunoproteasomes, a proteasome complex that possesses increased chymotrypsin-like activity and participates in efficient antigen presentation and immune responses (51). On the other hand, the newly identified catalytic subunit β5t is incorporated into the 20S proteasome instead of β5 or β5i, together with β1i and β2i (46). Because this novel proteasome containing β5t is specifically expressed in the thymus and exclusively in cTEC, it is termed a thymoproteasome.

In comparison to β5-containing standard proteasomes and β5i-containing immunoproteasomes, β5t-containing thymoproteasomes exhibit reduced chymotrypsin-like activity but normal caspase-like activity and normal trypsin-like activity (46). Proteasomes are responsible for the production of MHC class I-binding peptides and are the sole enzymes that determine the C-termini of the peptides (52, 53). Hydrophobic C-terminal anchor residues of the peptides are essential for high-affinity peptide binding into the clefts of MHC class I complexes (54). Chymotrypsin-like activity carried by β5 and β5i is important for the production of high-affinity MHC class I ligands (55). Thus, it is possible that cTEC generate a unique set of MHC class I-associated peptides that are different from those present in any other cells.

The generation of $CD4^-$ $CD8^+$ (CD8SP) thymocytes that express high levels of TCR is severely reduced in β5t-deficient mice. The selective reduction of CD8SP

T lymphocytes is also observed in the spleen of these mice. On the other hand, DP and CD4SP thymocytes as well as peripheral CD4 T lymphocytes are unaffected. The absence of β5t does not affect cortical or medullary architecture or overall thymus size, indicating that β5t is essential for neither the development of cTEC nor the generation of normal thymic architecture. These results demonstrate that β5t is required for the development of CD8SP T lymphocytes in the thymus and suggest the possibility that β5t is associated with positive selection of CD8SP T lymphocytes (46).

It is possible that thymoproteasomes in cTEC may be somehow involved in providing costimulatory signals that are specifically required for the generation of CD8SP T lymphocytes rather than CD4SP T lymphocytes. However, since the generation of CD8SP T lymphocytes is specifically affected in β5t-deficient mice, and as the surface expression of MHC class I molecules on cTEC of β5t-deficient mice is comparable to that of normal mice, β5t-containing thymoproteasomes in cTEC are likely involved in producing class I MHC-loaded peptides that provide TCR signals required for positive selection of class I MHC-restricted CD8SP T lymphocytes (46). β5t specifically limits chymotryptic activity that cleaves peptide bonds after hydrophobic amino acid residues in cTEC, and therefore, thymoproteasomes predominantly produce low-affinity class I MHC ligands specifically in cTEC. These low-affinity class I MHC ligands may limit the duration and/or avidity of interaction with TCR and contribute to inducing positive selection of the majority of CD8SP T lymphocytes (46, 56, 57).

The results from β5t-deficient mice reveal that cTEC possess unique protein degradation activity that might lead to the production of a unique set of class I MHC-associated peptides necessary for the generation of CD8 T lymphocytes. This unique protein degradation activity of cTEC might not be limited to class I MHC-associated peptides but might also occur in class II MHC-associated peptides, because cathepsin L, a lysosomal protease that is highly expressed by cTEC and not mTEC (58), is required for the optimal generation of CD4SP T lymphocytes (59, 60). A unique lysosomal degradation activity might be functional in cTEC, which is mediated by cathepsin L in a manner analogous to thymoproteasomes. Thus, the unique character of cTEC protein degradation and self-peptide presentation may be pivotal for the positive selection of thymocytes in both CD4SP and CD8SP lineages (56, 57). These findings of cTEC would not only highlight the significant roles of thymic cortex in T-lymphocyte development but also further our understanding of the molecular mechanisms of T-lymphocyte repertoire selection.

CCR7 Regulates Relocation of Positively Selected Thymocytes to Medulla

Newly generated immature DP thymocytes move randomly in the thymic cortex, as shown by in vitro real-time imaging of intact thymus lobes (11, 61). This “random walk motility” is also observed by noninvasive intravital imaging of thymocytes in the fish thymus (12). On the other hand, immature thymocytes at early ontogeny

before CD4 and CD8 expression appear dormant in the thymus (12). Thus, the differentiation into DP thymocytes possibly coincides with the acquisition of cellular motility, which represents the activity of cells that dynamically seek TCR interaction with the MHC–peptide complex in the cortical microenvironment. DP thymocytes that actively move within the cortex interact with cTEC and pause their motility upon TCR interaction with MHC–peptide ligands (62).

Positively selected thymocytes are induced to survive and to relocate from the cortex to the medulla. Positive selection coincides with the appearance of a thymocyte population that displays rapid and directed migration toward the medulla (11). Upon positive selection, DP thymocytes elevate CCR7 expression on the cell surface (63–65). CCR7 ligands, CCL19 and CCL21, in the thymus are predominantly expressed by mTEC and mostly localized in the medulla (65). Consequently, positively selected thymocytes are attracted to the medulla through CCR7-mediated chemotaxis. We found that positively selected thymocytes in mice deficient for CCR7 or CCR7 ligands are defective in accumulation in the medulla and are localized in the cortex (65, 66). Mice deficient for CCR7 signals exhibit autoimmunity to peripheral tissues (66–68). Thymocytes generated without CCR7 ligands are potent in inducing autoimmune exocrinopathy in mice, and thus are defective in establishing central tolerance (66). Therefore, the migration of positively selected thymocytes to the medulla is essential for the establishment of central tolerance, and the proper relocation of developing thymocytes within multiple thymic microenvironments is necessary for repertoire formation of T lymphocytes (20, 66).

TNFSF Regulation of Medulla Formation

The microenvironment of thymic medulla is mainly composed of mTEC and hematopoietic cells, including mature thymocytes and DC. Similar to cTEC, mTEC are derived from endodermal precursor cells that are generated at the third pharyngeal pouch (25, 26, 69). Thymic medulla is a specialized microenvironment where developing thymocytes establish tolerance to systemic self-antigens, including peripheral tissue-specific antigens. Indeed, T-lymphocyte development within the thymus that is defective in thymic medulla formation leads to failure in establishing self-tolerance, resulting in autoimmune disorders (70–72). In the thymic medulla, mTEC express a variety of "tissue-specific" genes, for example, the gene encoding insulin whose expression is restricted to β-islet cells in the pancreas (73–76). This "ectopic" expression of tissue-specific genes by mTEC is called "promiscuous gene expression" and is responsible for the establishment of self-tolerance through the presentation of tissue-specific antigens to developing thymocytes (21, 77, 78). AIRE, a nuclear protein that is predominantly expressed by mTEC, is associated with the promiscuous gene expression of mTEC (22, 79–82).

The formation of thymic medulla is associated with the development of mature thymocytes in the thymus. An early study showed that medulla formation is defective in *scid* mice, in which thymocyte development is arrested at the DN stage and is restored by reconstitution with wild-type hematopoietic cells (33). Studies of mice

deficient for positive selection, including TCRα-deficient mice, ZAP70-deficient mice, and MHC class I and class II double-deficient mice, confirmed that the formation of thymic medulla is dependent on the generation of positively selected mature thymocytes (83–86). In mice deficient for CCR7 or CCR7 ligands, medulla formation is mildly defective (65, 66), suggesting that optimum development of thymic medulla requires the relocation of positively selected thymocytes. Thus, signals produced by positively selected thymocytes crucially regulate mTEC development and medulla formation.

We recently identified that positive selection promotes mTEC proliferation and thereby nurtures the formation of thymic medulla (87). We found that positively selected thymocytes express RANKL, a TNFSF member ligand (87). The number of mTEC is reduced in mice deficient for RANKL, and the enforced expression of RANKL in mice deficient for positive selection restores mTEC cellularity and medulla formation, indicating that RANKL mediates thymic crosstalk signals for the optimal formation of thymic medulla (87). Osteoprotegerin, a naturally occurring soluble RANKL inhibitor that binds to RANKL and inhibits RANKL binding to its signaling receptor RANK, is expressed by mTEC and regulates mTEC development and medulla formation, because mice deficient for osteoprotegerin exhibit hypercellularity of mTEC and an enlarged thymic medulla (87). The RANKL receptor, RANK, is more strongly expressed in mTEC than in cTEC and is required for the development of mTEC expressing AIRE (87, 88). RANKL is also expressed by $CD4^+$ $CD3^-$ lymphoid tissue inducer (LTi) cells and is involved in the differentiation of mTEC during embryogenesis (88–90).

Positively selected thymocytes also produce CD40L, another TNFSF member ligand (87, 91). In contrast to RANKL, CD40L is not expressed in thymic LTi cells (87). The enforced expression of CD40L in vivo produces an enlarged thymic medulla, suggesting that CD40L signals can promote thymic medulla formation (92, 93). Analysis using fetal thymus organ culture shows that CD40L as well as RANKL facilitates mTEC development through classical and nonclassical NF-κB pathways (94). Mice deficient for both CD40 and RANKL exhibit severe defect in mTEC development and thymic medulla formation, whereas the single deficiency of CD40 causes only a mild defect in thymic medulla (94). Thus, it is likely that RANKL and CD40 cooperate with each other to promote mTEC development. It is also possible that RANKL and CD40 may sequentially regulate mTEC development; RANKL produced by LTi cells plays a role in mTEC development during embryogenesis, whereas RANKL and CD40L produced by positively selected mature thymocytes essentially promote postnatal increase of mTEC cellularity (87, 94).

Concluding Remarks

The fact that the thymus contains at least two distinct microenvironments, the cortex and the medulla, has been known for more than 100 years (95–98). Studies conducted over a span of 40 years since the discovery of the immunological function of the

thymus have remarkably advanced our understanding of lymphocyte biology in relationship to T-lymphocyte development and selection in the thymus. However, the developmental and molecular biology of thymic stromal cells has remained quite vague until recently. Recent achievements have enabled us to study the biology of thymic microenvironments using several molecules that represent key functions of thymic stromal cells. Those molecules include Foxn1, Delta-like ligands, AIRE, and β5t. Several molecules that mediate the development of thymic stromal cells, such as RANKL and CD40L, have also been identified. These outcomes should provide a solid foundation for further studies of thymic microenvironments to better understand the molecular mechanism of the development and repertoire formation of T cells and the therapeutic reconstitution of functional thymus for various clinical situations (99, 100). Unveiling of the molecular identities of thymic microenvironments has just begun.

Acknowledgments The support by Uehara Memorial Foundation and MEXT was acknowledged. T.N. was a JSPS Research Fellow.

References

1. Miller, J. F. A. P. (1961) Immunological function of the thymus. Lancet 2:748–749.
2. Sainte-Marie, G. and Leblond, C. P. (1964) Cytologic features and cellular migration in the cortex and medulla of thymus in the young adult rat. Blood 23:275–299.
3. Kingston, R., Jenkinson, E. J., and Owen, J. J. (1985) A single stem cell can recolonize an embryonic thymus, producing phenotypically distinct T-cell populations. Nature (Lond) 317:811–813.
4. von Boehmer, H. (1988) The developmental biology of T lymphocytes. Annu. Rev. Immunol. 6:309–326
5. Jenkinson, E. J., Owen, J. J., and Aspinall, R. (1980). Lymphocyte differentiation and major histocompatibility complex antigen expression in the embryonic thymus. Nature (Lond) 284:177–179.
6. Le Douarin, N. M. and Jotereau, F. V. (1975) Tracing of cells of the avian thymus through embryonic life in interspecific chimeras. J. Exp. Med. 142:17–40.
7. Bhandoola, A., Sambandam, A., Allman, D., Meraz, A., and Schwarz, B. (2003) Early T lineage progenitors: new insights, but old questions remain. J. Immunol. 171:5653–5658.
8. Scollay, R., Wilson, A., D'Amico, A., Kelly, K., Egerton, M., Pearse, M., Wu, L., and Shortman, K. (1988) Developmental status and reconstitution potential of subpopulations of murine thymocytes. Immunol. Rev. 104:81–120.
9. Lind, E. F., Prockop, S. E., Porritt, H. E., and Petrie, H. T. (2001). Mapping precursor movement through the postnatal thymus reveals specific microenvironments supporting defined stages of early lymphoid development. J. Exp. Med. 194, 127-134.
10. Wilson, A., Petrie, H. T., Scollay, R. and Shortman, K. (1989). The acquisition of CD4 and CD8 during the differentiation of early thymocytes in short-term culture. Int. Immunol. 1:605–612.
11. Witt, C. M., Raychaudhuri, S., Schaefer, B., Chakraborty, A. K., and Robey, E. A. (2005) Directed migration of positively selected thymocytes visualized in real time. PLoS Biol. 3:e160.
12. Li, J., Iwanami, N., Hoa, V. Q., Furutani-Seiki, M., and Takahama, Y. (2007) Noninvasive intravital imaging of thymocyte dynamics in medaka. J. Immunol. 179:1605–1615.
13. von Boehmer, H. (1994) Positive selection of lymphocytes. Cell 76:219–228.

14. Allen, P. M. (1994) Peptides in positive and negative selection: a delicate balance. Cell 76:593–596.
15. Ashton-Rickardt, P. G., Van Kaer, L., Schumacher, T. N., Ploegh, H. L., and Tonegawa, S. (1993) Peptide contributes to the specificity of positive selection of CD8+ T cells in the thymus. Cell 73:1041–1049.
16. Takahama, Y., Suzuki, H., Katz, K. S., Grusby, M.J., and Singer, A. (1994) Positive selection of CD4+ T cells by TCR ligation without aggregation even in the absence of MHC. Nature (Lond) 371:67–70.
17. Ashton-Rickardt, P. G. and Tonegawa, S. (1994) A differential-avidity model for T-cell selection. Immunol. Today 15:362–366.
18. Sebzda, E., Wallace, V. A., Mayer, J., Yeung, R.S., Mak, T. W., and Ohashi, P. S. (1994) Positive and negative thymocyte selection induced by different concentrations of a single peptide. Science 263:1615–1618.
19. Singer, A. (2002) New perspectives on a developmental dilemma: the kinetic signaling model and the importance of signal duration for the CD4/CD8 lineage decision. Curr. Opin. Immunol. 14:207–215.
20. Takahama, Y. (2006) Journey through the thymus: stromal guides for T-cell development and selection. Nat. Rev. Immunol. 6:127–135.
21. Klein, L. and Kyewski, B. (2000) “Promiscuous” expression of tissue antigens in the thymus: a key to T-cell tolerance and autoimmunity? J. Mol. Med. 78:483–494.
22. Anderson, M. S., Venanzi, E. S., Klein, L., Chen, Z., Berzins, S. P., Turley, S. J., von Boehmer, H., Bronson, R., Dierich, A., Benoist, C., and Mathis, D. (2002) Projection of an immunological self shadow within the thymus by the aire protein. Science 298:1395–1401.
23. Boyd, R. L., Tucek, C. L., Godfrey, D. I., Izon, D. J., Wilson, T. J., Davidson, N. J., Bean, A. G., Ladyman, H. M., Ritter, M. A., and Hugo, P. (1993) The thymic microenvironment. Immunol. Today. 14:445–459.
24. Manley, N. R. and Blackburn, C. C. (2003) A developmental look at thymus organogenesis: where do the non-hematopoietic cells in the thymus come from? Curr. Opin. Immunol. 15:225–232.
25. Rossi, S. W., Jenkinson, W. E., Anderson, G., and Jenkinson, E. J. (2006) Clonal analysis reveals a common progenitor for thymic cortical and medullary epithelium. Nature (Lond) 441:988–991.
26. Bleul, C. C., Corbeaux, T., Reuter, A., Fisch, P., Monting, J. S., and Boehm, T. (2006) Formation of a functional thymus initiated by a postnatal epithelial progenitor cell. Nature (Lond) 441:992–996.
27. Lindsay, E. A., Vitelli, F., Su, H., Morishima, M., Huynh, T., Pramparo, T., Jurecic, V., Ogunrinu, G., Sutherland, H. F., Scambler, P. J., Bradley, A., and Baldini, A. (2001) Tbx1 haploinsufficiency in the DiGeorge syndrome region causes aortic arch defects in mice. Nature (Lond) 410:97–101.
28. Manley, N. R. and Capecchi, M. R. (1998) Hox group 3 paralogs regulate the development and migration of the thymus, thyroid, and parathyroid glands. Dev. Biol. 195:1–15.
29. Su, D. M. and Manley, N. R. (2000) Hoxa3 and pax1 transcription factors regulate the ability of fetal thymic epithelial cells to promote thymocyte development. J. Immunol. 164:5753–5760.
30. Nehls, M., Pfeifer, D., Schorpp, M., Hedrich, H., and Boehm, T. (1994) New member of the winged-helix protein family disrupted in mouse and rat nude mutations. Nature (Lond) 372:103–107.
31. Anderson, G., Jenkinson, E. J., Moore N. C., and Owen, J. J. T. (1993) MHC class II-positive epithelium and mesenchyme cells are both required for T-cell development in the thymus. Nature (Lond) 362:70–73.
32. Jenkinson, W. E., Jenkinson, E. J., and Anderson, G. (2003) Differential requirement for mesenchyme in the proliferation and maturation of thymic epithelial progenitors. J. Exp. Med. 198:325–332.
33. Shores, E.W., Van Ewijk, W., and Singer, A. (1991) Disorganization and restoration of thymic medullary epithelial cells in T cell receptor-negative scid mice: evidence that receptor-bearing lymphocytes influence maturation of the thymic microenvironment. Eur. J. Immunol. 21:1657–1661.

34. Ritter, M. A. and Boyd, R. L. (1993) Development in the thymus: it takes two to tango. Immunol. Today 14:462–469.
35. van Ewijk, W., Shores, E. W., and Singer, A. (1994) Crosstalk in the mouse thymus. Immunol. Today 15:214–217.
36. Starr, T. K., Jameson, S. C., and Hogquist, K. A. (2003) Positive and negative selection of T cells. Annu. Rev. Immunol. 21:139–176.
37. Ignatowicz, L., Kappler, J., and Marrack, P. (1996) The repertoire of T cells shaped by a single MHC/peptide ligand. Cell 84:521–529.
38. Huseby, E. S., White, J., Crawford, F., Vass, T., Becker, D., Pinilla, C., Marrack, P., and Kappler, J. W. (2005) How the T cell repertoire becomes peptide and MHC specific. Cell 122:247–260.
39. Pawlowski, T., Elliott, J. D., Loh, D. Y., and Staerz, U. D. (1993) Positive selection of T lymphocytes on fibroblasts. Nature (Lond) 364:642–645.
40. Hugo, P., Kappler, J. W., McCormack, J. E., and Marrack, P. (1993) Fibroblasts can induce thymocyte positive selection in vivo. Proc. Natl. Acad. Sci. U. S. A. 90:10335–10339.
41. Yasutomo, K., Lucas, B., and Germain, R. N. (2000) TCR signaling for initiation and completion of thymocyte positive selection has distinct requirements for ligand quality and presenting cell type. J. Immunol. 165:3015–3022.
42. Li, W., Kim, M. G., Gourley, T. S., McCarthy, B.P., Sant'Angelo, D. B., and Chang, C. H. (2005) An alternate pathway for CD4 T cell development: thymocyte-expressed MHC class II selects a distinct T cell population. Immunity 23:375–386.
43. Choi, E. Y., Jung, K. C., Park, H. J., Chung, D. H., Song, J. S., Yang, S. D., Simpson, E., and Park, S. H. (2005) Thymocyte–thymocyte interaction for efficient positive selection and maturation of CD4 T cells. Immunity 23:387–396.
44. Horai, R., Mueller, K. L., Handon, R. A., Cannons, J. L., Anderson, S. M., Kirby, M. R., and Schwartzberg, P. L. (2007) Requirements for selection of conventional and innate T lymphocyte lineages. Immunity 27:775–785.
45. Kirberg, J., Bosco, N., Deloulme, J. C., Ceredig, R., and Agenes, F. (2008) Peripheral T lymphocytes recirculating back into the thymus can mediate thymocyte positive selection. J. Immunol. 181:1207–1214.
46. Murata, S., Sasaki, K., Kishimoto, T., Niwa, S., Hayashi, H., Takahama, Y., and Tanaka, K. (2007) Regulation of $CD8^+$ T cell development by thymus-specific proteasomes. Science 316:1349–1353.
47. Rock, K. L. and Goldberg, A. L. (1999) Degradation of cell proteins and the generation of MHC class I-presented peptides. Annu. Rev. Immunol. 17:739–779.
48. Kloetzel, P. M. (2001) Antigen processing by the proteasome. Nat. Rev. Mol. Cell. Biol. 2:179–187.
49. Coux, O., Tanaka, K., and Goldberg, A. L. (1996) Structure and functions of the 20S and 26S proteasomes. Annu. Rev. Biochem. 65:801–847.
50. Baumeister, W., Walz, J., Zühl, F., and Seemüller, E. (1998) The proteasome: paradigm of a self-compartmentalizing protease. Cell 92:367–380.
51. Tanaka, K. and Kasahara, M. (1998) The MHC class I ligand-generating system: roles of immunoproteasomes and the interferon-gamma-inducible proteasome activator PA28. Immunol. Rev. 163:161–176.
52. Cascio, P., Hilton, C., Kisselev, A. F., Rock, K. L., and Goldberg, A.L. (2001) 26S proteasomes and immunoproteasomes produce mainly N-extended versions of an antigenic peptide. EMBO J. 20:2357–2366.
53. Rock, K. L., York, I. A., and Goldberg, A. L. (2004) Post-proteasomal antigen processing for major histocompatibility complex class I presentation. Nat. Immunol. 5:670–677.
54. Young, A. C., Nathenson, S. G., and Sacchettini, J. C. (1995) Structural studies of class I major histocompatibility complex proteins: insights into antigen presentation. FASEB J. 9:26–36.
55. Fehling, H. J., Swat, W., Laplace, C., Kühn, R., Rajewsky, K., Müller, U., and von Boehmer, H. (1994) MHC class I expression in mice lacking the proteasome subunit LMP-7. Science 265:1234–1237.

56. Murata, S., Takahama, Y., and Tanaka, K. (2008) Thymoproteasome: probable role in generating positively selecting peptides. Curr. Opin. Immunol. 20(2):192–196.
57. Takahama, Y., Tanaka, K., and Murata, S. (2008) Modest cortex and promiscuous medulla for thymic repertoire formation. Trends Immunol. 29:251–255.
58. Honey, K. and Rudensky, A. Y. (2003) Lysosomal cysteine proteases regulate antigen presentation. Nat. Rev. Immunol. 3:472–482.
59. Nakagawa, T., Roth, W., Wong, P., Nelson, A., Farr, A., Deussing, J., Villadangos, J. A., Ploegh, H., Peters, C., and Rudensky, A. Y. (1998) Cathepsin L: critical role in Ii degradation and CD4 T cell selection in the thymus. Science 280:450–453.
60. Honey, K., Nakagawa, T., Peters, C., and Rudensky, A. (2002) Cathepsin L regulates $CD4^+$ T cell selection independently of its effect on invariant chain: a role in the generation of positively selecting peptide ligands. J. Exp. Med. 195:1349–1358.
61. Bousso, P., Bhakta, N. R., Lewis, R. S., and Robey, E. (2002) Dynamics of thymocyte-stromal cell interactions visualized by two-photon microscopy. Science 296:1876–1880.
62. Bhakta, N. R., Oh, D. Y., and Lewis, R. S. (2005) Calcium oscillations regulate thymocyte motility during positive selection in the three-dimensional thymic environment. Nat. Immunol. 6:143–151.
63. Ngo, V. N., Tang, H. L., and Cyster, J. G. (1998) Epstein-Barr virus-induced molecule 1 ligand chemokine is expressed by dendritic cells in lymphoid tissues and strongly attracts naive T cells and activated B cells. J. Exp. Med. 188:181–191.
64. Campbell, J. J., Pan, J., and Butcher, E. C. (1999) Developmental switches in chemokine responses during T cell maturation. J. Immunol. 163:2353–2357.
65. Ueno, T., Saito, F., Gray, D. H., Kuse, S., Hieshima, K., Nakano, H., Kakiuchi, T., Lipp, M., Boyd, R. L., and Takahama, Y. (2004) CCR7 signals are essential for cortex-medulla migration of developing thymocytes. J. Exp. Med. 200:493–505.
66. Kurobe, H., Liu, C., Ueno, T., Saito, F., Ohigashi, I., Seach, N., Arakaki, R., Hayashi, Y., Kitagawa, T., Lipp, M., Boyd, R. L., and Takahama, Y. (2006) CCR7-dependent cortex-to-medulla migration of positively selected thymocytes is essential for establishing central tolerance. Immunity 24:165–177.
67. Höpken, U. E., Wengner, A. M., Loddenkemper, C., Stein, H., Heimesaat, M. M., Rehm, A., and Lipp, M. (2007) CCR7 deficiency causes ectopic lymphoid neogenesis and disturbed mucosal tissue integrity. Blood 109:886–895.
68. Davalos-Misslitz, A. C. M, Rieckenberg, J., Willenzon, S., Worbs, T., Kremmer, E., Bernhardt, G., and Förster R. (2007) Generalized multi-organ autoimmunity in CCR7-deficient mice. Eur. J. Immunol. 37:613–622.
69. Rodewald, H. R., Paul, S., Haller, C., Bluethmann, H., and Blum, C. (2001) Thymus medulla consisting of epithelial islets each derived from a single progenitor. Nature (Lond) 414:763–768.
70. Weih, F., Carrasco, D., Durham, S. K., Barton, D. S., Rizzo, C. A., Ryseck, R. P., Lira, S. A., and Bravo, R. (1995) Multiorgan inflammation and hematopoietic abnormalities in mice with a targeted disruption of RelB, a member of the NF-kB/Rel family. Cell 80:331–340.
71. DeKoning, J., DiMolfetto, L., Reilly, C., Wei, Q., Havran, W., and Lo, D. (1997) Thymic cortical epithelium is sufficient for the development of mature T cells in relB-deficient mice. J. Immunol. 158:2558–2566.
72. Boehm, T., Scheu, S., Pfeffer, K., and Bleul, C. C. (2003) Thymic medullary epithelial cell differentiation, thymocyte emigration, and the control of autoimmunity require lympho-epithelial cross talk via LTbR. J. Exp. Med. 198:757–769.
73. Heath, V. L., Moore, N. C., Parnell, S. M., and Mason, D.W. (1998) Intrathymic expression of genes involved in organ specific autoimmune disease. J. Autoimmun. 11:309–318.
74. Klein, L., Klein, T., Rüther, U., and Kyewski, B. (1998) CD4 T cell tolerance to human C-reactive protein, an inducible serum protein, is mediated by medullary thymic epithelium. J. Exp. Med. 188:5–16.
75. Sospedra, M., Ferrer-Francesch, X., Domínguez, O., Juan, M., Foz-Sala, M., and Pujol-Borrell, R. (1998) Transcription of a broad range of self-antigens in human thymus suggests a role for central mechanisms in tolerance toward peripheral antigens. J. Immunol. 161:5918–5929.

76. Werdelin, O., Cordes, U., and Jensen, T. (1998) Aberrant expression of tissue-specific proteins in the thymus: a hypothesis for the development of central tolerance. Scand. J. Immunol. 47:95–100.
77. Klein, L., Klugmann, M., Nave, K. A., Tuohy, V.K., and Kyewski, B. (2000) Shaping of the autoreactive T-cell repertoire by a splice variant of self protein expressed in thymic epithelial cells. Nat. Med. 6:56–61.
78. Derbinski, J., Schulte, A., Kyewski, B., and Klein, L. (2001) Promiscuous gene expression in medullary thymic epithelial cells mirrors the peripheral self. Nat. Immunol. 2:1032–1039.
79. Heino, M., Peterson, P., Kudoh, J., Nagamine, K., Lagerstedt, A., Ovod, V., Ranki, A., Rantala, I., Nieminen, M., Tuukkanen, J., Scott, H. S., Antonarakis, S. E., Shimizu, N., and Krohn, K. (1999) Autoimmune regulator is expressed in the cells regulating immune tolerance in thymus medulla. Biochem. Biophys. Res. Commun. 257:821–825.
80. Heino, M., Peterson, P., Sillanpää, N., Guérin, S., Wu, L., Anderson, G., Scott, H. S., Antonarakis, S. E., Kudoh, J., Shimizu, N., Jenkinson, E. J., Naquet, P., and Krohn, K. J. (2000) RNA and protein expression of the murine autoimmune regulator gene (Aire) in normal, RelB-deficient and in NOD mouse. Eur. J. Immunol. 30:1884–1893.
81. Zuklys, S., Balciunaite, G., Agarwal, A., Fasler-Kan, E., Palmer, E., and Holländer, G. A. (2000) Normal thymic architecture and negative selection are associated with Aire expression, the gene defective in the autoimmune-polyendocrinopathy-candidiasis-ectodermal dystrophy (APECED) J. Immunol. 165:1976–1983.
82. Derbinski, J., Gäbler, J., Brors, B., Tierling, S., Jonnakuty, S., Hergenhahn, M., Peltonen, L., Walter, J., and Kyewski, B. (2005) Promiscuous gene expression in thymic epithelial cells is regulated at multiple levels. J. Exp. Med. 202:33–45.
83. Philpott, K. L., Viney, J. L., Kay, G., Rastan, S., Gardiner, E. M., Chae, S., Hayday, A. C., and Owen, M. J. (1992) Lymphoid development in mice congenitally lacking T cell receptor αβ-expressing cells. Science 256:1448–1452.
84. Surh, C. D., Ernst, B., and Sprent, J. (1992) Growth of epithelial cells in the thymic medulla is under the control of mature T cells. J. Exp. Med. 176:611–616.
85. Negishi, I., Motoyama, N., Nakayama, K., Nakayama, K., Senju, S., Hatakeyama, S., Zhang, Q., Chan, A. C., and Loh, D. Y. (1995) Essential role for ZAP-70 in both positive and negative selection of thymocytes. Nature (Lond) 376:435–438.
86. Nasreen, M., Ueno, T., Saito, F., and Takahama, Y. (2003) In vivo treatment of class II MHC-deficient mice with anti-TCR antibody restores the generation of circulating CD4 T cells and optimal architecture of thymic medulla. J. Immunol. 171:3394–3400.
87. Hikosaka, Y., Nitta, T., Ohigashi, I., Yano, K., Ishimaru, N., Hayashi, Y., Matsumoto, M., Matsuo, K., Penninger, J. M., Takayanagi, H., Yokota, Y., Yamada, H., Yoshikai, Y., Inoue, J., Akiyama, T., and Takahama, Y. (2008) The cytokine RANKL produced by positively selected thymocytes fosters medullary thymic epithelial cells that express autoimmune regulator. Immunity 29(3):438–450.
88. Rossi, S. W., Kim, M. Y., Leibbrandt, A., Parnell, S. M., Jenkinson, W. E., Glanville, S.H., McConnell, F. M., Scott, H. S., Penninger, J. M., Jenkinson, E. J., Lane, P. J., and Anderson, G. (2007) RANK signals from $CD4^{+}3^{-}$ inducer cells regulate development of Aire-expressing epithelial cells in the thymic medulla. J. Exp. Med. 204:1267–1272.
89. Anderson, G., Lane, P. J., and Jenkinson, E. J. (2007) Generating intrathymic microenvironments to establish T-cell tolerance. Nat. Rev. Immunol. 7:954–963.
90. White, A. J., Withers, D. R., Parnell, S. M., Scott, H. S., Finke, D., Lane, P. J., Jenkinson, E. J., and Anderson, G. (2008) Sequential phases in the development of Aire-expressing medullary thymic epithelial cells involve distinct cellular input. Eur. J. Immunol. 38:942–947.
91. Fuleihan, R., Ahern, D., and Geha, R. S. (1995) CD40 ligand expression is developmentally regulated in human thymocytes. Clin. Immunol. Immunopathol. 76:52–58.
92. Dunn, R. J., Luedecker, C. J., Haugen, H. S., Clegg, C. H., and Farr, A. G. (1997) Thymic overexpression of CD40 ligand disrupts normal thymic epithelial organization. J. Histochem. Cytochem. 45:129–141.
93. Clegg, C. H., Rulffes, J. T., Haugen, H. S., Hoggatt, I. H., Aruffo, A., Durham, S. K., Farr, A. G., and Hollenbaugh, D. (1997) Thymus dysfunction and chronic inflammatory disease in gp39 transgenic mice. Int. Immunol. 9:1111–1122.

94. Akiyama, T., Shimo, Y., Yanai, H., Qin, K., Ohshima, D., Maruyama, Y., Asaumi, Y., Kitazawa, J., Takayanagi, T., Penninger, J. M., Matsumoto, M., Nitta, T., Takahama, Y., and Inoue, J. (2008) The tumor necrosis factor family receptors RANK and CD40 cooperatively establish the thymic medullary microenvironment and self-tolerance. Immunity 29:423–437.
95. Hassall, A. H. (1849) The Microscopic Anatomy of the Human Body, in Health and Disease. Highley, London.
96. Symington, J. (1898) The thymus gland in the marsupialia. J. Anat. Physiol. 32(Pt 2):278–291.
97. Lewis, T. (1904) Observations upon the distribution and structure of haemolymph glands in mammalia and aves, including a preliminary note on the thymus. J. Anat. Physiol. 38(Pt 3):312–324.
98. Goodall, A. (1905) The post-natal changes in the thymus of guinea-pigs, and the effect of castration on thymus structure. J. Physiol. 32:191–198.
99. van den Brink, M. R., Alpdogan, O., Boyd, R. L. (2004) Strategies to enhance T-cell reconstitution in immunocompromised patients. Nat. Rev. Immunol. 4:856–867.
100. Gray, D. H., Ueno, T., Chidgey, A. P., Malin, M., Goldberg, G. L., Takahama, Y., and Boyd, R. L. (2005) Controlling the thymic microenvironment. Curr. Opin. Immunol. 17:137–143.

The Mechanisms of Motor Programming for Learned Vocalization in Songbirds

Hisataka Fujimoto, Taku Hasegawa, Ryosuke Matsui, Kentaro Abe, and Dai Watanabe

Introduction

Vocal signals, the fundamental interface for communication, convey information in their acoustic and temporal structures. Neural systems must extract the information from complex sequences of sound elements and, in turn, generate the motor commands for vocal sequences. Because humans acquire vocal communication after birth, the neural systems must establish a precise correspondence between sensory and motor representations of the vocal signals and control vocal behavior under the guidance of auditory information [1]. Recent advances in noninvasive technologies, such as functional magnetic resonance imaging (MRI) and positron emission tomography, have revealed brain areas involved in human vocal communication and imaged the metabolic signals reflecting their auditory–vocal association [2]. However, little is known about the neural processing that underlies sensory–motor integration for the learned vocal signals.

Songbirds, a diverse group of avian species classified as the order Passeriformes, provide an attractive model system. These avian species, much like humans, learn to imitate complex vocal signals of their elders during early life and maintain their spectral and temporal structures throughout their whole life [3–6]. Toward the understanding of the brain function to enable learned vocal communication, recent studies investigating the neural basis of songbird vocal behavior have been addressing a key issue: How do individual neurons establish sensory–motor correspondence for learned communication signals?

H. Fujimoto, T.Hasegawa, R.Matsui, K.Abe, and D.Watanabe
Department of Biological Sciences, Faculty of Medicine, and Department of Molecular and System Biology, Graduate School of Biostudies, Kyoto University, Yoshida, Sakyo-ku, Kyoto 606-8501, Japan

S. Nakanishi et al. (eds.), *Systems Biology*,
DOI:10.1007/978-4-431-87704-2_8, © Springer 2009

Neural Substrates for Learned Vocal Communication in Songbirds

In the songbird brain circuits, two subsystems play significant roles in the perception and expression of the learned vocal signals [7]. One subsystem is the telencephalic auditory system that comprises the primary and secondary auditory areas [8] (Fig. 1). Another subsystem is the song control system, a motor system specialized for learned vocalization [9], including the motor control pathway critical for vocal patterning [9,10] and the basal ganglia pathway necessary for audition-dependent vocal plasticity [11–13] (Fig. 1). The nucleus HVC (used as a proper name; formerly called the high vocal center), the hierarchically highest telencephalic motor area in the song control system, links the motor control pathway with the basal ganglia pathway (Fig. 1). Importantly, HVC receives input indirectly from the primary and secondary auditory areas [8,14] (Fig. 1). HVC could, therefore, serve essential functions as a sensorimotor integration site for vocal communication and as a gateway for auditory information flow into the song control system.

BOS Selectivity and Auditory Gating in the Vocal Control System

Because auditory feedback is required both before and after establishment of song vocalization [3,13,15–17], the neurons sensitive to self-generated vocalization could play an important role in learning and maintenance of the vocal signals [18].

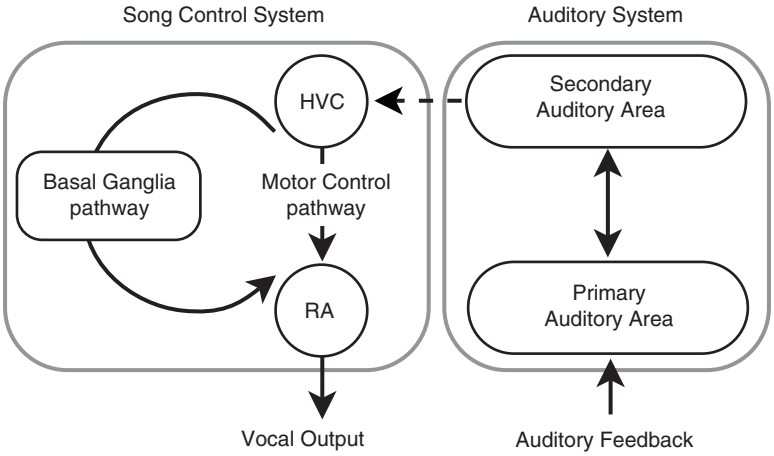

Fig. 1 Simplified diagram of the avian auditory system and song control system (*RA*, the robust nucleus of arcopallium). Not all nuclei of the song control system are shown

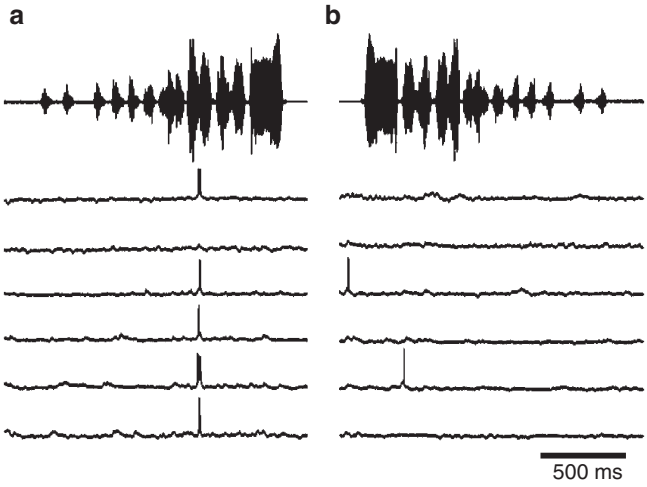

Fig. 2 Individual bird's own song (BOS)-selective response in the song control system. Auditory responses of a HVC neuron were recorded intracellularly under anesthetized states. Stereotyped time-locked spike bursts were evoked in the presence of BOS (**a**), whereas not in the presence of reversed song (**b**). *Upper traces* and the *lower six traces* represent auditory stimuli and membrane potentials, respectively

Neural recordings from an anesthetized songbird have revealed that neurons in the song control system display highly selective auditory response to the individual bird's own song (BOS) [19–24] (Fig. 2). Although neurons in the primary and secondary auditory areas also show activity in response to BOS playback [23,25], they preferentially respond to the conspecific song sequences rather than to the individual BOS [25,26]. At present, the precise origin of BOS selectivity remains unclear, but a distinct enhancement of BOS selectivity begins to emerge at the level of HVC in the song control system [23,27] (Fig. 2). The presence of the auditory selectivity to the self-generated vocal signals in HVC is consistent with the idea that HVC plays a critical part in the modification of motor commands for vocal signals under the guidance of auditory feedback.

Generally, single-neuron sensory responses can change depending on the states of the neural networks, reflecting the behavioral states of the animals [28]. It is, therefore, important to investigate the effects of behavioral state changes on auditory responses in the song control system. A remarkable state-dependency of the auditory response in the song control system was first demonstrated in HVC [29]; auditory responses of HVC neurons observed in anesthetized or sleep states are greatly suppressed to the same stimuli under awake unrestrained conditions [29]. Although mechanisms and functions of the state-dependent gating of auditory responses remain unknown, the absence of state-dependent modulation in the primary or secondary auditory areas indicates that auditory signaling is elaborately regulated in HVC [29], acting as the junction point between the auditory and song control system (Fig. 1). In addition, these findings emphasize the importance of

studying properties of high-order integrative neural systems, such as HVC, carefully under natural conditions [29–35].

Recording Neural Activity in Songbirds Under Natural Conditions

Characterizing the activities of individual neurons involved in songbird vocal communication poses some technical challenges. Song vocalization is a natural social behavior, and songbirds will sing only under unrestrained conditions. The device for measuring neural activities should be compact and lightweight so as not to disturb their communication behavior. Moreover, the positioning of electrodes should be remotely and flexibly manipulated to isolate single-neuron signals.

To overcome the difficulties in recording, various recording devices have been developed [30,32,35,36]. We have devised a miniature motorized microdrive system, whose basic design was previously described [36]. In brief, the microdrive system, which weighs less than 1.5 g, includes three motorized positioners and headstage preamplifiers. The individual electrodes are held by shuttles that travel along motor shafts. Each motor is equipped with a planetary gear system, whose reduction ratio is 337 to 1. As the result, the output torque is sufficient to drive shuttles, and the motion of each electrode is controlled with a positional resolution of less than 0.2 μm.

The Auditory–Vocal Association in HVC Neurons

On the basis of anatomical studies, HVC neurons are classified into three types: projection neurons that innervate telencephalic motor area, the robust nucleus of arcopallium (RA) (HVC_{RA} neurons) [9], projection neurons that extend their axons into basal ganglia area X (HVC_X neurons) [9], and interneurons.

Both HVC_{RA} neurons and HVC_X neurons are almost silent in awake nonsinging state and generate brief bursts of firing sparsely during vocalization [32,35,37]. The bursts of these projection neurons are highly stereotyped, tightly time-locked to the song sequences [32,37], suggesting that the robustness of the song vocalization is most likely to reflect this remarkable feature of the neural ensemble in HVC. Although HVC_{RA} neurons display no response to the auditory stimuli [35,37], a substantial proportion of HVC_X neurons respond selectively to the individual BOS playback [35]. Furthermore, the firing patterns of BOS-selective response observed in these HVC_X neurons are nearly identical to the firing patterns when the birds vocalize the same song sequences [35]. This observation raises the possibility that activity during singing is the result of auditory feedback. However, disruption of auditory feedback does not alter the pattern of this singing-related activity [35]. This evidence indicates that the activity in BOS-selective HVC_X neurons during vocalization carries not auditory feedback but motor-related information. Because HVC_X neurons project to the basal ganglia (Fig. 1), as is necessary for audition-dependent vocal

plasticity, the motor-related information represented in these neurons might be compared to the auditory feedback to improve vocal performance.

Both HVC_{RA} and HVC_{X} neurons are reciprocally interconnected with interneurons [38], which extend their axons locally within HVC. Because the activity and plasticity of the HVC_{RA} and HVC_{X} neurons are strictly regulated by GABA-mediated synaptic actions of these interneurons [38,39], it is of interest whether and how auditory information modulates GABA-mediated inhibition of the HVC interneurons. To address this question, we studied the interneuronal activity in HVC under awake unrestrained conditions using the microdrive system described above (Fujimoto, unpublished data).

HVC interneurons can be identified by their spontaneous activity in the awake nonsinging state [32,35,37]. A subclass of HVC interneurons displays tonic bursts of spiking in response to the BOS playback. The background spontaneous activities of these interneurons are greatly suppressed by auditory stimuli other than the individual BOS playback. Thus, the auditory responses observed in these HVC interneurons are BOS selective. In contrast to BOS-selective HVC_{X} neurons, the firing properties of these interneurons in singing behavior are quite different from those in sensory state. The BOS-selective interneurons become active before the onset of the song vocalization, and the burst firings continue until vocalization is terminated. BOS-selective HVC interneurons may, therefore, suppress the auditory information before onset of singing and act as a switch from the auditory state to the auditory-insensitive motor state.

Conclusions

Recent studies of songbird vocal communication have revealed that two types of neurons in the HVC, the telencephalic motor area for vocal behavior, display selective response to self-generated learned vocal signals. One is a subtype of projection neurons that transmit similar codes to the basal ganglia both in experiencing and in executing the learned vocal signals [35] (Fig. 1). The other is a subtype of interneurons that regulate local circuits differently between sensory phase and motor phase. Studies focusing on the connectivity, activity, and plasticity of these neuronal cell types will be helpful for the further understanding of the neural basis not only of songbird vocal behavior but also of human vocal communication.

Acknowledgments This work was supported by a grant from the Uehara Memorial Foundation.

References

1. Kuhl PK (1993) Developmental speech perception: implications for models of language impairment. Ann N Y Acad Sci 682:248–263.
2. Rizzolatti G, Craighero L (2004) The mirror-neuron system. Annu Rev Neurosci 27:169–192.
3. Konishi M (1965) The role of auditory feedback in the control of vocalization in the white-crowned sparrow. Z Tierpsychol 22:770–783.

4. Immelmann K (1969) Song development in the zebra finch and other estrildid finches. In: Hinde RA (ed) Bird Vocalizations. Cambridge University Press, Cambridge.
5. Doupe AJ, Kuhl PK (1999) Birdsong and human speech: common themes and mechanisms. Annu Rev Neurosci 22:567–631.
6. Tchernichovski O, Mitra PP, Lints T, Nottebohm F (2001) Dynamics of the vocal imitation process: how a zebra finch learns its song. Science 291:2564–2569.
7. Jarvis ED, Güntürkün O, Bruce L, Csillag A, Karten H, Kuenzel W, Medina L, Paxinos G, Perkel DJ, Shimizu T, Striedter G, Wild JM, Ball GF, Dugas-Ford J, Durand SE, Hough GE, Husband S, Kubikova L, Lee DW, Mello CV, Powers A, Siang C, Smulders TV, Wada K, White SA, Yamamoto K, Yu J, Reiner A, Butler AB, Avian Brain Nomenclature Consortium (2005) Avian brains and a new understanding of vertebrate brain evolution. Nat Rev Neurosci 6:151–159.
8. Reiner A, Perkel DJ, Bruce LL, Butler AB, Csillag A, Kuenzel W, Medina L, Paxinos G, Shimizu T, Striedter G, Wild M, Ball GF, Durand S, Güntürkün O, Lee DW, Mello CV, Powers A, White SA, Hough G, Kubikova L, Smulders TV, Wada K, Dugas-Ford J, Husband S, Yamamoto K, Yu J, Siang C, Jarvis ED, Gütürkün O, Avian Brain Nomenclature Forum (2004) Revised nomenclature for avian telencephalon and some related brainstem nuclei. J Comp Neurol 473:377–414.
9. Nottebohm F, Stokes TM, Leonard CM (1976) Central control of song in the canary, *Serinus canarius*. J Comp Neurol 165:457–486.
10. Vicario DS (1991) Organization of the zebra finch song control system: II. Functional organization of outputs from nucleus *Robustus archistriatalis*. J Comp Neurol 309:486–494.
11. Bottjer SW, Halsema KA, Brown SA, Miesner EA (1989) Axonal connections of a forebrain nucleus involved with vocal learning in zebra finches. J Comp Neurol 279:312–326.
12. Scharff C, Nottebohm F (1991) A comparative study of the behavioral deficits following lesions of various parts of the zebra finch song system: implications for vocal learning. J Neurosci 11:2896–2913.
13. Brainard MS, Doupe AJ (2000) Interruption of a basal ganglia-forebrain circuit prevents plasticity of learned vocalizations. Nature (Lond) 404:762–766.
14. Vates GE, Broome BM, Mello CV, Nottebohm F (1996) Auditory pathways of caudal telencephalon and their relation to the song system of adult male zebra finches. J Comp Neurol 366:613–642.
15. Leonardo A, Konishi M (1999) Decrystallization of adult birdsong by perturbation of auditory feedback. Nature (Lond) 399:466–470.
16. Sakata JT, Brainard MS (2006) Real-time contributions of auditory feedback to avian vocal motor control. J Neurosci 26:9619–9628.
17. Tumer EC, Brainard MS (2007) Performance variability enables adaptive plasticity of ‘crystallized’ adult birdsong. Nature (Lond) 450:1240–1244.
18. Konishi M (2004) The role of auditory feedback in birdsong. Ann N Y Acad Sci 1016:463–475.
19. McCasland JS, Konishi M (1981) Interaction between auditory and motor activities in an avian song control nucleus. Proc Natl Acad Sci U S A 78:7815–7819.
20. Doupe AJ, Konishi M (1991) Song-selective auditory circuits in the vocal control system of the zebra finch. Proc Natl Acad Sci U S A 88:11339–11343.
21. Margoliash D, Fortune ES (1992) Temporal and harmonic combination-sensitive neurons in the zebra finch’s HVc. J Neurosci 12:4309–4326.
22. Vicario DS, Yohay KH (1993) Song-selective auditory input to a forebrain vocal control nucleus in the zebra finch. J Neurobiol 24:488–505.
23. Lewicki MS, Arthur BJ (1996) Hierarchical organization of auditory temporal context sensitivity. J Neurosci 16:6987–6998.
24. Dave AS, Yu AC, Margoliash D (1998) Behavioral state modulation of auditory activity in a vocal motor system. Science 282:2250–2254.
25. Grace JA, Amin N, Singh NC, Theunissen FE (2003) Selectivity for conspecific song in the zebra finch auditory forebrain. J Neurophysiol 89:472–487.

26. Theunissen FE, Amin N, Shaevitz SS, Woolley SM, Fremouw T, Hauber ME (2004) Song selectivity in the song system and in the auditory forebrain. Ann N Y Acad Sci 1016:222–245.
27. Janata P, Margoliash D (1999) Gradual emergence of song selectivity in sensorimotor structures of the male zebra finch song system. J Neurosci 19:5108–5118.
28. Fontanini A, Katz DB (2008) Behavioral states, network states, and sensory response variability. J Neurophysiol 100:1160–1168.
29. Schmidt MF, Konishi M (1998) Gating of auditory responses in the vocal control system of awake songbirds. Nat Neurosci 1:513–518.
30. Hessler NA, Doupe AJ (1999) Singing-related neural activity in a dorsal forebrain-basal ganglia circuit of adult zebra finches. J Neurosci 19:10461–10481.
31. Luo M, Fee MS, Katz LC (2003) Encoding pheromonal signals in the accessory olfactory bulb of behaving mice. Science 299:1196–1201.
32. Hahnloser RH, Kozhevnikov AA, Fee MS (2002) An ultra-sparse code underlies the generation of neural sequences in a songbird. Nature (Lond) 419:65–70.
33. Leonardo A (2004) Experimental test of the birdsong error-correction model. Proc Natl Acad Sci U S A 101:16935–16940.
34. Leonardo A, Fee MS (2005) Ensemble coding of vocal control in birdsong. J Neurosci 25:652–661.
35. Prather JF, Peters S, Nowicki S, Mooney R (2008) Precise auditory-vocal mirroring in neurons for learned vocal communication. Nature (Lond) 451:305–310.
36. Fee MS, Leonardo A (2001) Miniature motorized microdrive and commutator system for chronic neural recording in small animals. J Neurosci Methods 112:83–94.
37. Kozhevnikov AA, Fee MS (2007) Singing-related activity of identified HVC neurons in the zebra finch. J Neurophysiol 97:4271–4283.
38. Mooney R, Prather JF (2005) The HVC microcircuit: the synaptic basis for interactions between song motor and vocal plasticity pathways. J Neurosci 25:1952–1964.
39. Rosen MJ, Mooney R (2003) Inhibitory and excitatory mechanisms underlying auditory responses to learned vocalizations in the songbird nucleus HVC. Neuron 39:177–194.

Dynamic Model of the Basal Ganglia Functions and Movement Disorders

Atsushi Nambu

Introduction

For control of voluntary movements, interactions between the cerebral cortex and the basal ganglia through the corticobasal ganglia loop are essential. The basal ganglia receive cortical inputs, process the information, and send it back to the original cerebral cortex via the thalamus to assist cortical activity (Fig. 1). The internal segment of the globus pallidus (GPi) and the substantia nigra pars reticulata (SNr) are the output nuclei of the basal ganglia. On the other hand, the striatum is the input station and receives direct excitatory cortical inputs. In the current model of basal ganglia organization, the striatum projects to the output nuclei, via two major projection systems, the *direct* and *indirect* pathways [2]. The direct pathway arises from GABAergic striatal neurons containing substance P and projects monosynaptically to the GPi/SNr. The indirect pathway arises from GABAergic striatal neurons containing enkephalin and projects polysynaptically to the GPi/SNr by way of a sequence of connections involving the external segment of the globus pallidus (GPe) and subthalamic nucleus (STN).

Cortico-STN-GPi/SNr *Hyperdirect* Pathway

The cerebral cortex projects topographically to the STN, as well as to the striatum [8,17]. Thus, recent studies propose the idea that the STN is another input station of the basal ganglia, forming the cortico-STN-GPi/SNr *hyperdirect* pathway [19], whose conduction velocity is faster than those of the direct and indirect pathways (Fig. 1). Indeed, stimulation of the motor cortices induces an early, short-latency excitation, followed by an inhibition and a late excitation in monkey GPe, GPi, and

A. Nambu
Division of System Neurophysiology, National Institute for Physiological Sciences, and Department of Physiological Sciences, Graduate University for Advanced Studies (SOKENDAI), 38 Nishigonaka, Myodaiji, Okazaki 444-8585, Japan

S. Nakanishi et al. (eds.), *Systems Biology*,
DOI:10.1007/978-4-431-87704-2_9, © Springer 2009

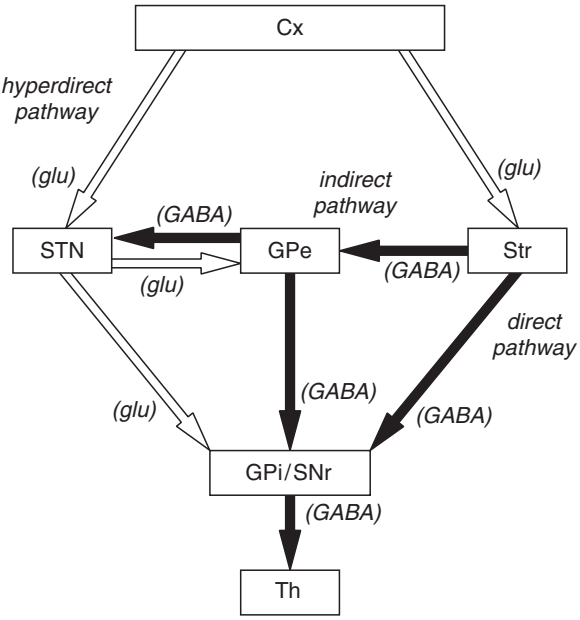

Fig. 1 Basic circuitry of the basal ganglia, comprising the Cx-STN-GPi/SNr *hyperdirect*, Cx-Str-GPi/SNr *direct*, and Cx-Str-GPe-STN-GPi/SNr *indirect* pathways. *Open* and *filled arrows* represent excitatory glutamatergic (*glu*) and inhibitory GABAergic (*GABA*) projections, respectively. *Cx*, cerebral cortex; *GPe*, external segment of the globus pallidus; *GPi*, internal segment of the globus pallidus; *SNr*, substantia nigra pars reticulata; *STN*, subthalamic nucleus; *Str*, striatum; *Th*, thalamus. (Modified from [19])

SNr neurons [12,18,21,23]. The early excitation in the GPi is derived from the cortico-STN-GPi/SNr hyperdirect pathway, whereas the inhibition and late excitation are mediated by the cortico-striato-GPi/SNr direct and cortico-striato-GPe-STN-GPi/SNr indirect pathways, respectively.

Activity of GPi Neurons

The GPi receives topographical inputs from the cerebral cortex through the hyperdirect, direct, and indirect pathways. GPi neurons in the forelimb region of the motor territory (ventral two-thirds of caudal GPi) change their activity, either inhibitory or excitatory, relating to forelimb movements [6,7,20,22]. These changes are presumably the result of the combination of inhibitory GABAergic inputs from the striatum, and excitatory glutamatergic inputs from the STN, which reflects the flow of information through the direct, indirect, and hyperdirect pathways. We do not know much about the extent of the contribution of each input to GPi activity during movements. However, an interesting finding is that GPi activity during voluntary limb movements always displays an increase rather than a decrease in discharge [6,7,20,22], suggesting a large contribution of inputs from the STN.

Dynamic Model of the Basal Ganglia Functions

GPi/SNr neurons are GABAergic and fire at high frequency; thus, neurons in their target structures, such as the thalamus, are inhibited continuously (Fig. 2). When striatal neurons are activated by cortical inputs, the striatal neurons inhibit GPi/SNr activity through the striato-GPi/SNr direct pathway. The continuous inhibition from the output nuclei to the target structures is transiently removed (disinhibition), and thalamic neurons are activated. The increased activity of the thalamus is transmitted to the motor cortex, and finally evokes a selected motor program. On the other hand, signals through the hyperdirect and indirect pathways have excitatory effects on the GPi/SNr and thus have inhibitory effects on thalamic neurons. Considering the respective axonal conduction velocities, signals through the hyperdirect pathway first actively inhibit thalamic neurons, then those through the direct pathway disinhibit them, and finally those through the indirect pathway inhibit them again. Thus, signals through the hyperdirect and indirect pathways make clear initiation and termination of the selected motor program [19].

In addition to such a temporal aspect, the enhancement by differential inputs through the hyperdirect, direct, and indirect pathways may work in a spatial domain as well. The *center-surround model* of basal ganglia functions proposes focused selection of an appropriate motor program and inhibition of competing motor

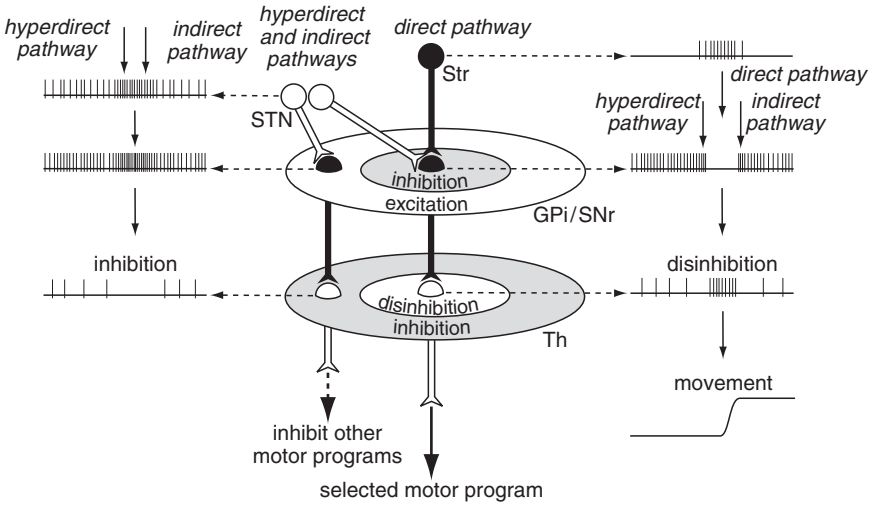

Fig. 2 Spatial and temporal distributions of basal ganglia activity during voluntary movements based on the dynamic model. Signals through the *direct pathway* inhibit GPi neurons in the center area, activate thalamic neurons by disinhibition, and finally release a selected motor program. On the other hand, signals through the *hyperdirect* and *indirect pathways* have broad excitatory effects on *GPi* neurons in temporal and spatial domains, make clear initiation and termination of the selected motor program, and inhibit other unnecessary competing motor programs. *Open* and *filled* neurons represent excitatory glutamatergic and inhibitory GABAergic neurons, repectively. *STN*, subthalamic nucleus; *Str*, striatum. (Modified from [16])

programs [10,14,15,19] (Fig. 2). Thalamic neurons are usually inhibited by continuous GABAergic inputs from the GPi. Signals through the direct pathway inhibit a specific group of GPi neurons in the center area, and thalamic and cortical neurons are released from inhibition and become active, resulting in the release of the selected motor program. On the other hand, signals through the hyperdirect and indirect pathways excite other groups of GPi neurons in the surrounding area and increase inhibition on thalamic neurons that mediate other competing motor programs. Inhibition in the center area of the GPi by striatal GABAergic inputs and excitation in the surrounding area by glutamatergic STN inputs coordinate the execution of the selected motor program and the inhibition of other competing motor programs.

Based on the *temporal* and *spatial* inputs to the target structures through the hyperdirect, direct, and indirect pathways, only the selected motor program is executed at the selected timing, and other competing motor programs are canceled.

Pathophysiology of Movement Disorders

The neural mechanisms underlying hypokinetic and hyperkinetic movement disorders are currently explained as changes in the *static* state of the basal ganglia by the standard model. The impaired balance of activity between the direct and indirect pathways causes an increase or decrease in the mean firing rate of GPi/SNr neurons [1,5]. For example, in Parkinson's disease, activity through the indirect pathway is increased and activity through the direct pathway is reduced. Both changes enhance the mean firing rate of GPi/SNr neurons, suppress the activity of thalamic and cortical neurons, and finally cause akinesia. On the other hand, in dystonia, activity through both direct and indirect pathways is increased, reduces the mean firing rate of GPi/SNr neurons, excites the activity of thalamic and cortical neurons by disinhibitory mechanism, and finally causes involuntary movements.

The dynamic model can better explain the pathophysiology of hypokinetic and hyperkinetic movement disorders by introducing the temporal and spatial aspects of the basal ganglia functions (Fig. 3). In normal monkeys, cortical stimulation evokes a triphasic response composed of an early excitation, an inhibition, and a late excitation in GPi neurons. In monkeys rendered parkinsonian by infusion of 1-methyl-4-phenyl-1,2,3,6-tetrahydropyridine (MPTP), the duration of the inhibition in GPi neurons evoked by cortical stimulation is reduced, and the amplitude of early and late excitations is increased. The intravenous injection of L-DOPA transiently improves parkinsonian akinesia, and the cortically evoked response pattern in the GPi is restored to the normal triphasic pattern. These observations suggest that in parkinsonian state, when a voluntary movement is about to be initiated by cortical mechanisms, signals through the hyperdirect and indirect pathways expand and suppress larger areas of the thalamus and cortex than in the normal state, and a signal through the direct pathway is reduced (Fig. 3, left). Thus, smaller areas of the thalamus and cortex are disinhibited for a shorter period of time than in the normal state, and not only the competing motor program, but also the selected motor program, cannot be released, resulting in the akinesia of Parkinson's disease.

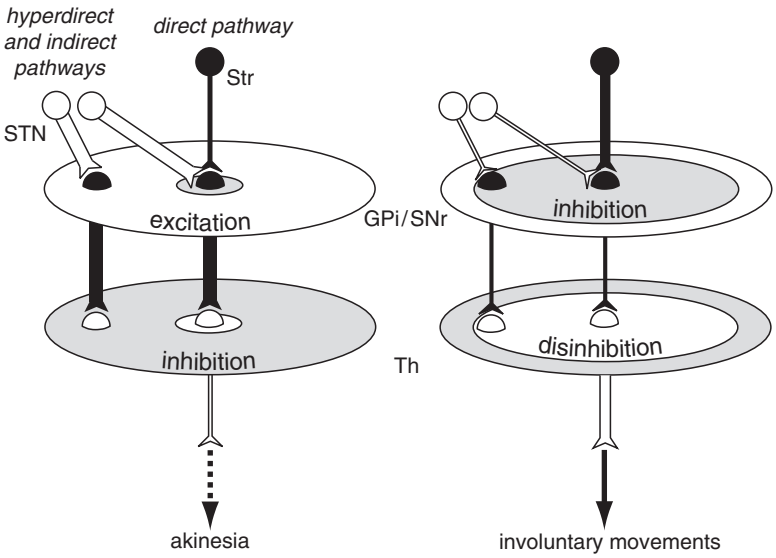

Fig. 3 Schematic diagram showing the activity changes in the basal ganglia during movement disorders. Increased signals through the *hyperdirect and indirect pathways* and a reduced signal through the *direct pathway* result in reduced disinhibition in the Th/Cx, leading to hypokinetic disorders (*left*). An increased signal through the direct pathway and reduced signals through the hyperdirect and indirect pathways result in increased disinhibition in the Th/Cx, leading to the involuntary movements observed in hyperkinetic disorders (*right*)

On the other hand, cortical stimulation produces long inhibitions in the GPe/GPi of monkeys during hemiballism, which is induced by STN blockade. In the transgenic mouse model of dystonia, cortical stimulation also induces a long-lasting inhibition in the GPe/GPi [4]. Thus, cortically evoked a long-lasting inhibition is considered to be a common feature of hyperkinetic disorders. Even a tiny neuronal activity originating in the cortex is transmitted through the basal ganglia circuitry and finally induces a strong and long-lasting inhibition in the wide areas of the GPi (Fig. 3, right). Therefore, the wide areas of the thalamus and cortex that mediate both the selected and competing motor programs are activated in an uncontrollable manner, resulting in the involuntary movements observed in hyperkinetic disorders.

Mechanism of the Effectiveness of Stereotaxic Surgery

Recent advances in stereotaxic surgery have highlighted the STN as a target structure. In monkeys and humans, a lesion or high-frequency stimulation (HFS) of the STN can ameliorate parkinsonian motor symptoms [3,9,11,13]. In our experiments, blockade of STN activity by the local injection of $GABA_A$ agonist muscimol also improves the motor activity of parkinsonian monkeys. The blockade of the STN diminishes the early and late excitations evoked by cortical stimulation and prolongs the duration of the inhibition in the GPi. According to the dynamic model, the main

cause of akinesia is a reduced disinhibition in the thalamus and cortex during movements. The blockade of the STN restores the disinhibition in the cortex and thalamus during movement, and releases the selected motor program. On the other hand, the mechanism of STN-HFS is not clear, and whether HFS excites or inhibits STN neuronal activity is open to argument [13].

Concluding Remarks

I have introduced the dynamic model of the basal ganglia functions: Information through the hyperdirect, direct and indirect pathways dynamically controls the activity of the thalamus and cortex, and releases only the selected motor program at the selected timing. The dynamic model can also explain the pathophysiology of movement disorders and the mechanism of the effectiveness of stereotaxic surgery. The dynamic model will lead us not only to better understanding of the normal functions of the basal ganglia, but also to better treatment of movement disorders.

Acknowledgments This study was supported by the Uehara Memorial Foundation and Grants-in-Aid for Scientific Research (B) from the Ministry of Education, Culture, Sports, Science and Technology of Japan.

References

1. Albin RL, Young A B, Penney, JB (1989) The functional anatomy of basal ganglia disorders. Trends Neurosci 12:366–375
2. Alexander GE, Crutcher MD (1990) Functional architecture of basal ganglia circuits: neural substrates of parallel processing. Trends Neurosci 13:266–271
3. Bergman H, Wichmann T, DeLong MR (1990) Reversal of experimental parkinsonism by lesions of the subthalamic nucleus. Science 249:1436–1438
4. Chiken S, Shashidharan P, Nambu A (2008) Cortically evoked long-lasting inhibition of pallidal neurons in a transgenic mouse model of dystonia. J Neurosci 28:13967–13977
5. DeLong MR (1990) Primate models of movement disorders of basal ganglia origin. Trends Neurosci 13:281–285
6. Georgopoulos AP, DeLong MR, Crutcher MD (1983) Relations between parameters of step-tracking movements and single cell discharge in the globus pallidus and subthalamic nucleus of the behaving monkey. J Neurosci 3:1586–1598
7. Hamada I, DeLong MR, Mano N (1990) Activity of identified wrist-related pallidal neurons during step and ramp wrist movements in the monkey. J Neurophysiol 64:1892–1906
8. Hartmann-von Monakow K, Akert K, Künzle H (1978) Projections of the precentral motor cortex and other cortical areas of the frontal lobe to the subthalamic nucleus in the monkey. Exp Brain Res 33:395–403
9. Hashimoto T, Elder CM, Okun MS, Patrick SK, Vitek JL (2003) Stimulation of the subthalamic nucleus changes the firing pattern of pallidal neurons. J Neurosci 23:1916–1923
10. Hikosaka O, Takikawa Y, Kawagoe R (2000) Role of the basal ganglia in the control of purposive saccadic eye movements. Physiol Rev 80:953–978

11. Jahanshahi M, Ardouin CMA, Brown RG, Rothwell JC, Obeso J, Albanese A, Rodriguez-Oroz MC, Moro E, Benabid AL, Pollak P, Limousin-Dowsey P (2000) The impact of deep brain stimulation on executive function in Parkinson's disease. Brain 123:1142–1154
12. Kita H, Nambu A, Kaneda K, Tachibana Y, Takada M (2004) Role of ionotropic glutamatergic and GABAergic inputs on the firing activity of neurons in the external pallidum in awake-monkeys. J Neurophysiol 92:3069–3084
13. Lozano AM, Dostrovsky J, Chen R, Ashby P (2002) Deep brain stimulation for Parkinson's disease: disrupting the disruption. Lancet Neurol 1:225–231
14. Mink JW (1996) The basal ganglia: focused selection and inhibition of competing motor programs. Prog Neurobiol 50:381–425
15. Mink JW, Thach WT (1993) Basal ganglia intrinsic circuits and their role in behavior. Curr Opin Neurobiol 3:950–957
16. Nambu A (2007) Globus pallidus internal segment. In: Tepper JM, Abercrombie ED, Bolam JP (eds) GABA and the Basal Ganglia: From Molecules to Systems. Progress in Brain Research, vol 160. Elsevier, Amsterdam, pp 135–150
17. Nambu A, Takada M, Inase M, Tokuno H (1996) Dual somatotopical representations in the primate subthalamic nucleus: evidence for ordered but reversed body-map transformations from the primary motor cortex and the supplementary motor area. J Neurosci 16:2671–2683
18. Nambu A, Tokuno H, Hamada I, Kita H, Imanishi M, Akazawa T, Ikeuchi Y, Hasegawa N (2000) Excitatory cortical inputs to pallidal neurons via the subthalamic nucleus in the monkey. J Neurophysiol 84:289–300
19. Nambu A, Tokuno H, Takada M, (2002) Functional significance of the cortico-subthalamo-pallidal "hyperdirect" pathway. Neurosci Res 43:111–117
20. Nambu A, Yoshida S, Jinnai K (1990) Discharge patterns of pallidal neurons with input from various cortical areas during movement in the monkey. Brain Res 519:183–191
21. Tachibana Y, Kita H, Chiken S, Takada M, Nambu A (2008) Motor cortical control of internal pallidal activity through glutamatergic and GABAergic inputs in awake monkeys. Eur J Neurosci 27:238–253
22. Turner RS, Anderson ME (1997) Pallidal discharge related to the kinematics of reaching movements in two dimensions. J Neurophysiol 77:1051–1074
23. Yoshida S, Nambu A, Jinnai K (1993) The distribution of the globus pallidus neurons with input from various cortical areas in the monkey. Brain Res 611:170–174

A Posttranslational Chemical Circadian Oscillator in Cyanobacteria

Hideo Iwasaki

Introduction

To understand dynamic biological behaviors at the system level in the "post-genome" era, it is important to elucidate the complicated molecular network generating biological information in addition to classical analysis on a single gene–function relationship. Periodic temporal (rhythmic) and spatial (morphological) pattern formations are both typical examples of dynamic and complex phenomena widely observed in organisms from bacteria to plants and humans. To elucidate such spatiotemporal dynamics at the molecular systems level, integration of molecular genetics, molecular biology, biochemistry, comprehensive genomic and post-genomic approaches, quantitative analyses, and mathematical considerations is necessary. In addition, synthetic biological approaches to reconstitute such phenomena in vitro and/or in vivo are also helpful to validate reality and find problems in the proposed molecules or models. For this type of analysis, we have analyzed cyanobacteria as one of the simplest organisms to exhibit circadian rhythms and regular pattern formations with cell differentiation. Here, I summarize a brief history and the current state of molecular, biochemical, and synthetic analysis on the cyanobacterial circadian clock and refer to some prospects on extensive researches on morphological development in filamentous cyanobacteria.

Circadian Rhythms

Life is full of a variety of rhythms, such as brain waves, calcium waves, metabolic oscillations, respiration rhythms, heart rate, the sleep/wake cycle, and annual cycles of flowering and reproduction. This variety is most likely because rhythmicity can

H. Iwasaki
Department of Electrical Engineering & Bioscience, Waseda University, and PRESTO, Japan Science & Technology Agency (JST), 2-2 Wakamatsu-cho, Shinjuku, Tokyo 162-8480, Japan

S. Nakanishi et al. (eds.), *Systems Biology*,
DOI:10.1007/978-4-431-87704-2_10,

be the origin of a variety of biological functions and information. First, autonomous reproduction or propagation per se is essentially periodic. It is inevitable because it is a replicating process based on rebuilding something that takes some time (or time delay). Second, rhythmicity enables biological processes to occur at their proper timing, thereby prohibiting mix-ups in complicated reaction networks. Rhythms may be important as a basis for frequency responses, even in biological informatics. Recent studies suggest that frequency responses are observed not only in higher-order brain informative processes but also in cellular signal transduction (see chapter by Dr. Shinya Kuroda). Third, rhythms are recursive and, therefore, predictable. Thus, they are useful tools to predict and adapt to periodic environmental changes such as day/night alternation and seasonal cycles. Circadian, circatidal, and circannual rhythms are typical examples of such biological oscillations.

Circadian rhythm, an endogenous oscillation with a period of ~24 h, is one of the most intensively analyzed biological oscillations. It is observed in cellular, physiological, behavioral, and population parameters, which are ubiquitously observed in many organisms. Circadian rhythms are characterized by three features. First, the rhythms persist even in the absence of external cues with a period length (free-running period) that is close to, but not always exactly equal to, the 24-h period of the earth's rotation. Second, circadian rhythms can be entrained to the external earth's cycles, such as the predictable alternation of light and dark. Third, the period length is relatively stable at different constant temperatures: that is, the free-running period is temperature compensated. All these features support the idea that circadian clocks are physiologically significant for organisms as adaptive systems to daily changes in environmental conditions on the earth, such as light, temperature, and humidity. Furthermore, the circadian clock is suggested as a fundamental basis of photoperiodic behavior in plants, insects and mammals). In humans, circadian clocks are involved in many physiological regulations, such as the wake/sleep cycle, hormone secretions, and body temperature. Such a human circadian control has recently become a medical consequence, because a loss of clock function causes depression, jet lag, or insomnia.

Schematically, the circadian organization can be considered to be organized by three elements: the circadian oscillator that generates basic oscillation, input pathways that transfer external environmental information to the oscillator, and output pathways from the oscillator which regulate many temporal events. Among them, here I focus on the molecular mechanism of the circadian oscillator in cyanobacteria.

Molecular Model of the Circadian Oscillator: A Transcription-Translation-Based Oscillator (TTO) Model

Circadian rhythms are observed in unicellular organisms and even in an isolated nerve cell. Thus, the circadian clock consists of an intracellular molecular network. Molecular genetics of circadian clocks started from isolation of three *Drosophila*

eclosion rhythm mutants and mapping them to a single genomic locus named *period* (*per*) in 1971 (Konopka and Benzer, 1971). It took 19 years, however, to develop the experimental suggestion of the first molecular model for the *per* gene function in circadian rhythm generation (Hardin et al., 1990). This model is based on a rhythmic expression of a clock gene itself via an autofeedback control in which the clock gene expression is negatively inhibited by its own translational product (clock protein) with a time delay (transcription-translation feedback oscillator model; TTO model). Retrospectively, this type of transcription rhythms was theoretically proposed for the first time in 1965 by Goodwin (Goodwin, 1965), which required 25 years to obtain experimental validation at the level of molecular biology. After the first *per* model, many more factors and reactions have been found and therefore the models have become much more complicated (e.g., Ueda et al., 2005; see also chapter by Dr. Hiroki R. Ueda). For example, to ensure such a long-period rhythmicity, it was suggested that a time lag was important between cytosolic accumulation of PER protein and suppression of its own transcription in the nucleus. Accordingly, the stability of PER protein is likely regulated by multiple pathways including complex formation, phosphorylation, and ubiquitination.

Interestingly, amino acid sequences of clock proteins are not conserved among animals, plants, fungi, and bacteria. Nevertheless, the TTO model has become a milestone in not only circadian clock research in any organisms (reviewed by Dunlap, 2004) but also in developmental clock in somitogenesis (Hirata et al., 2002). However, we have found an alternative mechanism to generate circadian oscillation in cyanobacteria, which persisted even after complete elimination of transcription and translation reactions (Tomita et al., 2005).

Dilemma in Diazotrophic Cyanobacteria and Adaptive Periodic Spatiotemporal Pattern Formations

Among many model organisms, cyanobacteria, the simplest organisms to exhibit circadian rhythms, have become intensively analyzed to address fundamental questions in circadian biology. How was such a prokaryotic circadian control discovered in nature?

Several cyanobacterial strains are able to fix molecular nitrogen, as are some other prokaryotic organisms. A key enzyme for this reaction, nitrogenase, is extremely sensitive to oxygen that is inevitably generated by photosynthesis. Therefore, nitrogen-fixing (diazotrophic) Cyanobacteria have developed two different strategies to divide the contradictory metabolic pathways. One is a spatial separation of two metabolisms specifically adopted in filamentous (multicellular) diazotrophic cyanobacteria that differentiate a cell specialized for nitrogen fixation, named the heterocyst. The heterocyst shuts off photosystem II (PSII) activity and induces the nitrogenase protein, in contrast to the vegetative cells producing oxygen through full-chain photosynthesis. Interestingly, the spatial pattern of heterocyst development varies among cyanobacterial stains. Most noticeably, *Anabaena* (*Nostoc*) sp. PCC

7120, a genetically tractable filamentous strain, develops the heterocyst at every 8–12 cells in dividing filaments. Thus, heterocyst formation can be an interesting model system to analyze spatial pattern formation with bona fide cell differentiation.

However, this design cannot explain the ability of fixing nitrogen and oxygenic photosynthesis in unicellular or nonheterocystous diazotrophic cyanobacteria. An alternative strategy, "temporal separation," has been proposed for these cyanobacteria. In 1985, nitrogenase activity in the nonheterocystous, filamentous cyanobacterium *Oscillatoria* sp. was shown to exhibit daily rhythms peaking at night that persisted even after transfer to continuous light (LL) conditions (Stal and Krumbein, 1985). Thereafter, two other groups also reported robust daily oscillation of nitrogenase activity in unicellular cyanobacteria under constant conditions (Mitsui et al., 1986; Grobbelaar et al., 1986). Especially, Huang and colleagues were the first researchers who realized the cause was endogenous circadian oscillation, as reported for eukaryotes (Grobbelaar et al., 1986).

Cyanobacterial Circadian Clock Mechanism: Ticking Time Beyond TTO

Among the many cyanobacterial strains, *Synechococcus elongatus* PCC 7942 is most intensively analyzed in circadian biology because this strain is genetically tractable and exhibits highly reproducible high-amplitude gene expression rhythms monitored by a bioluminescence reporter (Fig. 1; Kondo et al., 1993; Iwasaki and Dunlap, 2000; Iwasaki and Kondo, 2000; Iwasaki and Kondo, 2004). Note that this strain is not a diazotrophic strain and cannot fix nitrogen. Interestingly, by promoter-trap analysis, this strain shows circadian rhythms in essentially all gene promoter activities (Liu et al., 1995). Cyanobacterial transcription rhythms require each of three clock

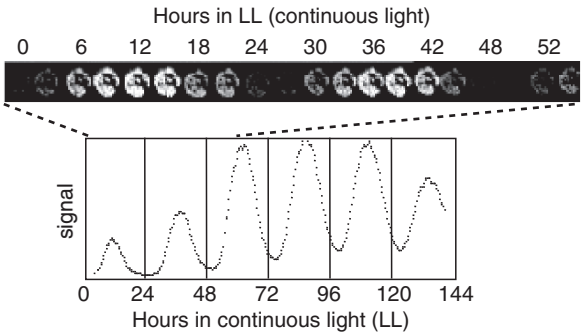

Fig. 1 Circadian *kaiBC* promoter activity rhythm monitored by a bioluminescence reporter under continuous light (*LL*) conditions. The *kaiBC* promoter was fused to a promoter-less bacterial luciferase operon, *luxAB*, from *Vibrio harveyi*, and introduced into *Synechococcus elongatus*. The transformed cells were grown on solid media under the light, transferred to the dark for 12 h to reset the clock, returned to continuous light (*LL*) conditions, and then subjected to bioluminescence monitoring using a cooled charge-coupled device (-CCD) camera or photomultiplier tubes

genes, *kaiA*, *kaiB*, and *kaiC*, which form a gene cluster (Ishiura et al., 1998). *kai* means "cycle" in Japanese, and many clock mutations with a period ranging from 14 to 80 h, and even arrhythmia, have been mapped to the *kai* genes. *kaiB* and *kaiC* form an operon to be coexpressed in a circadian fashion with very high amplitude. Note that, differing from eukaryotic clock proteins such as CLOCK and BMAL1 (CYCLE), all Kai proteins lack DNA-binding motifs. However, overexpression of *kaiC* suppresses its own transcription to be arrhythmic. Disruption and overexpression of *kaiA* suppresses and enhances *kaiBC* expression level, respectively. Based on these genetic experiments, Ishiura et al. (1998) proposed that circadian *kaiBC* expression is based on an autoregulatory feedback mechanism in which KaiC negatively regulates its own transcription, whereas KaiA activates it. This scheme is essentially the same as the classical TTO mechanism proposed for eukaryotic clocks.

Nevertheless, we found that circadian rhythm in the phosphorylation state of KaiC protein persisted after transfer to continuous darkness (DD), under which *kai* gene transcription was completely suppressed even in the presence of excess amounts of transcription/translation inhibitors (Fig. 2; Tomita et al., 2005). Importantly, the

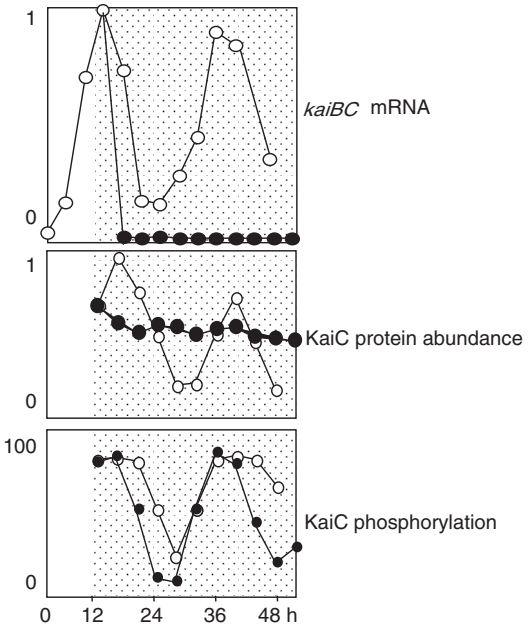

Fig. 2 KaiC phosphorylation cycle in the absence of transcription/translation feedback. Under continuous light (LL) conditions (*open circles*), mRNA from the *kaiBC* operon (*top*) exhibits a high-amplitude circadian rhythm, and the level of KaiC protein accumulation (*middle*) and the magnitude of KaiC phosphorylation (*bottom*) also cycle in a circadian fashion with a delay by several hours. When cells are transferred from hour 12 in the light to continuous darkness (DD) (*filled circles*), most of the mRNAs including *kaiA* and *kaiBC* transcripts were dramatically and immediately nullified to an undetectable level. Interestingly, the KaiA, KaiB, and KaiC proteins become stabilized in the dark to be constantly (arrhythmically) present without de novo protein synthesis. Nevertheless, the KaiC phosphorylation cycle persisted normally. Note that this KaiC phosphorylation rhythm in DD is not affected at all in the presence of an excess amount of transcription/translation inhibitors

period length of the circadian KaiC phosphorylation rhythm under DD was temperature compensated and affected by known clock mutations mapped to the *kai* genes, as was observed under continuous light (LL) conditions. This finding was the first experimental evidence of circadian control that is not dependent on the TTO scheme.

More dramatically, Nakajima et al. (2005) succeeded in reconstitution of the KaiC phosphorylation cycle in vitro by simply incubating KaiA, KaiB, and KaiC recombinant proteins at an appropriate molecular ratio in the presence of ATP. Again, the period of the in vitro reconstituted KaiC phosphorylation rhythm is temperature compensated, and the period in bioluminescence in particular *kai* mutants is consistent with the period in the in vitro phosphorylation cycle using the same mutant variants of KaiC (Nakajima et al. 2005). Therefore, it was concluded that this posttranslational oscillation is the core to the temporal integration of the cyanobacterial circadian system. This observation is particularly important because it was the first experiment to determine a "sufficient condition (factors)" for driving circadian rhythms. Conversely, molecular genetic approaches have been powerful tools to identify molecules essential for rhythm generation, i.e., to search for the "necessary condition." It was surprising that such a robust and long period oscillation as circadian rhythms was based on a chemical network composed of only three kinds of proteins. Although autocatalytic chemical oscillations such as Belousov–Zhabotinsky (BZ) reactions have been well known, the period length of these is much shorter than that of circadian rhythms: incorporating a time delay by separating molecules with semipermeable membranes was necessary for known chemical oscillations with a period of more than a couple of hours. Temperature compensation of chemical oscillations in a homogeneous aqueous solution has been rarely known.

How is the KaiC phosphorylation cycle generated? Interestingly, KaiC itself harbors both autophosphorylating and autodephosphorylating activities for Ser 431 and Thr 432 residues. KaiA activates the KaiC autophosphorylation, while KaiB antagonizes the KaiA function both in vitro and in vivo (Nishiwaki et al., 2000; Iwasaki et al., 2002; Kitayama et al., 2003; Williams et al., 2002). To generate enzymatic oscillation, the ratio of the Kai proteins and sequential dynamic complex formations among Kai proteins are important (Kageyama et al., 2006). Consistent with this, the importance of such cyclic protein complex formation has been also suggested in vivo (Iwasaki et al., 1999; Iwasaki et al., 2000; Iwasaki et al., 2002; Kageyama et al., 2003). KaiC has two ATP-binding motifs and exhibits ATP-dependent hexamer formation (Nishiwaki et al., 2000; Mori et al., 2002). Terauchi et al. (2007) recently found a weak ATPase activity of KaiC, and revealed that 1 molecule of KaiC catalyzed only 15 ATP molecules per day. This enzymatic rate is much slower than that of known slow enzymes such as AAA-type ATPases (less than 1/1000). They also found that KaiC ATPase activity showed a circadian cycle in a reaction mixture exhibiting KaiC phosphorylation rhythm. Importantly, the ATPase activity of KaiC is temperature compensated regardless of the presence or absence of KaiA or KaiB protein. This nature was also observed even two phosphorylation residues were substituted with alanines, indicating that this is not dependent on the phosphorylation state of KaiC (Terauchi et al., 2007). Generally, in an oscillating system, total energy in the system is in proportion to its frequency. Consistent with this

idea, Terauchi et al. (2007) examined ATPase activities of five KaiC mutant proteins that gave rise to a different period length in vivo and in vitro. Strikingly, the result demonstrated that the ATPase activity even in the absence of KaiA and KaiB proteins was proportional to the frequency of resulting rhythmicity in the presence of KaiA and KaiB in vitro. This finding strongly supports that energy from ATP hydrolysis by KaiC is the key factor in determining the period length (Terauchi et al., 2007).

More recently, Kitayama et al. (2008) demonstrated that even in the absence of the rhythmic KaiC phosphorylation cycle some *kai* mutant strains in vivo exhibited temperature-compensated transcription/translation rhythms under LL conditions. In a *kaiA*-overexpressor mutant strain, the level of KaiC phosphorylation was constitutively elevated, whereas circadian rhythm in the *kaiBC* promoter activity persisted. Moreover, the rhythms in *kaiBC* expression and KaiB and KaiC accumulation were observed even after two phosphorylation residues of KaiC were replaced with Glu to mimic a constitutively phosphorylated form. Again, the KaiC phosphorylation cycle per se is not likely to be an essential process for Kai-dependent temperature-compensated transcriptional rhythms (Kitayama et al., 2008). Retrospectively, this situation is reminiscent of the residual low-amplitude, unstable transcription cycle in a *sasA*-null mutant strain, in which extremely downregulated KaiC protein was constitutively phosphorylated (Iwasaki et al., 2000; Takai et al., 2006). SasA is a KaiC-interacting sensory histidine kinase necessary for robust circadian oscillations (Iwasaki et al., 2000). Because the KaiC ATPase activity is the simplest reaction that is directly associated with basic circadian properties, it may independently regulate both the KaiC phosphorylation cycle and the transcriptional cycle. Thus, there is much accumulated information on the coexistence of at least four types of feedback loops in the circadian system. The detailed molecular mechanism of all these circuits and the relationships among them remain to be resolved.

Toward Understanding Spatial Pattern Formation in Multicellular (Filamentous) Cyanobacteria

Spatial extension of dynamic networks generating rhythms can be used also for a mechanism generating spatial pattern formations (morphology), represented by the clock-and-wavefront model for somitogenesis and the Turing model. Thus, methods and models used for circadian biology may be applied and extended to studies on periodic pattern formations. As described here, filamentous (multicellular) diazotrophic cyanobacteria often develop heterocysts (Fig. 3A). Particularly, *Anabaena* sp. PCC 7120 differentiates heterocysts at about every ten cells. Many mutations affecting heterocyst formations have been isolated, while a basis for such regular pattern formation still remains to be solved (reviewed by Golden and Yoon, 2003; Zhang et al., 2006).

Thus, we are interested in four questions to be addressed in *Anabaena*. First, what is the mechanism for the one-dimensional periodic pattern formation? Second,

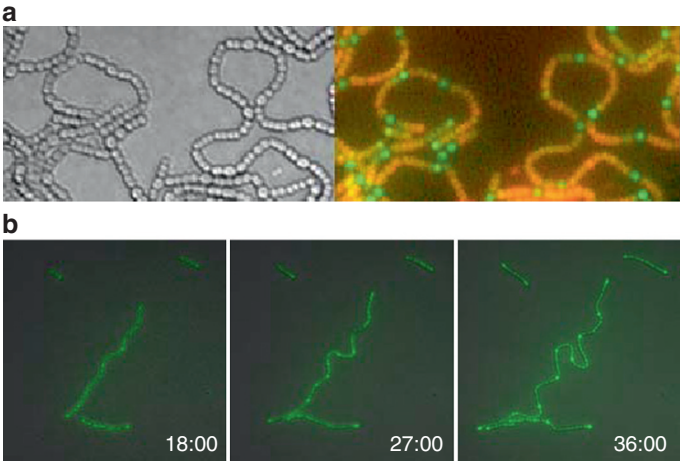

Fig. 3 Heterocyst formation in *Anabaena*. **a** *Anabaena* cells harboring a *gfp* reporter gene fused to the promoter of a gene named *hetR*, essential for heterocyst formation, were grown in the absence of nitrogen in solid media to develop heterocysts, which are larger than vegetative cells (*left*, bright field) and accumulate *hetR::gfp* signals (*green* signals in the *right panel*). *Red* signals in the *right panel* indicate autofluorescence from chlorophyll in vegetative cells. Note that the red signal correlating to the photosynthetic activity is nullified in the heterocysts. **b** Example of time-lapse fluorescence observation during heterocyst formation in the *hetR::gfp* strain. *Numbers* indicate hours after nitrogen depletion

are neighboring clock cells coupled to each other? Third, are clock systems equivalent between normal (vegetative) cells and heterocysts? Finally, is differentiation gated by the circadian clock? We initially set up an automated monitoring system to grow bacteria and to observe morphogenesis and gene expression profiles under the microscope (Fig. 3B). Using this system, we succeeded in obtaining the first "bacterial cell lineage" (Iwasaki, unpublished results). Moreover, we observed low-amplitude circadian rhythms in expression of genes involved in morphogenesis.

For experimentally validating models of circadian rhythms, pulsed (transient) administration of a genetic inducer or reagents is quite effective to perturb the oscillatory network that gives rise to phase-shift of the rhythm, for example. Such a perturbation experiment for spatial patterns similarly requires local administration of a reagent, metabolite, or inducer. Thus, application of microelectrical mechanical systems (MEMS) and microfluidic techniques seems very useful for administrating reagents to specific cells in an *Anabaena* filament to test which type of perturbation would be observed following morphogenesis. Such studies are now underway.

Acknowledgments I thank Dr. Takao Kondo and his laboratory members for the fruitful long-term collaboration in the *Synechococcus* circadian clock project. I also thank our laboratory members, especially Hironori Asai and Shunsuke Iwamori, for the *Anabaena* pattern formation project. This work was supported in part by the Uehara Memorial Foundation, grants-in-aid from the Japanese Society for Promotion of Science (No. 19657019 and 20370072), and the ERATO Aihara complexity modeling project (Japan Science and Technology Agency).

References

Dunlap JC (2004) The molecular mechanism of circadian oscillators. In: Chronobiology: Biological Timekeeping. Sinauer Associates, Sunderland, MA, pp 212–253

Golden JW, Yoon HS (2003) Heterocyst development in *Anabaena*. Curr Opin Microbiol 6:557–563

Goodwin BC (1965) Oscillatory behavior in enzymatic control processes. Adv Enzyme Regul 3:425–438

Grobbelaar N, Huang T-C, Lin H-Y, Chow T-J (1986) Dinitrogen-fixing endogenous rhythm in *Synechococcus* RF-1. FEMS Microbiol Lett 37:173–177

Hardin PE, Hall JC, Rosbash M (1990) Feedback of the *Drosophila period* gene product on circadian cycling of its messenger RNA levels. Nature (Lond) 343:536–540

Hirata H, Yoshiura S, Ohtsuka T, Bessho Y, Harada T, Yoshikawa K, Kageyama R (2002) Oscillatory expression of the bHLH factor Hes1 regulated by a negative feedback loop. Science 298:840–843

Ishiura M, Kutsuna S, Aoki S, Iwasaki H, Andersson CR, Tanabe A, Golden SS, Johnson CH, Kondo T (1998) Expression of a gene cluster *kaiABC* as a circadian feedback process in cyanobacteria. Science 281:1519–1523

Iwasaki H, Dunlap JC (2000) Microbial circadian oscillatory systems in *Neurospora* and *Synechococcus*: models for cellular clocks. Curr Opin Microbiol 3:189–196

Iwasaki H, Kondo T (2000) The current state and problems of circadian clock studies in cyanobacteria. Plant Cell Physiol 41:1013–1020

Iwasaki H, Kondo T (2004) Circadian timing mechanism in the prokaryotic clock system of cyanobacteria. J Biol Rhythms 19:436-444

Iwasaki H, Taniguchi Y, Ishiura M, Kondo T (1999) Physical interactions among circadian clock proteins, KaiA, KaiB and KaiC, in cyanobacteria. EMBO J 18:1137–1145

Iwasaki H, Williams SB, Kitayama Y, Ishiura M, Golden SS, Kondo T (2000) A KaiC-interacting sensory histidine kinase, SasA, necessary to sustain robust circadian oscillation in cyanobacteria. Cell 101:223–233

Iwasaki H, Nishiwaki T, Kitayama Y, Nakajima M, Kondo T (2002) KaiA-stimulated KaiC phosphorylation in circadian timing loops in cyanobacteria. Proc Natl Acad Sci U S A 99:15788–15793

Kageyama H, Kondo T, Iwasaki H (2003) Circadian formation of clock protein complexes by KaiA, KaiB, KaiC, and SasA in cyanobacteria. J Biol Chem 278:2388–2395

Kageyama H, Nishiwaki T, Nakajima M, Iwasaki H, Oyama T, Kondo T (2006) Cyanobacterial circadian pacemaker: Kai protein complex dynamics in the KaiC phosphorylation cycle in vitro. Mol Cell 23:161–171

Kitayama Y, Iwasaki H, Nishiwaki T, Kondo T (2003) KaiB functions as an attenuator of KaiC phosphorylation in the cyanobacterial clock system. EMBO J 22:2127–2134

Kitayama Y, Nishiwaki T, Terauchi K, Kondo T (2008) Dual KaiC-based oscillations constitute the circadian system of cyanobacteria. Genes Dev 22:1513–1521

Kondo T, Strayer CA, Kulkarni RD, Taylor W, Ishiura M, Golden SS, Johnson CH (1993) Circadian rhythms in prokaryotes: luciferase as a reporter of circadian gene expression in cyanobacteria. Proc Natl Acad Sci U S A 90:5672–5676

Konopka RJ, Benzer S (1971) Clock mutants of *Drosophila melanogaster*. Proc Natl Acad Sci U S A 68:2112–2116

Liu Y, Tsinoremas NF, Johnson CH, Lebedeva NV, Golden SS, Ishiura M, Kondo T (1995) Circadian orchestration of gene expression in cyanobacteria. Genes Dev 9:1469–1478

Mitsui A, Kumazawa S, Takahashi A, Ikemoto H, Cao S, Arai T (1986) Strategy by which nitrogen-fixing unicellular cyanobacteria grow photoautotrophically. Nature (Lond) 323:720–722.

Mori T, Saveliev SV, Xu Y, Stafford WF, Cox MM, Inman RB, Johnson CH (2002) Circadian clock protein KaiC forms ATP-dependent hexameric rings and binds DNA. Proc Natl Acad Sci U S A 99:17203–7208

Nakajima M, Imai K, Ito H, Nishiwaki T, Murayama Y, Iwasaki H, Oyama T, Kondo T (2005) Reconstitution of circadian oscillation of cyanobacterial KaiC phosphorylation in vitro. Science 308:414–415

Nishiwaki T, Iwasaki H, Ishiura M, Kondo T (2000) Nucleotide binding and autophosphorylation of clock protein KaiC as a circadian timing process of cyanobacteria. Proc Natl Acad Sci U S A 97:495–499

Stal LJ, Krumbein WE (1985) Nitrogenase activity in the non-heterocystous cyanobacterium *Oscillatoria* sp. grown under alternating light-dark cycles. Arch Microbiol 143:67–71

Takai N, Nakajima M, Oyama T, Kito R, Sugita C, Sugita M, Kondo T, Iwasaki H (2006) A KaiC-associating SasA–RpaA two-component regulatory system as a major circadian timing mediator in cyanobacteria. Proc Natl Acad Sci U S A 103:12109–12114

Terauchi K, Kitayama Y, Nishiwaki T, Miwa K, Murayama Y, Oyama T, Kondo T (2007) ATPase activity of KaiC determines the basic timing for circadian clock of cyanobacteria. Proc Natl Acad Sci U S A 104:16377–16381

Tomita J, Nakajima M, Kondo T, Iwasaki H (2005) No transcription–translation feedback in circadian rhythm of KaiC phosphorylation. Science 307:251–254

Ueda HR, Hayashi S, Chen W, Sano M, Machida M, Shigeyoshi Y, Iino M, Hashimoto S (2005) System-level identification of transcriptional circuits underlying mammalian circadian clocks. Nat Genet 37:187–192

Williams SB, Vakonakis I, Golden SS, LiWang AC (2002) Structure and function from the circadian clock protein KaiA of *Synechococcus elongatus*: a potential clock input mechanism. Proc Natl Acad Sci U S A 99:15357–15362

Zhang CC, Laurent S, Sakr S, Peng L, Bédu S (2006) Heterocyst differentiation and pattern formation in cyanobacteria: a chorus of signals. Mol Microbiol 59:367–375

The Apoptotic Signaling Network Dynamically Interprets the Outputs of Individual Signaling Pathways in an Early Analog and Late Digital Manner

Kevin A. Janes, H. Christian Reinhardt, and Michael B. Yaffe

Introduction

Changes in cell behavior are determined by a network of proteins that actively transmits signaling information (Irish et al., 2004; Jordan et al., 2000; Pawson, 2004). Modulation of total levels of key proteins, as well as their posttranslational states and enzymatic activities, could all potentially act as "molecular signals" that are monitored and interpreted. To understand how complex signal-transduction events control cell responses, these molecular signals must be measured dynamically and then mapped to downstream changes in cell outcome (Gaudet et al., 2005; Janes et al., 2005). Such approaches can accurately predict diverse cellular responses and suggest how molecular information is organized and propagated within the cell (Miller-Jensen et al., 2007).

One crucial cell decision is whether to die or to survive (Green and Evan, 2002; Kyriakis, 2001; Tran et al., 2004). Apoptosis is a common mechanism of cell death in response to many intrinsic and extrinsic cytotoxic cues such as cytokines and DNA damage (Strasser et al., 2000; Zhou and Elledge, 2000). Neighboring cells can also directly induce apoptosis in a target cell by secreting prodeath factors. Although cell death is important for normal development and tissue homeostasis, it is irreversible, requiring apoptosis to be tightly controlled. Deregulated apoptosis is known to be involved in many human diseases such as cancer (Rudin and Thompson, 1997; Vaux, 1993).

Tumor necrosis factor (TNF) is the founding member of a family of death ligands that plays critical roles in the regulation of apoptosis and inflammation (Aggarwal, 2003; Baud and Karin, 2001). In response to TNF, both pro-apoptotic and pro-survival

K.A. Janes, H.C. Reinhardt, and M.B. Yaffe
Koch Institute for Integrative Cancer Research, Center for Cell Decision Processes, Department of Biology, and Department of Biological Engineering, Massachusetts Institute of Technology, Cambridge, MA, USA

K.A. Janes
Department of Cell Biology, Harvard Medical School, Boston, MA 02115, USA

S. Nakanishi et al. (eds.), *Systems Biology*,
DOI:10.1007/978-4-431-87704-2_11, © Springer 2009

pathways are activated via caspases and IKK–NF-κB (Karin and Ben-Neriah, 2000; Riedl and Shi, 2004). TNF also activates stress pathways, including JNK and p38–MK2, which play pro- or anti-apoptotic roles depending upon the timing and duration of signaling and the activation state of other pathways (Deng et al., 2003; Janes et al., 2005; Lamb et al., 2003; Roulston et al., 1998; Ventura et al., 2004). Thus, predicting the apoptotic response of cells to TNF is complicated because the pathways and molecular signals involved are dynamic, context dependent, and directly antagonistic (Micheau and Tschopp, 2003; Miller-Jensen et al., 2007; Wajant et al., 2003).

In addition to direct signaling through the TNF receptor, TNF drives secretion of the cytokines transforming growth factor-α (TGF-α), interleukin-1α (IL-1α), and interleukin-1 receptor antagonist (IL-1ra) to initiate a cascade of autocrine signaling events through the epidermal growth factor (EGF) and IL-1 receptors (Janes et al., 2006). These induced autocrine ligands collaborate with circulating growth factors, such as EGF and insulin, to influence cell sensitivity to TNF (Garcia-Lloret et al., 1996; Remacle-Bonnet et al., 2000). How the collective information from pro-death, pro-survival, and autocrine ligands is processed through the same network of molecular signals to control apoptosis is unclear.

We have recently formalized a data-driven computational approach for investigating the TNF apoptotic-signaling network together with the pro-survival networks of EGF and insulin (Gaudet et al., 2005; Janes et al., 2006; Janes et al., 2004). The state of the network was estimated by measuring signaling proteins within various pathways that were directly implicated in the mechanisms of cytokine signaling, apoptosis, or both. We collected large-scale dynamic measurements of molecular signals that included the phosphorylation of critical receptors, adaptors, and transcription factors, the catalytic activity of protein kinases, and the cleavage state of caspases. In parallel, several apoptotic readouts induced by ten different cytokine–stimulus combinations were measured in human HT-29 colon adenocarcinoma cells. The complete set of 7980 molecular signals and 1440 apoptotic responses allowed us to model network function from primary data without the need to agglomerate kinetic parameters, intracellular concentrations, and protein–protein interactions from the literature.

We modeled how molecular signals may work together to control apoptosis using partial least squares regression (Janes and Yaffe, 2006). In a partial least squares model, signaling events (“variables”) conveying similar information are combined into supervariables called principal components that are trained to predict outcomes such as cell death. Applying this approach to our dataset revealed many statistically coupled molecular signals whose dynamics were linked to apoptosis. The resulting model accurately captured the apoptotic responses induced by various cytokine combinations and correctly predicted the effect of perturbations, which were outside the initial model training (Janes et al., 2005). The success of the model also led to mechanistic hypotheses about apoptotic regulation that were subsequently verified by follow-up experiments, validating the usefulness of the data-driven modeling approach (Janes et al., 2005).

Counterintuitively, one can learn as much from failures of a model as from its successes. In engineering sciences, where modeling is a much more established

technique, "failure analysis" is routinely used to define the normal operating range of complex systems, such as engines, bridges, and circuit boards (for recent examples, see Chansawat et al., 2006; Khatir et al., 2007; and Truman and Booker, 2007). Failure-directed approaches have not yet been applied to models of biological systems, but failed models can identify gaps in existing knowledge (Price et al., 2003) and reveal new mechanisms that were not captured by the original model (Hua et al., 2005; Miller-Jensen et al., 2007).

Here, we investigated whether the failure regimes of data-driven models could be used to identify fundamental properties of signal transduction in biological networks—namely, whether integrated cellular response networks could interpret the state of distinct signal transduction pathways in a digital (i.e., binary '1' or '0') or analog manner. To accomplish this, we reduced signaling dynamic range by grouping similar levels of signaling into a finite number of "bins" and then assessed the ability of the binned signals to predict apoptosis. We found for the TNF-induced autocrine circuits (Janes et al., 2006) that the signals induced by autocrine IL-1α can be selectively perceived by the network as digital information when dynamic range is compressed into a single steplike threshold. The response to autocrine TGF-α, conversely, requires analog signaling, with dynamic range spread evenly across signal strength.

Results

To investigate the relative importance of signal strength and dynamic range in a biologically relevant network, it was necessary to start with both a high-quality signaling dataset and a validated data-driven model. Our signaling dataset comprised 19 molecular signals measured at 13 time points from 0 to 24 h after stimulation with one of ten different combinations of TNF, EGF, and insulin (see Experimental Procedures for details). We analyzed molecular signals that were mechanistically connected to pathways downstream of the TNF, EGF, or insulin receptors and upstream of apoptosis. Measurements were collected from three or six biological replicates for a total of 7980 individual protein measurements.

Signaling dynamics are critical for many cell responses (Marshall, 1995; Pawson, 2004), but there is only a limited understanding of how dynamic signals are interpreted (Murphy and Blenis, 2006). Therefore, using the time course data, we extracted 30–40 time-dependent descriptors ("signaling metrics") that summarize the duration, activation, and deactivation of each molecular signal (Janes et al., 2005). Together, these metrics capture the information in a time course that is conceivably available to mediate cell outcomes, such as apoptosis. For each stimulus combination, four different cell-death markers were measured in triplicate by flow cytometry at three time points from 12 to 48 h to quantify the percentage of cells undergoing apoptosis. Together, the fused signaling-apoptosis dataset that served as the basis for model training consisted of 6600 signaling metrics (660 metrics per treatment × 10 treatments) and 120 apoptotic readouts (4 readouts × 3 time points × 10 treatments).

Our goal was to predict apoptosis (Y) from the measured signaling network state (X). The simplest relationship between these two datasets is a linear one: $Y = X\beta$, where Y is a matrix of 10 rows of treatments and 12 columns of apoptotic readouts at different time points, X is a matrix of 10 rows of treatments and 660 columns of signaling metrics, and β is a matrix of regression coefficients that describes how each metric contributes to each apoptotic readout (660 rows × 12 columns). There are not enough treatment conditions to calculate unique solutions for the complete matrix of regression coefficients (β), in the way that is commonly done for linear regression, curve fitting, etc. However, one can break down the matrix of signaling metrics into a series of vector products, which multiply a "scores" vector (s) and a "loadings" vector (Equation l):

$$X \approx \begin{bmatrix} s_{1,1} \\ s_{2,1} \\ \vdots \\ s_{10,1} \end{bmatrix} [l_{1,1}\ l_{1,2} \ldots l_{1,660}] + \begin{bmatrix} s_{1,2} \\ s_{2,2} \\ \vdots \\ s_{10,2} \end{bmatrix} [l_{2,1}\ l_{2,2} \ldots l_{2,660}] + \ldots = s_1 l_1{}^T + S_2 l_2{}^T + \ldots$$

where s is a vector of 10 rows (1 for each observation), l is a vector of 660 rows (1 for each signaling metric), and ^{T} is the vector transpose (a function that swaps row and column elements). Each score-loading product ($s_1 l_1{}^T$, $s_2 l_2{}^T$, etc.) represents a "principal component" of the dataset. Often, data matrices can be approximated with only a few principal components (our model requires three, for example).

This approximation simplifies the dataset by reducing its dimensionality. Dimensionality reduction is advantageous in many other biological applications: colorimetric assays (using a one-dimensional calibration line that relates the two dimensions of absorbance and concentration), multiple sequence alignments (reducing many sequences to a few phylogenies), etc. Here, the reduced number of scores vectors is used to predict Y more efficiently: $Y = TB$, where T is a matrix of concatenated scores vectors (10 rows of treatments × 3 columns of principal components), and B is a matrix of regression coefficients, describing how each element in a score vector contributes to each apoptotic readout (3 rows × 12 columns). (Note that the number of elements in B that need to be estimated from the data is far smaller than the number of elements in β.) Numerical algorithms are available to extract the optimal principal components from X for predicting the data in Y (Geladi and Kowalski, 1986). The result is a "partial least squares" model linking X and Y through a small set of principal components derived from the data (Janes and Yaffe, 2006). By using molecular signals in X that are mechanistically connected to apoptosis (Y, see above), these principal components can give insight into the events directly responsible for the apoptotic phenotype.

Applying the partial least squares algorithms to our dataset yielded a three-component model that could fit the apoptotic readouts to within 99% (Janes et al., 2005). To assess the stability of the model, we cross-validated the predictions by leaving out one of the cytokine treatments and training a model that contained only nine treatments. This "leave-one-out" model was then used to predict the withheld

treatment condition, and the cross-validation procedure was iterated for all treatments in the dataset. Apoptotic readouts induced by stimulus combinations withheld from the training dataset were captured to within 94% of their measured values (Janes et al., 2005), indicating that the full model is stable and quantitatively predictive.

Importantly, the success of these predictions is not simply a consequence of starting with a high number of signaling metrics, a subset of which might always predict any Y matrix. Using the same metrics and treatment conditions in a three-component model, we were unable to predict the starting TNF-EGF-insulin concentrations (36% accuracy) or the receptor occupancy for the stimulating cytokines (0% accuracy, data not shown). These Y matrices have fourfold fewer elements (three cytokine levels or receptor occupancies, compared to 12 apoptotic readouts) and yet cannot be predicted. We conclude that the apoptotic model is not based on false discovery and can be used as the foundation for exploring signaling dynamic range.

Autocrine-Feedback Circuits Are Selectively Perceived as Analog or Digital Signals

Signal-transduction and gene-regulatory networks have a dense feedback connectivity that resembles the layout of electrical circuits (Hasty et al., 2002; McAdams and Shapiro, 1995). This observation raises the question of whether natural and engineered circuits transmit the same types of information with similar requirements for signal strength and dynamic range. The discrete, four-base code of the genome and the binary nature of many cell fate responses suggests that the intervening signaling networks might operate digitally (Hood and Galas, 2003). If true, then dynamic range would be of limited importance, because all the information would be encoded in the abrupt transitions from one digital state to the next. However, mathematical models based on digital regulation have often required additional analog pathways to capture experimental observations, suggesting that dynamic range could be essential for many pathways (Altan-Bonnet and Germain, 2005; McAdams and Shapiro, 1995; McAdams and Shapiro, 2003; Ruf et al., 2006). It is not known whether network-level data quantitatively support digital or analog signal processing as a mechanism for controlling cellular outcomes.

The original data-driven apoptosis model is based on analog signal processing: across the full range of observations for each metric, the model assumes a smooth, mathematically continuous relationship between measured values ("signal activation") and how that value is interpreted as a contributor to apoptosis ("signal output") (Janes et al., 2005; Janes and Yaffe, 2006) (Fig. 1A: "Analog response"). To test whether this analog relationship was required, we explored the predictive power of discretized models that incorporate digital signaling elements by grouping similar observations into discrete "bins" (Fig. 1A). Each bin for a signaling metric reflects an interval of activation states that has lost its dynamic range and thus relays the same output. Using many bins is only slightly different from the starting dataset. As the number of bins decreases, however, more dynamic range is lost and the observations become coarse grained, with two bins representing an entirely on–off digital signal.

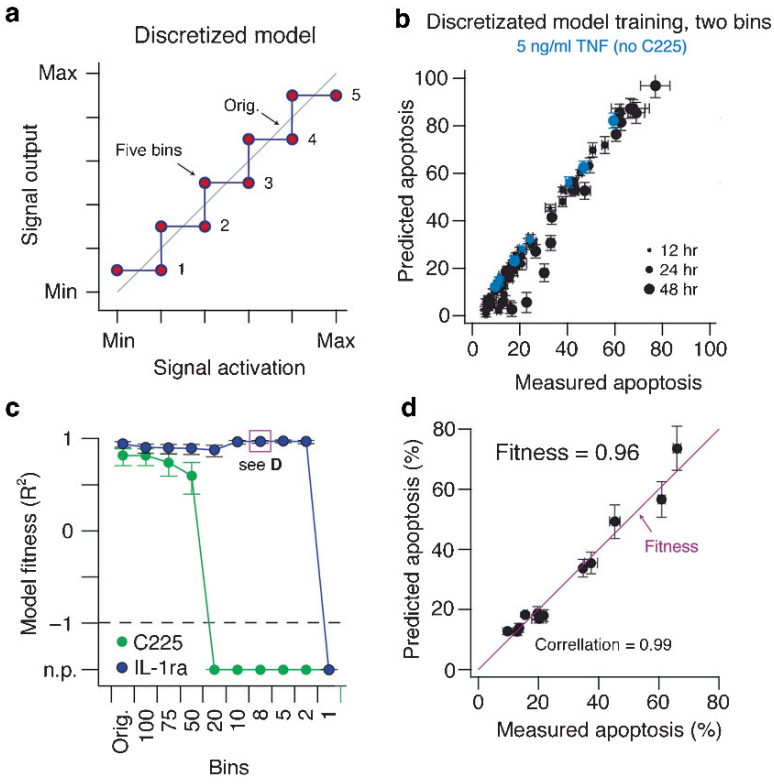

Fig. 1 Selective failure of progressively discretized models linking signal activation to signal output for predicting apoptosis. **a** Discretization of the experimentally measured signal activation state (abscissa) into with five bins of signal output (*ordinate*) used for model construction. Signal activation and signal output were uniformly discretized into a fixed number of bins (here, five bins) based on the minimum (*Min*) and maximum (*Max*) observed values for each signaling metric. Points at the discontinuities (*vertical lines*) were assigned to the upper bin values. The original continuous "analog" model was constructed using the measured signal activation-modeled signal output response shown by the *diagonal line*. **b** Training of the apoptosis prediction model using discretized signal outputs from ten different conditions of tumor necrosis factor (TNF), insulin, and epidermal growth factor (EGF) stimulation. In model training, data from one of the ten conditions were removed, the model was trained on the remaining nine datasets, and then used to predict four different readouts of apoptosis at 12, 24, and 48 h after the omitted treatment using the discretized signaling metrics from that treatment. This approach was then iteratively repeated for all ten conditions. Results of a two-bin model are shown. Sample data from one specific condition (5 ng/ml TNF) are highlighted in *blue*. **c** Predictions of apoptosis after perturbation of autocrine feedback in models with increasing discretization. Model fitness was calculated for predictions of the C225 (*green*) and interleukin (IL)-1ra (*blue*) perturbations after discretizing the signaling metrics as described in **a**. The specific data point for the model fitness shown in **d** is *boxed in purple*. **d** An example of good model fitness for modeling apoptosis after disruption of the IL-1 feedback loop using an eight-bin discretized model. The Pearson correlation coefficient is indicated. Perfect model fitness (fitness = 1) is represented by the *purple line*

After each discretization, we trained a new "discretized model" using the binned signaling data to capture the original measurements of apoptosis induced by TNF, EGF, and insulin. This retraining is necessary, because manipulating the dataset without updating the model will mathematically violate the underlying equations of the partial least squares approach (scores and loadings vectors, for example, will no longer approximate X; see above). To restrict discretization to the data itself, all models were fit with continuous regression coefficients. We found that the ability of the discretized models to predict the observed cytokine-induced apoptotic responses was indistinguishable from the original analog model based on predictions of cytokine treatments that were withheld from the training data (Fig. 1B). Therefore, discretization did not prevent the construction of a stable data-driven model that predicts apoptosis induced by TNF, EGF, and insulin.

To gauge the predictive power of the discretized models in a manner independent of the training data, we used perturbations of two TNF-induced autocrine circuits that were not present in the training set: (1) 5 ng/ml TNF in the presence of C225 (Fig. 1C, "C225"), a monoclonal antibody that blocks binding of autocrine TGF-α to its cognate receptor; and (2) 100 ng/ml TNF in the presence of exogenous IL-1ra (Fig. 1C, "IL-1ra"), a receptor antagonist that prevents signaling from autocrine IL-1α. The original analog apoptosis model could accurately predict the extent of apoptosis resulting from both of these perturbations (Janes et al., 2005) (Fig. 1C, "Analog"), thus providing a validated test set to compare the quality of the discretized model variants.

For each variant, we compared the prediction of four apoptotic readouts—phosphatidyl serine exposure, membrane permeability, nuclear fragmentation, and cleaved caspase-3/cleaved cytokeratin-18—against the values measured experimentally at 12, 24, and 48 h (Janes et al., 2005). Failed models often lose the quantitative accuracy of their predictions but still retain a qualitative ability to discriminate high versus low levels of cell responses (K.A.J. and M.B.Y., unpublished observations; see below). We therefore quantified the accuracy of predictions by using a formula for model "fitness" (Gaudet et al., 2005) that postulates a one-to-one match between apoptosis predicted by the model and that measured by experiment (Fig. 1D, "Perfect fitness"). This definition of fitness is more stringent because it penalizes model variants that are correlative qualitatively but not predictive quantitatively (Fig. 1C, "n.p.").

When the signaling data were progressively discretized from 100 bins down to 1 bin, we observed two distinct patterns of model failure (Fig. 1C). For the C225-antibody blockade of autocrine TGF-α, the extent of TNF-induced apoptosis could not be captured accurately by models when fewer than 50 bins were used to discretize the signaling metrics. This finding indicates that fine gradations in signaling are critical for the network to interpret TGF-α autocrine signals and suggests that the intracellular network interprets TGF-α feedback in an analog manner. By contrast, IL-1ra perturbation of TNF-induced apoptosis appeared largely insensitive to the level of discretization. High-quality predictions could be achieved by a model derived from as few as two signaling bins (i.e., "on" or "off"), raising the possibility that autocrine IL-1α signaling is perceived in a digital manner in these cells. Thus, although TNF activates both the TGF-α and IL-1α autocrine circuits (Janes et al., 2006), our

analysis raises the possibility that the molecular signals activated by these extracellular feedbacks are transmitted or interpreted differently within the intracellular network.

Discussion

The selective failure of the autocrine perturbations during discretization matches the apparent function of the autocrine ligands that were blocked. For example, C225 disrupts binding of autocrine TGF-α, which is constitutively released in HT-29 cells but upregulated by around twofold within minutes after TNF addition (Janes et al., 2006). This autocrine tuning of a preexisting stimulus suggests that TGF-α signaling is interpreted as an analog input, which would explain the rapid failure of the C225 prediction after discretization. Conversely, IL-1ra prevents binding of autocrine IL-1α, which is barely detectable in the medium of unstimulated cells but is induced dramatically between 4 and 8 h after TNF is added (Janes et al., 2006). The extracellular "state" of IL-1α is thus essentially digital (present or absent). Accordingly, predictions of apoptosis following IL-1α blockade with IL-1ra show no sensitivity to discretization with as few as two bins.

In addition, the sequential release of TGF-α (early) and IL-1α (late) parallels the transition from analog decision making at early times to digital cell-death execution at late times. Autocrine TGF-α collaborates with direct signaling from the TNF receptor to interpret the cellular microenvironment and decide whether to undergo apoptosis, whereas IL-1α further amplifies the extent of caspase activation and drives a larger percentage of cells to death (Janes et al., 2006). This observation indicates that an analog-to-digital conversion of signaling is taking place at some point between cytokine receptors and caspase-effector proteins. Future network breakpoint analyses using perturbations of signaling proteins will allow us to determine the analog and digital nodes of the intracellular network, as we have done here for the TNF-induced autocrine cascade.

References

Aggarwal, B. B. (2003). Signalling pathways of the TNF superfamily: a double-edged sword. Nat Rev Immunol 3:745–756.

Alon, U., Camarena, L., Surette, M. G., Aguera y Arcas, B., Liu, Y., Leibler, S., and Stock, J. B. (1998). Response regulator output in bacterial chemotaxis. EMBO J 17:4238–4248.

Altan-Bonnet, G., and Germain, R. N. (2005). Modeling T cell antigen discrimination based on feedback control of digital ERK responses. PLoS Biol 3:e356.

Baud, V., and Karin, M. (2001). Signal transduction by tumor necrosis factor and its relatives. Trends Cell Biol 11:372–377.

Chansawat, K., Yim, S. C. S., and Miller, T. H. (2006). Nonlinear finite element analysis of a FRP-strengthened reinforced concrete bridge. J Bridge Eng 11:21–32.

Deng, Y., Ren, X., Yang, L., Lin, Y., and Wu, X. (2003). A JNK-dependent pathway is required for TNF-alpha-induced apoptosis. Cell 115:61–70.

Garcia-Lloret, M. I., Yui, J., Winkler-Lowen, B., and Guilbert, L. J. (1996). Epidermal growth factor inhibits cytokine-induced apoptosis of primary human trophoblasts. J Cell Physiol 167:324–332.

Gaudet, S., Janes, K. A., Albeck, J. G., Pace, E. A., Lauffenburger, D. A., and Sorger, P. K. (2005). A compendium of signals and responses triggered by prodeath and prosurvival cytokines. Mol Cell Proteomics 4:1569–1590.

Geladi, P., and Kowalski, B. R. (1986). Partial least-squares regression: a tutorial. Anal Chim Acta 185:1–17.

Green, D. R., and Evan, G. I. (2002). A matter of life and death. Cancer Cell 1:19–30.

Hasty, J., McMillen, D., and Collins, J. J. (2002). Engineered gene circuits. Nature (Lond) 420:224–230.

Hood, L., and Galas, D. (2003). The digital code of DNA. Nature (Lond) 421:444–448.

Hua, F., Cornejo, M. G., Cardone, M. H., Stokes, C. L., and Lauffenburger, D. A. (2005). Effects of bcl-2 levels on fas signaling-induced caspase-3 activation: molecular genetic tests of computational model predictions. J Immunol 175:985–995.

Irish, J. M., Hovland, R., Krutzik, P. O., Perez, O. D., Bruserud, O., Gjertsen, B. T., and Nolan, G. P. (2004). Single cell profiling of potentiated phospho-protein networks in cancer cells. Cell 118:217–228.

Janes, K. A., and Yaffe, M. B. (2006). Data-driven modelling of signal-transduction networks. Nat Rev Mol Cell Biol 7:820–828.

Janes, K. A., Kelly, J. R., Gaudet, S., Albeck, J. G., Sorger, P. K., and Lauffenburger, D. A. (2004). Cue-signal-response analysis of TNF-induced apoptosis by partial least squares regression of dynamic multivariate data. J Comput Biol 11:544–561.

Janes, K. A., Albeck, J. G., Gaudet, S., Sorger, P. K., Lauffenburger, D. A., and Yaffe, M. B. (2005). A systems model of signaling identifies a molecular basis set for cytokine-induced apoptosis. Science 310:1646–1653.

Janes, K. A., Gaudet, S., Albeck, J. G., Nielsen, U. B., Lauffenburger, D. A., and Sorger, P. K. (2006). The response of human epithelial cells to TNF involves an inducible autocrine cascade. Cell 124:1225–1239.

Jordan, J. D., Landau, E. M., and Iyengar, R. (2000). Signaling networks: the origins of cellular multitasking. Cell 103:193–200.

Karin, M., and Ben-Neriah, Y. (2000). Phosphorylation meets ubiquitination: the control of NF-[kappa]B activity. Annu Rev Immunol 18:621–663.

Khatir, Z., Lefebvre, S., and Saint-Eve, F. (2007). Experimental and numerical investigations on delayed short-circuit failure mode of single chip IGBT devices. Microelectron Reliab 47:422–428.

Kyriakis, J. M. (2001). Life-or-death decisions. Nature (Lond) 414:265–266.

Lamb, J. A., Ventura, J. J., Hess, P., Flavell, R. A., and Davis, R. J. (2003). JunD mediates survival signaling by the JNK signal transduction pathway. Mol Cell 11:1479–1489.

Marshall, C. J. (1995). Specificity of receptor tyrosine kinase signaling: transient versus sustained extracellular signal-regulated kinase activation. Cell 80:179–185.

McAdams, H. H., and Shapiro, L. (1995). Circuit simulation of genetic networks. Science 269:650–656.

McAdams, H. H., and Shapiro, L. (2003). A bacterial cell-cycle regulatory network operating in time and space. Science 301:1874–1877.

Micheau, O., and Tschopp, J. (2003). Induction of TNF receptor I-mediated apoptosis via two sequential signaling complexes. Cell 114:181–190.

Miller-Jensen, K., Janes, K. A., Brugge, J. S., and Lauffenburger, D. A. (2007). Common effector processing mediates cell-specific responses to stimuli. Nature (Lond) 448:604–608.

Murphy, L. O., and Blenis, J. (2006). MAPK signal specificity: the right place at the right time. Trends Biochem Sci 31:268–275.

Pawson, T. (2004). Specificity in signal transduction: from phosphotyrosine-SH2 domain interactions to complex cellular systems. Cell 116:191–203.

Price, N. D., Papin, J. A., Schilling, C. H., and Palsson, B. O. (2003). Genome-scale microbial in silico models: the constraints-based approach. Trends Biotechnol 21:162–169.

Remacle-Bonnet, M. M., Garrouste, F. L., Heller, S., Andre, F., Marvaldi, J. L., and Pommier, G. J. (2000). Insulin-like growth factor-I protects colon cancer cells from death factor-induced apoptosis by potentiating tumor necrosis factor alpha-induced mitogen-activated protein kinase and nuclear factor kappaB signaling pathways. Cancer Res 60:2007–2017.

Riedl, S. J., and Shi, Y. (2004). Molecular mechanisms of caspase regulation during apoptosis. Nat Rev Mol Cell Biol 5:897–907.

Roulston, A., Reinhard, C., Amiri, P., and Williams, L. T. (1998). Early activation of c-Jun N-terminal kinase and p38 kinase regulate cell survival in response to tumor necrosis factor alpha. J Biol Chem 273:10232–10239.

Rudin, C. M., and Thompson, C. B. (1997). Apoptosis and disease: regulation and clinical relevance of programmed cell death. Annu Rev Med 48:267–281.

Ruf, F., Park, M. J., Hayot, F., Lin, G., Roysam, B., Ge, Y., and Sealfon, S. C. (2006). Mixed analog/digital gonadotrope biosynthetic response to gonadotropin-releasing hormone. J Biol Chem 281:30967–30978.

Strasser, A., O'Connor, L., and Dixit, V. M. (2000). Apoptosis signaling. Annu Rev Biochem 69:217–245.

Tran, S. E., Meinander, A., and Eriksson, J. E. (2004). Instant decisions: transcription-independent control of death-receptor-mediated apoptosis. Trends Biochem Sci 29:601–608.

Truman, C. E., and Booker, J. D. (2007). Analysis of a shrink-fit failure on a gear hub/shaft assembly. Eng Fail Anal 14:557–572.

Vaux, D. L. (1993). Toward an understanding of the molecular mechanisms of physiological cell death. Proc Natl Acad Sci U S A 90:786–789.

Ventura, J. J., Cogswell, P., Flavell, R. A., Baldwin, A. S., Jr., and Davis, R. J. (2004). JNK potentiates TNF-stimulated necrosis by increasing the production of cytotoxic reactive oxygen species. Genes Dev 18:2905–2915.

Wajant, H., Pfizenmaier, K., and Scheurich, P. (2003). Tumor necrosis factor signaling. Cell Death Differ 10:45–65.

Zhou, B. B., and Elledge, S. J. (2000). The DNA damage response: putting checkpoints in perspective. Nature (Lond) 408:433–439.

Specific Features of Transient Ras and Sustained Rap1 Activation

Yu-ichi Ozaki, Shinsuke Uda, and Shinya Kuroda

Epidermal growth factor (EGF) and nerve growth factor (NGF) induce transient and sustained extracellular signal-regulated kinase (ERK) activation, respectively, and regulate cell growth and differentiation in PC12 cells (Fig. 1a) (Gotoh et al. 1990; Qiu and Green 1992; Traverse et al. 1992; Vaudry et al. 2002). Transient and sustained ERK activation in PC12 cells depends on transient Ras activation and sustained Rap1 activation, respectively (Fig. 1b) (Vaudry et al. 2002; York et al. 1998). We have previously modeled EGF- and NGF-dependent ERK activation in PC12 cells, and found that transient Ras and consequent ERK activation depends on rapidly increasing rates of EGF and NGF, whereas sustained Rap1 and consequent ERK activation depends on the final concentration of NGF (Sasagawa et al. 2005). We here construct simple Ras and Rap1 models whose inactivation is dependent on and independent of stimulation, respectively (Fig. 1c), and summarize how the modes of inactivation of Ras and Rap1 makes the features distinct.

We described the Ras model in dimensionless form as follows:

$$\frac{d}{dt}GEF = R - (1+R)\cdot GEF \tag{1}$$

$$\frac{d}{dt}GAP = q\left(p\cdot R - \left(1+p\cdot R\right)\cdot GAP\right) \tag{2}$$

$$\frac{d}{dt}Ras = s\left(k\cdot GEF - \left(k\cdot GEF + GAP\right)\cdot Ras\right) \tag{3}$$

where *R*, *GEF*, *GAP*, and *Ras* correspond, respectively, to phosphorylated receptors, activated SOS, activated RasGAP, and activated Ras. Parameters *p*, *q*, *k*, and *s*, denote, respectively, the association constant of *GAP* activation, the relative rate constant of *GAP* activation compared to *GEF* activation, the equilibrium constant of *Ras*, and the rate constant of *Ras* activation (see Appendix). Total amounts of

Y. Ozaki, S. Uda, and S. Kuroda
Department of Biophysics and Biochemistry, Graduate School of Science,
University of Tokyo, CREST, Japan Science and Technology Agency, Hongo 7-3-1,
Bunkyo-ku, Tokyo 113-0033, Japan

S. Nakanishi et al. (eds.), *Systems Biology*,
DOI:10.1007/978-4-431-87704-2_12, © Springer 2009

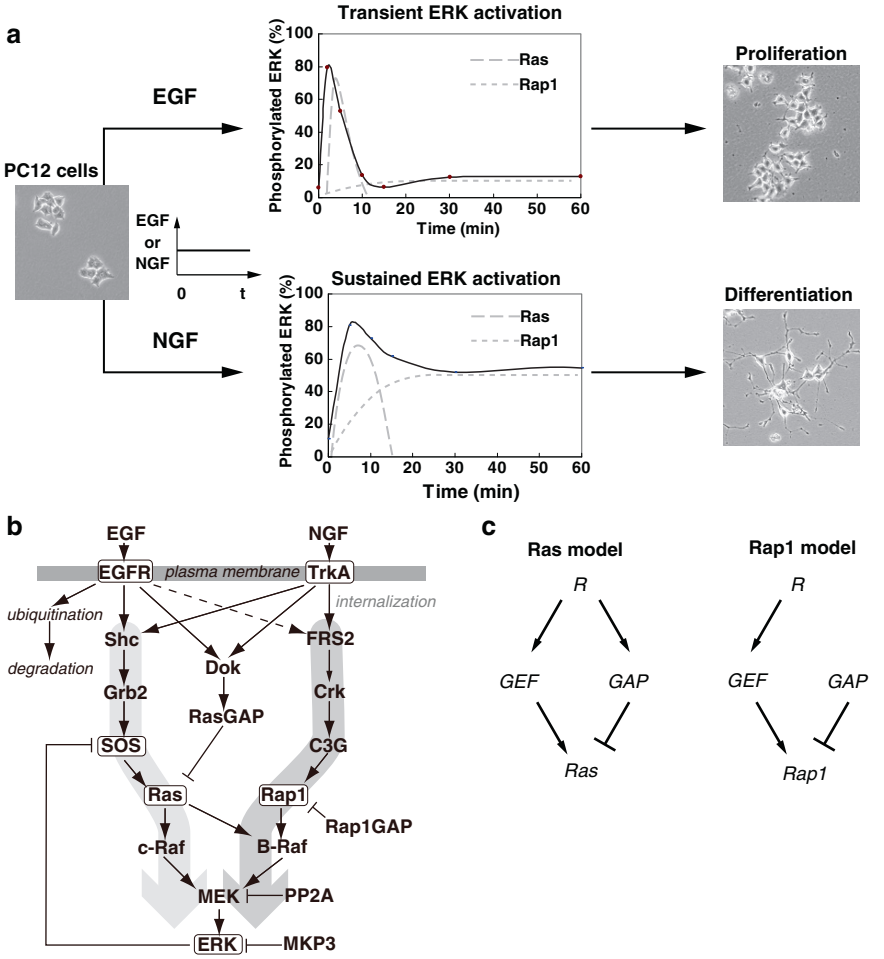

Fig. 1 Transient and sustained extracellular signal-regulated kinase (ERK) activation in PC12 cells. **a** Constant epidermal growth factor (EGF) and nerve growth factor (NGF) stimulation induces transient, and transient and sustained ERK activation, resulting in cell proliferation and differentiation, respectively. **b** EGF- and NGF-dependent ERK signaling networks in PC12 cells. *Thick arrows* denote Ras- and Rap1-dependent networks, which are responsible for transient and sustained ERK activation, respectively. **c** Overview of Ras and Rap1 models. *Arrows and bars* indicate activation and inactivation, respectively. *R* corresponds to phosphorylated receptors in **b**; *GEF* in the Ras and Rap1 models correspond to SOS- and C3G-dependent networks in **b**, respectively; *GAP* in the Ras and Rap1 models correspond to the RasGAP-dependent network and Rap1GAP in **b**, respectively. GEF, guanine nucleotide exchange factor; GAP, GTPase-activating protein

GEF, *GAP*, and *Ras* are set at 1, and the dissociation constant of *GEF* is set at 1. The rate constant of *GEF* activation becomes 1 when *R* is small.

Similarly, we described the Rap1 model in dimensionless form as follows:

$$\frac{d}{dt}GEF = R - (1+R)\cdot GEF \tag{4}$$

$$GAP = p \tag{5}$$

$$\frac{d}{dt} Rap1 = s\left(k \cdot GEF - \left(k \cdot GEF + GAP\right) \cdot Rap1\right) \tag{6}$$

where the parameters and assumptions are the same as those in the Ras model except that *GAP* is a constant *p* regardless of stimulation.

From Equations 1–3, we derived a steady-state solution of the Ras model as follows:

$$GEF = \frac{R}{1+R} \tag{7}$$

$$GAP = \frac{p \cdot R}{1 + p \cdot R} \tag{8}$$

$$Ras = \frac{k}{k + p \cdot \dfrac{1+R}{1+p \cdot R}} \tag{9}$$

When $p > 1$ and $R < 1/p$, *GEF* and *GAP* are asymptotically proportional to *R* (Fig. 2a, upper panel), and *Ras* is constant regardless of *R* (Fig. 2a, lower panel). When $1/p < R < 1$, *GAP* becomes saturated while *GEF* is still proportional to *R*, and *Ras* is increased with *R*. When $R > 1$, both *GEF* and *GAP* are saturated and *Ras* becomes constant.

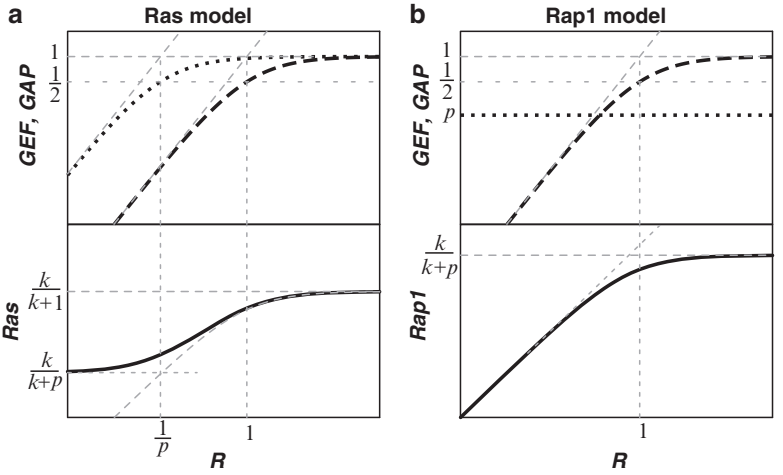

Fig. 2 Steady-state responses of Ras and Rap1 models: Ras model (**a**); Rap1 model (**b**). *Upper panels* indicate steady-state responses of *GEF* and *GAP* as indicated by *dashed and dotted lines*, respectively. K_d values, which give 50% of the maximum values, of *GEF* and *GAP* are 1 and 1/p, respectively. *Lower panels* indicate steady-state response of *Ras* and *Rap1*. Note that the log-log plot is used for all panels

From Equations 4–6, we also derived a steady-state solution of *GEF* and *Rap1* in response to *R*:

$$GEF = \frac{R}{1+R} \tag{10}$$

$$Rap1 = \frac{k}{k + p\left(1 + \frac{1}{R}\right)} \tag{11}$$

Note that *GAP* is constant in the Rap1 model. When $R < 1$, *GEF* is proportional to *R* (Fig. 2b, upper panel), and *Rap1* is also proportional to *R* (Fig. 2b, lower panel). When $R > 1$, *GEF* becomes saturated, and *Rap1* becomes constant.

In particular, when *R* is small, *Ras* becomes constant and independent from *R*, whereas *Rap1* is proportional to *R*. This result highlights one of the unique features of Rap1 systems: Rap1 captures amplitude of stimulation. Because *GEF*, *GAP*, *Ras*, and *Rap1* are not saturated when *R* is small, we can further simplify both Ras and Rap1 models:

$$\frac{d}{dt}GEF = R - GEF \tag{1′}$$

$$\frac{d}{dt}GAP = q\left(p \cdot R - GAP\right) \tag{2′}$$

$$\frac{d}{dt}Ras = s\left(k \cdot GEF - GAP \cdot Ras\right) \tag{3′}$$

$$\frac{d}{dt}GEF = R - GEF \tag{4′}$$

$$GAP = p \tag{5′}$$

$$\frac{d}{dt}Rap1 = s\left(k \cdot GEF - GAP \cdot Rap1\right) \tag{6′}$$

Initial conditions of *GEF*, *GAP*, *Ras*, and *Rap1* are set at those of the steady-state solution with $R = 1$, $p = 1$, and $k = 1$ without loss of generality. Hereafter, we used these simplified Ras and Rap1 models for further analyses. Note that constant *R* induces transient *Ras* activation when $0 < q < 1$.

Step stimulation of *R* induces transient increase of *Ras* (Fig. 3a–c). When $t < 1/q$, *GEF* and *GAP* are similarly increased (Fig. 3b), and *Ras* is also increased (Fig. 3c). When $t > 1/q$, *GEF* becomes constant while *GAP* is increased, and *Ras* is decreased; this makes a transient peak of *Ras*. From Equation 3′, *Ras* becomes closer to the *GEF*/*GAP* ratio as *s* becomes larger (Fig. 3c).

We did ramp stimulation of *R* by modified ramp function $R = (1 - e^{-rt}) + 1$, where *r* denotes increasing rate of *R*. Therefore, the ramp stimulation remains a

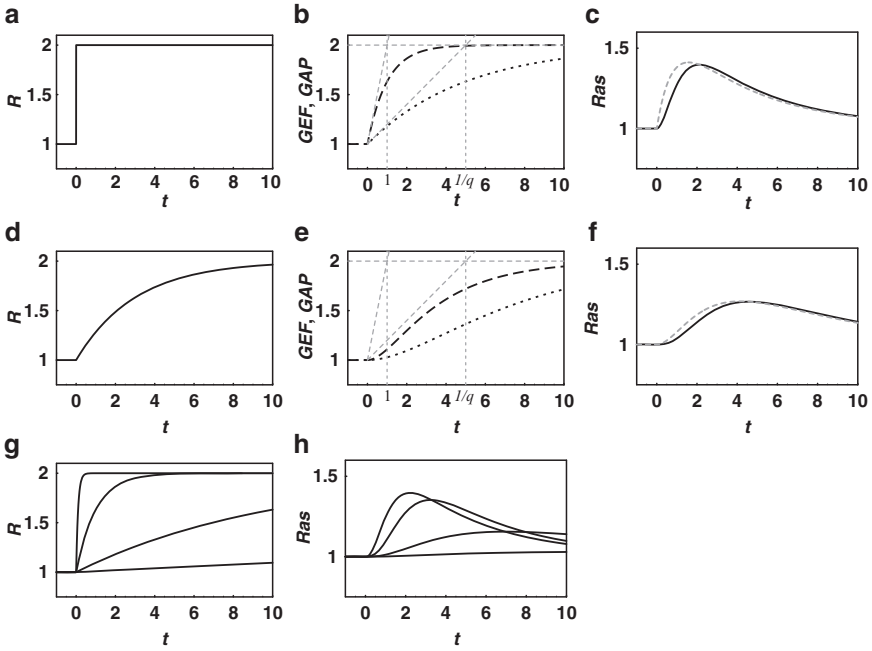

Fig. 3 Transient *Ras* response to step and ramp stimulation. **a–c** Responses to step stimulation. **d–f** Responses to ramp stimulation. **a**, **d** The step and ramp stimulation of *R*. Ramp stimulation of *R* is given by $R = (1 - e^{-rt}) + 1$ with $r = 0.333$. **b**, **e** *GEF* (*dashed line*) and *GAP* (*dotted line*) responses with $q = 0.2$. The time constant of *GEF* and *GAP* are 1 and $1/q$ as indicated, respectively. **c**, **f** *Ras* response with $s = 2$. *Gray dashed lines* in **c** and **f** indicate the *GEF*/*GAP* ratio. **h** *Ras* responses to various ramp stimulations of *R* with $r = 0.01$, 0.1, 1, and 10 (**g**)

finite dose at $t \to \infty$. Ramp stimulation of *R* induces slower *GEF* and *GAP* increase (Fig. 3d, e), resulting in a smaller *GEF*/*GAP* ratio (Fig. 3f); this delays and decreases the transient peak of *Ras* (Fig. 3f). Importantly, the transient peak of *Ras* is delayed and decreased as *r* decreases (Fig. 3g,h). Note that the final amplitude of *R* is the same regardless of the value of *r*, indicating that the Ras system captures the increasing rate of stimulation, rather than the final amplitude of stimulation. Thus, the Ras and Rap1 systems capture both the increasing rate and final amplitude of stimulation, respectively.

In PC12 cells, Ras activation occurs more rapidly than Rap1 activation (Sasagawa et al. 2005; York et al. 1998), suggesting faster and slower GEF activation for Ras and Rap1, respectively. Therefore, we analyzed the case where *GEF* activation for *Ras* is faster than that for *Rap1* (Fig. 4). Step stimulation of *R* induces transient *Ras* and sustained *Rap1* increase, respectively (Fig. 4a–c). The impulse stimulation of *R*, approximated by a pulse, sufficiently induces transient *Ras* increase, but not sustained *Rap1* increase (Fig. 4d–f). In contrast, the ramp stimulation of *R* sufficiently induces sustained *Rap1* increase but not transient *Ras* increase

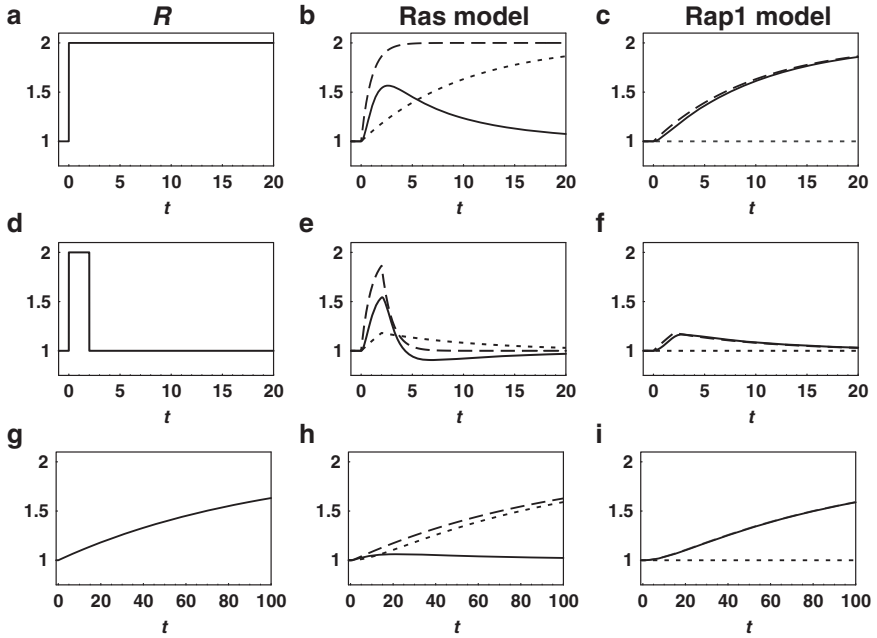

Fig. 4 Distinct *Ras* and *Rap1* responses to step, impulse, and ramp stimulation. **a–c** Responses to step stimulation. **d–f** Responses to impulse stimulation. The pulse width is set at 2. **g–i** Responses to ramp stimulation with $r = 0.01$. **a**, **d**, **g** Stimulation of R; **b**, **e**, **h** responses in *Ras* model; **c**, **f**, **i** responses in the *Rap1* model. The time constant of *GEF* activation for the Rap1 model is set at 10. All responses are calculated with $q = 0.1$ and $s = 2$. Notation for line styles is the same as in Fig. 3

(Fig. 4g–i). These results indicate that the impulse and ramp stimulation of R can specifically induce *Ras* and *Rap1* increase, respectively. This finding highlights the distinct features of the Ras and Rap1 systems. The Ras system specifically captures a rapid temporal pattern of stimulation rather than a slow temporal pattern, whereas the Rap1 system specifically captures a slow temporal pattern of stimulation rather than a rapid temporal pattern.

Appendix

We derive Equations 1–6 from Fig. 1c as follows. Molecule A has two states, inactive (A_i) and active (A^*). Conversion of A between the two states is catalyzed by effector molecules E_1^* and E_2^* as indicated in the following reaction:

$$A_i \underset{r_2 \cdot E_2^*}{\overset{r_1 \cdot E_1^*}{\rightleftarrows}} A^*$$

Forward reaction rate from A_i to A^* is assumed to be proportional to the product of A_i and E_1^* with rate constant r_1, and backward reaction rate is similarly assumed. We obtain the equation of molecule A as follows:

$$\frac{d}{dt}A^* = r_1 \cdot E_1^* \cdot A_i - r_2 \cdot E_2^* \cdot A^*.$$

A_i can be eliminated when an amount of A is conserved throughout the reaction. Similarly, we obtain Equations 1–6. Similar to biochemical reactions, we define dissociation and association constants by r_2/r_1 and r_1/r_2, respectively.

Acknowledgments We thank laboratory members for critically reading this manuscript, and the Uehara Memorial Foundation for the grant of systems biology.

References

Gotoh Y, Nishida E, Yamashita T et al (1990) Microtubule-associated-protein (MAP) kinase activated by nerve growth factor and epidermal growth factor in PC12 cells. Identity with the mitogen-activated MAP kinase of fibroblastic cells. Eur J Biochem 193:661–669.

Qiu MS, Green SH (1992) PC12 cell neuronal differentiation is associated with prolonged p21ras activity and consequent prolonged ERK activity. Neuron 9:705–717.

Sasagawa S, Ozaki Y, Fujita K et al (2005) Prediction and validation of the distinct dynamics of transient and sustained ERK activation. Nat Cell Biol 7:365–373.

Traverse S, Gomez N, Paterson H et al (1992) Sustained activation of the mitogen-activated protein (MAP) kinase cascade may be required for differentiation of PC12 cells. Comparison of the effects of nerve growth factor and epidermal growth factor. Biochem J 288(pt 2):351–355.

Vaudry D, Stork PJ, Lazarovici P et al (2002) Signaling pathways for PC12 cell differentiation: making the right connections. Science 296:1648–1649.

York RD, Yao H, Dillon T et al (1998) Rap1 mediates sustained MAP kinase activation induced by nerve growth factor. Nature (Lond) 392:622–666.

Control and Alteration of Protein Traffic in the Cell

Toshiya Endo

Mitochondrial Protein Traffic

Normal eukaryotic cell functions rely on cellular systems of protein trafficking control that ensure correct targeting and assembly of specific sets of proteins for membrane-bounded compartments or organelles. The known principles of protein traffic are that destination signals are encoded in the transported proteins themselves and that they are decoded by receptors in the target membranes, for example [1].

Mitochondria are two-membrane-bounded organelles consisting of 1000–2000 different proteins, more than 99% of which are synthesized in the cytosol as precursor proteins and subsequently imported into mitochondria. Mitochondrial protein import and sorting to one of the four subcompartments, the outer membrane, intermembrane space, inner membrane, and matrix, are mediated by proteinaceous machineries called translocators in the outer and inner mitochondrial membranes [2–5] (Fig. 1). The translocators cooperate with each other to achieve precise as well as efficient protein delivery to their intramitochondrial destinations. A translocator is a protein complex that performs multiple functions. It functions as a receptor for recognition of the targeting as well as sorting signals, and it provides a protein-conducting channel through which precursor proteins go across the membrane in an unfolded state. It also offers a driving force to achieve a vectorial movement of the translocating polypeptide chain.

Recognition of Mitochondrial Targeting Signals

The first step of mitochondrial protein traffic is the entry into the mitochondria at the outer membrane. There are multiple gates to enter mitochondria: Tom20, Tom22, and Tom70 [6]. Those receptors are the subunits of the outer membrane translocator, the TOM40 complex, and have receptor domains facing the cytosol.

T. Endo
Department of Chemistry, Graduate School of Science, Nagoya University, Nagoya, Japan

S. Nakanishi et al. (eds.), *Systems Biology*,
DOI:10.1007/978-4-431-87704-2_13, © Springer 2009

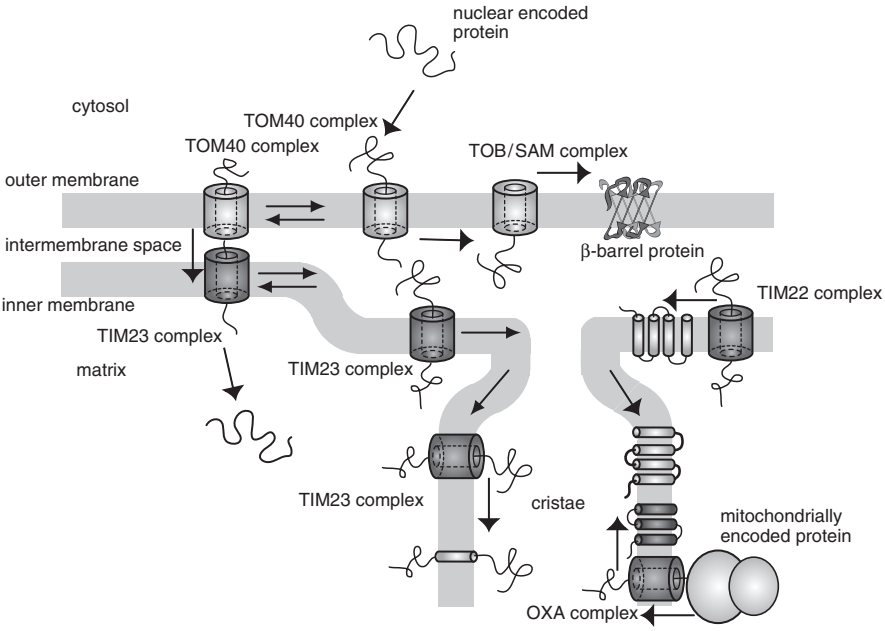

Fig. 1 Mitochondrial protein traffic. The translocators, the *TOM40* and *TOB/SAM* complexes in the outer membrane, and the *TIM23*, *TIM22*, and *OXA* complexes in the inner membrane control traffic of 1000–2000 different mitochondrial proteins

Mitochondrial precursor proteins can be classified into two groups, which are recognized by different receptors. Most mitochondrial proteins destined for the matrix or inner membrane are synthesized as precursor proteins with an N-terminal cleavable presequence. The presequence contains a mitochondrial targeting signal, which is mainly recognized by Tom20 and Tom22. On the other hand, many polytopic inner membrane proteins including the carrier protein family lack presequences. They have instead internal mitochondrial targeting signals in the mature part, which are recognized by Tom70.

We previously revealed the mechanism of discrimination of the mitochondrial targeting signal in the presequence from secretory signals in the signal sequence of secretory proteins by the receptor Tom20 [6,7]. Mitochondrial presequences do not share distinct consensus sequences, but instead display common physicochemical properties. Presequences are rich in positively charged residues and have the potential to form an amphiphilic helical structure. On the other hand, signal sequences of secretory proteins that are recognized by the cytosolic receptor SRP (signal recognition particle) contain a cluster of hydrophobic amino acids with two or more positive charges at the N-terminal region. We determined the nuclear magnetic resonance (NMR) structure of the receptor domain of rat Tom20 in a complex with a presequence peptide [7]. The presequence peptide of rat aldehyde dehydrogenase does not take an ordered structure in solution, but when bound to

the hydrophobic groove of Tom20, it takes a helical structure. Because the hydrophobic groove of Tom20 is shallow, the amphiphilic helical structure of the presequence nicely fits the hydrophobic groove. The side chains of the hydrophobic residues are aligned on one side of the amphiphilic helix and are oriented toward the hydrophobic binding groove. On the other hand, hydrophilic and/or positively charged residues are located on the other side of the helix, thereby exposing their side chains to the aqueous solution.

In contrast to Tom20, because the binding groove of SRP is much deeper than that of Tom20 [8], the helical structure of the secretory signal peptide is fully accommodated into the binding groove of SRP, so that hydrophobic residues on both sides of the helix can interact with hydrophobic residues of the groove. Therefore, the difference in the depths of the hydrophobic grooves between Tom20 and SRP could allow precise recognition of the amphiphilic helix and the hydrophobic helix by their cognate receptors. This concept explains well the fact that mitochondrial targeting signals lack a strict consensus sequence motif and mitochondrial receptors have to recognize rather a broad range of sequences of mitochondrial targeting signals. Nevertheless, recognition by Tom20 may not be sufficient to explain the highly precise targeting of mitochondrial precursor proteins.

Our current understanding is that mitochondrial presequences are recognized by an array or chain of presequence-binding receptor proteins [2–5]. For example, after crossing the outer membrane through the TOM40 channel, the presequence is recognized by another receptor site (*trans* site) of the TOM40 complex on the intermembrane-space side of the outer membrane. Then, proteins destined for the matrix have to cross the inner membrane, and therefore they are recognized by Tim50, another receptor of the TIM23 complex, which is a translocator in the inner membrane for protein translocation across the inner membrane [9,10]. The presequence is transferred from the outer membrane receptor Tom20 and the *trans* site of the TOM40 complex to the inner membrane receptor Tim50, most likely following the affinity gradient between Tom20 and Tim50.

What receives the presequence next? It is Tim23 of the TIM23 complex that receives the presequence from Tim50. This step now requires input of energy, i.e., the membrane potential across the inner membrane. The energy is likely required for clearance of the presequence from the high-affinity presequence binding site. The presequence is then transferred to the matrix side through the import channel of the TIM23 complex, to be bound by mitochondrial Hsp70 in the matrix. Mitochondrial Hsp70 pulls in the presequence to achieve vectorial movement of the precursor protein.

Alteration of the Targeting Signal–Receptor Pair

Because we now understand the details of the recognition mechanism of mitochondrial targeting signals by receptor components along the import pathway, it is time for us to attempt to artificially alter the mitochondrial protein traffic by changing

the import receptors. The basic idea is that mitochondrial proteins have a mitochondrial targeting signal, which is recognized by mitochondrial import receptors such as Tom20. Then, we change the signal recognition site of the receptor proteins, so that standard mitochondrial targeting signals cannot be recognized by the altered receptor. Then we screen for new targeting signals that are recognized by the altered receptor. Combination of the altered receptor and new targeting signals could be used to change the bulk of resident proteins in mitochondria, resulting in formation of mitochondria with a new function.

Generation of Mutant Tom20 with Altered Substrate Specificity

Although we determined the NMR structure of rat Tom20 in a complex with a presequence, the three-dimensional structure of yeast Tom20 or its complex with a presequence is not available. Therefore, we estimated the structure of yeast Tom20 by homology modeling using the software DS Modeling (Accelrys, San Diego, CA, USA). Then we put a presequence of yeast cytochrome oxidase subunit IV onto the yeast Tom20 structure. As we know that Tom20 has a hydrophobic groove that can accommodate the hydrophobic side of the amphiphilic helix of the presequence, we replaced several hydrophobic residues in the groove with hydrophilic and positively charged lysine. When we replaced wild-type Tom20 with those mutant Tom20s in yeast cells, the mutant cells cannot grow rapidly, as we expected for mutant Tom20 with altered substrate specificity.

To choose a Tom20 mutant that fits our purpose best, we analyzed protein levels of the Tom20 mutants. Some mutant Tom20s showed lowered protein levels, suggesting that they are not stable in cells. We thus chose Tom20 mutants including V97K-I133K, which exhibits a sufficiently high expression level.

Next, we checked that mutant Tom20s do not affect the assembly structures of the TOM40 complex. For this purpose, we performed blue-native polyacrylamide gel electrophoresis (BN-PAGE) analyses of the solubilized mitochondria with mutant Tom20s. The intact TOM40 complex with wild-type Tom20 showed a band of a 450-kDa complex on a BN-PAGE gel. Some mutant Tom20s caused breakdown of the TOM40 complex, but the others did not. Of note, mutant Tom20 V97K-I133K showed that it does not affect the 450-kDa complex of the TOM40 complex.

Screening System to Select Mutant Presequences Recognized by Mutant Tom20

Next, we set up a system to screen for mutant presequences that are recognized by mutant Tom20 (V97K-I133K) but not by wild-type Tom20 (Fig. 2). Yeast (*Saccharomyces cerevisiae*) can produce energy by both alcohol fermentation and respiration. Respiration requires the electron transport system on the inner membrane, including cytochrome oxidase. We thus first disrupted the *COX IV* gene for

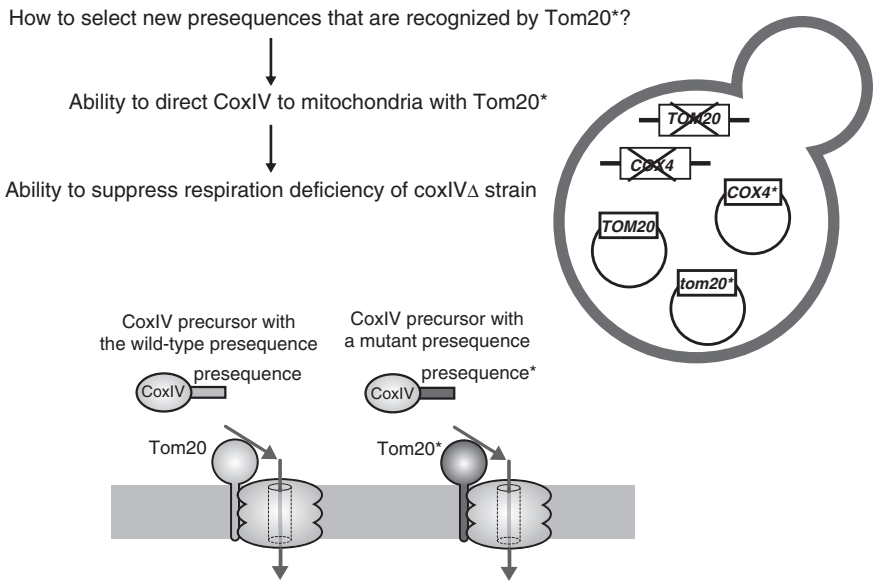

Fig. 2 Strategy to screen for mutant presequences to be recognized by altered Tom20

the cytochrome oxidase subunit IV precursor. This strain can grow on a fermentable medium such as glucose but not on a nonfermentable medium such as glycerol. However, when the gene for Cox IV precursor was inserted into a plasmid to be introduced in this cell, the expressed Cox IV was transported to mitochondria to make the mitochondria respiration competent.

Now, if expression of wild-type Tom20 is shut off, and instead mutant Tom20 is expressed, the CoxIV precursor cannot enter the mitochondria because its presequence is not recognized by mutant Tom20. Now we can use this system to screen for mutant presequences that can be recognized by mutant Tom20, because such a presequence can direct CoxIV to make the mitochondria respiration competent. We are at the moment screening for such presequences. Once we obtain altered presequences that can be recognized by altered Tom20 (V97K-I113K), but not by the original wild-type Tom20, we could introduce a set of mitochondria with a new presequence and their cognate Tom20 mutant into yeast cells to change the bulk of mitochondrial proteins.

Future Perspective

Even if we obtain a set of altered Tom20-preseuqence pairs, we need to overcome several practical problems to reach our goal. For example, mutant presequences for altered Tom20 should be adjusted for best recognition by a chain of downstream

receptors along the import pathway, otherwise the mutant presequences cannot guide passenger proteins to the desired intramitochondrial compartments in new mitochondria with altered Tom20. Another problem is the mitochondrial fusion. Because mitochondria frequently undergo fusion and fission that would cause mixing of mitochondrial contents [11], we need to prevent such mixing to keep distinct sets of mitochondria intact after their delivery to new mitochondria with altered Tom20. After successful resolution of those problems, we hope that we will be able to make new mitochondria with a new function by altering mitochondrial targeting signals and their cognate receptor protein.

Acknowledgments I thank K. Mizutani, T. Sato, and T. Yoshihisa for their collaboration in this work.

References

1. Schatz, G. and Dobberstein, B. (1996). Common principles of protein translocation across membranes. Science 271:1519–1526.
2. Endo, T., Yamamoto, H., and Esaki, M. (2003). Functional cooperation and separation of translocators in protein import into mitochondria, the double-membrane bounded organelles. J. Cell Sci. 116:3259–3267.
3. Wiedemann, N., Frazier, A.E., and Pfanner, N. (2004). The protein import machinery of mitochondria. J. Biol. Chem. 279:14473–14476.
4. Neupert, W. and Herrmann, J.M. (2007). Translocation of proteins into mitochondria. Annu. Rev. Biochem. 76:723–749.
5. Koehler, C.M. (2004). New developments in mitochondrial assembly. Annu. Rev. Cell Dev. Biol. 20:309–335.
6. Endo, T. and Kohda, D. (2002). Functions of outer membrane receptors in mitochondrial protein import. Biochim. Biophys. Acta 1592:3–14.
7. Abe, Y., Shodai, T., Muto, T., Mihara, K., Torii, H., Nishikawa, S., Endo, T., and Kohda, D. (2000). Structural basis of presequence recognition by the mitochondrial protein import receptor Tom20. Cell 100:551–560.
8. Keenan, R.J., Freyman, D.M., Walter, P., and Stroud, R.M. (1998). Crystal structure of the signal sequence binding subunit of the signal recognition particle. Cell 94:181–191.
9. Geissler, A., Chacinska, A., Truscott, K.N., Wiedemann, N., Brandner, K., Sickmann, A., Meyer, H.E., Meisinger, C., Pfanner, N., and Rehling, P. (2002). The mitochondrial presequence translocase: an essential role of Tim50 in directing preproteins to the import channel. Cell 111:507–518.
10. Yamamoto, H., Esaki, M., Kanamori, T., Tamura, Y., Nishikawa, S., and Endo, T. (2002.) Tim50 is a subunit of the TIM23 complex that links protein translocation across the outer and inner mitochondrial membranes. Cell 111:519–528.
11. Okamoto, K. and Shaw, J.M. (2005). Mitochondrial morpology and dynamics in yeast and multicellular eukaryotes. Annu. Rev. Genet. 39:503–536.

Plant Functional Genomics Based on Integration of Metabolomics and Transcriptomics: Toward Plant Systems Biology

Kazuki Saito

Introduction

By taking the advantages of development of sequencing technology, the genome sequences of several plant species have been revealed: these include *Arabidopsis thaliana* [1], *Oryza sativa* (rice) [2], *Populus trichocarpa* (poplar) [3], *Vitis vinifera* (grapevine) [4], and *Sorghum bicolor* (sorghum) (http://www.phytozome.net/sorghum). However, even in *Arabidopsis*, which is most extensively investigated in terms of gene function, only half the genes have been functionally annotated based on sequence similarity to known genes, and the function of only about 11% has been confirmed with evidence [5]. Therefore, the identification of the function of unknown genes is currently a major subject in plant genomics. Analyses of the changes in plants in which specific genes are either overexpressed (*gain-of-function* experiment) or knocked out (*loss-of-function* experiment) are generally used for decoding the functions of genes. Systematic analyses of the transcriptome and metabolome, in particular, correlating the expression pattern of genes with the accumulation pattern of metabolites, could be an excellent way for deducing the functions of genes, even if these engineered plants do not show apparent phenotypic alternation [6–9].

In plants, a large number of genes involved in primary and secondary metabolism are present to form multigene families, for example, in *Arabidopsis*, 30 terpene synthase genes, 272 cytochrome P450 genes, 107 glycosyltransferase genes, and 130 ABC protein genes [10]. These genes are believed to be involved in the synthesis, modification, degradation, and/or transport of particular metabolites in plants. Compared with the model plant *Arabidopsis*, the situation is more complicated in the case of other plants, even if their genome sequences are available, because of the lack of feasible genetic resources for functional investigation such as large mutant panels and full-length cDNA collections. The integration of metabolic profiles with gene expression profiles can provide hints for the identification of functions

K. Saito
Chiba University, Graduate School of Pharmaceutical Sciences, Inage-ku, Chiba 263-8522, Japan, and RIKEN Plant Science Center, Tsurumi-ku, Yokohama 230-0045, Japan

S. Nakanishi et al. (eds.), *Systems Biology*,
DOI:10.1007/978-4-431-87704-2_14, © Springer 2009

of unknown metabolic genes, regardless of model or nonmodel plants. With the recent advances of sophisticated bioinformatics tools and analytical technology, the systems biology approach becomes more realistic to solve biological problems. In this chapter, the functional genomics study of combining transcriptome and metabolome is discussed, leading to the development of plant systems biology.

Functional Identification of Genes Involved in Metabolism by Integration of Transcriptomics and Metabolomics

A set of genes involved in a certain biological process are generally coregulated and thus coexpressed under the control of a shared regulatory system. Therefore, if an unknown gene is coexpressed with known genes of a particular biological process, this unknown gene is likely to be involved in this process. This co-occurrence principle can be extended to metabolite co-accumulation relationships with the expression pattern of genes in the particular pathway in which the metabolite is involved. Given that a pathway is modulated by mutation or stress, this modulation can be characterized by metabolic profiling. By using this combined strategy of gene coexpression and metabolic profiling under given conditions, a comprehensive prediction of genes involved in a particular process can be achieved. Then, once the genes of interest are prioritized by gene-to-metabolite connection, reverse genetics and biochemistry of recombinant proteins are conducted by taking the advantages of the publicly available rich bioresources of *A. thaliana*. Finally, comprehensive gene identification and discovery of networks of genes and metabolites can be elucidated (Fig. 1) [9]. Several studies that successfully applied this principle are discussed hereafter.

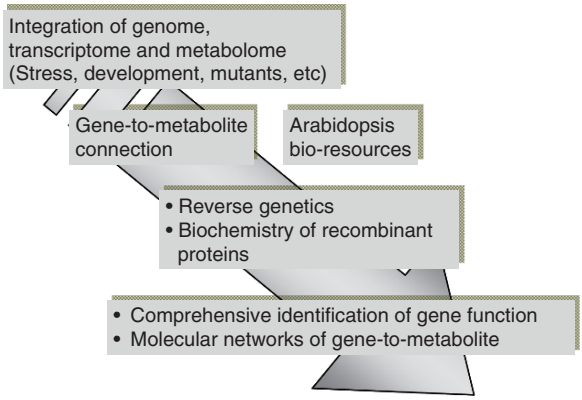

Fig. 1 Concept for integrated post-genomics study

Flavonoid-Related Genes

A comprehensive analysis of the metabolome and transcriptome of *A. thaliana* overexpressing the *PAP1* gene encoding an MYB transcription factor was carried out for the identification of novel gene functions involved in flavonoid biosynthesis [11]. For metabolome analysis, two metabolic profiling methods were applied: flavonoid-targeted analysis by high-performance liquid chromatography-mass spectrometry (LC-MS) and nontargeted analysis by Fourier transform ion-cyclotron mass spectrometry (FTICR-MS). The advantages of FTICR-MS are its ultrahigh-resolution capacity and high m/*z* accuracy. This combined analysis revealed the specific accumulation of cyanidin and quercetin derivatives and identified 8 novel anthocyanins from an array of putative 1,800 metabolites in *PAP1* overexpressing plants. The transcriptome analysis of more than 20,000 genes on a DNA microarray revealed the induction of 38 genes by ectopic overexpression of the *PAP1* transcription factor. Several genes with unidentified functions, encoding biosynthetic enzymes, transporters, and transcription factors, were induced by *PAP1*. Two putative glycosyltransferase genes (At5g17050 and At4g14090) induced by *PAP1* expression were confirmed to encode flavonoid 3-*O*-glucosytransferase and anthocyanin 5-*O*-glucosyltransferase, respectively, from the enzymatic activity of their recombinant proteins and results of the analysis of anthocyanins in the respective gene knockout mutants. Furthermore, the functions of a novel acyltransferase [12] and a glutathione *S*-transferase [13] were confirmed by the same approach. This innovative means of predicting novel gene functions has been further extended by using publicly available datasets of the *Arabidopsis* transcriptome.

Glycosylation plays a major role in the remarkable chemical diversity of flavonoids in plants, including *A. thaliana*. However, the wide diversity of proteins encoded by the large gene family of type 1 glycosyltransferases (UGT) hampers the determination of the biochemical function of each gene solely from its primary sequence. Transcriptome coexpression analysis combined with a reverse genetics approach led to the identification of a gene dominantly determining the flavonoid patterns in *Arabidopsis* [14]. This investigation efficiently applied transcriptome coexpression analysis with the ATTED-II database [15] and its mirror site Correlated Gene Search at PRIMe (http://prime.psc.riken.jp/), which are the secondary databases derived from a public *Arabidopsis* transcriptome dataset with Affymetrix ATH1 GeneChip [16]. The expression pattern of a UGT gene denoted as UGT1 in Fig. 2 was found to be highly correlated with known flavonoid biosynthetic genes. No C-7 rhamnosylated flavonols were detected in two knockout mutants by insertion of T-DNA into this *UGT89C1* gene. This specific metabolite deficiency in the mutants was restored by stable transformation with the genomic fragment containing intact *UGT89C1*. Biochemical tests using recombinant proteins also indicated that *UGT89C1* functions as flavonol 7-*O*-rhamnosyltransferase. As an another example, the metabolic profiling of the mutant lacking a methyltransferase gene *AtOMT1* (At5g54160) narrowed down by the coexpression analysis showed that gene is involved not only in the production of lignins and sinapoyl

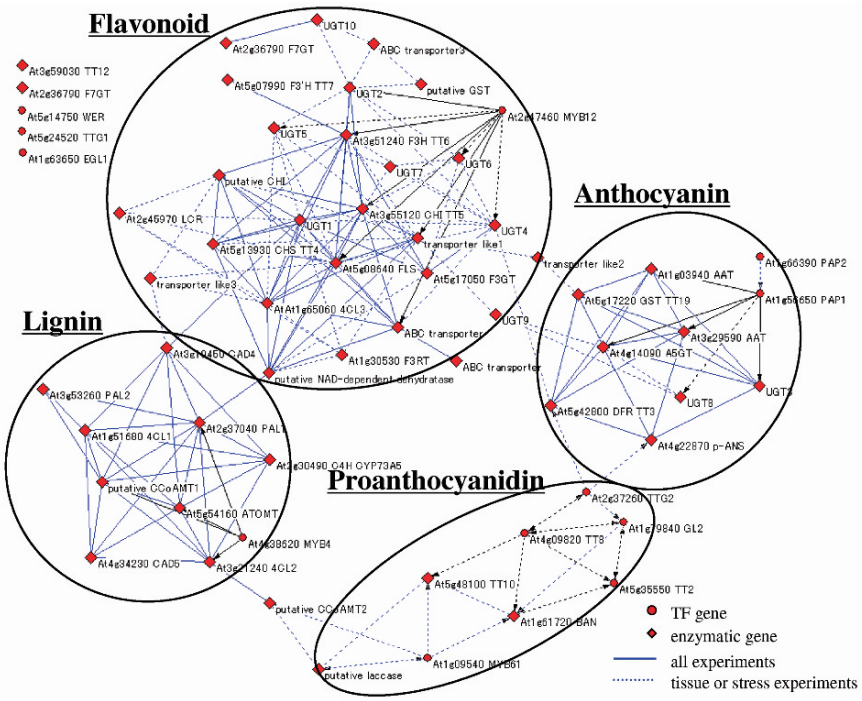

Fig. 2 Coexpression graph of *Arabidopsis* genes related to phenylpropanoid and flavonoids (courtesy of T. Tohge and K. Yonekura-Sakakibara)

esters but also in the methylation of flavonols forming isorhamnetin [17]. These study demonstrates that the integration of transcriptome coexpression analysis with a reverse genetic approach is a versatile tool for elucidation of the multigene family of metabolic pathways in *Arabidopsis*.

Sulfur Metabolism-Related Genes

The feasibility of the batch-learning self-organizing map (BL-SOM) for high-throughput analysis of post-genomic data on plant biology has been illustrated [18]. BL-SOM is a modification of the conventional self-organizing map (SOM), which provides colored feature maps independent of the order of data input. The nutritional stress experiments on *A. thaliana* were analyzed by computation with BL-SOM for the data sets of metabolome and transcriptome obtained by FTICR-MS and DNA array. BL-SOM analyses of nontargeted metabolome data provided metabolic fingerprinting of global responses to nutritional stress and development. The excellent clustering performance of BL-SOM led to metabolite annotation from accurate m/z values, suggesting a metabolic mechanism responding to sulfur deficiency. Transcriptome data were also analyzed by BL-SOM, and genes responding

to sulfur deficiency were classified according to their expression patterns. The results showed that functionally related genes were nicely clustered in the same or neighbor lattice points on BL-SOM feature maps.

This principle of coexpression and co-accumulation by BL-SOM analysis was further applied to metabolomic and transcriptomic data of *Arabidopsis* grown under sulfur deficiency to decode novel gene function [19, 20]. The metabolism of glucosinolates was shown to be coordinately regulated under sulfur starvation. Three uncharacterized putative sulfotransferase genes clustering together with known glucosinolate biosynthesis genes were candidates for involvement in biosynthesis. In vitro enzymatic assays of the recombinant gene products prioritized by the integrated analysis confirmed their functions as desulfoglucosinolate sulfotransferases. Several genes involved in sulfur assimilation clustered with *O*-acetylserine, which is considered a positive regulator of these genes. The genes involved in anthocyanin biosynthesis clustered with the gene encoding a transcriptional factor that upregulates specifically anthocyanin biosynthesis genes.

The discovery of two R2R3-MYB transcription factors that positively control the biosynthesis of glucosinolates in *Arabidopsis* was achieved by an integrated omics approach [21]. Combined transcriptome coexpression analysis of publicly available condition-independent data and the condition-specific (i.e., sulfur deficiency in this case) data identified *MYB28* and *MYB29* as candidate transcription factor genes specifically involved in the regulation of aliphatic glucosinolate production. Analysis of a knockout mutant and ectopic expression of the gene demonstrated that *MYB28* is a positive regulator for basal-level production of aliphatic glucosinolates. In contrast, *MYB29* presumably plays an accessory function for methyl jasmonate-mediated induction of a set of aliphatic glucosinolate biosynthetic genes. Overexpression of *MYB28* in *Arabidopsis* cultured suspension cells resulted in the production of large amounts of glucosinolates. Because an *Arabidopsis* cell suspension produces no glucosinolates, this study indicates the possibility of efficient industrial production of glucosinolates by manipulation of these transcription factors. A working model for regulation of glucosinolate production involving these genes was postulated.

Systems Analysis of Genotype-Dependent Metabolic Regulation by Metabolomic Approach

Metabolites are not only the catalytic products of enzymatic reactions but also the active regulators or the ultimate phenotypic representatives of homeostasis in highly complex cellular processes. Such a mode of regulation can be revealed by biochemical networks. The metabolic network between wild-type and two mutant [*methionine-over accumulation 1* (*mto1*) and *transparent testa4* (*tt4*)] plants was investigated regarding the alteration of metabolite accumulation in *A. thaliana* [22]. In the GC-TOF/MS analysis, quantitative information was acquired regarding more than 170 metabolites. In addition to the conventional analysis regarding the levels of metabolites, metabolite-to-metabolite correlations across individual plants caused

by tiny environmental fluctuations was analyzed by a novel score, z-score of index metabolite, describing the correlation of a given metabolite to others. Although the two mutants showed no apparent morphological abnormalities, the overall correlation values in *mto1* were much lower than those of the wild-type and *tt4* plants. These findings suggested the loss of overall network stability caused by the uncontrolled accumulation of methionine. In the *tt4* mutant, a new correlation between malate and sinapate was observed, although the levels of malate, sinapate, and sinapoylmalate remain unchanged, suggesting an adaptive reconfiguration of the network module by this mutation. Gene expression correlations presumably responsible for these metabolic networks were determined using the metabolite correlations as clues. As the conclusions, two Arabidopsis mutants, *mto1* and *tt4*, exhibited the following changes in the entire metabolome network: the overall loss of metabolic stability (*mto1*) or the generation of a metabolic network of a backup pathway for the lost physiological functions (*tt4*). The expansion of metabolite correlation to gene expression correlation provides detailed insights into the systemic understanding of the plant cellular process regarding metabolomes and transcriptomes.

Conclusions and Future Prospects

Recent advances of sophisticated bioinformatics tools and analytical technology allowed the systems biological approach to be more realistic for solving biological problems that have not been well addressed by simple reductionism. We foresee the development of systems biology driven by large datasets of transcriptome, metabolome, proteome, and fluxome. The recently developed ultrahigh-speed sequencing technology is likely to be exploited for meeting the challenge of sequencing a whole genome or large cDNA collections of a variety of plant species, including crops and pharmaceutical plants. The systems biology approach based on construction of mathematical models using large omics datasets will open a new avenue for our better understanding of hidden networks of molecular elements (gene, transcripts, proteins, and metabolites) in plant life. This information will be eventually applicable to biotechnology in the new era where plant biotechnology could play a more indispensable role in our lives.

Acknowledgments I thank my colleagues who have participated in this project. Part of this study has been supported by Uehara Memorial Foundation, Japan.

References

1. The Arabidopsis Genome Initiative (2000) Analysis of the genome sequence of the flowering plant *Arabidopsis thaliana*. Nature (Lond) 408:796–815.
2. International Rice Genome Sequencing Project (2005) The map-based sequence of the rice genome. Nature (Lond) 436:793–800.

3. Tuskan, G. A., Difazio, S., Jansson, S., Bohlmann, J., Grigoriev, I., Hellsten, U., Putnam, N., Ralph, S., Rombauts, S., Salamov, A., Schein, J., Sterck, L., Aerts, A., Bhalerao, R. R., Bhalerao, R. P., Blaudez, D., Boerjan, W., Brun, A., Brunner, A., Busov, V., Campbell, M., Carlson, J., Chalot, M., Chapman, J., Chen, G. L., Cooper, D., Coutinho, P. M., Couturier, J., Covert, S., Cronk, Q., Cunningham, R., Davis, J., Degroeve, S., Dejardin, A., Depamphilis, C., Detter, J., Dirks, B., Dubchak, I., Duplessis, S., Ehlting, J., Ellis, B., Gendler, K., Goodstein, D., Gribskov, M., Grimwood, J., Groover, A., Gunter, L., Hamberger, B., Heinze, B., Helariutta, Y., Henrissat, B., Holligan, D., Holt, R., Huang, W., Islam-Faridi, N., Jones, S., Jones-Rhoades, M., Jorgensen, R., Joshi, C., Kangasjarvi, J., Karlsson, J., Kelleher, C., Kirkpatrick, R., Kirst, M., Kohler, A., Kalluri, U., Larimer, F., Leebens-Mack, J., Leple, J. C., Locascio, P., Lou, Y., Lucas, S., Martin, F., Montanini, B., Napoli, C., Nelson, D. R., Nelson, C., Nieminen, K., Nilsson, O., Pereda, V., Peter, G., Philippe, R., Pilate, G., Poliakov, A., Razumovskaya, J., Richardson, P., Rinaldi, C., Ritland, K., Rouze, P., Ryaboy, D., Schmutz, J., Schrader, J., Segerman, B., Shin, H., Siddiqui, A., Sterky, F., Terry, A., Tsai, C. J., Uberbacher, E., Unneberg, P., et al. (2006) The genome of black cottonwood, *Populus trichocarpa* (Torr. & Gray). Science 313:1596–604.
4. Jaillon, O., Aury, J. M., Noel, B., Policriti, A., Clepet, C., Casagrande, A., Choisne, N., Aubourg, S., Vitulo, N., Jubin, C., Vezzi, A., Legeai, F., Hugueney, P., Dasilva, C., Horner, D., Mica, E., Jublot, D., Poulain, J., Bruyere, C., Billault, A., Segurens, B., Gouyvenoux, M., Ugarte, E., Cattonaro, F., Anthouard, V., Vico, V., Del Fabbro, C., Alaux, M., Di Gaspero, G., Dumas, V., Felice, N., Paillard, S., Juman, I., Moroldo, M., Scalabrin, S., Canaguier, A., Le Clainche, I., Malacrida, G., Durand, E., Pesole, G., Laucou, V., Chatelet, P., Merdinoglu, D., Delledonne, M., Pezzotti, M., Lecharny, A., Scarpelli, C., Artiguenave, F., Pe, M. E., Valle, G., Morgante, M., Caboche, M., Adam-Blondon, A. F., Weissenbach, J., Quetier, F. & Wincker, P. (2007) The grapevine genome sequence suggests ancestral hexaploidization in major angiosperm phyla. Nature (Lond) 449:463–7.
5. The Multinational Arabidopsis Steering Commitee (2007) The Multinational Coordinated *Arabidopsis thaliana* Functional Genomics Project. Annual Report 2007.
6. Bino, R. J., Hall, R. D., Fiehn, O., Kopka, J., Saito, K., Draper, J., Nikolau, B. J., Mendes, P., Roessner-Tunali, U., Beale, M. H., Trethewey, R. N., Lange, B. M., Wurtele, E. S. & Sumner, L. W. (2004) Potential of metabolomics as a functional genomics tool. Trends Plant Sci 9:418–25.
7. Oksman-Caldentey, K. M. & Saito, K. (2005) Integrating genomics and metabolomics for engineering plant metabolic pathways. Curr Opin Biotechnol 16:174–9.
8. Schauer, N. & Fernie, A. R. (2006) Plant metabolomics: towards biological function and mechanism. Trends Plant Sci 11:508–16.
9. Saito, K., Hirai, M. & Yonekura-Sakakibara, K. (2008) Decoding genes by coexpression network and metabolomics: 'majority report by precogs.' Trends Plant Sci 13:36–43.
10. D'Auria, J. C. & Gershenzon, J. (2005) The secondary metabolism of *Arabidopsis thaliana*: growing like a weed. Curr Opin Plant Biol 8:308–16.
11. Tohge, T., Nishiyama, Y., Hirai, M. Y., Yano, M., Nakajima, J., Awazuhara, M., Inoue, E., Takahashi, H., Goodenowe, D. B., Kitayama, M., Noji, M., Yamazaki, M. & Saito, K. (2005) Functional genomics by integrated analysis of metabolome and transcriptome of *Arabidopsis* plants over-expressing an MYB transcription factor. Plant J 42:218–35.
12. Luo, J., Nishiyama, Y., Fuell, C., Taguchi, G., Elliott, K., Hill, L., Tanaka, Y., Kitayama, M., Yamazaki, M., Bailey, P., Parr, A., Michael, A. J., Saito, K. & Martin, C. (2007) Convergent evolution in the BAHD family of acyl transferases: identification and characterization of anthocyanin acyl transferases from *Arabidopsis thaliana*. Plant J 50:678–95.
13. Wangwattana, B., Koyama, Y., Nishiyama, Y., Kitayama, M., Yamazaki, M. & Saito, K. (2008) Characterization of PAP1-upregulated glutathione S-transferase genes in *Arabidopsis thaliana*. Plant Biotechnol 25:191–6.
14. Yonekura-Sakakibara, K., Tohge, T., Niida, R. & Saito, K. (2007) Identification of a flavonol 7-*O*-rhamnosyltransferase gene determining flavonoid pattern in *Arabidopsis* by transcriptome coexpression analysis and reverse genetics. J Biol Chem 282:14932–41.

15. Obayashi, T., Kinoshita, K., Nakai, K., Shibaoka, M., Hayashi, S., Saeki, M., Shibata, D., Saito, K. & Ohta, H. (2007) ATTED-II: a database of co-expressed genes and cis elements for identifying co-regulated gene groups in *Arabidopsis*. Nucleic Acids Res 35:D863–9.
16. Goda, H., Sasaki, E., Akiyama, K., Maruyama-Nakashita, A., Nakabayashi, K. et al. (2008) The AtGenExpress hormone- and chemical-treatment data set: Experimental design, data evaluation, model data analysis, and data access. Plant J 55:526–42.
17. Tohge, T., Yonekura-Sakakibara, K., Niida, R., Watanabe-Takahashi, A. & Saito, K. (2007) Phytochemical genomics in *Arabidopsis thaliana*: a case study for functional identification of flavonoid biosynthesis genes. Pure Appl Chem 79:811–23.
18. Yano, M., Kanaya, S., Altaf-UI-Amin, M., Kurokawa, K., Hirai, M. Y. & Saito, K. (2006) Integrated data mining of transcriptome and metabolome based on BL-SOM. J Comput Aid Chem 7:125–36.
19. Hirai, M. Y., Yano, M., Goodenowe, D. B., Kanaya, S., Kimura, T., Awazuhara, M., Arita, M., Fujiwara, T. & Saito, K. (2004) Integration of transcriptomics and metabolomics for understanding of global responses to nutritional stresses in *Arabidopsis thaliana*. Proc Natl Acad Sci U S A 101:10205–10.
20. Hirai, M. Y., Klein, M., Fujikawa, Y., Yano, M., Goodenowe, D. B., Yamazaki, Y., Kanaya, S., Nakamura, Y., Kitayama, M., Suzuki, H., Sakurai, N., Shibata, D., Tokuhisa, J., Reichelt, M., Gershenzon, J., Papenbrock, J. & Saito, K. (2005) Elucidation of gene-to-gene and metabolite-to-gene networks in *Arabidopsis* by integration of metabolomics and transcriptomics. J Biol Chem 280:25590–5.
21. Hirai, M. Y., Sugiyama, K., Sawada, Y., Tohge, T., Obayashi, T., Suzuki, A., Araki, R., Sakurai, N., Suzuki, H., Aoki, K., Goda, H., Nishizawa, O. I., Shibata, D. & Saito, K. (2007) Omics-based identification of *Arabidopsis* Myb transcription factors regulating aliphatic glucosinolate biosynthesis. Proc Natl Acad Sci U S A 104:6478–83.
22. Kusano, M., Fukushima, A., Arita, M., Jonsson, P., Moritz, T., Kobayashi, M., Hayashi, N., Tohge, T. & Saito, K. (2007) Unbiased characterization of genotype-dependent metabolic regulations by metabolomic approach in *Arabidopsis thaliana*. BMC Syst Biol 1:53.

A Possible Role of Homeostasis Between Monomeric and Filamentous Actin in Filament Nucleation Revealed by Pharmacokinetic Modeling

Naoki Watanabe and Chiharu Higashida

Introduction

The currently prevailing method to elucidate molecular functions in vivo is to knock out or knock down gene expression and to observe the resultant phenotypic changes. For example, fibroblasts extend pseudopods called lamellipodia toward the source of the platelet-derived growth factor (PDGF) gradient. We now know tens of molecules, both cell signaling intermediates and cytoskeleton regulators, involved in such cell polarization and migration. They interact with each other in a complicated manner both spatially and temporally. Our laboratory has recently carried out a screening to examine the effect of knockdown of Rho family GTPases on PDGF-induced chemotaxis. Many of these molecules have been implicated in the regulation of the cytoskeleton. Depletion of several Rho family GTPases had profound and distinct effects on cell morphology during migrating (Monypenny, J. et al., submitted). But given the complexity of the molecular interplay, it often remains unclear whether the induced phenotype is a direct or an indirect consequence of individual treatment. Even with the data showing clear morphological phenotypes, the question as to whether individual molecules function locally or globally, for example, is not easy to answer.

How, then, can we investigate such fast and complex mechanisms in detail?

Currently, we are applying several approaches to solve this question. One is directly capturing biochemical reactions quantitatively in living cells using "single-molecule observation of cytoskeletal reorganization." The second is "fast perturbation of the system using small compounds." Drug treatment provides useful information in combination with time-lapse imaging as it enables us to capture initial effects of perturbation. Then, we apply "systematic configuration of biochemistry" to discover hidden connections between biochemical functions in the system. The actin system is one of the best characterized systems biochemically in

N. Watanabe and C. Higashida
Department of Pharmacology, Kyoto University Faculty of Medicine,
Yoshida Konoe-cho, Sakyo-ku, Kyoto 606-8501, Japan

S. Nakanishi et al. (eds.), *Systems Biology*,
DOI:10.1007/978-4-431-87704-2_15, © Springer 2009

vitro, and much information is available. Here we describe a specific topic on our recent discovery of a role of homeostasis between monomeric and filamentous actin in filament nucleation. In this example, systematic integration of biochemical parameters by the use of pharmacokinetic simulation gave us an insight into an unexpected outcome induced by drug manipulation of cellular actin systems.

Turnover Between Filamentous and Globular Actin in Cells

In cells, actin exists in two forms, monomeric G-actin and filamentous F-actin. Current modern microscopy allows single-molecule observation of fluorescently labeled actin at the filamentous state in living cells. Cytoskeletal proteins stay attached to cellular structures on the order of seconds and stop random diffusion temporarily. This property makes it feasible to visualize single molecules of cell structure-associated probes when introduced at a very low density. In this way, we can visualize and measure spatiotemporal dynamics of assembly and disassembly of cytoskeletons in living cells [1,2].

As observed in our single-molecule imaging using GFP-actin as a probe [1], F-actin turnover is very dynamic. In typical cultured cells, the conversion between G-actin and F-actin occurs in every one-half minute to several minutes [1,3–5]. Another property commonly found in cultured cells is that G-actin and F-actin exist at roughly a 1:1 ratio. The cellular concentration of G-actin may exceed 100 μM. Therefore, similarly abundant G-actin-sequestering proteins are required to bind and prevent G-actin from polymerization (Fig. 1).

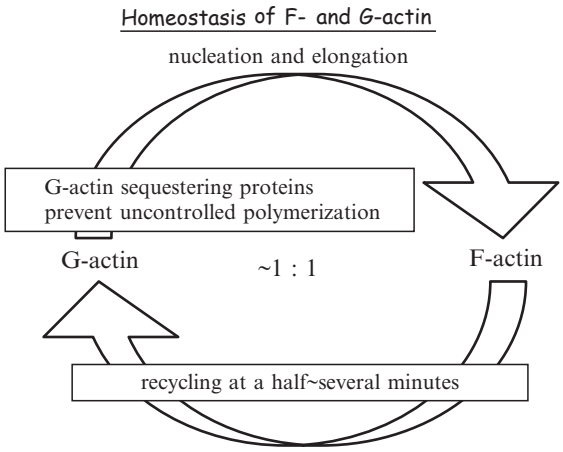

Fig. 1 Actin filament turnover in cells. In typical cultured cells, conversion between monomeric G-actin and filamentous F-actin occurs in every one-half minute to a few minutes. Another common property is that G-actin and F-actin exist roughly at a 1:1 ratio. The concentration of G-actin in cells may exceed 100 μM. G-actin-sequestering proteins bind G-actin and prevent it from polymerization

To form de novo filaments from G-actin, actin assembly undergoes two steps, nucleation and elongation [6]. In the nucleation step, the formation of actin dimers and trimers occurs frequently in solution. However, dissociation of subunits is also very fast, and this reaction barely proceeds forward. Once filament nuclei consisting of four actin subunits are formed, they act as a filament, and actin elongation proceeds steadily. In cells, elongation is driven largely by the profilin–actin complex. The rate of actin nucleation depends on free G-actin squared to cubed concentration. Filament nucleation occurs spontaneously in physiological salt condition, but this step requires a long time in typical in vitro experiments.

In cells, to nucleate filaments efficiently, actin nucleators are required. One of the major actin nucleators is Arp2/3 complex [7,8]. Arp2/3 complex nucleates the filaments off the side of preexisting filaments. This branched network is abundantly found at the leading edge of migrating cells. On the other hand, the Formin family (Formins) is responsible for the formation of a different set of actin filaments such as actin stress fibers and cytokinetic contractile rings. These Formin-dependent actin structures are characterized as being composed of long actin filaments.

There is another difference between two actin nucleators. The Arp2/3 complex binds the slow-growing end of the new filament and allows filament growth at the fast-growing end. By contrast, after nucleating new actin filament, Formins stay associated with its fast-growing end during filament growth. This unique property is useful to assemble long actin filaments because it can prevent the association of Capping protein. Capping protein inhibits elongation of actin. The anti-Capping protein activity of Formins thus explains why Formin-dependent filaments are long.

Low-Dose Actin Monomer Inhibitors Promote Actin Nucleation by mDia1 in Cells But Not In Vitro

Previously, we identified a member of Formins called mDia1 as an effector of the small GTPase Rho [9]. Rho is a molecular switch that regulates cytokinesis, smooth muscle contraction, and actin stress fiber formation in cells. Formins share conserved FH1 and FH2 regions in their C-terminal halves and also play a critical role in cytokinesis and cell polarity of various species. The GTP-bound form of Rho binds the N-terminal region of mDia1. This binding opens autoinhibited mDia1 to release the activity of its FH1–FH2 unit [10]. The FH1–FH2 region of mDia1 has a strong promoting effect on actin stress formation in cells [10]. With the FH2 domain, Formins nucleate actin filaments and bind the growing ends of filaments [11,12]. Remarkably, our single-molecule observation of the FH1–FH2 domain mutant of mDia1 has revealed fast long-range directional movement of molecules [13]. By marked contrast, however, we barely observed processive movement of full-length mDia1 in cells.

Recently, we sought cellular conditions where directional movement of native full-length mDia1 is induced frequently [14]. Interestingly, we came across an unexpected drug, latrunculin B, as a strong inducer of processive movement of mDia1. LatB binds G-actin near its ATP-binding site. LatB prevents actin monomer

from assembling into filaments. LatB is a drug widely used to probe actin-dependent cellular processes. When administrated at a high concentration, over 1 μM, LatB stops the movement of mDia1 because of a loss in the polymerization-competent G-actin. However, we observed that at a low dose, LatB dramatically increases the frequency of emergence of processively moving full-length mDia1. Processive mDia1Full was frequently observed as early as 10 s after the perfusion of 100 nM LatB. In addition, the speed of mDia1 rapidly decreased to less than 40%. This finding provided important information in our simulation, which is described next.

After a series of experiments, we found that the FH1–FH2 or FH2 region of mDia1 alone can respond to low-dose LatB and exhibit increased frequency of processive movement. We also confirmed that Rho is required for full-length mDia1 being in an open conformation but is not a direct mediator of LatB-increased actin nucleation by mDia1 in cells. We also tested if LatB directly promotes mDia1-catalyzed actin assembly in vitro. However, under various conditions tested, LatB only had a negative effect on mDia1FH2-mediated actin filament assembly in vitro.

Paradoxical Increase in Free G-Actin Revealed by Pharmacokinetic Simulation of Latrunculin B Treatment

Given the distinct effects of LatB on mDia1-catalyzed actin nucleation between in cells and in vitro, we reevaluated the pharmacological effect of LatB in cellular actin systems. We built a pharmacokinetic simulation to estimate changes in the cytoplasmic concentration of G-actin, either free or bound to thymosin-β4 (Tβ4), profilin, and latrunclin B (LatB) in our experiments. In the model, two major G-actin-sequestering proteins are considered. Profilin binds G-actin noncompetitively with latrunculin. On the other hand, the binding of latrunculin to G-actin substantially reduces the affinity between Tβ4 and G-actin [15]. Given the large amounts of the two proteins, we expect that the effect of other minor G-actin-binding proteins can largely be represented by these two proteins with different competitiveness against LatB.

The simulation scheme is illustrated in Fig. 2. The scheme can be described by simultaneous differential equations. Involvement of actin filament turnover was also considered based on the observed decreased speed of mDia1. Unexpectedly, simulation analysis predicted a rapid several-fold increase in free G-actin concentration that occurs within 1 min. Although some parameters such as the ratio between G-actin and Tβ4 have not been precisely defined yet, we consistently observed several-fold increases in free G-actin within a reasonable range of parameter values in calculation. The estimated increases were in good agreement with the time course of the increase in the number of processively moving mDia1Full molecules. It is of note that the increase in free G-actin occurs despite LatB accumulating in the cytoplasm at the several micromolar level.

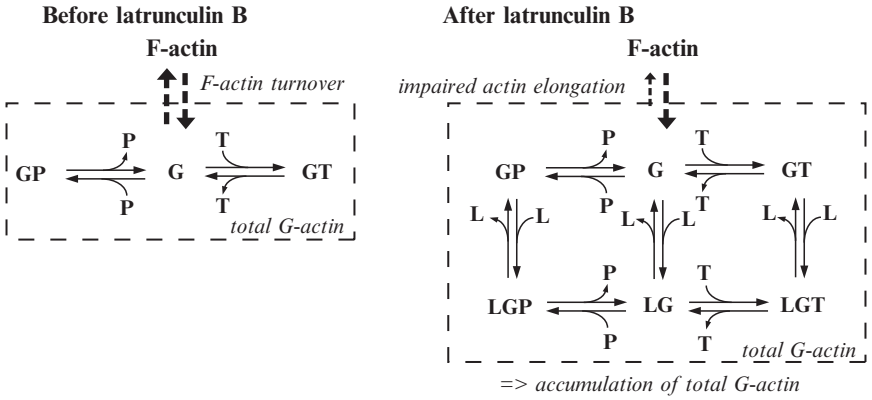

Fig. 2 Pharmacokinetic modeling of latrunculin B treatment. *G*, *L*, *T*, and *P* represent G-actin, LatB, thymosin-β4 (Tβ4), and profilin, respectively. The scheme was described by differential equations that estimated time-dependent concentration changes of each G-actin species either free or bound to LatB, Tβ4, and/or profilin. LatB is a widely used research tool to probe actin-dependent cellular processes. Intuitively, LatB is conceived of decreasing polymerization-competent G-actin (*downward on the right scheme*). However, our simulation revealed the more complex behavior of the system. LatB binds G-actin noncompetitively with profilin, whereas LatB-bound G-actin binds Tβ4 with a substantially reduced affinity [15]. Might this property cause a paradoxical increase in drug-free G-actin? Just the addition of low-dose LatB in the circuit (*squares surrounded by dashed lines*) affected the free G-actin concentration only marginally. Instead, a change in the balance between F-actin and total G-actin had a profound effect on the free G-actin concentration. In experiments, we observed a decrease in actin elongation speed by mDia1 and an ~30% F-actin decrease in cells treated with low-dose LatB. Incorporation of the observed shift from F- to G-actin into the model led us to find a paradoxical effect of LatB, which is to increase free G-actin several fold [14]

F-actin turnover and its modulation by LatB are the key for the induction of the paradoxical G-actin increase in the simulation. If we turned off the term for mimicking the imbalance between actin assembly and disassembly in the calculation, no obvious change in the free G-actin concentration was observed over time. This finding indicates that an increase in total G-actin plays a pivotal role. Our model predicts that a ~30% increase in the total G-actin results in the several-fold increase in free G-actin regardless of various changes in other parameters. Hence, although the primary pharmacological effect of LatB is inactivation of G-actin, LatB treatment also induces a 1.2- to 1.3-fold increase in total G-actin, which may lead to a several-fold free G-actin increase accompanied by saturation of the buffering capacity of G-actin-sequestering proteins. Our finding highlights an unprecedented example of pharmacological effects in which an antagonist increases the concentration of drug-free targets in a complex biological system [14].

Figure 3 summarizes our current model for dual regulation of mDia1-catalyzed actin assembly. We predict that Rho signaling determines the ratio of the opened and closed forms of mDia1, whereas an increase in free G-actin efficiently converts

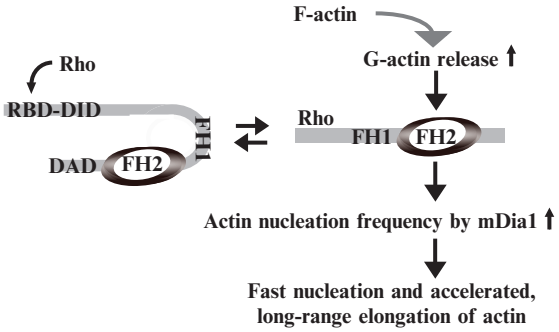

Fig. 3 The feedback actin polymer restoration mechanism involving *mDia1*. Rho signaling determines the ratio between the closed (*left*) and the opened (*right*) form of mDia1, whereas an increase in free G-actin efficiently converts "opened" mDia1 to the fully active actin nucleating state, leading to fast long-range actin filament assembly in cells

"opened" mDia1 to the fully active actin-nucleating and processive actin-capping state, leading to fast, long-range actin filament assembly.

Concluding Remarks

Currently, we are investigating the physiological relevance of G-actin regulation of actin nucleation. Our single-molecule imaging results suggest that the G-actin regulation mechanism may apply not only for mDia1 but also for some other actin nucleators. We also observed coupling of subcellular localization between mDia1-associated actin nucleation and actin-depolymerizing molecules [14]. We therefore predict that concentration fluctuation of G-actin and its partners may play a role in various cell morphological regulations.

Modeling and computational analysis would be vital to our understanding of complex biological systems in the near future. Yet, we need well-defined parameters and better understanding of individual interconnections between biological functions. Our current analysis highlights that we still do not realize "systems" as simple as this case. We anticipate step-by-step revelation of hidden secrets in biology by the joint approach between various research fields, including systems biology.

References

1. Watanabe, N., and Mitchison, T. J. (2002). Single-molecule speckle analysis of actin filament turnover in Lamellipodia. Science 295:1083–1086.
2. Miyoshi, T., Tsuji, T., Higashida, C., Hertzog, M., Fujita, A., Narumiya, S., Scita, G., and Watanabe, N. (2006). Actin turnover-dependent fast dissociation of capping protein in the

dendritic nucleation actin network: evidence of frequent filament severing. J Cell Biol 175:947–955.
3. Theriot, J. A., and Mitchison, T. J. (1991). Actin microfilament dynamics in locomoting cells. Nature (Lond) 352:126–131.
4. McGrath, J. L., Tardy, Y., Dewey, C. F., Jr., Meister, J. J., and Hartwig, J. H. (1998). Simultaneous measurements of actin filament turnover, filament fraction, and monomer diffusion in endothelial cells. Biophys J 75:2070–2078.
5. Mallavarapu, A., and Mitchison, T. (1999). Regulated actin cytoskeleton assembly at filopodium tips controls their extension and retraction. J Cell Biol 146:1097–1106.
6. Pollard, T. D., Blanchoin, L., and Mullins, R. D. (2000). Molecular mechanisms controlling actin filament dynamics in nonmuscle cells. Annu Rev Biophys Biomol Struct 29:545–576.
7. Welch, M. D., Rosenblatt, J., Skoble, J., Portnoy, D. A., and Mitchison, T. J. (1998). Interaction of human Arp2/3 complex and the Listeria monocytogenes ActA protein in actin filament nucleation. Science 281:105–108.
8. Mullins, R. D., Heuser, J. A., and Pollard, T. D. (1998). The interaction of Arp2/3 complex with actin: nucleation, high affinity pointed end capping, and formation of branching networks of filaments. Proc Natl Acad Sci U S A 95:6181–6186.
9. Watanabe, N., Madaule, P., Reid, T., Ishizaki, T., Watanabe, G., Kakizuka, A., Saito, Y., Nakao, K., Jockusch, B. M., and Narumiya, S. (1997). p140mDia, a mammalian homolog of *Drosophila diaphanous*, is a target protein for Rho small GTPase and is a ligand for profilin. EMBO J 16:3044–3056.
10. Watanabe, N., Kato, T., Fujita, A., Ishizaki, T., and Narumiya, S. (1999). Cooperation between mDia1 and ROCK in Rho-induced actin reorganization. Nat Cell Biol 1:136–143.
11. Evangelista, M., Zigmond, S., and Boone, C. (2003). Formins: signaling effectors for assembly and polarization of actin filaments. J Cell Sci 116:2603–2611.
12. Watanabe, N., and Higashida, C. (2004). Formins: processive cappers of growing actin filaments. Exp Cell Res 301:16–22.
13. Higashida, C., Miyoshi, T., Fujita, A., Oceguera-Yanez, F., Monypenny, J., Andou, Y., Narumiya, S., and Watanabe, N. (2004). Actin polymerization-driven molecular movement of mDia1 in living cells. Science 303:2007–2010.
14. Higashida, C., Suetsugu, S., Tsuji, T., Monypenny, J., Narumiya, S. and Watanabe, N. (2008). G-actin regulates rapid induction of actin nucleation by mDia1 to restore cellular actin polymers. J Cell Sci 121:3403–3412.
15. Yarmola, E. G., Somasundaram, T., Boring, T. A., Spector, I., and Bubb, M. R. (2000). Actin-latrunculin A structure and function. Differential modulation of actin-binding protein function by latrunculin A. J Biol Chem 275:28120–28127.

Molecules, Networks, and Memory

Upinder S. Bhalla

Introduction

A profound evolution of modeling scope and scale has occurred in the field as we have sought to understand how memory works at the level of molecular networks. We have moved from an initial concept of a small number of relatively simple synaptic functions to the current appreciation of the complexity of function and cellular mechanisms that support these functions.

One of the initial triumphs of the field was to find a molecular correlate of the crucial property of Hebbian associativity [1]. A list of further functional modules of the synapse might include the detection and selection of memory-triggering activity patterns; chemical circuits that store information through feedback and switching; presynaptic release control; movement of key molecules into and out of the synapse; and activity-triggered protein synthesis (Fig. 1). More recent data suggest further modules for the formation and maintenance of synaptic contacts and pre- and postsynaptic structure. This long list of synaptic functions may suggest a pessimistic view of our ability to either complete the list or understand the signaling mechanisms. I propose, instead, that the list is a roadmap, and hence a clear statement of where modeling studies need to go. The system is undoubtedly complex, and therein lies the challenge for the field. Typical models for these functional modules contain tens to hundreds of molecular species and reactions. In keeping with the theme of this symposium and book, I suggest that the challenge of biological complexity is best met squarely, by developing models that embrace the complexity but are not overwhelmed by it. This systematic process of model building, one synaptic function at a time, is the basis for an eventual quantitative understanding of the synapse and its role in memory.

We owe our initial view of synaptic function in memory to two streams of neuroscience: anatomy, from Cajal, and psychology, from Donald Hebb. At the risk of

U.S. Bhalla
National Centre for Biological Sciences, TIFR, Bellary Road, Bangalore 560065, India

S. Nakanishi et al. (eds.), *Systems Biology*,
DOI:10.1007/978-4-431-87704-2_16,

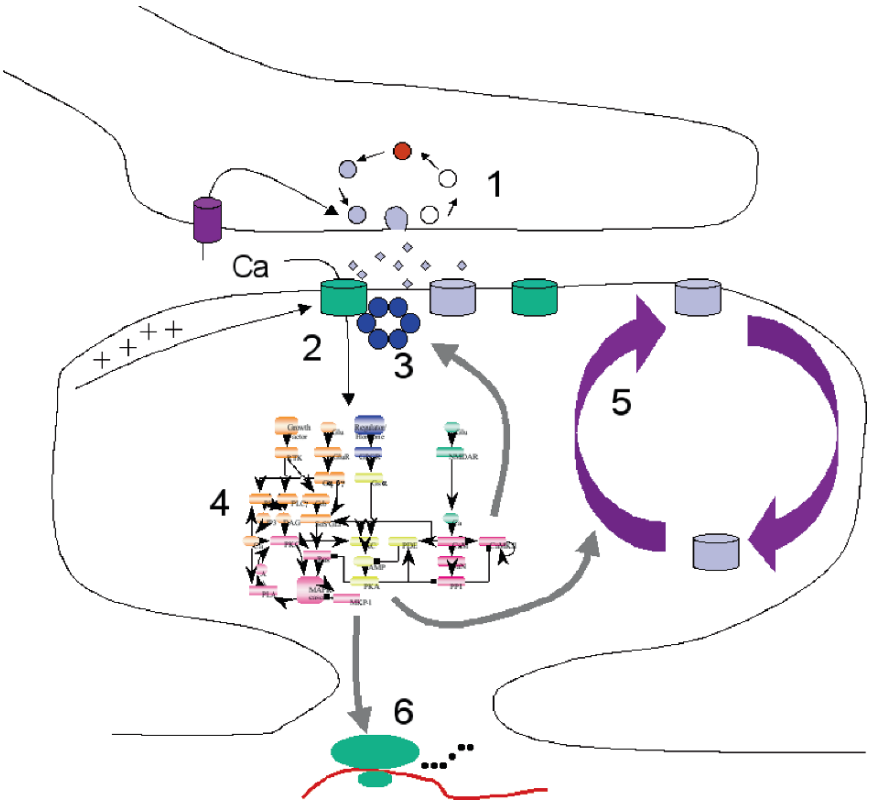

Fig. 1 Modules in synaptic function. *1* Presynaptic vesicle release control. *2* Associativity. The *N*-methyl D-asparate (NMDA) channel opens only when the input neurotransmitter is associated with postsynaptic depolarization. *3* Bistability. The hexagonal set of molecules represents calcium calmodulin-dependent type II kinase (CaMKII), which may act as a bistable switch. *4* Pattern selectivity. The complex of signaling pathways leads to different outcomes depending on input patterns in time and on cellular context. *5* Molecular movement. Here the movement of the alpha-amino-3-hydroxy-5-methyl-4-isoxazolepropionic acid (AMPA) receptor is shown, which is regulated by activity. *6* Dendritic protein synthesis

doing many contemporary scientists an injustice, one could attribute the ideas of connectivity to Cajal and the ideas of associativity to Hebb. The key breakthrough that completed this early picture of associative memories came from the work of Ascher and Nowak in the 1980s. They showed that the *N*-methyl D-asparate (NMDA) receptor could implement the crucial function of input-output associativity at the synapse [2]. This function turned out to be a relatively simple process of magnesium ion blockage of the receptor until the channel was depolarized. Thus, ion flow through the NMDA receptor could only occur if input activity (glutamate neurotransmitter) were associated with output activity (depolarization of the postsynaptic cell). This finding was the first indication of how synaptic logic could

implement crucial memory functions. Thus, at this stage the field had a satisfyingly consistent view of memory in terms of connectivity and the rules that led to change in connectivity.

The next level of inquiry led into the mechanistic details of synaptic function and into intracellular signaling networks. To recapitulate, some of the key functional modules are chemical circuits that store information; presynaptic release control; selection of memory triggering activity patterns; movement of synaptic molecules; and activity-triggered protein synthesis. We have pursued development of detailed signaling models of these functional modules as a roadmap to understanding synaptic function.

Information Storage

After associativity, there followed one of the central questions of synaptic function: How do synapses store information? By the time this question was addressed at the molecular level, the electrical properties of synaptic modification were well established [1]. It was known that synaptic conductances increased and stayed elevated for long periods following even a brief calcium influx. This sustained change suggested that some structural or chemical activity was causing the synapse to switch to a new state of higher conductance. This was remarkable enough, but the duration of the change posed a special problem, because individual molecules turn over in days or less [3]. Taking a cue from computer memories, the concept of a bistable chemical "switch" became a central theme of these studies. Such switches typically have a feedback process such that they can either remain in a quiescent state or a self-sustaining state of high activity (Fig. 2i–iii). One candidate switching molecule was calcium calmodulin-dependent type II kinase (CaMKII). Many theoretical models [4,5] have suggested that CaMKII may act as a bistable switch. However, experimental studies have revealed a great deal of complexity in this putative switch, and the details are still being worked out. For example, CaMKII translocates between a soluble fraction in the synapse and a particulate fraction at the postsynaptic density (PSD) [6]. We have shown in our models that this translocation process may be a critical contributor to long-lasting bistability [7]. In the soluble form, CaMKII can be rapidly dephosphorylated by protein phosphatase 2A (PP2A). However, at the PSD the access to the kinase is restricted to protein phosphatase 1 (PP1), which is saturable. The balance of CaMKII autophosphorylation and PP1 dephosphorylation at the PSD may therefore be in the range where bistability is possible (Fig. 2iv).

Other pathways have also been proposed for synaptic switching, and several of these now have experimental support. We have proposed that the mitogen-activated protein kinase (MAPK) pathway forms a positive feedback loop with phospholipase A2 and protein kinase C [8] (Fig. 2v). We have subsequently provided experimental evidence that this feedback loop does indeed function in fibroblasts [9].

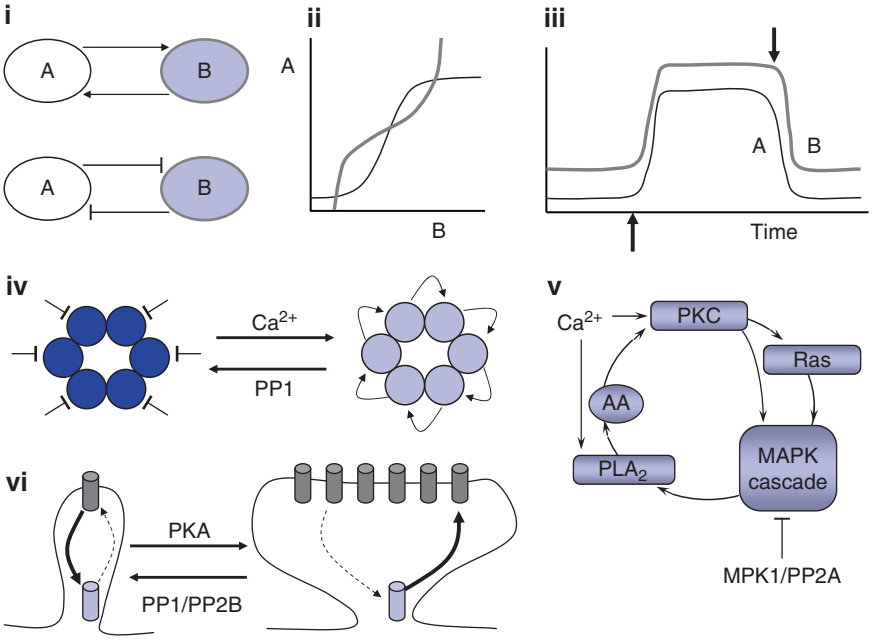

Fig. 2 Bistability in synaptic plasticity. **i** Two possible feedback circuits that may give bistability. The *top* one is mutually excitatory; the *bottom* one is mutually inhibitory. The *net sign* around the loop is positive in both cases. **ii** Bistability analysis using superimposed dose–response curves for *A* and *B* with respect to each other. The presence of three intersection points indicates bistability. **iii** Functioning of a bistable switch. The system remains stable in a low state of activity until a brief stimulus arrives (*lower arrow*). It then switches to a state of high activity, thus "remembering" the first stimulus. It remains active until an inhibitory stimulus arrives (*upper arrow*), at which point it switches back to the low state. **iv** CaMKII bistability. The CaMKII subunits phosphorylate and therefore activate each other. The initial trigger is Ca^{2+} influx. To turn the system off, protein phosphatase 1 (PP1) must dephosphorylate enough subunits to arrest the feedback cycle. **v** Mitogen-activated protein kinase (MAPK) bistability through a feedback loop involving phospholipase A2 (PLA2) and protein kinase C (PKC). Ca^{2+} is an activating stimulus, and the phosphatases MKP1 and PP2A can turn off the activity. **vi** AMPA receptor cycling and bistability. In the low state, only a few receptors are present at the synaptic junction. In the high state, many receptors are present, and this saturates the dephosphorylation process required to remove them

Other groups have investigated its role in cerebellar long-term depression (LTD) [10], and very recent experimental evidence for this is presented in this volume. We have reported a further, unexpected switch that emerged from an analysis of receptor trafficking (Fig. 2vi) [7]. This switch behaves somewhat differently from the feedback loops of the CaMKII and MAPK switches. Instead of self-activating feedback, the bistability arises from saturation of transport to and from the synapse. Interestingly, one of the saturated molecules is the same phosphatase (PP1) that is involved in CaMKII regulation.

Overall, there are now several candidate mechanisms for synaptic information storage. It is now considered likely that multiple biochemical switches may act in

concert to pass synaptic "memory" through multiple phases of formation and consolidation [1,11]. Our current models of such switches incorporate tens to hundreds of molecular species and many hundreds of reaction steps [7,8,12]. This unresolved complexity has come as a challenge to the field, specially given the simplicity of the initial synaptic operation of associativity.

Presynaptic Release Control

The presynaptic terminal has been somewhat neglected from a modeling point of view, despite its crucial role in synaptic transmission and considerable experimental and theoretical evidence for its role in information storage. This is partly accounted for by its relative experimental inaccessibility, which deprives us of the wealth of signaling and physiological data that have contributed so much to understanding postsynaptic signaling. Recent experimental and modeling studies have begun to make inroads into this system [13]. Short-term plasticity effects such as paired-pulse facilitation or depression have been modeled in terms of the calcium dynamics at the presynaptic terminal. One of the key unknowns is the mechanisms by which presynaptic signaling contributes to changes in the total synaptic efficacy. This mechanism presumably involves some form of retrograde signal from the postsynaptic side to account for associativity with postsynaptic activity. Clearly, any complete picture of synaptic function must account for the details of these presynaptic events.

Pattern Selectivity

Synapses are highly selective about circumstances that may lead to plasticity. These circumstances may include strong activity, specific temporal patterns of activity, and context in the form of other synaptic inputs to the cell as well as hormonal and broadcast neurotransmitter input. The synapse must continually monitor all these inputs to decide whether to maintain its synaptic weight at a steady level or to increase or decrease it. Such decisions tie into plasticity switches as well as to structural change and control of protein synthesis.

We began analyzing this issue with the observation that different signaling pathways exhibit a very wide range of time courses. Using this as a starting point, we tested our models to see if a set of four major kinase pathways at the synapse might exhibit selectivity for different activity patterns [14,15]. This turned out to be the case, and the models also predicted mechanisms by which these tuning properties might be modulated by neurotrophins or hormones. We followed this initial observation with a systematic analysis of patterns used to elicit long-term potentiation (LTP), and found that the MAPK pathway was tuned to spaced synaptic input in a manner reminiscent of one of the strongest LTP-inducing patterns

[16]. In contrast, CaMKII was best activated for brief, strong input. We experimentally tested these predictions and confirmed that the MAPK cascade, but not the CaMKII pathway, exhibited tuned activity tuning to spaced input in a manner very similar to our initial predictions [16]. In ongoing work, we find that the protein synthesis pathways may also be capable of some degree of pattern selectivity.

These studies converge to indicate that synapses implement a very effective system of pattern selectivity through their signaling networks.

Movement of Synaptic Molecules

Synapses are highly dynamic structures. They undergo changes in their morphology as a function of time, activity, and system cues such as stress and neurotrophins. As a first step to characterizing the complex details of synaptic remodeling, researchers have begun to look at how molecules move around in the synapse. Such studies have been carried out at exquisite, single-molecule detail to look at how synaptic ultrastructure affects molecular diffusion [17]. We have been examining less spatially detailed, but chemically complex, active movement of molecules at the synapse and dendrite.

One of the simple mechanisms for such movement harnesses diffusion by the regulation of binding sites at different target locations. We examined control of two important synaptic molecules by this mechanism: CaMKII and the alpha-amino-3-hydroxy-5-methyl-4-isoxazolepropionic acid (AMPA) receptor. CaMKII moves into the PSD following strong calcium influx, whereas the AMPA receptor translocation is governed by its phosphorylation state. Although our model was designed primarily to monitor receptor movement, this system turned out to have the unexpected emergent property of bistability [7]. The “down” state of the system had very few AMPA receptors at the PSD and hence corresponded to a weak or silent synapse. In this state, the basal levels of PP1 at the PSD were sufficient to rapidly dephosphorylate the receptor and thus mark it for movement back into the reserve pools (Fig. 2vi). The “up” state had ~150 receptors at the PSD, a level comparable to active synapses. In this condition, the PP1 became saturated, and therefore the removal of AMPA receptors was balanced by their insertion into the PSD. We predicted that the saturation of PP1 could also be a mechanism for coupling with the movement of CaMKII to the PSD. One of the particularly striking features of this coupled bistable system was that it was robust with respect to stochasticity. Chemical noise compromises the stability of bistable chemical switches, leading to spontaneous state changes, which would be disastrous for a memory switch. In the AMPAR-CaMKII switch, we found that the spontaneous switching time was well over a year, making it an attractive candidate for long-term memory storage [7].

Although these initial models are interesting, they are clearly at a very early stage for characterizing the complex structural and molecular movement events that are involved in synapse formation and memory. It seems likely that more complete

models will require the integration of three-dimensional reaction-diffusion calculations [17] along with mechanical models of structural components of the synapse.

Activity-Triggered Protein Turnover

In concert with regulating the movement of its constituent molecules, the synapse must also regulate their supply. This control involves a delicate balance between molecular import and export to the soma and local synthesis and degradation. We have very recently developed models for one aspect of this process: activity-dependent protein at dendritic sites adjacent to synapses. This site turns out to be a convergence point for multiple signals, including neurotrophins, at least two calcium-responsive pathways, and cellular metabolic inputs. Our simulations show that the pathways are capable of differential activation to different activity patterns involved in LTP and LTD, potentially leading to selective expression of different proteins depending on context. We had anticipated that activity-dependent protein synthesis might be a locus for yet another synaptic bistable switch, because it has numerous potential positive feedback loops. For example, several components of the protein synthesis machinery are themselves synthesized locally. Furthermore, brain-derived neurotrophic factor (BDNF), one of the factors that activates the pathway, is also synthesized. Nevertheless, our quantitative analysis suggests that none of the known feedback mechanisms can give rise to bistability in this system. We speculate that this is an illustration of functional modularity in the synapse, in that the switching properties are separate from the protein synthesis control mechanisms.

Discussion

Associativity, information storage, presynaptic release, pattern selectivity, molecular movement, and protein synthesis: this weighty list accounts for many of the known functions the synapse must support to store memories. It is an intimidating list of functions, encompassing as it does much of cell biology and physiology. Nevertheless, it also serves as a roadmap for experiments and, increasingly, for models that can encapsulate the complexity and define the essential steps.

Over the years, my group and others have built a parts list of these key processes that underlie memory, in the form of increasingly detailed biochemical and biophysical computer models. Although these modules already are complex, we have been impelled by our own and other experiments to introduce still more detail. These elaborations include stochastic “noisy” chemical steps, diffusion, and interactions with ion channels and cellular biophysics. I propose that one of the key lessons of these modeling studies is that synaptic complexity is neither an accident, nor something that can easily be abstracted away. Instead, it is an essential part of how the cell constructs a reliable submicrometer machine that performs complex decisions and stores information for a lifetime.

References

1. Bliss TV, Collingridge GL (1993) A synaptic model of memory: long-term potentiation in the hippocampus. Nature (Lond) 361:31–39.
2. Ascher P, Nowak L (1988) The role of divalent cations in the *N*-methyl-D-aspartate responses of mouse central neurones in culture. J Physiol 399:247–266.
3. Ehlers MD (2003) Activity level controls postsynaptic composition and signaling via the ubiquitin-proteasome system. Nat Neurosci 6:231–242.
4. Miller P, Zhabotinsky AM, Lisman JE, Wang XJ (2005) The stability of a stochastic CaMKII switch: dependence on the number of enzyme molecules and protein turnover. PLoS Biol 3:e107.
5. Zhabotinsky AM (2000) Bistability in the Ca(2+)/calmodulin-dependent protein kinase-phosphatase system. Biophys J 79:2211–2221.
6. Shen K, Teruel MN, Connor JH, Shenolikar S, Meyer T (2000) Molecular memory by reversible translocation of calcium/calmodulin-dependent protein kinase II. Nat Neurosci 3:881–886.
7. Hayer A, Bhalla US (2005) Molecular switches at the synapse emerge from receptor and kinase traffic. PLoS Comput Biol 1:137–154.
8. Bhalla US, Iyengar R (1999) Emergent properties of networks of biological signaling pathways. Science 283:381–387.
9. Bhalla US, Ram PT, Iyengar R (2002) MAP kinase phosphatase as a locus of flexibility in a mitogen-activated protein kinase signaling network. Science 297:1018–1023.
10. Kuroda S, Schweighofer N, Kawato M (2001) Exploration of signal transduction pathways in cerebellar long-term depression by kinetic simulation. J Neurosci 21:5693–5702.
11. Kennedy MB, Beale HC, Carlisle HJ, Washburn LR (2005) Integration of biochemical signalling in spines. Nat Rev Neurosci 6:423–434.
12. Bhalla US (2004) Signaling in small subcellular volumes. II. Stochastic and diffusion effects on synaptic network properties. Biophys J 87:745–753.
13. Hosoi N, Sakaba T, Neher E (2007) Quantitative analysis of calcium-dependent vesicle recruitment and its functional role at the calyx of Held synapse. J Neurosci 27:14286–14298.
14. Bhalla US (2002) Biochemical signaling networks decode temporal patterns of synaptic input. J Comput Neurosci 13:49–62.
15. Bhalla US (2002) Mechanisms for temporal tuning and filtering by postsynaptic signaling pathways. Biophys J 83:740–752.
16. Ajay SM, Bhalla US (2004) A role for ERKII in synaptic pattern selectivity on the time-scale of minutes. Eur J Neurosci 20:2671–2680.
17. Coggan JS, Bartol TM, Esquenazi E, Stiles JR, Lamont S, et al. (2005) Evidence for ectopic neurotransmission at a neuronal synapse. Science 309:446–451.

Systems Biology Meets Single-Cell Physiology: Role of a Positive-Feedback Signal Transduction Network in Cerebellar Long-Term Synaptic Depression

Keiko Tanaka and George J. Augustine

Introduction

It is widely assumed that persistent changes in the brain, such as those occurring during learning, memory, development, and various pathological conditions, are mediated by long-lasting, plastic changes in synaptic efficacy [1]. Long-term depression (LTD) of excitatory transmission at cerebellar Purkinje cells is an attractive system for studies of such long-lasting synaptic plasticity [2]. LTD arises from interaction of the two excitatory synaptic inputs that innervate Purkinje cells: climbing fibers (CF) and parallel fibers (PF). Simultaneous activation of these inputs causes a LTD of the efficacy of PF synapses [2].

The signals generated by the activity of these synapses are well understood. CF activation depolarizes the Purkinje cell and produces a rise in the intracellular Ca^{2+} This rise in $[Ca^{2+}]_i$ is necessary and sufficient to account for the CF contribution to LTD [3–5]. PF synapses produce several signals that are important for LTD. PF activity produces two messengers within Purkinje cells: diacylglycerol (DAG) and inositol trisphosphate (IP3). DAG is important for LTD induction, via its well-known ability to activate protein kinase C (PKC) [6–8], while IP3 contributes to LTD signaling by releasing Ca^{2+} from intracellular stores and thereby elevating $[Ca^{2+}]_i$ [9–12]. PF activity also appears to activate nitric oxide synthase in the presynaptic terminals of PFs, generating the membrane-permeant gas, nitric oxide (NO), that is also involved in LTD [13–17].

As its name implies, LTD is a slow process that gradually develops over 10–30 min and lasts for hours and perhaps for much longer (Fig. 1A). An initial phase of LTD results from a reduction in the number of functional alpha-amino-3-hydroxy-5-methyl-4-isoxazolepropionic acid (AMPA)-type glutamate receptors

K. Tanaka
Department of Biophysics and Biochemistry, Graduate School of Science, University of Tokyo, Tokyo, Japan, and PRESTO, Japan Science and Technology Agency, Tokyo, Japan

G.J. Augustine
Department of Neurobiology, Duke Medical Center, Box 3209, Durham, NC 27710, USA

S. Nakanishi et al. (eds.), *Systems Biology*,
DOI:10.1007/978-4-431-87704-2_17,

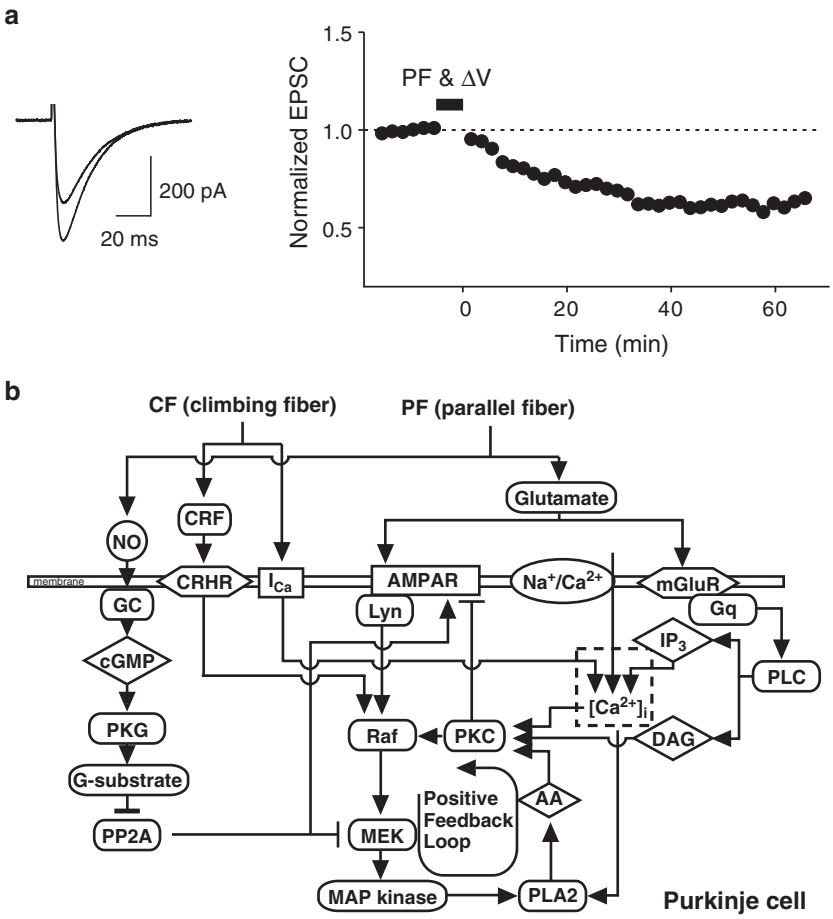

Fig. 1 **a** Long-term depression (LTD) can be elicited by pairing parallel fiber (*PF*) synaptic activity with depolarization of the Purkinje cell membrane potential, which causes a time-dependent (*right*) reduction in the amplitude of excitatory postsynaptic currents (*EPSCs*) elicited by stimulating PFs (*left*). **b** Diagram of the signaling components incorporated in the computational model of Kuroda et al. [24]

that mediate PF synaptic transmission [18]. This reduction is caused by internalization of these receptors via a clathrin-dependent endocytosis process [19,20] that is triggered by PKC phosphorylation of the GluR2 and GluR3 subunits of the AMPA receptors. A second component of LTD occurs more than an hour after LTD induction (at room temperature). This component is caused by changes in gene transcription and translation [21–23], although the affected genes have not yet been identified.

It is important to understand how the second messenger signals produced by synaptic activity, which typically disappear within a few seconds or less after synaptic activity ends [3,11], are converted into the slow reactions that cause LTD of PF

synaptic transmission. A comprehensive "systems biology" style computational model was (Fig. 1B) [24]. This computational model accounts for the component of LTD that is caused by changes in AMPA receptor trafficking and uses AMPA receptor phosphorylation as a readout for LTD. The model is capable of predicting many of the features of LTD, including the stimulus requirements for LTD induction and the response of LTD to several experimental manipulations. The central feature of this model is a Ca^{2+}-triggered positive feedback loop involving many signal transduction proteins, including protein kinase C (PKC), the mitogen-activated protein kinase (MAPK), and phospholipase A2 (PLA2) [25]. This feedback loop is postulated to create a bistable system that allows PKC to be activated in a regenerative way once the positive feedback loop is activated by the signals generated by synaptic activity. Thus, the model predicts that the positive feedback loop translates the brief signals produced by synaptic activity into enduring biochemical events, specifically a sustained activation of PKC, that yield the slow and gradual development of LTD after synaptic activity ends. The goal of the work described in this chapter was to provide experimental tests of this computational model.

Calcium Requirements of LTD

Our first experimental indication of the positive feedback loop in LTD was observed when we investigated the relationship between $[Ca^{2+}]_i$ and the amount of LTD [20]. In these studies, we photolysed a "caged" Ca^{2+} compound, DMNPE-4, to increase $[Ca^{2+}]_i$ directly in the postsynaptic Purkinje cells. In this way, we could also control the length of time that $[Ca^{2+}]_i$ was elevated. As seen in Fig. 2A, for a given duration of $[Ca^{2+}]_i$ elevation, the relationship between $[Ca^{2+}]_i$ and the amount of LTD was sigmoidal, with no LTD produced at lower $[Ca^{2+}]_i$ and full LTD elicited at higher $[Ca^{2+}]_i$. These relationships could be described by the Hill equation, with a Hill coefficient of approximately 5 indicating cooperative triggering of LTD by Ca^{2+}. Prolonging the duration of $[Ca^{2+}]_i$ elevation caused a leftward shift in this relationship (closed triangles and diamonds in Fig. 2A), while decreasing the duration of $[Ca^{2+}]_i$ elevation caused a rightward shift (closed circles and squares in Fig. 2A). Thus, the duration of $[Ca^{2+}]_i$ elevation influences the Ca^{2+} requirements for LTD induction. This dynamic property indicates that LTD is induced by a "leaky integrator" process [20], similar to the "leaky integrate and fire" concept often used in models of neuronal electrical signaling [26,27].

These features of the triggering of LTD by Ca^{2+} suggest that LTD results from Ca^{2+} activating signaling processes that have regenerative properties but behave as a leaky integrator. Because such properties could arise from a positive feedback process, our collaborators T. Doi, H. Ogasawara, and M. Kawato determined whether the computational model of Kuroda et al. [24] could explain our results. Even though this model (Fig. 1B) was not originally designed to simulate the results of our experiments that manipulated $[Ca^{2+}]_i$, in fact only a few minor

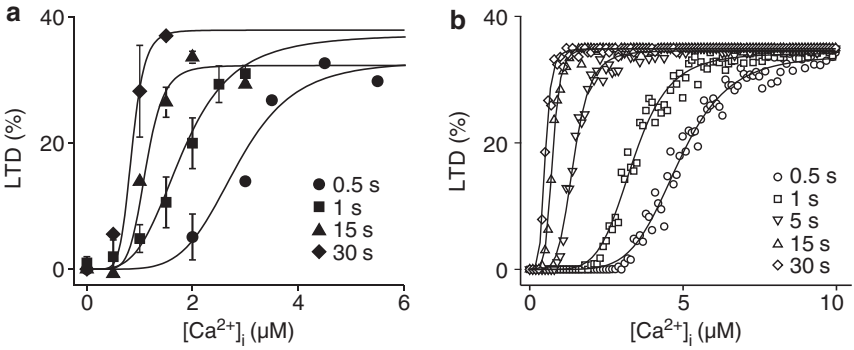

Fig. 2 Relationship between peak $[Ca^{2+}]_i$ and *LTD* for different durations of $[Ca^{2+}]_i$ elevation, obtained from experimental measurements (**a**) and predicted by computational simulations (**b**). (From Tanaka et al. [20])

modifications were needed for this model to reproduce all major features of our experimental measurements of the Ca^{2+} dependence of LTD (Fig. 2B).

The computational model predicted that disruption of the positive feedback loop, by preventing activation of PKC via arachidonic acid (AA), should reduce the Ca^{2+} sensitivity of LTD induction. This prediction was tested experimentally by examining the effect of a PLA2 inhibitor on the $[Ca^{2+}]_i$ dependence of LTD. We found a close correspondence between the experimental results and the predictions of the computational model [20], supporting the idea that both the cooperative activation and the leaky integrator properties of LTD triggering by Ca^{2+} arise, at least in part, from the positive feedback loop working downstream of Ca^{2+}.

Reciprocal Activation of PKC and MAPK Required for LTD

Although the experimental measurements of the relationship between $[Ca^{2+}]_i$ and LTD were consistent with the computational model, we sought more direct tests of the positive feedback loop model. We next tested the essence of this loop, the predicted mutual activation of PKC and MAPK by each other, by determining experimentally (1) whether MAPK is downstream of PKC, and (2) whether PKC is also downstream of MAPK [28].

To address the first question, we first measured activation of MAPK by biochemical and immunohistochemical analysis using an antibody that selectively recognizes the phosphorylated, activated form of MAPK [29,30]. LTD induction caused a pronounced increase in MAPK phosphorylation in Purkinje cells, and this phosphorylation was blocked by a PKC inhibitor, bisindolylmaleimide I (BIM), indicating that activation of MAPK during LTD induction requires an upstream action of PKC. We then tested whether this interaction between PKC and MAPK is required for LTD. For this purpose, a PKC activator, 12-*O*-tetradecanoyl

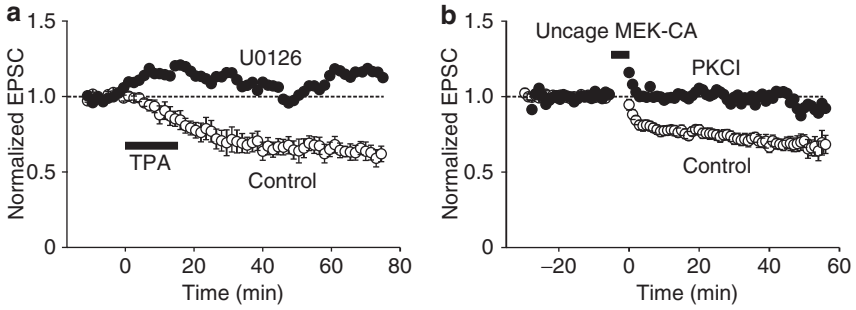

Fig. 3 **a** LTD induced by activating protein kinase C (PKC) by 12-*O*-tetradecanoyl phorbol-13-acetate (TPA) was blocked by U0126, indicating that PKC works by activating mitogen-activated protein kinase (MAPK). **b** LTD induced by activating MAPK by uncaged MEK-CA was blocked by PKCI, indicating that MAPK works by activating PKC. (From Tanaka and Augustine [28])

phorbol-13-acetate (TPA), was used to induce LTD; as previously reported [31–33], TPA treatment caused LTD (open circles in Fig. 3A). This LTD resulting from direct activation of PKC was blocked by an inhibitor that blocks the MAPK pathway, U0126 (closed circles in Fig. 3A), indicating that MAPK works downstream of PKC. Thus, these results demonstrate that PKC activates MAPK during LTD and that this interaction is required for LTD induction.

A similar strategy was used to determine whether MAPK also acts upstream of PKC. Prolonged activation of PKC, detected by translocation of PKC to the plasma membrane [34], was observed after LTD induction and was blocked by U0126. This finding indicates that PKC activation is sustained via an upstream action of MAPK. To determine whether this interaction is required for LTD, we asked whether a PKC inhibitor could prevent LTD induced by direct activation of MAPK. Toward this goal, we covalently attached a NVOC-Cl caging group [35] onto a pseudophosphorylated, constitutively active form of MEK (MEK-CA), a kinase that phosphorylates/activates MAPK [30]. In vitro analysis demonstrated that applying UV light to the caged MEK-CA permits temporally precise activation of MAPK. We then introduced the caged MEK-CA into Purkinje cells through the patch pipette. Photolysis of caged MEK-CA induced LTD of PF synaptic transmission (open circles in Fig. 3B). This LTD induced by direct activation of MAPK was blocked by a PKC inhibitor, the PKC inhibitory peptide (PKCI; closed circles in Fig. 3B). Taken together with the results showing MAPK-dependent PKC activation during LTD, these results indicate that MAPK also activates PKC.

In summary, our results demonstrate that the reciprocal activation of PKC and MAPK is important for LTD, as predicted by the computational model. We thus conclude that the positive feedback loop is active during LTD and is required for LTD.

Positive Feedback Loop Prolongs Duration of PKC Activation

The computational model [24] predicts that the main purpose of the positive feedback loop is to prolong the duration of PKC activity in time. We tested this prediction via two series of experiments. The first examined the time window of PKC activity by applying a PKC inhibitor, BIM, at several time points after LTD-inducting stimuli. In the absence of BIM treatment, LTD was produced by pairing of PF stimulation with depolarization of the Purkinje cell membrane potential (PF&ΔV) [3,36] (open circles of Fig. 4A). However, when BIM was applied as late as 20 min after the PF&ΔV stimulus, LTD was reduced or eliminated. The closed circles of Fig. 4A show the results of an experiment where BIM was applied 10 min after the stimulus: while the stimulus caused excitatory postsynaptic current (EPSC) amplitude to depress initially, this depression reversed after BIM treatment. In contrast, applying BIM 30 min or later after the stimulus did not affect LTD. The relationship between the time of BIM application and the degree of LTD impairment indicated that PKC remains active for at least 20–30 min after the LTD-inducing stimulus ends (Fig. 4B). Thus, activation of PKC is prolonged, as predicted by the model.

The second series of experiments determined whether this prolonged activation of PKC is the result of the positive feedback loop. For this purpose, we applied a PLA2 inhibitor (OBAA) at different times after the stimulus, just as already described for BIM. As was the case for BIM, OBAA was effective in reducing LTD even when applied 20–30 min after the end of the stimulus. The relationship between the time of OBAA application and the degree of LTD impairment closely paralleled the relationship for BIM application. We therefore conclude that the positive feedback loop is responsible for sustaining activation of PKC for at least the first 20–30 min after synaptic activity.

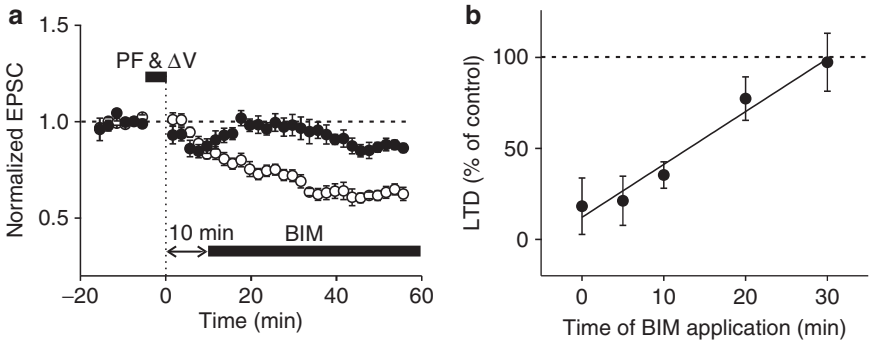

Fig. 4 **a** Application of bisindolylmaleimide I (*BIM*) 10 min after pairing of PF stimulation with depolarization of the Purkinje cell membrane potential (*PF&ΔV*) caused LTD. **b** Relationship between the time of BIM application and the degree of LTD impairment. (From Tanaka and Augustine [28])

Summary

Our experimental results provide several lines of evidence consistent with the hypothesis that the positive feedback loop first proposed on the basis of "systems biology" computational models is important for LTD:

1. Elevating postsynaptic $[Ca^{2+}]_i$, by photolysis of a caged Ca^{2+} compound, indicated a sigmoidal relationship between $[Ca^{2+}]_i$ and LTD. This cooperative behavior was predicted by the computational model.
2. The duration of the rise in $[Ca^{2+}]_i$ influenced the apparent Ca^{2+} affinity of LTD, being described by a leaky integrator process. The computational model was also capable of simulating these properties of Ca^{2+}-triggered LTD.
3. Disrupting this cycle experimentally also produced changes in the Ca^{2+} dependence of LTD that were predicted by the computational model.
4. Histochemical "epistasis" experiments demonstrate the reciprocal activation of PKC and MAPK during LTD.
5. Physiological experiments demonstrate that such reciprocal activation of PKC and MAPK is required for LTD.
6. Timed application of enzyme inhibitors reveals that this positive feedback loop causes PKC to be active for more than 20 min, allowing sufficient time for LTD expression.

Based on these results, we conclude that the positive feedback loop is an essential component of the molecular signaling cascade responsible for LTD induction (Fig. 5). Our work therefore provides experimental support for the proposal that the PKC/MAPK positive feedback loop serves as a general mechanism for sustaining intracellular signaling in time [25].

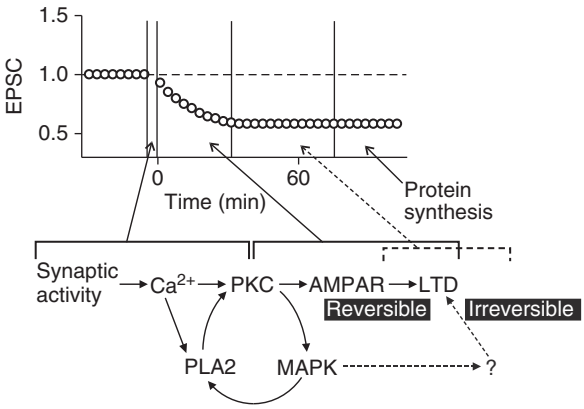

Fig. 5 Model for time course of signal transduction events involved in LTD. (From Tanaka and Augustine [28])

It appears that the increases in $[Ca^{2+}]_i$ associated with synaptic activity disappear within 1 s after synaptic activity ceases. However, the resulting activation of PKC turns on the positive feedback loop, which sustains PKC activity for at least 20–30 min and leads to the gradual expression of LTD as AMPA receptors are phosphorylated [37,38] and internalized [19,20]. Because application of either BIM or OBAA caused LTD to be reversed, it appears that initially the internalization of AMPA receptors can be reversed if the positive feedback loop is not maintained. Application of these inhibitors at later times does not reverse LTD, indicating that internalization becomes stabilized by this time point (Fig. 5). At times later than 60–90 min after stimulation, synthesis of new proteins maintains LTD [22]. Whether this phase of LTD relies on the positive feedback loop or any of its components remains to be determined.

This positive feedback model of LTD is reminiscent of the regenerative molecular mechanisms that have been implicated in other forms of long-lasting synaptic plasticity, such as autophosphorylation of the Ca/CaM-dependent protein kinase II that is important for hippocampal long-term synaptic potentiation [39] and activation of the prion-like protein, CPEB, which is important for long-term synaptic plasticity in *Aplysia* [40]. Thus, it is possible that positive feedback loops are a general mechanism for translating transient signals generated by brief synaptic activity into sustained biochemical activity during long-term synaptic plasticity.

References

1. Pittenger C, and Kandel ER (2003) In search of general mechanisms for long-lasting plasticity: *Aplysia* and the hippocampus. Philos Trans R Soc Lond B Biol Sci 358:757–763
2. Ito M (2001) Cerebellar long-term depression: characterization, signal transduction, and functional roles. Physiol Rev 81:1143–1195
3. Konnerth A, Dreessen J, and Augustine GJ (1992) Brief dendritic calcium signals initiate long-lasting synaptic depression in cerebellar Purkinje cells. Proc Natl Acad Sci U S A 89:7051–7055
4. Sakurai M (1990) Calcium is an intracellular mediator of the climbing fiber in induction of cerebellar long-term depression. Proc Natl Acad Sci U S A 87:3383–3385
5. Linden DJ, Dickinson MH, Smeyne M, et al (1991) A long-term depression of AMPA currents in cultured cerebellar Purkinje neurons. Neuron 7:81–89
6. Crépel F, and Krupa M (1988) Activation of protein kinase C induces a long-term depression of glutamate sensitivity of cerebellar Purkinje cells. An in vitro study. Brain Res 458:397–401
7. Linden DJ (1994) Input-specific induction of cerebellar long-term depression does not require presynaptic alteration. Learn Mem 1:121–128
8. Matsuda S, Launey T, Mikawa S, et al (2000) Disruption of AMPA receptor GluR2 clusters following long-term depression induction in cerebellar Purkinje neurons. EMBO J 19:2765–2774
9. Khodakhah K, and Armstrong CM (1997) Induction of long-term depression and rebound potentiation by inositol trisphosphate in cerebellar Purkinje neurons. Proc Natl Acad Sci U S A 94:14009–14014
10. Inoue T, Kato K, Kohda K, et al (1998) Type 1 inositol 1,4,5-trisphosphate receptor is required for induction of long-term depression in cerebellar Purkinje neurons. J Neurosci 18:5366–5373

11. Finch EA, and Augustine GJ (1998) Local calcium signalling by inositol-1,4,5-trisphosphate in Purkinje cell dendrites. Nature (Lond) 396:753–756
12. Miyata M, Finch EA, Khiroug L, et al (2000) Local calcium release in dendritic spines required for long-term synaptic depression. Neuron 28:233–244
13. Ito M, and Karachot L (1990) Messengers mediating long-term desensitization in cerebellar Purkinje cells. Neuroreport 1:129–132
14. Daniel H, Hemart N, Jaillard D, et al (1993) Long-term depression requires nitric oxide and guanosine 3′:5′ cyclic monophosphate production in rat cerebellar Purkinje cells. Eur J Neurosci 5:1079–1082
15. Boxall AR, and Garthwaite J (1996) Long-term depression in rat cerebellum requires both NO synthase and NO-sensitive guanylyl cyclase. Eur J Neurosci 8:2209–2212
16. Lev-Ram V, Jiang T, Wood J, et al (1997) Synergies and coincidence requirements between NO, cGMP, and Ca^{2+} in the induction of cerebellar long-term depression. Neuron 18:1025–1038
17. Reynolds T, and Hartell NA (2001) Roles for nitric oxide and arachidonic acid in the induction of heterosynaptic cerebellar LTD. Neuroreport 12:133–136
18. Linden DJ (2001) The expression of cerebellar LTD in culture is not associated with changes in AMPA-receptor kinetics, agonist affinity, or unitary conductance. Proc Natl Acad Sci U S A 98:14066–14071
19. Wang YT, and Linden DJ (2000) Expression of cerebellar long-term depression requires postsynaptic clathrin-mediated endocytosis. Neuron 25:635–647
20. Tanaka K, Khiroug L, Santamaria F, et al (2007) Ca^{2+} requirements for cerebellar long-term synaptic depression: role for a postsynaptic leaky integrator. Neuron 54:787–800
21. Nakazawa K, Karachot L, Nakabeppu Y, et al (1993) The conjunctive stimuli that cause long-term desensitization also predominantly induce c-Fos and Jun-B in cerebellar Purkinje cells. Neuroreport 4:1275–1278
22. Linden DJ (1996) A protein synthesis-dependent late phase of cerebellar long-term depression. Neuron 17:483–490
23. Karachot L, Shirai Y, Vigot R, et al (2001) Induction of long-term depression in cerebellar Purkinje cells requires a rapidly turned over protein. J Neurophysiol 86:280–289
24. Kuroda S, Schweighofer N, and Kawato M (2001) Exploration of signal transduction pathways in cerebellar long-term depression by kinetic simulation. J Neurosci 21:5693–5702
25. Bhalla US, and Iyengar R (1999) Emergent properties of networks of biological signaling pathways. Science 283:381–387
26. Knight BW (1972) Dynamics of encoding in a population of neurons. J Gen Physiol 59:734–766
27. Fohlmeister JF, Poppele RE, and Purple RL (1977) Repetitive firing: a quantitative study of feedback in model encoders. J Gen Physiol 69:815–848
28. Tanaka K, and Augustine GJ (2008) A positive feedback signal transduction loop determines timing of cerebellar long-term depression. Neuron 59:608–620
29. Nishida E, and Gotoh Y (1993) The MAP kinase cascade is essential for diverse signal transduction pathways. Trends Biochem Sci 18:128–131
30. Cobb MH, and Goldsmith EJ (1995) How MAP kinases are regulated. J Biol Chem 270:14843–14846
31. Linden DJ, and Connor JA (1991) Participation of postsynaptic PKC in cerebellar long-term depression in culture. Science 254:1656–1659
32. Endo S, and Launey T (2003) ERKs regulate PKC-dependent synaptic depression and declustering of glutamate receptors in cerebellar Purkinje cells. Neuropharmacology 45:863–872
33. Kondo T, Kakegawa W, and Yuzaki M (2005) Induction of long-term depression and phosphorylation of the δ2 glutamate receptor by protein kinase C in cerebellar slices. Eur J Neurosci 22:1817–1820
34. Newton AC (2001) Protein kinase C: structural and spatial regulation by phosphorylation, cofactors, and macromolecular interactions. Chem Rev 101:2353–2364
35. Marriott G, Roy P, and Jacobson K (2003) Preparation and light-directed activation of caged proteins. Methods Enzymol 360:274–288

36. Crépel F, and Jaillard D (1991) Pairing of pre- and postsynaptic activities in cerebellar Purkinje cells induces long-term changes in synaptic efficacy *in vitro*. J Physiol 432:123–141
37. Chung HJ, Steinberg JP, Huganir RL, et al (2003) Requirement of AMPA receptor GluR2 phosphorylation for cerebellar long-term depression. Science 300:1751–1755
38. Steinberg JP, Takamiya K, Shen Y, et al (2006) Targeted in vivo mutations of the AMPA receptor subunit GluR2 and its interacting protein PICK1 eliminate cerebellar long-term depression. Neuron 49:845–860
39. Sanhueza M, McIntyre CC, and Lisman JE (2007) Reversal of synaptic memory by Ca^{2+}/calmodulin-dependent protein kinase II inhibitor. J Neurosci 27:5190–5199
40. Bailey CH, Kandel ER, and Si K (2004) The persistence of long-term memory: a molecular approach to self-sustaining changes in learning-induced synaptic growth. Neuron 44:49–57

Computational Models of Cerebellar Long-Term Memory

Hideaki Ogasawara and Mitsuo Kawato

Introduction

Our brain is capable of learning new things while maintaining old memory. Retention of information requires stability, and new learning requires plasticity. As a memory device, neurons have to meet these contradictory requirements (the "stability versus plasticity dilemma" [1]), but stochastic noise makes this duty still more difficult. The dendritic spine, the key unit of neuronal information processing, is very small (~1 μm or less in diameter) and contains only a limited number of each molecular species. For instance, the number of α-amino-3-hydroxy-5-methylisoxazole-4-propionic acid (AMPA)-type glutamate receptors (AMPARs) in a parallel fiber (PF)–Purkinje cell (PC) synapse is as small as 4 to 73 [2]. In such a minute environment, stochastic fluctuations come into play and, affect the signaling pathways underlying memory formation and maintenance. How do neurons handle the stability versus plasticity dilemma without being overwhelmed by the noise? In this chapter, we address this issue by reviewing several theoretical studies of cerebellar long-term depression (LTD) and simulating simple models.

Cerebellar LTD

The main neurons and wirings in the cerebellar cortex include PCs, PFs, and climbing fibers (CFs). PCs provide the sole output from the cortex, and each PC receives two types of excitatory inputs: one from hundreds of thousands of PFs and the other from a single CF. Marr-Albus-Ito theory [3–5] states that their neuronal circuit underlies

H. Ogasawara
National Institute of Information and Communications Technology. 2-2-2, Hikaridai, Seika, Kyoto, 619-0288, Japan

H. Ogasawara and M. Kawato
ATR Computational Neuroscience Laboratories, 2-2-2 Hikaridai, Seika, Kyoto 619-0288, Japan

S. Nakanishi et al. (eds.), *Systems Biology*,
DOI:10.1007/978-4-431-87704-2_18,

supervised learning of the cerebellum. In this theory, PFs provide a sensorimotor context to PCs, while CFs carry teaching signals that modify PF-PC synapses in an associative manner.

In fact, the transmission efficacy of a PF–PC synapse is reduced when the CF and PF are repetitively and synchronously activated (cerebellar LTD). The molecular mechanisms are comprehensively reviewed elsewhere [6–11]. Briefly, PF firing induces production of inositol 1,4,5-trisphosphate (IP_3) through the mGluR1 metabotropic glutamate receptor pathway. CF firing depolarizes the PC and induces Ca^{2+} influx through voltage-gated calcium channels (Fig. 1a). Therefore, [IP_3] and [Ca^{2+}] represent PF and CF activities, respectively (In this chapter, [substance] stands for the concentration of the substance.) Synergistic increase of [IP_3] and [Ca^{2+}] activates IP_3 receptors (IP_3Rs) located in a calcium store of the dendritic spine and results in an enormous Ca^{2+} release. Ca^{2+} activates protein kinase C (PKC), which in turn phosphorylates the GluR2 subunit of AMPARs. Phosphorylated receptors are removed from the postsynaptic membrane through endocytosis.

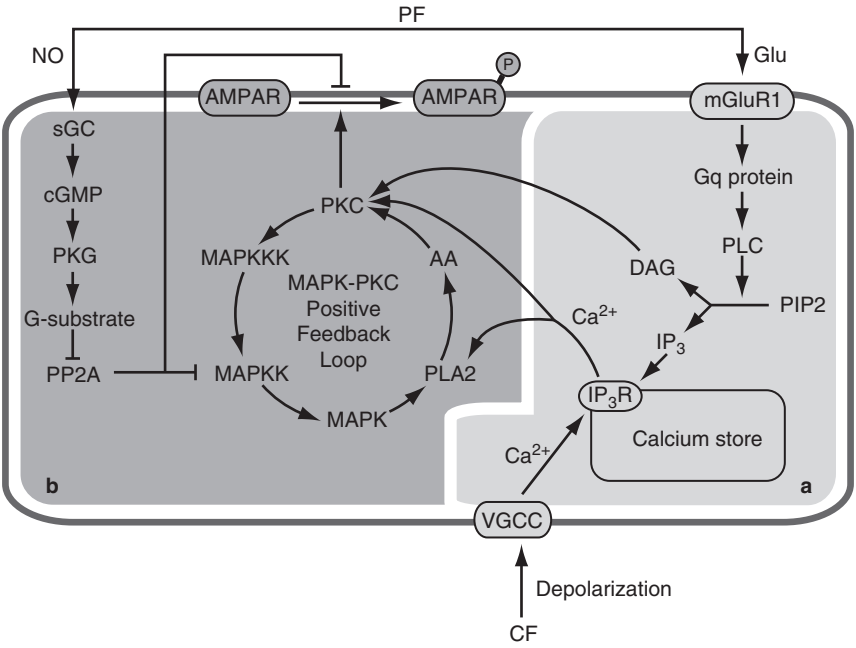

Fig. 1 Schematic view of signaling cascades in cerebellar long-term depression (LTD). Reactions surrounded by the *bold gray line* take place inside the dendritic spine. **a** Parallel fiber–climbing fiber (PF-CF) coincidence detection mechanisms (*light gray area; right side*) [14]. *Glu*, glutamate; *PKG*, cGMP-dependent protein kinase; *PIP2*, phosphatidylinositol bisphosphate. **b** The mitogen-activated protein kinase (MAPK)–PKC positive feedback loop [13] and its peripherals (*dark gray area; left side*). *AA*, arachidonic acid; *AMPA*, α-amino-3-hydroxy-5-methylisoxazole-4-propionic acid; *AMPAR*, AMPA-type glutamate receptor; *DAG*, diacyl glycerol. (From [15], with permission of S. Karger AG, Basel)

Essential molecules for LTD include mitogen-activated protein kinase (MAPK), MAPK kinase (MAPKK), MAPKK kinase (MAPKKK), PKC, phospholipases A2 (PLA2) and C (PLC), arachidonic acid (AA), IP_3, and many others [6–11].

Models to Explain Cerebellar LTD

In numerous situations such as development and cell-cycle progression, cells take discrete states and jump from one to another, avoiding intermediate states. For example, frog eggs are either mature or immature, and there is no half-mature egg [12]. This kind of switch-like behavior is termed "bistability." Bistability is particularly important in neurobiology because it is implicated in the storage of cellular information. Previous studies have shown that Ca^{2+}-induced Ca^{2+} release (CICR) and the MAPK-PKC positive feedback loop in the PC are among many bistable dynamics of the cell (Fig. 1) [13,14] (reviewed in [15]).

Calcium Dynamics Model

Calcium release via IP_3Rs is a supralinear function of calcium influx; the greater an input stimulus (calcium influx) is, the much more greater the output signal (calcium release) is. Doi et al. [14] simulated the molecular mechanism and demonstrated that a positive feedback loop $Ca^{2+} \rightarrow IP_3Rs \rightarrow Ca^{2+}$ is responsible for the supralinearity of calcium release. They also showed that the optimal PF-CF delay (~100 ms) for calcium release and LTD is attributable to the slow mGluR1 pathway that takes time to biochemically produce IP_3, rather than to calcium kinetics and the binding properties of the receptor [16] (see also comments in [17]).

MAPK-PKC Positive Feedback Loop

Kuroda et al. [13] modeled the intracellular signaling cascade of cerebellar LTD (Fig. 1b). Their model predicted that MAPK and PKC form a bistable positive feedback loop, which mediates the intermediate phase (<~40 min) of LTD. Subsequent neurobiological experiments strongly supported their predictions [18,19].

Cascade of Excitable Dynamics

How do neurons resolve the stability versus plasticity dilemma [1] in stochastic noise? Taking into account the fact that bistability is ubiquitous in signaling pathways [20], one of us has proposed a cascade of excitable dynamics as a likely

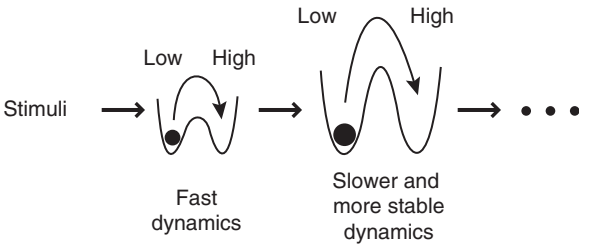

Fig. 2 Threshold cascade model (see text for explanation). (From [15], with permission of S. Karger AG, Basel)

mechanism (Fig. 2) [21]. In the model (detailed in [15]), multiple bistable dynamics with various time constants are connected in tandem, in the order of fast to slow. Each dynamics has an energy barrier that correlates with its time constant (the faster a switch is, the lower its barrier is), and an active dynamics stimulates the next one that is more stable and requires larger inputs for activation. In this way, when external stimuli activate the fastest system, the activity is transmitted from one to another slower one, and finally to the slowest one. Such a cascade of multiple bistable dynamics will form long-term memory that is stable, still open to modifications, and robust to noise. The model is applicable to at least the first two steps of cerebellar LTD, that is, CICR and the MAPK-PKC positive feedback loop (Fig. 1).

Protein Kinase Mζ Model

Based on these studies and an abundance of biological literature, we have proposed a conceptual model [15] in which cerebellar LTD is induced and maintained by successive activation of three bistable dynamics with different time scales: CICR, the MAPK-PKC positive feedback loop, and protein kinase Mζ (PKMζ)-induced PKMζ synthesis.

PKMζ is a persistently active enzyme, consisting of the catalytic domain of an atypical PKC isoform, PKCζ. It is expressed in a brain-specific manner. A series of experiments performed mainly by Sacktor's group demonstrates accumulating evidence that PKMζ plays a pivotal role in long-term maintenance of memory (exhaustively reviewed in [22]). Briefly, a procedure to induce hippocampal LTP (LTD) upregulates (downregulates) PKMζ. Injection of a PKMζ inhibitor, ZIP, to the hippocampus reverses LTP in vivo and produces persistent loss of 1-day-old spatial information. More surprisingly, an injection of ZIP to the rat neocortex, which is regarded as the long-term repository of memory, erases associative memories as old as 1 month [23]. These findings strongly suggest that PKMζ is the (semi-)permanent form of memory trace. PKMζ is also expressed in the cerebellar cortex [24,25]. Because cerebellar plasticity is regarded as a mirror image of hippocampal plasticity and they share much of their signaling networks [6,7,9,10,26], PKMζ activity is likely to be central to cerebellar LTD, as it is to hippocampal LTP.

Sometimes hippocampal studies advance far ahead of its cerebellar counterparts. For instance, calmodulin-dependent protein kinase II was discovered to be essential for hippocampal plasticity and learning in 1992 [27], but it was not until 2006 that the kinase was shown to be also necessary for cerebellar memory [28]. One of the main purposes of this model is to shorten the interval by calling for experiments to characterize the role of PKMζ in the cerebellum.

Pathways

PKMζ induces PKMζ expression, and this enzyme can act in two steps; either directly on its expression or on actin polymerization, which facilitates protein synthesis (Fig. 3a). Thus, we postulate that PKMζ forms a bistable switch by a combination of multistep ultrasensitivity and positive feedback [29,30]. Central to the model are three positive feedback loops, i.e., CICR (Fig. 3b, circle 1), the MAPK-PKC positive feedback loop (Fig. 3b, circle 2), and PKMζ-induced PKMζ expression (Fig. 3b, circle 3). Their decay time constants are less than 1 s, tens of minutes, and weeks or longer, respectively. Importantly, these excitable dynamics of different time scales are connected in tandem. When stimuli activate the quickest dynamics (Fig. 3b, loop 1) repetitively, activity is transmitted from the quickest, to the intermediate (Fig. 3b, loop 2), and thereafter to the slowest and most stable dynamics (Fig. 3b, loop 3). As a consequence, long-term stability and plasticity of memory are established. In this sense, this model is a more concrete representation of the cascade model of excitable dynamics [21] (Figs. 2, 3c).

Various States of Memory

This model schematizes various experimental observations of cerebellar synaptic plasticity. In the basal state, PP2A is active and inhibits the MAPK-PKC positive feedback loop (Fig. 3d).

LTP Induction

Postsynaptic LTP is induced in an NO-dependent manner at low [Ca^{2+}] [31,32]. NO, whose synthesis is triggered by PF spikes, facilitates exocytosis of AMPARs in a *N*-ethylmaleimide-sensitive factor (NSF)-dependent manner [33] (Fig. 3e).

Induction and Maintenance of LTD

When [Ca^{2+}] and [NO] are increased by conjunctive PF–CF activity, NO releases the MAPK-PKC positive feedback loop from PP2A inhibition, and Ca^{2+} activates PKC, which then phosphorylates and internalizes AMPARs (Fig. 3f). In the intermediate phase (Fig. 3g), the activated MAPK-PKC positive feedback loop maintains PKC activity and receptor endocytosis. During, and subsequent to, the late phase (Fig. 3h),

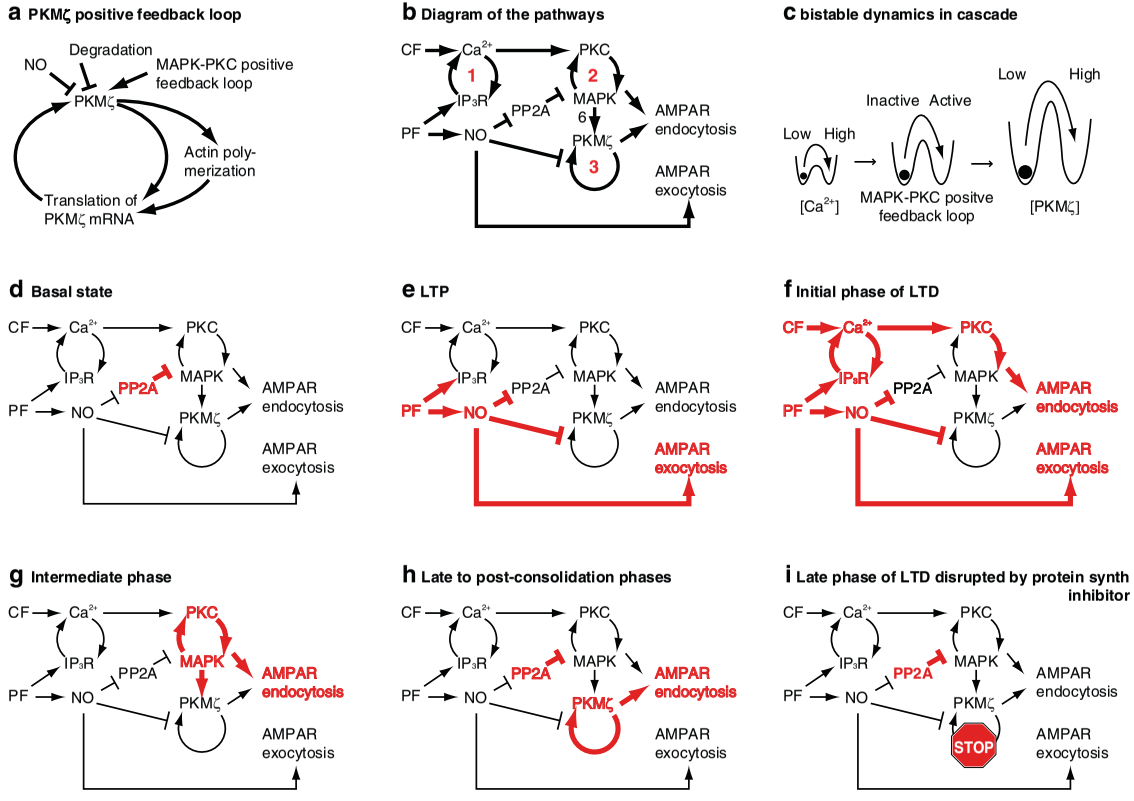

Fig. 3 Conceptual model of cerebellar long-term memory (see text for explanation). **a** Schematic diagram of long-term memory. *Sharp and blunt arrows* indicate excitatory and inhibitory pathways, respectively. **b** The protein kinase Mζ (PKMζ) positive feedback loop. **c** The cascade model [21] representation of the cerebellar long-term memory model. **d–i** Various states of memory. *Bold lines* and *thin lines* indicate activated and inactivated pathways, respectively; *bold text* and *thin text* indicate active or increased molecules and inactive or decreased molecules, respectively. **d** The basal state. **e** LTP. **f** The initial, intermediate (**g**), and late to post-consolidation (**g**) phases of LTD. i The late phase of LTD disrupted by application of a protein synthesis inhibitor. (From [15], with permission of S. Karger AG, Basel)

newly synthesized PKMζ maintains AMPAR phosphorylation and internalization for a long period.

Disruption of Late-Phase LTD by Application of a Protein Synthesis Inhibitor

The model predicts that protein synthesis inhibitor disrupts late-phase LTD by preventing PKMζ expression (Fig. 3i), whereas it does not affect the initial and intermediate phases. Once PKMζ is sufficiently expressed, only minimal synthesis of PKMζ is required to compensate for its degradation and maintain LTD. During this period, transient application of a protein synthesis inhibitor will fail to switch off the PKMζ positive feedback loop, so long as the level of remaining PKMζ is above the threshold for maintaining loop activity.

Simulation Study of Single or Interlinked Bistable Switches

We have proposed that a cascade of bistable dynamics is a possible mechanism that resolves the stability versus plasticity dilemma in stochastic noise (Figs. 2, 3) [15,21]. To test this hypothesis computationally, we build simple simulation models. One model contains a single loop (Fig. 4a), and the other contains two interlinked

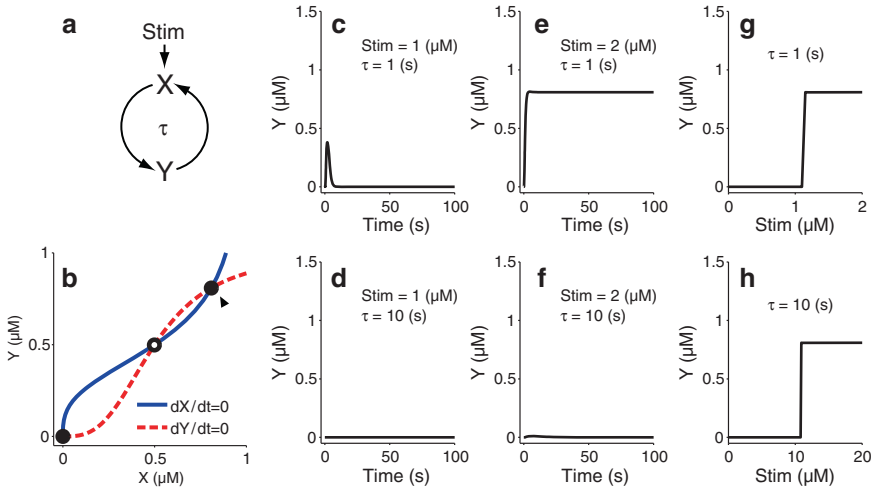

Fig. 4 Deterministic runs of the single-loop model. **a** Schematic diagram of the model. *X* and *Y* activate each other, and a stimulus (*stim*) is given to *X*. **b** Nullclines and stable (*filled circles*) and unstable (*open circle*) steady states. In the stable steady states, the system is either active (*arrowhead*) or inactive. Stim = 0 throughout. **c–f** Time courses of *Y* during and after stimulation. Stim is either 1 μM (**c, d**) or 2 μM (**e, f**) and given for 1 s in the beginning of each run. **g, h** Dose–response relationship. The loop with the smaller τ is more sensitive to stimulation. τ is 1 s (**c, e, g**) or 10 s (**d, f, h**)

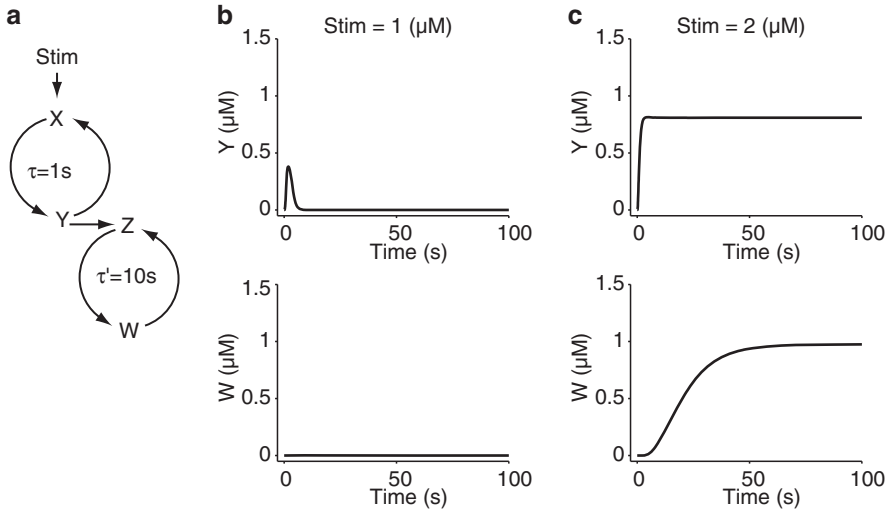

Fig. 5 Deterministic runs of the double-loop model. **a** Schematic diagram of the model. A stimulus (Stim) activates *X* of the first loop, and *X* and *Y* activate each other. *Y* also activates *Z* of the second loop, and *Z* and *W* activate each other. The first loop is faster than the second loop. **b, c** Time courses of *Y* and *W* during and after stimulation. The second loop has the same time constant as the single loop in Fig. 4d,f,h, but is more sensitive to stimuli because the first loop boosts the inputs. τ and τ' are 1 s and 10 s, respectively. Stim is either 1 μM (**b**) or 2 μM (**c**) and given for 1 s in the beginning of each run

loops (Fig. 5a). Note that our aim here is to capture the basic properties of isolated or coupled switches by using least complicated models, and not to realistically represent biological signaling pathways. Each loop consists of a couple of mutually activating molecules (X and Y as well as Z and W in Figs. 4a, 5a). The ordinary differential equations (ODEs) for the single loop model and the first loop of the double loop model are as follows:

$$\tau \frac{dX}{dt} = \frac{Y^n}{Y^n + K^n} X_{inact} - X + Stim(t)$$

$$\tau \frac{dY}{dt} = \frac{X^n}{X^n + K^n} Y_{inact} - Y$$

where $n = 3$ and $K = 0.5\,\mu M$. The inactive forms of *X* and *Y*, X_{inact} and Y_{inact}, are constant at 1 μM and do not change in concentrations even when they are consumed (buffered molecules)[1]. *Stim* is a time-dependent stimulus that induces *X*. Similarly, the ODEs for the second loop of the double loop model are as follows:

[1] The buffered species (e.g. X_{inact}) may appear to violate mass conservation, but actually do not; we assume a situation in which these molecules are abundant in the cell and freely diffuse into or out of the system, keeping their concentrations constant.

$$\tau' \frac{dZ}{dt} = \frac{W^n}{W^n + K^n} Z_{inact} - Z + Y$$
$$\tau' \frac{dW}{dt} = \frac{Z^n}{Z^n + K^n} W_{inact} - W$$

The inactive forms of Z and W, Z_{inact} and W_{inact}, are constant at 1 μM. The time constants τ and τ' determine the rates of reactions; for instance, the bigger (smaller) τ is, the more slowly (faster) X and Y change. Numerical integration of the ODEs yields deterministic solutions, and a Monte-Carlo method [34] serves for stochastic simulations.

Although the interlinked loops superficially resemble the model of Brandman et al. [35], there are crucial differences between these dynamic systems. First, the stimulus acts on the first loop in our model (Fig. 5a), whereas it acts directly on both loops in theirs. Second, in contrast to our model, the bistable property of the positive feedback loops in [35] is not inherent but depends on the level of the stimulus.

Single-Loop Model

First, we need to characterize the single-loop model (Fig. 4a) by performing deterministic simulations. Figure 4b indicates steady-state solutions given that one of the two variables (X or Y) is kept constant (nullclines); the points of intersection are equilibrium points of the system. The figure indicates that the loop is a bistable system, having two stable steady states and an unstable saddle point. In one stable steady state, X and Y are active (~0.8 μM; arrowhead), and in the other stable steady state they are inactive. Figure 4c–f shows the time course of Y during and after transient stimulation. When fast kinetics is assumed (τ = 1 s), the loop responds only transiently to a weak stimulus (Fig. 4c), whereas it is fully and permanently activated by a strong stimulus (Fig. 4e). At equilibrium, the loop is totally inactive or stereotypically active depending on the strength of the stimulus (Fig. 4g), which reflects the all-or-none nature of the bistable switch. A loop of slower kinetics (τ = 10 s) is less sensitive to stimuli (Fig. 4d,f,h) because the stimuli are too short in duration (for 1 s) and end before the state of the loop crosses the threshold.

Next, we consider stochasticity. In deterministic simulations, X and Y do not change once they reach the active state (Fig. 4b; arrowhead), but it does not mean that no reaction is taking place there. Rather, each molecule is constantly being activated and inactivated at the same rate, appearing to be static. However, in a very small system such as a dendritic spine where the number of molecules is severely limited, stochastic fluctuations are no longer negligible. Figure 6 plots several stochastic runs of a minute system (0.05 μm^3) corresponding to a tiny spine [36]. In this system, a concentration of 1 μM is equivalent to 30 molecules. Starting from the active state, the system is shaken by stochastic fluctuations and eventually pushed off to the inactive state (Fig. 6a–c); it would permanently

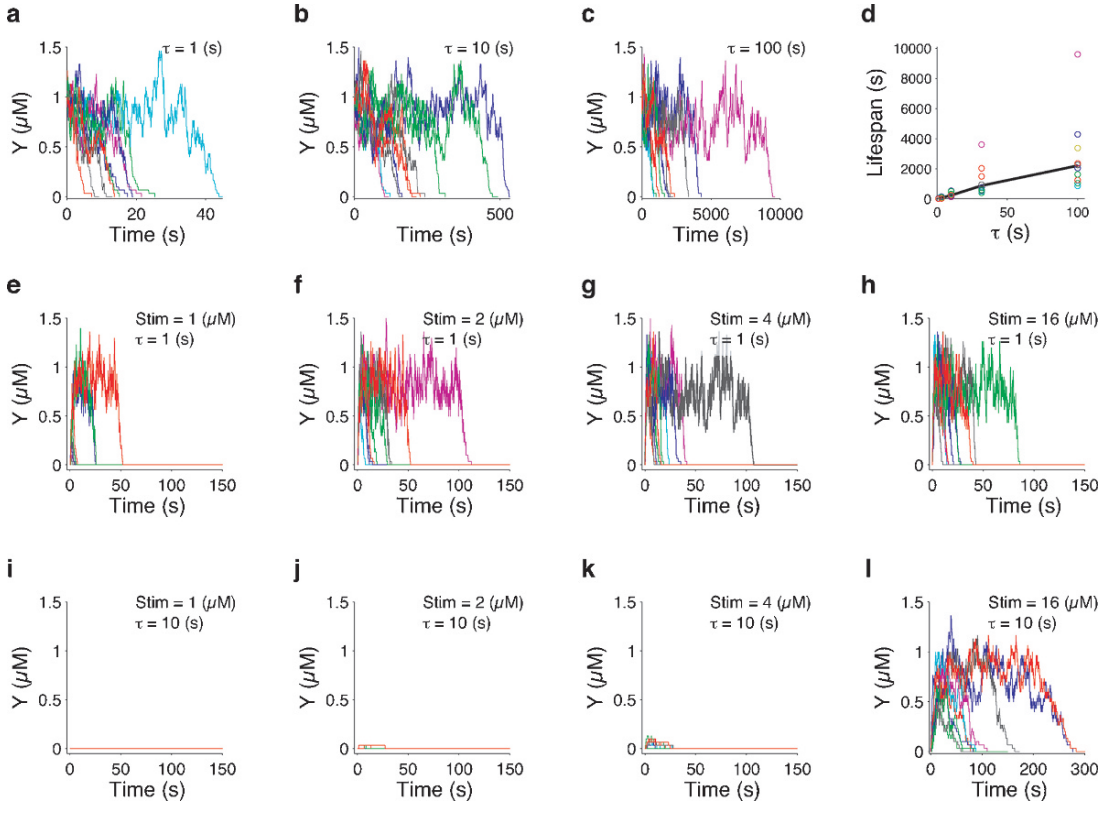

Fig. 6 Stochastic runs of the single-loop model. **a–c** Time courses of *Y* starting from the active state. The larger τ is, the longer the lifespan of the active state tends to be. τ is either 1 s (**a**), 10 s (**b**), or 100 s (**c**). **d** Linear relationship between τ and average lifespan. *Circles* indicate lifespan observed in individual runs and the *bold line* indicates their averages. **f–l** Time courses of *Y* during and after stimulation. The loop with a small τ (1 s) is sensitive to stimulation but, it can remain at the active state only for a short period. In contrast, the loop with a larger τ (10 s) is less sensitive to stimuli, but once activated, it maintains activity for a long time. Note the different time scale of **l**. Stim is either 1 μM (**e, i**), 2 μM (**f, j**), 4 μM (**g, k**), or 16 μM (**h, l**) and is given for 1 s in the beginning of each run

remain at the active state in deterministic simulation. The lifespan of the active state is proportional to τ (Fig. 6d); the slower (faster) the loop is, the longer (shorter) period its activity persists for. It should be noted that no further reaction will take place once both X and Y reach zero, as the Monte Carlo method [34] assumes that the probability of any reaction to occur in the future is proportional to X and Y. Thus, in stochastic simulations the inactive state is practically the only stable steady state, and the active state is no longer permanent. When τ is small (1 s), the loop is activated for a while by transient stimuli that are sufficiently strong (Fig. 6e–h). In contrast, when τ is larger (10 s), the loop is less sensitive to stimulation (Fig. 6i–k); once activated by a very strong stimulus, however, the loop often maintains its activity for a long time (Fig. 6l). These findings indicate that in a stochastic situation there is a trade-off between stability and sensitivity.

Interlinked Loop Model

What if two loops are coupled? We expect that a cascade of bistable dynamics makes stable and plastic memory. In particular, we are interested in a slow loop interlinked with and activated by a faster loop (Fig. 5a) because it mimics some of the cerebellar LTD steps (Fig. 3c). Figure 5b,c shows deterministic runs of the model. The faster loop (X and Y) behaves similarly as the single-loop model with fast kinetics (Fig. 4c,e). It is activated only transiently by a weak stimulus (Fig. 5b) and permanently by a strong stimulus (Fig. 5c). The slower loop (Z and W), which would not be activated by the direct input of a strong stimulus (Fig. 4f), is gradually activated by the same size of stimulus (Fig. 5c), and eventually reaches the active state. This increase in sensitivity is caused by amplification of the signal by the faster loop; its time-integrated output ($\int Ydt$) is infinitely larger than the time integral of the transient stimulus ($\int Stim(t)dt$). The interlinked loops are concluded to be as sensitive as the single fast loop.

When stochasticity is considered, a more interesting feature emerges. As is seen in the stochastic runs of the single loop model (Fig. 6e–h), a strong stimulus brings the faster loop to the active state, where the loop hangs around for a while before it eventually returns to the inactive state (Fig. 7, upper panels). Although activity of the fast loop is only transient, in some cases it contributes sufficiently large input to the slower loop (Fig. 7, lower panels). Once activated by the first loop, the second loop more often than not maintains its activity for a considerably long time. If the system did not consist of two loops but rather a single slow loop, it would be much less sensitive to the stimuli, as is evident from Fig. 6i–k. The output of the system, W, indicates an important feature that the couple of fast and slow loops is more sensitive to stimuli than a single loop with slow kinetics, whereas its activity is more stable than that of a single loop with fast kinetics.

This simple model demonstrates that a cascade of bistable dynamics has a combination of highly desirable features for a memory device, that is, robustness to noise (stability) and sensitivity to input stimuli (plasticity). Such switch cascades

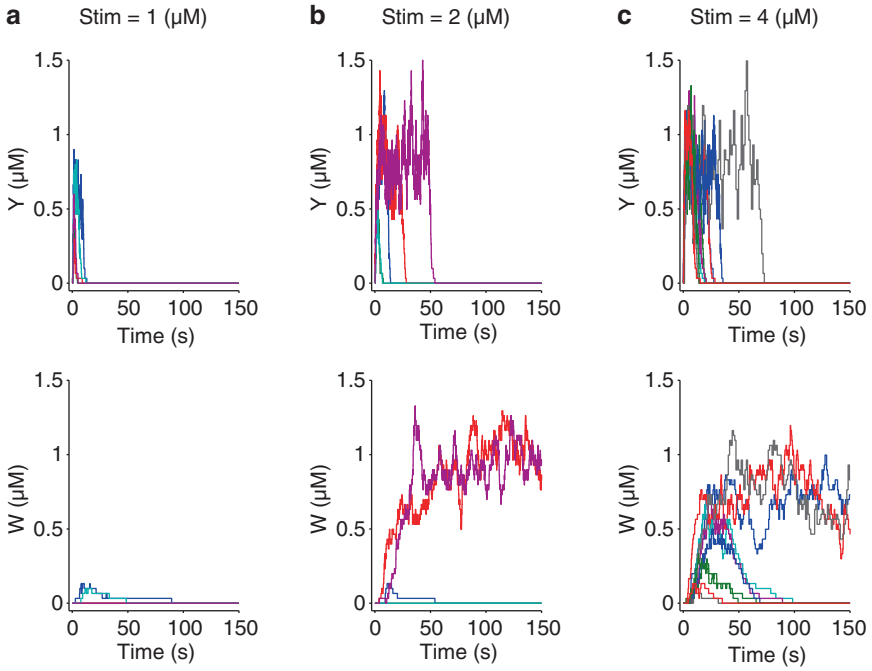

Fig. 7 Stochastic runs of the double-loop model. The *upper and lower panels* show time courses of the first loop and its downstream slower loop, respectively. The output of the system, *W*, shows that this double loop model is more sensitive to stimuli than a single loop with slow kinetics, whereas its activity is more stable than that of a single loop with fast kinetics. τ and τ' are 1 s and 10 s, respectively. Stim is either 1 μM (**a**), 2 μM (**b**), or 4 μM (**c**) and is given for 1 s in the beginning of each run

are biologically implementable, as is exemplified by the pairing of CICR and MAPK-PKC positive feedback loops [13,14].

Conclusions

In this chapter, we reviewed theoretical studies on cerebellar LTD. CICR and the MAPK-PKC positive feedback loop form bistable switches connected in tandem, and we hypothesize that PKMζ is another switch that follows. Simulations of single or interlinked bistable positive feedback loops supported our hypothesis that a cascade of excitable dynamics is a likely mechanism that resolves the stability versus plasticity dilemma.

Acknowledgments We thank Dr. Sungho Hong of Okinawa Institute of Science and Technology for his helpful comments. This work was supported by a grant from the Uehara Memorial Foundation.

References

1. Abraham WC, Robins A (2005) Memory retention: the synaptic stability versus plasticity dilemma. Trends Neurosci 28:73–78
2. Masugi-Tokita M, Tarusawa E, Watanabe M, Molnar E, Fujimoto K, Shigemoto R (2007) Number and density of AMPA receptors in individual synapses in the rat cerebellum as revealed by SDS-digested freeze-fracture replica labeling. J Neurosci 27:2135–2144
3. Marr D (1969) A theory of cerebellar cortex. J Physiol 202:437–470
4. Ito M (1970) Neurophysiological aspects of the cerebellar motor control system. Int J Neurol 7:162–176
5. Albus JS (1971) A theory of cerebellar function. Math Biosci 10:25–61
6. Ito M (2001) Cerebellar long-term depression: characterization, signal transduction, and functional roles. Physiol Rev 81:1143–1195
7. Ito M (2002) The molecular organization of cerebellar long-term depression. Nat Rev Neurosci 3:896–902
8. Hartell NA (2002) Parallel fiber plasticity. Cerebellum 1:3–18
9. Ito M (2006) Cerebellar circuitry as a neuronal machine. Prog Neurobiol 78:272–303
10. Jörntell H, Hansel C (2006) Synaptic memories upside down: bidirectional plasticity at cerebellar parallel fiber-Purkinje cell synapses. Neuron 52:227–238
11. Iino M (2006) Ca^{2+}-dependent inositol 1,4,5-trisphosphate and nitric oxide signaling in cerebellar neurons. J Pharmacol Sci 100:538–544
12. Ferrell JE Jr, Machleder EM (1998) The biochemical basis of an all-or-none cell fate switch in *Xenopus* oocytes. Science 280:895–898
13. Kuroda S, Schweighofer N, Kawato M (2001) Exploration of signal transduction pathways in cerebellar long-term depression by kinetic simulation. J Neurosci 21:5693–5702
14. Doi T, Kuroda S, Michikawa T, Kawato M (2005) Inositol 1,4,5-trisphosphate-dependent Ca^{2+} threshold dynamics detect spike timing in cerebellar Purkinje cells. J Neurosci 25:950–961
15. Ogasawara H, Doi T, Kawato M (2008) Systems biology perspectives on cerebellar long-term depression. NeuroSignals 16:300–317
16. Sarkisov DV, Wang SS (2008) Order-dependent coincidence detection in cerebellar Purkinje neurons at the inositol trisphosphate receptor. J Neurosci 28:133–142
17. Ogasawara H (2008) The calcium kinetics and inositol trisphosphate receptor properties shape the asymmetric timing window of coincidence detection. J. Neurosci 28:4293–4294
18. Tanaka K, Khiroug L, Santamaria F, Doi T, Ogasawara H, Ellis-Davies GC, Kawato M, Augustine GJ (2007) Ca^{2+} requirements for cerebellar long-term synaptic depression: role for a postsynaptic leaky integrator. Neuron 54:787–800
19. Tanaka K, Augustine GJ (2008) A positive feedback signal transduction loop determines timing of cerebellar long-term depression. Neuron 59:608–620
20. Ramakrishnan N, Bhalla US (2008) Memory switches in chemical reaction space. PLoS Comput Biol 4:e1000122
21. Kawato M (2008) From 'understanding the brain by creating the brain' towards manipulative neuroscience. Philos Trans R Soc Lond B Biol Sci 363:2201–2214
22. Sacktor TC (2008) PKMζ, LTP maintenance, and the dynamic molecular biology of memory storage. Prog Brain Res 169:27–40
23. Shema R, Sacktor TC, Dudai Y (2007) Rapid erasure of long-term memory associations in the cortex by an inhibitor of PKMζ. Science 317:951–953
24. Hernandez AI, Blace N, Crary JF, Serrano PA, Leitges M, Libien JM, Weinstein G, Tcherapanov A, Sacktor TC (2003) Protein kinase Mζ synthesis from a brain mRNA encoding an independent protein kinase Cζ catalytic domain. Implications for the molecular mechanism of memory. J Biol Chem 278:40305–40316
25. Oster H, Eichele G, Leitges M (2004) Differential expression of atypical PKCs in the adult mouse brain. Brain Res Mol Brain Res 127:79–88
26. Lynch MA (2004) Long-term potentiation and memory. Physiol Rev 84:87–136

27. Silva AJ, Stevens CF, Tonegawa S, Wang Y (1992) Deficient hippocampal long-term potentiation in alpha-calcium-calmodulin kinase II mutant mice. Science 257:201–206
28. Hansel C, de Jeu M, Belmeguenai A, Houtman SH, Buitendijk GH, Andreev D, De Zeeuw CI, Elgersma Y (2006) αCaMKII Is essential for cerebellar LTD and motor learning. Neuron 51:835–843
29. Goldbeter A, Koshland DE Jr (1981) An amplified sensitivity arising from covalent modification in biological systems. Proc Natl Acad Sci U S A 78:6840–6844
30. Ferrell JE Jr (1999) Building a cellular switch: more lessons from a good egg. Bioessays 21:866–870
31. Shibuki K, Kimura S (1997) Dynamic properties of nitric oxide release from parallel fibres in rat cerebellar slices. J Physiol 498(pt 2):443–452
32. Lev-Ram V, Wong ST, Storm DR, Tsien RY (2002) A new form of cerebellar long-term potentiation is postsynaptic and depends on nitric oxide but not cAMP. Proc Natl Acad Sci U S A 99:8389–8393
33. Kakegawa W, Yuzaki M (2005) A mechanism underlying AMPA receptor trafficking during cerebellar long-term potentiation. Proc Natl Acad Sci U S A 102:17846–17851
34. Gillespie DT (1977) Exact stochastic simulation of coupled chemical reactions. J Phys Chem 81:2340–2361
35. Brandman O, Ferrell JE Jr, Li R, Meyer T (2005) Interlinked fast and slow positive feedback loops drive reliable cell decisions. Science 310:496–498
36. Nimchinsky EA, Sabatini BL, Svoboda K (2002) Structure and function of dendritic spines. Annu Rev Physiol 64:313–353

Biogenesis and Function Mechanisms of Micro-RNAs and Their Role as Oncogenes and Tumor Suppressors

Soken Tsuchiya, Kazuya Terasawa, Ryo Kunimoto, Yasushi Okuno, Fumiaki Sato, Kazuharu Shimizu, and Gozoh Tsujimoto

Introduction

Micro-RNAs (miRNAs) are evolutionarily conserved small noncoding RNAs (20–23 nucleotides). MiRNAs regulate various physiological pathways such as differentiation, proliferation, and apoptosis by negative regulation of the gene expressions at the posttranscriptional level [1–3]. Currently, more than 800 human miRNAs have been identified and registered in the miRNA database miRBase [4]. Strikingly, 30% of protein-coding transcripts in humans is predicted to be regulated by miRNAs [5,6]. Recently, miRNAs have been reported to work as oncogenes or tumor suppressor genes and be directly involved in the initiation, progression, and metastasis of various cancers [7–9]. Therefore, we focus on the role that miRNAs play in cancer and the use of miRNAs in drug discovery. Collection of evidence suggests that miRNAs can be potentially useful for understanding tumorigenesis and finding novel strategies for cancer diagnosis and therapy.

Biogenesis of miRNAs

MiRNAs are generated in multiple steps (Fig. 1). Initially, miRNAs are transcribed by RNA polymerase II as long RNA precursors (pri-miRNAs) [10–12]. Pri-miRNAs are usually several kilobases in length, and contain a 7-methyl

S. Tsuchiya, F. Sato, K. Shimizu
Department of Nanobio Drug Discovery, Graduate School of Pharmaceutical Sciences, Kyoto University, Kyoto, Japan

K. Terasawa and G. Tsujimoto
Department of Genomic Drug Discovery Science, Kyoto University, 46-29 Yoshida Shimoadachi, Sakyo-ku, Kyoto 606-8501, Japan

R. Kunimoto and Y. Okuno
Department of PharmacoInformatics, Graduate School of Pharmaceutical Sciences, Kyoto University, Kyoto, Japan

S. Nakanishi et al. (eds.), *Systems Biology*,
DOI:10.1007/978-4-431-87704-2_19, © Springer 2009

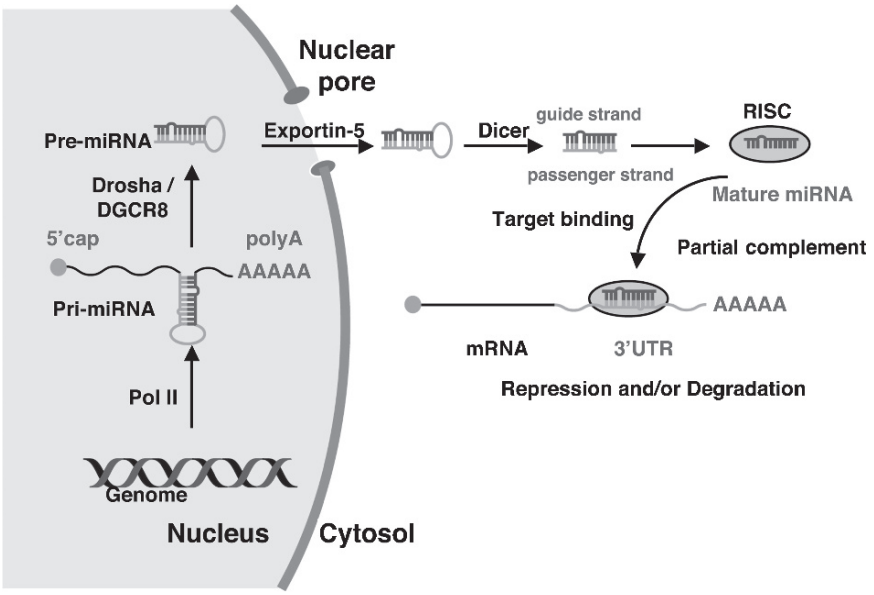

Fig. 1 Schematic diagram of biogenesis and function in micro-RNAs (miRNAs). MiRNAs are transcribed by RNA polymerase II and sequentially processed by Drosha/DGCR8 and Dicer. MiRNA-loaded RNA-induced silencing complex (*RISC*) causes the cleavage or translational silencing of target mRNAs

guanosine cap structure and a poly(A) tail similar to protein-coding mRNAs. The pri-miRNAs are processed into precursors of approximately 70 nucleotides (pre-miRNAs) with a stem-loop structure and a two-nucleotide 3′-overhang by the RNase III enzyme, Drosha, and a double-stranded RNA-binding protein, DGCR8/Pasha [13–15]. Then, pre-miRNAs are transported to the cytoplasm by a member of the Ran transport receptor family, exportin-5 [16,17]. Pre-miRNAs exported in the cytoplasm are further processed by another RNase III enzyme, Dicer, and unwound by a helicase [18]. Finally, only one mature miRNA strand (guide strand) is incorporated into a RNA-induced silencing complex (RISC) that mediates cleavage or translational inhibition of target mRNAs, while the other strand (passenger strand) is quickly degraded [19–21]. The stability of the base pairs at the 5′-end of the duplex determines which strand is incorporated in RISC [22,23]. RISC is composed of Dicer, Argonaute2 (Ago2), and the double-strand RNA-binding protein, TRBP [21,24], and cleaves target mRNAs more efficiently by using pre-miRNAs rather than the duplex RNAs that do not have the stem-loop structure, suggesting that processing by Dicer may be coupled with assembly of the mature miRNA into RISC [21]. The incorporated miRNA guides the RISC to the complementary sequence in the 3′-untranslated region (UTR) of target mRNAs. MiRNAs base-pair to the 3′-UTR of target mRNA with perfect or near-perfect complementarity, leading to the target mRNA degradation by Ago2,

a component of RISC [25]. In contrast, partial base-pairing between a miRNA and a target mRNA leads to translational silencing of a target mRNA without RNA degradation [26]. In partial base-pairing, the binding of some nucleotides in the 5′-region of miRNAs has been indicated to be functionally important by systematic mutation experiments [27,28].

The Role of miRNAs in Cancer

Recently, it has been reported that the expression of several miRNAs is altered in a variety of human cancers, suggesting potential roles of miRNAs in tumorigenesis [29]. Calin et al. [30] showed that more than 50% of miRNAs were located in cancer-associated genomic regions or in fragile sites. In fact, miR-15a and miR-16 genes exist as a cistronic cluster at 13q14, which is deleted or downregulated in most cases (~68%) of B-cell chronic lymphocytic leukemias [31]. Cimmino et al. [32] found that both these miRNAs negatively regulate the expression of B cell lymphoma 2 (BCL2), which inhibits apoptosis and is present in many types of cancer including leukemias. In fact, overexpression of miR-15 and miR-16 in the MEG-01 cell line induces apoptotic cell death.

Alterations in gene copy number of miRNAs are detected in a variety of human cancers [33–35]. Zhang et al. [33] showed that miRNAs exhibited high-frequency genomic alterations in human ovarian cancer, breast cancer, and melanoma using high-resolution array-based comparative genomic hybridization. Hayashita et al. [34] found that the expression and gene copy number of the miR-17–92 cluster composed of seven miRNAs is increased in lung cancer cell lines, especially with small-cell lung cancer histology. Enforced expression of miRNAs included in this polycistronic cluster enhances cell proliferation in a lung cancer cell line. The increase in expression and gene copy number of miR-17–92 cluster was also found in B-cell lymphomas [35]. The expression of miRNAs in this cluster is upregulated by c-Myc, whose expression and/or function is one of the most common abnormalities in human cancers, and miR-17-5p and miR-20a in this miR-17–92 cluster negatively regulate the expression of transcriptional factor E2F1 [36]. Furthermore, it was indicated that the miR-17–19b cluster included in miR-17–92 cluster inhibited apoptotic cell death and accelerated c-Myc-induced lymphomagenesis in mice reconstituted with miR-17–19b cluster-overexpressed hematopoietic stem cells [35]. Furthermore, the miR-17–92 cluster has been reported to augment angiogenesis in vivo by downregulation of antiangiogenic thrombospondin-1 and connective tissue growth factor in Ras-transformed colonocytes [37].

Global expression profiling analysis of protein-coding genes is known to be useful for cancer diagnoses and prognosis predictions [38]. Recently, Lu et al. [29] indicated that miRNA expression profiles can successfully classify poorly differentiated cancers that cannot be classified by mRNA expression profiles. Accordingly, miRNA expression profiles are more accurately correlated with clinical severity of cancer malignancy than protein-coding gene expression profiles. This result

indicates the potential of miRNA expression profiles in cancer classification and prognosis prediction [29].

Because miRNAs act as oncogenes or tumor suppressor genes, miRNAs are potential targets of therapeutic strategies. Recently, Krutzfeldt et al. [39] indicated that chemically engineered oligonucleotides, termed antagomirs, efficiently inhibited miRNAs in vivo. Additionally, it is reported that introduction of 2′-*O*-methoxyethyl phosphorothioate antisense oligonucleotide of miR-122 (abundant in the liver; regulates cholesterol and fatty acid metabolism) decreases plasma cholesterol levels and improves liver steatosis in mice with diet-induced obesity [40]. These findings indicate that antisense oligonucleotides are also potential targets for drug discovery, suggesting the possibility that intractable cancers may become curable by overexpression and/or inhibition of miRNAs. However, for miRNAs to be used in gene therapy, further improvements to make miRNAs more effective and less toxic than other cancer therapy are required.

Prediction of Target mRNAs

Identification of the miRNA-targeted genes provides deep biological insights to understand the new mechanisms of the physiopathological phenomena. Therefore, development of a comprehensive assay to rapidly identify target mRNAs would greatly assist understanding of miRNAs and lead to novel therapeutic approaches against cancer. Although there are many bioinformatics approaches for target prediction, which have predicted that a single miRNA may have hundreds of target genes [5,6,41–45], they have room for many improvements in accuracy and completeness of prediction, respectively. Thus, we have developed a new computational approach to extract regulatory networks between miRNAs and their target mRNAs (Fig. 2). We assumed that the expression pattern of miRNA would present inverse correlation with that of its corresponding target mRNA. Hence, selecting the inverse correlative pairs among the miRNA–target pairs predicted by the sequence-based algorism (ex. miRanda) from expression profiles of mRNAs and miRNAs, we have successfully reduced the false-positive pairs of target prediction results. Moreover, overlapping target information of the predicted pairs onto the coexpressed gene networks, we have also generated the gene networks coregulated by the common miRNA. We hope the inferred networks can be helpful to understand the biological systems of the miRNAs world.

It has been established that the abnormalities of specific miRNA expression contribute to tumorigenesis. Therefore, miRNAs are expected to be powerful tools for cancer classification, diagnosis, and prognosis prediction as well as potential targets of cancer therapy. Furthermore, identification of target mRNAs regulated by miRNAs, elucidation of the oncogenic or tumor suppressive molecular mechanisms by miRNAs and identification of genetic variation in miRNAs and miRNA–target sites of mRNAs may lead to the discovery of new molecular targets related to oncogenesis.

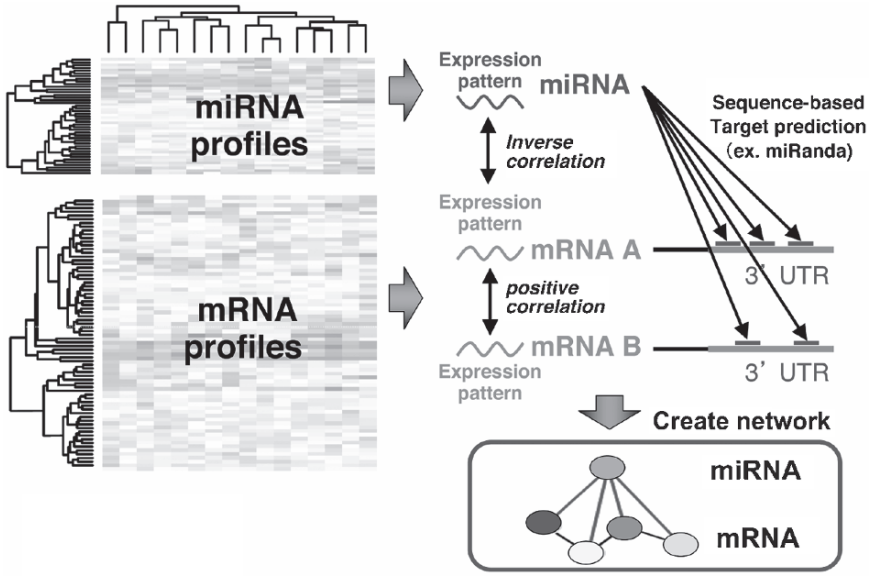

Fig. 2 Scheme of formulation of networks between miRNAs and their target mRNAs

References

1. Bartel DP (2004) MicroRNAs: genomics, biogenesis, mechanism, and function. Cell 116:281–297
2. Tsuchiya S, Okuno Y, Tsujimoto G (2006) MicroRNA: biogenetic and functional mechanisms and involvements in cell differentiation and cancer. J Pharmacol Sci 101:267–270
3. Pasquinelli AE, Reinhart BJ, Slack F et al (2000) Conservation of the sequence and temporal expression of let-7 heterochronic regulatory RNA. Nature (Lond) 408:86–89
4. Griffiths-Jones S, Grocock RJ, van Dongen S et al (2006) miRBase: microRNA sequences, targets and gene nomenclature. Nucleic Acids Res 34:D140–D144
5. Lewis BP, Burge CB, Bartel DP (2005) Conserved seed pairing, often flanked by adenosines, indicates that thousands of human genes are microRNA targets. Cell 120:15–20
6. Xie X, Lu J, Kulbokas EJ et al (2005) Systematic discovery of regulatory motifs in human promoters and 3′ UTRs by comparison of several mammals. Nature (Lond) 434:338–345
7. Esquela-Kerscher A, Slack FJ (2006) Oncomirs: microRNAs with a role in cancer. Nat Rev Cancer 6:259–269
8. Calin GA, Croce CM (2006) MicroRNA–cancer connection: the beginning of a new tale. Cancer Res 66:7390–7394
9. Calin GA, Croce CM (2006) MicroRNA signatures in human cancers. Nat Rev Cancer 6:857–866
10. Lee Y, Jeon K, Lee JT et al (2002) MicroRNA maturation: stepwise processing and subcellular localization. EMBO J 21:4663–4670
11. Cai X, Hagedorn CH, Cullen BR (2004) Human microRNAs are processed from capped, polyadenylated transcripts that can also function as mRNAs. RNA 10:1957–1966
12. Lee Y, Kim M, Han J et al (2004) MicroRNA genes are transcribed by RNA polymerase II. EMBO J 23:4051–4060
13. Lee Y, Ahn C, Han J et al (2003) The nuclear RNase III Drosha initiates microRNA processing. Nature (Lond) 425:415–419

14. Gregory RI, Yan KP, Amuthan G et al (2004) The Microprocessor complex mediates the genesis of microRNAs. Nature (Lond) 432:235–40
15. Han J, Lee Y, Yeom KH et al (2006) Molecular basis for the recognition of primary microRNAs by the Drosha-DGCR8 complex. Cell 125:887–901
16. Yi R, Qin Y, Macara IG et al (2003) Exportin-5 mediates the nuclear export of pre-microRNAs and short hairpin RNAs. Genes Dev 17:3011–3016
17. Lund E, Guttinger S, Calado A et al (2004) Nuclear export of microRNA precursors. Science 303:95–98
18. Hutvagner G, McLachlan J, Pasquinelli AE et al (2001) A cellular function for the RNA-interference enzyme Dicer in the maturation of the let-7 small temporal RNA. Science 293:834–838
19. Matranga C, Tomari Y, Shin C et al (2005) Passenger-strand cleavage facilitates assembly of siRNA into Ago2-containing RNAi enzyme complexes. Cell 123:607–620
20. Rand TA, Petersen S, Du F et al (2005) Argonaute2 cleaves the anti-guide strand of siRNA during RISC activation. Cell 123:621–629
21. Gregory RI, Chendrimada TP, Cooch N et al (2005) Human RISC couples microRNA biogenesis and posttranscriptional gene silencing. Cell 123:631–640
22. Khvorova A, Reynolds A, Jayasena SD (2003) Functional siRNAs and miRNAs exhibit strand bias. Cell 115:209–216
23. Schwarz DS, Hutvágner G, Du T et al (2003) Asymmetry in the assembly of the RNAi enzyme complex. Cell 115:199–208
24. Chendrimada TP, Gregory RI, Kumaraswamy E et al (2005) TRBP recruits the Dicer complex to Ago2 for microRNA processing and gene silencing. Nature (Lond) 436:740–744
25. Meister G, Landthaler M, Patkaniowska A et al (2004) Human Argonaute2 mediates RNA cleavage targeted by miRNAs and siRNAs. Mol Cell 15:185–197
26. Hutvágner G, Zamore PD (2002) A microRNA in a multiple-turnover RNAi enzyme complex. Science 297:2056–2060
27. Doench JG, Sharp PA (2004) Specificity of microRNA target selection in translational repression. Genes Dev 18:504–511
28. Kiriakidou M, Nelson PT, Kouranov A et al (2004) A combined computational-experimental approach predicts human microRNA targets. Genes Dev 18:1165–1178
29. Lu J, Getz G, Miska EA et al (2005) MicroRNA expression profiles classify human cancers. Nature (Lond) 435:834–838
30. Calin GA, Sevignani C, Dumitru CD et al (2004) Human microRNA genes are frequently located at fragile sites and genomic regions involved in cancers. Proc Natl Acad Sci U S A 101:2999–3004
31. Calin GA, Dumitru CD, Shimizu M et al (2002) Frequent deletions and down-regulation of micro-RNA genes miR15 and miR16 at 13q14 in chronic lymphocytic leukemia. Proc Natl Acad Sci U S A 99:15524–15529
32. Cimmino A, Calin GA, Fabbri M et al (2005) miR-15 and miR-16 induce apoptosis by targeting BCL2. Proc Natl Acad Sci U S A 102:13944–13949
33. Zhang L, Huang J, Yang N et al (2006) microRNAs exhibit high frequency genomic alterations in human cancer. Proc Natl Acad Sci U S A 103:9136–9141
34. Hayashita Y, Osada H, Tatematsu Y et al (2005) A polycistronic microRNA cluster, miR-17–92, is overexpressed in human lung cancers and enhances cell proliferation. Cancer Res 65:9628–9632
35. He L, Thomson JM, Hemann MT et al (2005) A microRNA polycistron as a potential human oncogene. Nature (Lond) 435:828–833
36. O'Donnell KA, Wentzel EA, Zeller KI ey al (2005) c-Myc-regulated microRNAs modulate E2F1 expression. Nature (Lond) 435:839–843
37. Dews M, Homayouni A, Yu D et al (2006) Augmentation of tumor angiogenesis by a Myc-activated microRNA cluster. Nat Genet 38:1060–1065
38. Ramaswamy S, Tamayo P, Rifkin R et al (2001) Multiclass cancer diagnosis using tumor gene expression signatures. Proc Natl Acad Sci U S A 98:15149–15154

39. Krutzfeldt J, Rajewsky N, Braich R et al (2005) Silencing of microRNAs in vivo with 'antagomirs'. Nature (Lond) 438:685–689
40. Esau C, Davis S, Murray SF et al (2006) miR-122 regulation of lipid metabolism revealed by in vivo antisense targeting. Cell Metab 3:87–98
41. John B, Enright AJ, Aravin A et al (2004) Human MicroRNA targets. PLoS Biol 2:e363
42. Kiriakidou M, Nelson PT, Kouranov A et al (2004) A combined computational-experimental approach predicts human microRNA targets. Genes Dev 18:1165–1178
43. Lewis BP, Shih IH, Jones-Rhoades MW et al (2003) Prediction of mammalian microRNA targets. Cell 115:787–798
44. Krek A, Grun D, Poy MN et al (2005) Combinatorial microRNA target predictions. Nat Genet 37:495–500
45. Miranda KC, Huynh T, Tay Y et al (2006) A pattern-based method for the identification of microRNA binding sites and their corresponding heteroduplexes. Cell 126:1203–1217

The Pathogenetic Significance of Deregulated Transcription Factors in Hematological Malignancies

Masahiro Nakagawa, Susumu Goyama, Motoshi Ichikawa, and Mineo Kurokawa

Introduction

Hematological malignancies have been treated with traditional chemotherapy, such as alkylating agents, anthracycline, or antimetabolites. These conventional chemotherapies are not specific to malignant cells, and severe side effects are unavoidable with intensive chemotherapy. Therefore, it might be difficult to improve the cure rate further with conventional chemotherapy. Hematopoietic stem cell transplantation (HSCT) is a powerful and curable treatment, but it is very invasive. Patients sometimes suffer from severe side effects, such as graft-versus-host disease (GVHD), and HSCT may also cause premature death. In addition, it is sometimes difficult to find appropriate donors. In recent years, with the great advances in molecular biology, genetics, biochemistry, and systems biology, we gradually come to understand the molecular mechanisms of pathogenesis in hematological malignancies. Molecular targeted therapy targets molecules or pathways that play critical roles in maintaining hematological malignancies. In contrast to conventional chemotherapy, molecular targeted therapy is highly specific to malignant cells and has minimal side effects. Currently, the most successful molecular targeted therapy is imatinib, a relatively specific inhibitor of the BCR-ABL tyrosine kinase in chronic myeloid leukemia (CML). Imatinib dramatically changed the standard therapy and indication of HSCT for CML [1,2]. However, in contrast to CML, which is relatively homogeneous, molecular pathogenesis and therapeutic targets are largely unknown in many hematological malignancies. Therefore, we definitely need to elucidate molecular mechanisms of pathogenesis in other types of hematopoietic malignancies. Classically, we analyzed the functions of molecules individually, which method was not necessarily efficient. To extensively clarify molecular pathogenesis in many hematological malignancies, we applied bioinformatics and systems biology. We made genome-wide analyses of intracellular

M. Nakagawa, S. Goyama, M. Ichikawa, and M. Kurokawa
Department of Hematology and Oncology, Graduate School of Medicine, University of Tokyo, The University of Tokyo Hospital, 7-3-1 Hongo, Bunkyo-ku, Tokyo, 113-8655, Japan

S. Nakanishi et al. (eds.), *Systems Biology*,
DOI:10.1007/978-4-431-87704-2_20,

changes caused by leukemia-associated transcriptional factors, with the intention to comprehend total molecular pathogenesis and to identify therapeutic targets.

Deregulation of Transcription Factors in Hematological Malignancies

Hematopoiesis is a precisely regulated process that generates terminally differentiated cells in the peripheral blood from immature progenitors from bone marrow. The number of mature cells is tightly maintained in spite of the short life of these cells. For this strict regulation, hematopoietic progenitors must proliferate, differentiate, or undergo apoptosis, according to the individual circumstances. These processes are controlled by the combined network of multiple hematopoietic transcription factors [3]. Deregulation of these process caused by genetic mutations results in the development of hematological malignancies (Fig. 1). Specific chromosomal translocations are detected in nearly half of cases with acute leukemia. It was revealed that hematopoietic transcription factors are frequent targets for leukemia-associated gene rearrangements. This finding is consistent with the fact that hematopoiesis can be achieved through well-organized cooperation between hematopoietic transcription factors: among these are *Evi-1* (ectopic viral integration site 1) and *AML1* (acute myeloid leukemia 1).

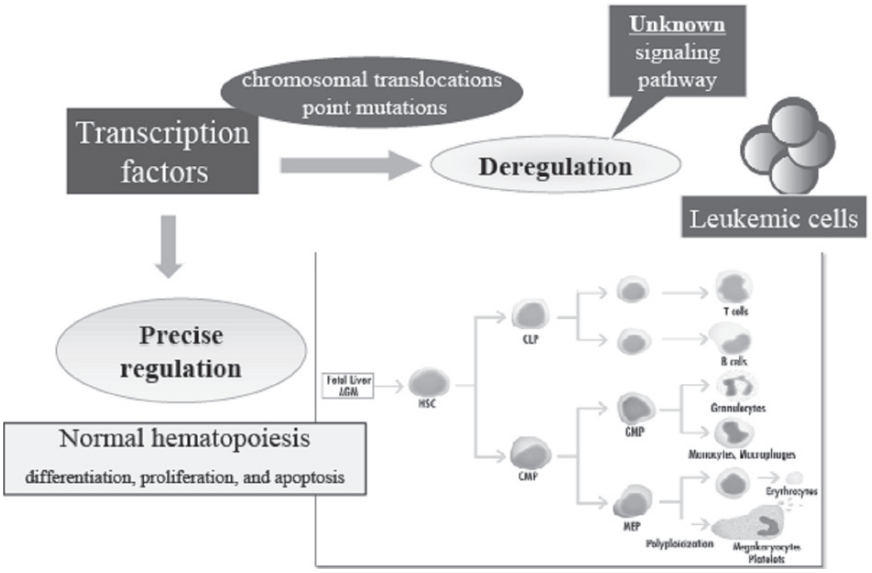

Fig. 1 Deregulation of transcription factors in leukemia. Transcription factors precisely regulate hematopoietic system for differentiation, proliferation, and apoptosis. Deregulation of transcription factors causes hematopoietic malignancies by unknown signaling pathways

AML1 in Normal and Malignant Hematopoiesis

AML1 is a transcription factor first isolated from t(8;21)(q21;q22) and later in t(3;21)(q26;q22), t(12;21)(p13;q22), and t(16;21)(q24;q21) translocations found in human leukemia in which the aberrant fusion genes AML1/ETO and AML1/Evi-1, TEL/AML1, and AML1/MTG16, respectively, were generated [4]. These fusion proteins have a common functional property whereby they act as a dominant negative inhibitor for the normal AML1 allele. For example, the AML1/ETO fusion protein retains the ability to bind to the *cis* elements of AML1 target genes but does not initiate gene transcription. This property enables the fusion protein to interfere with the transcriptional activity of native AML1. Similar in vitro data have been obtained for TEL/AML1 and AML1/Evi-1. In addition, AML1/ETO elicits a dominant inhibitory effect on AML1 function during hematopoietic development. AML1/ETO knock-in mice recapitulate an AML1-null phenotype; they die in utero, although they have one fully intact AML1 allele. It is shown that AML1 dimerizes with the common β-subunit, CBFβ, to bind to its target sequences known as PEBP2 sequences and regulates a variety of hematopoietic lineage-specific genes, including interleukin-3, granulocyte-macrophage colony-stimulating factor, macrophage colony-stimulating factor receptor, neutrophil elastase, granzyme B, myeloperoxidase, neutrophil defensin, and subunits of the T-cell and B-cell antigen receptor, in cooperation with other transcription factors [4]. AML1 is absolutely required for mouse embryogenesis and hematopoiesis, because AML1-null embryos die at midgestation (by E12.5) with massive hemorrhage in the central nervous system and complete effacement of definitive hematopoiesis in the fetal liver, although primitive erythropoiesis is preserved [5,6]. The analysis on AML1 function in adults has been hampered by premature lethality of AML1 knockout (KO) mice. Recently, we have generated AML1 conditional knockout (cKO) mice in which AML1 is disrupted specifically in hematopoietic compartments after birth, and found that AML1 negatively regulates quiescent hematopoietic stem cells (HSCs) in adult hematopoiesis, whereas it is required for megakaryocytic maturation and lymphocytic development [7,8].

Evi-1 in Normal and Malignant Hematopoiesis

Evi-1 was first identified as a common locus of retroviral integration in myeloid tumors in AKXD mice [9]. In humans, Evi-1 is located on chromosome 3q26, and rearrangements on chromosome 3q26 often activate Evi-1 expression in acute myeloid leukemia (AML) and myelodysplastic syndrome (MDS) [10,11]. Although these rearrangements are infrequent in AML, they are of remarkable prognostic value. Patients with these karyotypes are characterized by elevated platelet count and lack of response to antileukemic therapy [12]. Elevated Evi-1 expression occurs with high frequency in AML patients without 3q26 abnormalities and is associated with unfavorable outcomes [13,14]. Thus, Evi-1 is one of the key factors that predict poor survival in

leukemia patients. Previous studies revealed that Evi-1 possesses diverse functions as an oncoprotein. Evi-1 antagonizes growth-inhibitory effects of transforming growth factor-beta (TGF-β) by interacting with Smad3 [15], protects cells from stress-induced cell death by inhibiting c-Jun N-terminal kinase (JNK) [16], increases the expression of endogenous c-Jun and c-fos, resulting in activation of AP-1 [17], and blocks granulocytic differentiation of myeloid cells [18]. Evi-1 knockout mice die in utero by E10.5 exhibiting widespread hypocellularity, hemorrhaging, and disruption in the development of paraxial mesenchyme [22]. To investigate the physiological role of Evi-1 in adult hematopoiesis, we have generated Evi-1 cKO mice in which Evi-1 is disrupted specifically in hematopoietic compartments after birth, and found that Evi-1 is essential for proliferation of both HSCs and leukemic cells [19].

The Signaling Pathway Regulated by AML1 or Evi-1

Deregulation of the transcriptional network caused by functional impairments of AML1 or Evi-1 is the key to comprehend molecular pathogenesis of hematopoietic malignancies. Therefore, we focused on the signaling pathway regulated by them. In normal conditions, precise regulation of AML1 or Evi-1 maintains hematopoiesis. Once their functions are impaired, the deregulated network causes hematological malignancies. First, we obtained transcriptome from the cells just after deleting AML1. We purified lineage-negative, Sca-1-positive, c-kit-positive (LSK) cells as HSCs from cKO mice and retrovirally transduced Cre-ER to them. To detect immediate targets of AML1, we collected the cells just after deleting AML1 by activation of Cre-ER using 4-OHT and analyzed them with cDNA microarray. Next, we combined transcriptome analysis and knowledge-based database for various information networks. We used gene set enrichment analysis (GSEA) [20,21], which is a computational method that determines whether an a priori defined set of genes shows statistically significant, concordant differences between two biological states, such as AML1 deficient or AMLI competent. We found several signal pathways regulating cell proliferation, inflammation, or apoptosis are activated in AML1-deficient cells. Next, we obtained transcriptome from the cells shortly after deleting Evi-1, by retrovirus containing Cre instead of

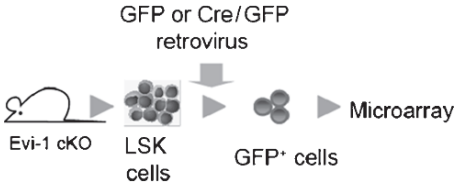

Fig. 2 Transcriptome from the cells just after deleting *Evi-1*. Lineage-negative, Sca-1-positive, c-kit-positive (*LSK*) cells were isolated as hematopoietic stem cells (HSCs) from *Evi-1* conditional knockout (*cKO*) mice. *GFP* or *Cre*/*GFP* retroviral infection was performed on these cells, and GFP-positive cells were collected shortly after deleting Evi-1 by Cre recombinase activity. Gene expression profiles were compared in cDNA microarray analysis between GFP and Cre/GFP cells, that is, Evi-1 wild-type and Evi-1 knockout cells

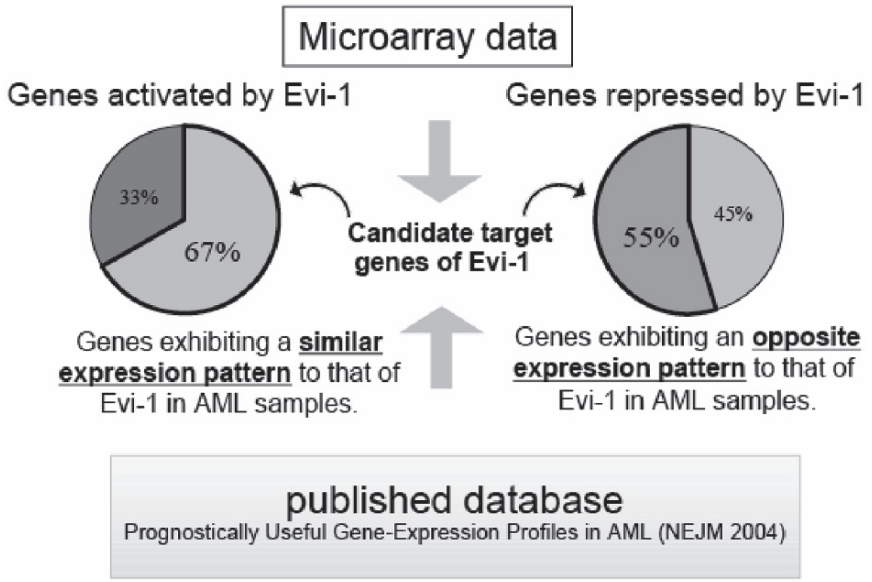

Fig. 3 Analysis of gene expression pattern using human acute myeloid leukemia (AML) samples. Gene expression pattern was compared with human AML samples. Candidate target genes of Evi-1 were extracted by investigating their expression pattern. Genes exhibiting similar expression pattern to that of Evi-1 are possibly activated by Evi-1. On the other hand, genes exhibiting the opposite expression pattern to that of Evi-1 are possibly repressed by Evi-1

Cre-ER (Fig. 2). This time, we compared gene expression patterns using human AML samples [14]. Candidate target genes of Evi-1 were extracted by investigating their expression pattern (Fig. 3). Genes exhibiting a similar expression pattern to that of Evi-1 are possibly activated by Evi-1. On the other hand, genes exhibiting the opposite expression pattern to that of Evi-1 may be repressed by Evi-1. From these two types of microarray analyses, we picked some candidates related to HSCs and platelet formation, because Evi-1 knockout mice exhibited decreased HSCs and platelet production. For example, GATA2 is an important gene that regulates HSCs, as previously reported that Evi-1 regulates fetal HSC proliferation through GATA2 expression [22]. It awaits further investigation whether these candidate target genes could be therapeutic targets in AML1 or Evi-1-related leukemia.

References

1. Druker BJ et al (2006) Five-year follow-up of patients receiving imatinib for chronic myeloid leukemia. N Engl J Med 35523:2408–2417
2. Hehlmann R et al (2007) Drug treatment is superior to allografting as first-line therapy in chronic myeloid leukemia. Blood 10911:4686–4692
3. Iwasaki H, Akashi K (2007) Hematopoietic developmental pathways: on cellular basis. Oncogene 2647:6687–6696

4. Lutterbach B, Hiebert SW (2000) Role of the transcription factor AML-1 in acute leukemia and hematopoietic differentiation. Gene (Amst) 2452:223–235
5. Okuda T et al (1996) AML1, the target of multiple chromosomal translocations in human leukemia, is essential for normal fetal liver hematopoiesis. Cell 842:321–330
6. Wang Q et al (1996) Disruption of the Cbfa2 gene causes necrosis and hemorrhaging in the central nervous system and blocks definitive hematopoiesis. Proc Natl Acad Sci U S A 938:3444–3449
7. Ichikawa M et al (2004) AML-1 is required for megakaryocytic maturation and lymphocytic differentiation, but not for maintenance of hematopoietic stem cells in adult hematopoiesis. Nat Med 103:299–304
8. Ichikawa M et al (2008) AML1/Runx1 negatively regulates quiescent hematopoietic stem cells in adult hematopoiesis. J Immunol 1807:4402–4408
9. Mucenski ML et al (1988) Identification of a common ecotropic viral integration site, Evi-1, in the DNA of AKXD murine myeloid tumors. Mol Cell Biol 81:301–308
10. Ogawa S et al (1996) Abnormal expression of Evi-1 gene in human leukemias. Hum Cell 94:323–332
11. Suzukawa K et al (1994) Identification of a breakpoint cluster region 3 of the ribophorin I gene at 3q21 associated with the transcriptional activation of the EVI1 gene in acute myelogenous leukemias with inv(3)(q21q26). Blood 848:2681–2688
12. Pintado T et al (1985) Clinical correlations of the 3q21;q26 cytogenetic anomaly. A leukemic or myelodysplastic syndrome with preserved or increased platelet production and lack of response to cytotoxic drug therapy. Cancer (Phila) 553:535–541
13. Barjesteh van Waalwijk van Doorn-Khosrovani S et al (2003) High EVI1 expression predicts poor survival in acute myeloid leukemia: a study of 319 de novo AML patients. Blood 1013:837–845
14. Valk PJ et al (2004) Prognostically useful gene-expression profiles in acute myeloid leukemia. N Engl J Med 35016:1617–1628
15. Kurokawa M et al (1998) The oncoprotein Evi-1 represses TGF-beta signalling by inhibiting Smad3. Nature (Lond) 3946688:92–96
16. Kurokawa M et al (2000) The evi-1 oncoprotein inhibits c-Jun N-terminal kinase and prevents stress-induced cell death. EMBO J 1912:2958–2968
17. Tanaka T et al (1994) Evi-1 raises AP-1 activity and stimulates c-fos promoter transactivation with dependence on the second zinc finger domain. J Biol Chem 26939:24020–24026
18. Morishita K et al (1992) Expression of the Evi-1 zinc finger gene in 32Dc13 myeloid cells blocks granulocytic differentiation in response to granulocyte colony-stimulating factor. Mol Cell Biol 121:183–189
19. Goyama S et al (in press) Cell Stem Cell
20. Mootha VK et al (2003) PGC-1alpha-responsive genes involved in oxidative phosphorylation are coordinately downregulated in human diabetes. Nat Genet 343:267–273
21. Subramanian A et al (2005) Gene set enrichment analysis: a knowledge-based approach for interpreting genome-wide expression profiles. Proc Natl Acad Sci U S A 10243: 15545–15550
22. Yuasa H et al (2005) Oncogenic transcription factor Evi1 regulates hematopoietic stem cell proliferation through GATA-2 expression. EMBO J 2411:1976–1987

Ultradian Oscillation Networks in Somite Segmentation and Other Biological Events

Yasutaka Niwa*, Hiromi Shimojo*, and Ryoichiro Kageyama

Introduction

When you observe the surrounding environment, you notice that it is composed of many events that are periodic, although they seem at first glance to be stable. Mesopotamian culture knew that the moon waxes and wanes in a monthly cycle and that the position of the sun changes with a period of a year. Our internal environment, which is kept relatively constant by forces that promote homeostasis, also consists of many cyclic events. We usually wake up in the morning and go to bed at night. When this rhythm is disturbed by jet lag, one feels uncomfortable for a few days. No one doubts that this circadian rhythm is one of the most famous and essential rhythms in our body. By contrast, developmental processes seem to be well organized and programmed in advance. However, from the perspective of a single cell, there is noise in both intracellular and intercellular environments, and there should be some mechanisms for being resistant to such noise.

Recently several groups showed that the expression of several genes is not just constant. Rather, expression oscillates, and does so robustly with a periodicity of less than 24 h. That is an ultradian rhythm, and it occurs in developmental tissues or cultured cells when you observe them not as a whole but at the single-cell level, or if you observe their synchronized behaviors [14,15,20,21,29,31]. Here we would like to review these ultradian rhythms and their biological meaning in a developmental and cellular context such as somitogenesis and neurogenesis in mice and several signaling pathways in cultured cells.

Y. Niwa, H. Shimojo, and R. Kageyama
Institute for Virus Research, Kyoto University, Kyoto, Japan and Japan Science and Technology Agency, CREST, Kyoto, Japan

*Equal contribution

S. Nakanishi et al. (eds.), *Systems Biology*,
DOI:10.1007/978-4-431-87704-2_21,

Somite Segmentation Clock

Somitogenesis

Considering the skeleton of the vertebrate body, one would conclude that our body consists of a beautiful segmental structure. Examples are the ribs and the vertebrae (Fig. 1a). These metameric structures are already defined at the developmental stage by their precursors, which are called somites (Fig. 1b). A somite is a transient structure and gives rise to skeletal muscle and dermis in addition to ribs and vertebrae. One new pair of somites is generated with a certain periodicity by being separated from the most anterior part of the presomitic mesoderm (PSM), which is located in the most caudal part of the embryo. This process is accompanied by morphological boundary formation, which is called segmentation. For mouse, chicken, and zebrafish, respectively, the segmentation period is 120, 90, and 30 min.

Discovery of Molecular Evidence

This extraordinarily periodical event has been the object of mathematical modeling for a long time [7]. However, its molecular mechanism has been examined for just a decade. The first molecular clue was the discovery of the oscillatory expression of *c-hairy1* in the chick PSM [25]. This gene expression pattern varied among littermates and moved from posterior to anterior with the same periodicity as the segmentation period [25]. This variation in gene expression pattern was thought to

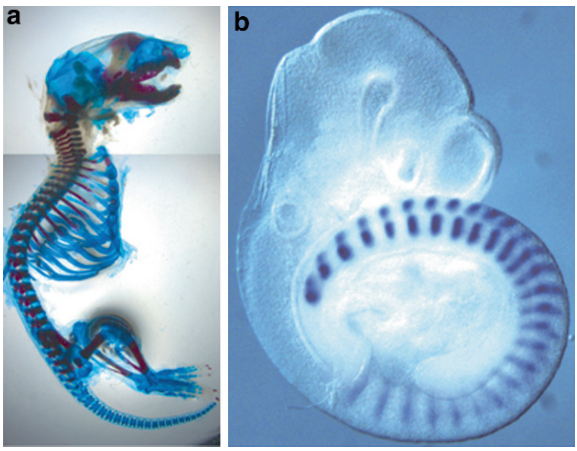

Fig. 1 Mouse skeleton and somites. **a** Skeletal staining of a mouse at P0. **b** Visualization of somites in a mouse embryo at E9.5 by in situ hybridization for *Uncx4.1*, which is a marker gene of the somite

be caused by the oscillatory changes in expression level in each cell. Subsequently, *c-hairy1* counterparts in mouse and zebrafish were found to show oscillatory expression patterns [16,26]. These molecules, or the system that generates these oscillatory expression patterns, were thought to account for the segmentation period, and they are now called a segmentation clock. Real-time imaging of the expression level of these genes recently showed that this oscillation continuously occurs at the single-cell level [21].

Molecular Mechanism of the Segmentation Clock

Negative Autoregulation of the Transcription Factor Hes7

In mouse somitogenesis, a gene for the basic helix-loop-helix (bHLH) transcription factor Hes7, a counterpart in mice of *c-hairy1*, has a critical role [5,6]. This gene is specifically expressed in the PSM in an oscillatory pattern [5]. This oscillatory expression is essential for proper somitogenesis because both persistent expression and loss of expression of Hes7 lead to irregular formation of ribs and vertebrae [5,13]. Furthermore, Hes7 represses its own promoter directly and is quickly removed by the ubiquitin-proteasome pathway [6]. This negative feedback loop targeting its own transcription seems to explain its oscillatory expression pattern in the PSM (Fig. 2).

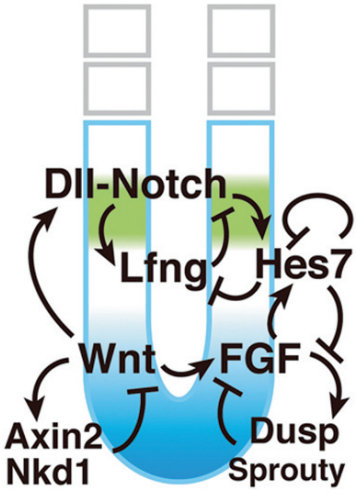

Fig. 2 Schematic representation of the mouse segmentation clock mechanism. Molecules in three major pathways and Hes7 interact with each other and form complex networks, which are thought to make the robustness of the mouse segmentation clock

Negative Feedback Loop in Notch Signaling

Another important molecule in mouse somitogenesis is Lunatic fringe (Lfng), which is a glycosyltransferase for Notch. As does Hes7, Lfng shows oscillatory expression in the PSM, and both persistent expression and loss of expression of Lfng result in the irregular formation of ribs and vertebrae [10,28,32]. Notch signaling induces Lfng expression, whereas Lfng inhibits Notch activity, forming another negative feedback loop (Fig. 2) [8]. This negative feedback loop generates oscillations in the activity of the Notch signaling pathway, and loss of Lfng leads to the failure of Notch signaling to oscillate [22], suggesting that Notch signaling plays an essential role in the segmentation clock. Furthermore, mutants with defects in somitogenesis in mice and zebrafish are mainly the result of the Notch pathway genes [16,26]. There is some controversy about the role of Notch signaling in the segmentation clock in mice, but there is no doubt that the Notch pathway is essential for proper somitogenesis.

Negative Feedback Loop in Wnt and FGF Signaling

In addition to Notch signaling, several molecules of Wnt and fibroblast growth factor (FGF) signaling also show oscillatory expression patterns in the PSM [9]. Among them, Axin2, which is an inhibitor of Wnt signaling, was first reported to oscillate out of phase from Lfng (Fig. 2) [3]. Recent genome-wide studies searching for oscillatory molecules in the PSM showed that many genes in Wnt and FGF signaling, as well as Notch signaling, show oscillatory expression in the PSM [9]. These results suggest that not only Hes7 but also Notch, Wnt, and FGF signaling have their own feedback loops, and that these feedback loops couple with each other and make the segmentation clock in the PSM robust.

Interaction Between Feedback Loops

Hes7 represses not only itself but also Lfng, which is thought to be an inhibitor of Notch signaling [5,6]. Hes7 also represses Dusp4, an inhibitor of FGF/MAPK signaling, which oscillates in the posterior PSM (Fig. 2) [23]. Periodic repression by Hes7 is essential for the oscillatory expression of Lfng and Dusp4 [23], which are thought to be important for their own negative feedback signaling loops. So, it is likely that Hes7 is a core of the segmentation clock and regulates oscillations in both Notch and FGF signaling pathways [23]. Actually, a recent report shows that Hes7 oscillation still remains even in the absence of Notch signaling [23]. On the other hand, the amplitude and anterior propagation of Hes7 oscillations are affected without Notch signaling [23]. Because dissociated, cultured PSM cells quickly lose their stable 2-h cycle oscillations, it is possible that, in mice, Notch signaling also

regulates the segmentation clock via intercellular synchronization of the unstable oscillators in different cells, as was first proposed in zebrafish [17,18,21].

Oscillations in Neural Progenitors

Neural Development and Notch Signaling

Neural development proceeds by strictly regulated steps: from a cell proliferation phase, to a neurogenic phase, and then to a gliogenic phase (Fig. 3). During these processes, neural progenitors change their competency, giving rise to distinct types of cells [1,12]; this means that maintenance of neural progenitors until later stages of development is essential to generate cells both in correct number and with full cell-type diversity. Notch signaling plays an important role in maintenance of neural progenitors [2,11]. When Notch ligands such as Delta-like1 (Dll1) expressed in neighboring cells bind to Notch receptors, the intracellular domain of Notch (act-Notch) is cleaved and released from the membrane and goes to the nucleus (Fig. 4).

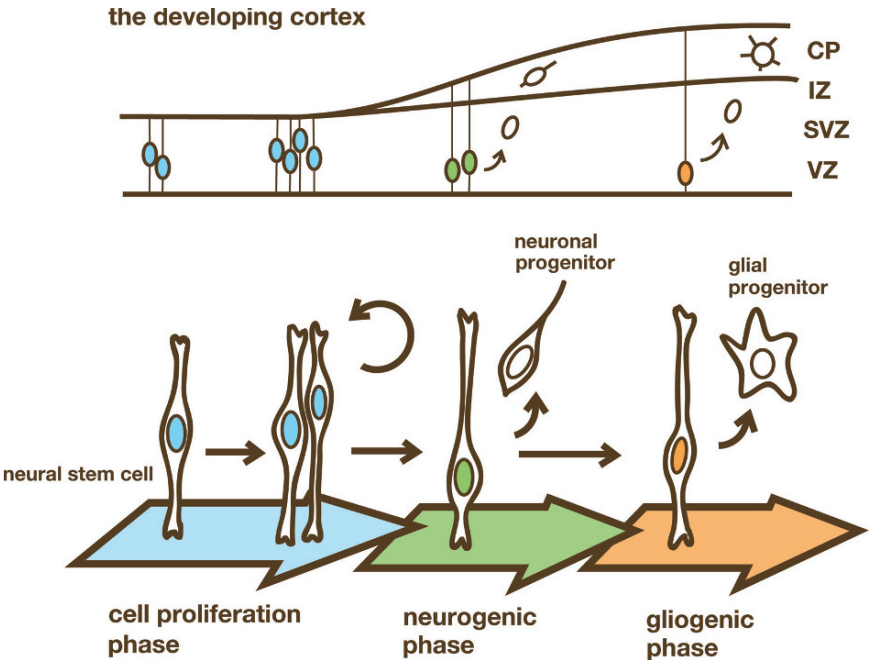

Fig. 3 Neural stem cells change their competency during neural development. Neural development proceeds according to the following steps: cell proliferation phase, neurogenic phase, and gliogenic phase. During these steps, neural stem cells change their competency and give rise to different cell types such as neuronal progenitors and glial progenitors. *VZ*, ventricular zone; *SVZ*, subventricular zone; *IZ*, intermediate zone; *CP*, cortical plate

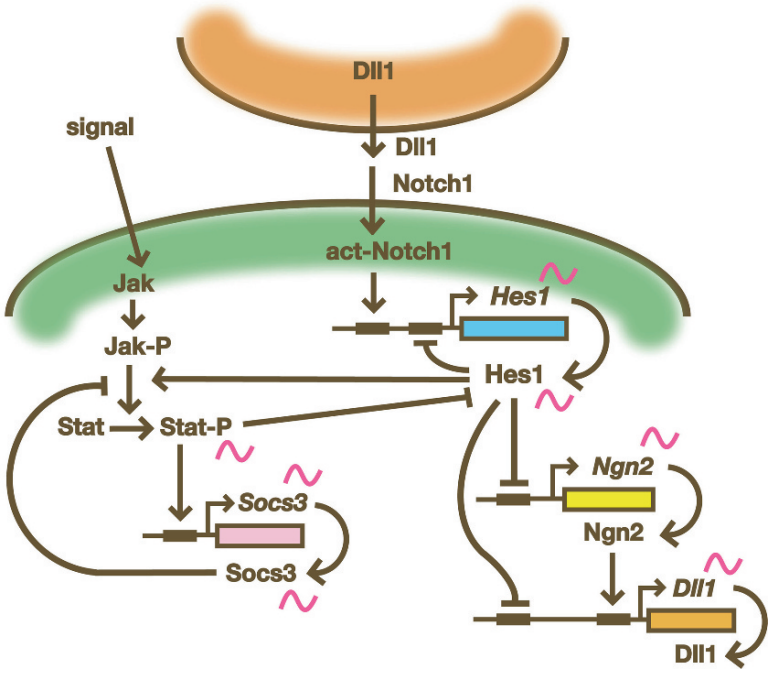

Fig. 4 Ultradian oscillation networks in neural progenitors. In neural progenitors, the expressions of Hes1, Ngn2, and Dll1 oscillate, thereby inducing mutual activation of Notch signaling in neighboring cells and maintaining Hes1 expression and the undifferentiated states. In addition to Notch signaling, Jak-Stat signaling molecules oscillate. Oscillations in Notch signaling and Jak-Stat signaling regulate each other

act-Notch forms a complex with RBP-J, and this complex activates expression of the bHLH transcriptional repressors Hes1 and Hes5 [24]. Hes genes downregulate the expression of proneural genes such as Neurogenin2 (Ngn2) and inhibit neuronal differentiation [4,27,19]. We now focus on oscillations in Notch signaling to better understand neural development.

Hes1 Oscillates in Dividing Neural Progenitors

In cultured cells, Hes1 expression oscillates with a period of about 2 h [14,21]. This oscillation is induced by serum stimulation or Notch activation, and is regulated by negative feedback: Hes1 can repress its own expression by directly binding to its own promoter [30], followed by rapid disappearance of both Hes1 mRNA and Hes1 protein, because they are extremely unstable, and then by the next round of expression. In this way, Hes1 autonomously displays an oscillatory expression mode.

In the developing central nervous system, Hes1 is expressed in the ventricular zone, a proliferative region, and the expression of Hes1 shows various levels in each dividing progenitor cell, suggesting the possibility that Hes1 expression oscillates in dividing neural progenitors. Using a real-time imaging method, Hes1 expression was found to be dynamically changing at the single-cell level (Fig. 4) [29].

Oscillations of Notch Signaling Regulate Maintenance of Neural Progenitors

The Hes1 target genes Ngn2 and Dll1 are expressed in dividing neural progenitors and show an inverse correlation with Hes1 expression, suggesting that these genes oscillate in neural progenitor cells. Interestingly, the expression of Ngn2 and Dll1 is found to be dynamically changing in dividing neural progenitors at the single-cell level (Fig. 4). Furthermore, inhibition of Notch signaling, a condition known to induce neuronal differentiation, leads to downregulation of Hes1 and sustained upregulation of Ngn2 and Dll1. These findings suggest that Hes1 oscillation leads to Ngn2 and Dll1 oscillations in dividing neural progenitors by periodically repressing their expression (Fig. 4). Oscillation of the expression of the Notch ligand Dll1 also activates Notch signaling in neighboring neural progenitors, thereby maintaining Hes1 oscillations and the undifferentiated state of these cells. As neural development proceeds, the expression of Hes1 is downregulated, whereas Ngn2 and Dll1 expressions are upregulated in a sustained manner, leading to neuronal differentiation. Ngn2 oscillation is apparently not sufficient, but sustained upregulation is required for neuronal differentiation. It is likely that Ngn2 oscillation induces expression of subsets of downstream genes such as Dll1 and is advantageous for maintenance of neural progenitors.

Jak-Stat Signaling Is Required for Hes1 Oscillation

In addition to Notch signaling, the expression of molecules of Jak-Stat and Smad signaling pathways also oscillates in response to serum in cultured fibroblast cells [31]. Furthermore, the stability of Hes1 protein is regulated by Stat signaling: Hes1 protein is stabilized in the absence of Stat signaling, whereas it is destabilized by constitutive activation of Stat signaling. Both sustained activation and inactivation of Stat signaling abolish Hes1 oscillation, suggesting that oscillations in Stat signaling regulate Hes1 oscillation by controlling the stability of Hes1 protein (Fig. 4). Moreover, loss of Hes1 oscillation leads to cell-cycle arrest, suggesting that the expression mode of signaling pathway molecules affect the downstream cellular event.

In the developing central nervous system, Hes1 oscillation disappears because of inhibition of Jak-Stat signaling, suggesting that Jak-Stat signaling also regulates Hes1 oscillation in neural progenitors.

Conclusions

A growing number of genes in various tissues and cells have been reported to be expressed cyclically with periods shorter than 24 h. These ultradian oscillation networks play an important role in biological events. During somitogenesis, the ultradian oscillation networks function as a segmentation clock, one of the biological clocks that regulate the timing of developmental events. Nevertheless, there are issues that remain to be determined. One of these questions is this: What is the master factor, acting as a pacemaker of the segmentation clock?

On the other hand, in non-PSM cells, there are few reports that discuss biological events, such as neural development, from the point of view of different gene expression modes. However, a growing number of oscillating genes have been reported. For instance, expression of NF-κB and p53 also oscillates [20,15]. These results suggest that oscillatory expression is more general and plays a more important role in cellular events than was previously thought, although the full significance of these systems remains unclear. The study of these ultradian oscillations in non-PSM cells is just getting started.

Many issues remain regarding ultradian rhythms, such as their molecular mechanisms, crosstalk of various signaling pathways, and downstream biological events. By elucidating the whole picture of oscillatory networks, we could characterize the sophisticated systems that regulate molecular events, cellular events, and biological events in more detail.

References

1. Alvarez-Buylla A, Garcia-Verdugo JM, Tramontin AD (2001) A unified hypothesis on the lineage of neural stem cells. Nat Rev Neurosci 2:287–293
2. Artavanis-Tsakonas S, Rand MD, Lake RJ (1999) Notch signaling: cell fate control and signal integration in development. Science 284:770–776
3. Aulehla A, Wehrle C, Brand-Saberi B, Kemler R, Gossler A, Kanzler B, Herrmann BG (2003) *Wnt3a* plays a major role in the segmentation clock controlling somitogenesis. Dev Cell 4:395–406
4. Bertrand N, Castro DS, Guillemot F (2002) Proneural genes and the specification of neural cell types. Nat Rev Neurosci 3:517–530
5. Bessho Y, Miyoshi G, Sakata R, Kageyama R (2001) Dynamic expression and essential functions of *Hes7* in somite segmentation. Genes Dev 15:2642–2647
6. Bessho Y, Hirata H, Masamizu Y, Kageyama R (2003) Periodic repression by the bHLH factor Hes7 is an essential mechanism for the somite segmentation clock. Genes Dev 17:1451–1456
7. Cooke J, Zeeman EC (1976) A clock and wavefront model for control of the number of repeated structures during animal morphogenesis. J Theor Biol 58:455–476
8. Dale JK, Maroto M, Dequeant ML, Malapert P, McGrew M, Pourquié O (2003) Periodic Notch inhibition by Lunatic Fringe underlies the chick segmentation clock. Nature (Lond) 421:275–278
9. Dequéant M-L, Glynn E, Gaudenz K, Wahl M, Chen J, Mushegian A, Pourquié O (2006) A complex oscillating network of signaling genes underlies the mouse segmentation clock. Science 314:1595–1598

10. Evrard YA, Lun Y, Aulehla A, Gan L, Johnson RL (1998) *lunatic fringe* is an essential mediator of somite segmentation and patterning. Nature (Lond) 394:377–381
11. Gaiano N, Fishell G (2002) The role of Notch in promoting glial and neural stem cell fates. Annu Rev Neurosci 25:471–490
12. Götz M, Huttner WB (2005) The cell biology of neurogenesis. Nat Rev Mol Cell Biol 6:777–788
13. Hirata H, Bessho Y, Kokubu H, Masamizu Y, Yamada S, Lewis J, Kageyama R (2004) Instability of Hes7 protein is crucial for the somite segmentation clock. Nat Genet 36:750–754
14. Hirata H, Yoshiura S, Ohtsuka T, Bessho Y, Harada T, Yoshikawa K, Kageyama R (2002) Oscillatory expression of the bHLH factor Hes1 regulated by a negative feedback loop. Science 298:840–843
15. Hoffmann A, Levchenko A, Scott ML, Baltimore D (2002) The IκB-NF-κB signaling module: temporal control and selective gene activation. Science 298:1241–1245
16. Holley SA (2007) The genetics and embryology of zebrafish metamerism. Dev Dyn 236:1422–1449
17. Horikawa K, Ishimatsu K, Yoshimoto E, Kondo S, Takeda H (2006) Noise-resistant and synchronized oscillation of the segmentation clock. Nature (Lond) 441:719–723
18. Jiang Y-J, Aerne BL, Smithers L, Haddon C, Ish-Horowicz D, Lewis J (2000) Notch signaling and the synchronization of the somite segmentation clock. Nature (Lond) 408:475–479
19. Kageyama R, Ohtsuka T, Kobayashi T (2007) The Hes gene family: repressors and oscillators that orchestrate embryogenesis. Development (Camb) 134:1243–1251
20. Lev Bar-Or R, Maya R, Segel LA, Alon U, Levine AJ, Oren M (2000) Generation of oscillations by the p53-Mdm2 feedback loop: a theoretical and experimental study. Proc Natl Acad Sci U S A 97:11250–11255
21. Masamizu Y, Ohtsuka T, Takashima Y, Nagahara H, Takenaka Y, Yoshikawa K, Okamura H, Kageyama R (2006) Real-time imaging of the somite segmentation clock: revelation of unstable oscillators in the individual presomitic mesoderm cells. Proc Natl Acad Sci U S A 103:1313–1318
22. Morimoto M, Takahashi Y, Endo M, Saga Y (2005) The Mesp2 transcription factor establishes segmental borders by suppressing Notch activity. Nature (Lond) 435:354–359
23. Niwa Y, Masamizu Y, Tianxiao L, Nakayama R, Deng Chu-Xia, Kageyama R (2007) The initiation and propagation of Hes7 oscillation are cooperatively regulated by Fgf and notch signaling in the somite segmentation clock. Dev Cell 13:298–304
24. Ohtsuka T, Ishibashi M, Gradwohl G, Nakanishi S, Guillemot F, Kageyama R (1999) *Hes1* and *Hes5* as Notch effectors in mammalian neuronal differentiation. EMBO J 18:2196–2207
25. Palmeirim I, Henrique D, Ish-Horowicz D, Pourquié O (1997) Avian hairy gene expression identifies a molecular clock linked to vertebrate segmentation and somitogenesis. Cell 91(5):639–648
26. Rida PC, Le Minh N, Jiang YJ (2004) A Notch feeling of somite segmentation and beyond. Dev Biol 265:2–22
27. Ross SE, Greenberg ME, Stiles CD (2003) Basic helix-loop-helix factors in cortical development. Neuron 39:13–25
28. Serth K, Schuster-Gossler K, Cordes R, Gossler A (2003) Transcriptional oscillation of lunatic fringe is essential for somitogenesis. Genes Dev 17:912–925
29. Shimojo H, Ohtsuka T, Kageyama R (2008) Oscillations in Notch signaling regulate maintenance of neural progenitors. Neuron 58:52–64
30. Takebayashi K, Sasai Y, Sakai Y, Watanabe T, Nakanishi S, Kageyama R (1994) Structure, chromosomal locus, and promoter analysis of the gene encoding the mouse helix-loop-helix factor HES-1, Negative autoregulation through the multiple N box elements. J Biol Chem 269:5150–5156
31. Yoshiura S, Ohtsuka T, Takenaka Y, Nagahara H, Yoshikawa K, Kageyama R (2007) Ultradian oscillations of Stat, Smad, and Hes1 expression in response to serum. Proc Natl Acad Sci U S A 104:11292–11297
32. Zhang N, Gridley T (1998) Defects in somite formation in lunatic fringe-deficient mice. Nature (Lond) 394:374–377

The Cellular Basis of *Dictyostelium* Morphogenesis

Cornelis J. Weijer

Introduction

One of the central aims of the study of development is to understand how distinct cellular behaviours, for example, division, differentiation, apoptosis, and movement, are coordinated in space and in time to result in reproducible pattern formation and morphogenesis. Coordination of these cellular behaviours requires extensive communication between cells of different types and between the cells and their environment. The social amoeba *Dictyostelium discoideum,* a simple genetically tractable organism situated at the threshold of single and multicellular organisms in the evolutionary tree of life, is well suited for the study of these interactions because its genome has been sequenced and it is amenable to experimental manipulation through targeted gene disruption and replacement (Kreppel, Fey et al. 2004; Eichinger, Pachebat et al. 2005). *Dictyostelium* cells normally live as single cells in the leaf litter of the soil where they feed on bacteria and divide by binary fission. Under starvation conditions, up to several hundred thousand cells aggregate chemotactically to form a multicellular structure the slug, that directed by light and temperature gradients migrates to the surface of the soil to form a fruiting body. The fruiting body is composed of a stalk supporting a mass of spores. The spores are a dormant stage which after dispersal may germinate to release amoebae, thus closing the life cycle (Fig. 1). We describe here key aspects of the signalling mechanisms coordinating cellular behaviours responsible for pattern formation and morphogenesis.

The Control of Cell Movement During Development

Because *Dictyostelium* development takes place in the absence of food under starvation conditions, only limited cell divisions occur during multicellular development. Morphogenesis therefore primarily results from the movement of

C.J. Weijer
Division of Cell and Developmental Biology, School of Life Sciences,
University of Dundee, Wellcome Trust Biocentre, Dundee DD1 5EH, UK

S. Nakanishi et al. (eds.), *Systems Biology*,
DOI:10.1007/978-4-431-87704-2_22,

Fig. 1 Colonie of Dictyostelium cells on a bacterial lawn, showing a cross section through the life cycle of *Dictyostelium*. A single amoeba was inoculated in a lawn of bacteria. The amoebae eat the bacteria and form a plaque. At the edge of the plaque (*bottom left*), the amoebae are feeding; behind the feeding front the cells start to starve and form aggregation streams. Once the cells have aggregated, they form tipped mounds that transform into standing slugs. The slugs topple over and migrate away, and after a variable period of migration the slugs stop moving and transform into fruiting bodies. The fruiting body stands on the substrate with a basal disk that anchors a 2- to 3-mm-long stalk, which supports a spore head containing hundreds of thousands of spores; 80% of the population of cells that aggregate form spores. Under suitable conditions spores disperse and germinate to form new colonies, while the stalk cells die and do not propagate. The whole cycle from the initiation of starvation to fruiting body formation takes 24 h at ~20°C

individual differentiating cells into a relatively complex structure, the proportions of which are essentially independent of how many cells exactly aggregate. Key questions are which signals guide the movement behaviour of thousands of cells during development, which signals control differentiation, and how do movement and differentiation interact?

Aggregation

Starvation induces changes in the gene expression programme that results in the cells acquiring the ability to produce and secrete and degrade cyclic adenosine monophosphate (cAMP) (Saran, Meima et al. 2002; Iranfar, Fuller et al. 2003). Through the expression of the cAMP receptor, the cells also acquire the ability to respond chemotactically to cAMP gradients. It has emerged that chemotaxis results from the polarisation of the cytoskeletal dynamics persistently along the cAMP gradient. Unstimulated amoeboid cells are continuously changing shape by extension and retraction of pseudopods in all directions, resulting in a random walk (Soll, Wessels et al. 2003; Sasaki, Janetopoulos et al. 2007). In the presence of an external

gradient of a chemoattractant such as cAMP the cells persistently extend successive pseudopods in the direction of rising cAMP concentration, while at the same time suppressing the extension of lateral pseudopods, which results in efficient movement up the gradient (Andrew and Insall 2007). Much current research is directed towards understanding how cells detect cAMP gradients, polarise their cytoskeleton, and move in response to these cAMP gradients (Chen, Iijima et al. 2007; Franca-Koh, Kamimura et al. 2007; Insall and Andrew 2007). Cells move by extending pseudopods at their leading edge, a process driven by actin polymerisation. For extension to occur, the assembly of the myosin thick filaments in the cortex at the site of extension needs to be inhibited, which involves phosphorylation of the tail of the myosin heavy chain on several threonine residues (Yumura, Yoshida et al. 2005; Bosgraaf and van Haastert 2006; Goldberg, Wolpin et al. 2006). Cells also need to pull up their back end and suppress the extension of lateral pseudopods, which involves, besides the well-characterised role of myosin II, also the action of members of the myosin I family and is dependent on internal cAMP levels (Falk, Wessels et al. 2003; Zhang, Heid et al. 2003). To move forward the cells must gain traction form the substrate on which they are moving, which involves the formation of multiple transient (10–20 s) actin contact sites that have been shown to transduce traction forces to the substrate (Bretschneider, Diez et al. 2004; Uchida and Yumura 2004). It appears that cells may undergo alternating phases of actin-driven extension at the front and myosin-driven contraction at the back (Iwadate and Yumura 2008). Much work is directed towards the investigation of the molecular mechanisms that result in signal detection, cell polarisation and its translation in directed movement. This work has been extensively reviewed elsewhere recently and is not covered here in detail (Willard and Devreotes 2006; Janetopoulos and Firtel 2008).

Aggregation is caused by periodic cAMP synthesis and secretion by cells in the aggregation centre. Binding of cAMP to the serpentine transmembrane cAMP receptor results in stimulation of the signal transduction cascade that leads to the activation of an adenylylcyclase (ACA), which within tens of seconds produces cAMP, part of which is secreted to the outside (Fig. 2). The secreted cAMP binds to the receptor and thus is part of an autocatalytic feedback loop, resulting in a rapid increase of cAMP production. However, stimulation of the receptor also activates an adaptation process that with a small time delay results in the inhibition of adenylyl cyclase activation and a cessation of cAMP production. As cAMP diffuses away into the extracellular medium and is also degraded by secreted cAMP phosphodiesterases, this results in a drop in cAMP levels, which in turn results in deadaptation of the cells (Fig. 2). Both excitation and adaptation depend on the receptor-dependent activation of a heterotrimeric G protein, resulting in activation of Ras, which in turn activates phosphatidyl inositide 3 kinase (PI3 kinase), which phosphorylates phosphatidylinositide(4,5)phosphate (PIP2) to phosphatidyl-(3,4,5)-phosphate (PIP3). PIP3 then activates many downstream pathways, leading to chemotaxis and adenylcyclase activation (Mahadeo and Parent 2006). The activation of adenylcyclase is critically dependent on the PIP3-dependent binding of CRAC (cytosolic regulator of adenylyl cyclase) to the membrane where it is

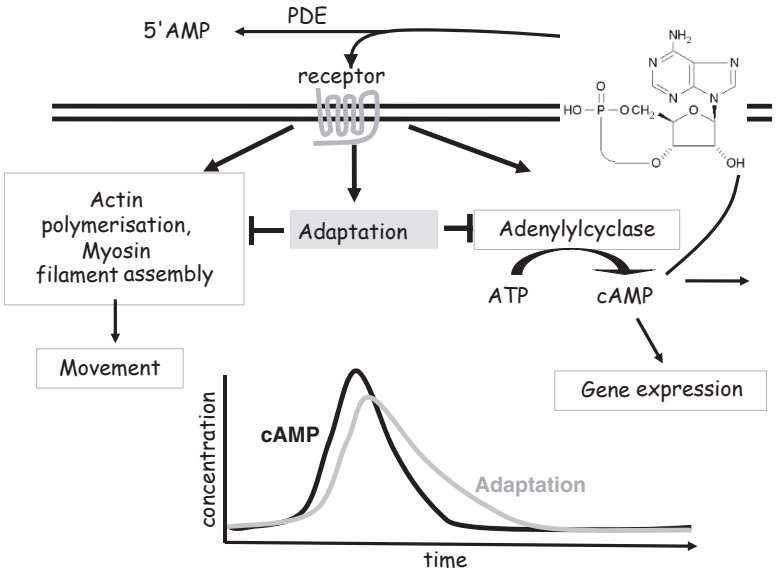

Fig. 2 Cyclic adenosine monophosphate (cAMP) signalling activates cAMP relay and chemotaxis. Extracellular cAMP binds to a transmembrane serpentine cAMP receptor and activates two distinct signal transduction pathways. One pathway leads to organisation of the actin myosin cytoskeleton and chemotaxis. The second pathway results in activation of the aggregation stage adenylylcyclase (ACA). Activation of ACA results in cAMP production, part of which is secreted and binds to the receptor to form a positive feedback loop, where a little extracellular cAMP results in the production of more. Binding of cAMP to the receptor also activates an adaptation process that inhibits both ACA activation and the chemotactic signal transduction pathway. Once adaptation reaches a full response, the production of cAMP ceases and cAMP secretion stops. As cAMP is continuously degraded by an extracellular cAMP phosphodiesterase, extracellular cAMP levels fall, which allows the cells to de-adapt and start a new cAMP response

activated, which is required for adenylyl cyclase activation and chemotaxis (Comer, Lippincott et al. 2005).

Detection and amplification of this signal by surrounding cells coupled with desensitisation of the cAMP-producing cells results in the propagation of waves of cAMP away from the aggregation centre (Fig. 3). Cells detect the rising phase of the wave and move in the direction of increasing cAMP concentration; once the waves passes, the cells are adapted and are insensitive to the falling phase of the wave and therefore do not turn around and chase the wave after it has passed. These cAMP waves therefore guide the cells towards the aggregation centre, where they accumulate into a three-dimensional aggregate, the mound (Dormann and Weijer 2001; Dormann and Weijer 2003). During the synchronised chemotactic movement phase cells elongate, while during the falling phase of the waves the cells are amoeboid in shape. The large-scale spatiotemporal patterns of cells behaviour can be visualised as changes in light scattering since moving elongated cells scatter more light (Fig. 3A) These waves can thus successfully be used to visualize and measure the spatiotemporal dynamics of wave propagation at all stages of development (Fig. 3B,C,D).

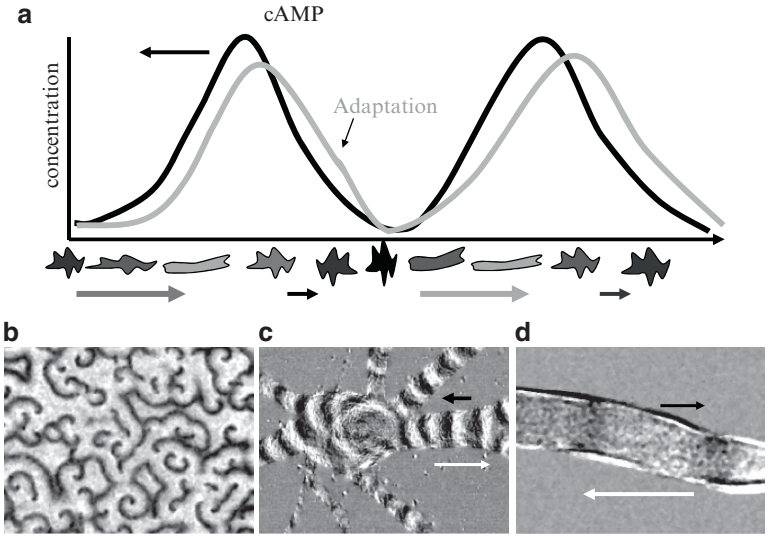

Fig. 3 Optical density waves reflect cAMP waves at different stages of development. **a** Aggregation centres initiate cAMP waves. These propagate from the centre outward (*black arrow*). Cells detect the rising phase of the cAMP wave and move in the direction of higher cAMP concentrations (*bottom figures and arrows*; colour of cells and arrows indicates degree of light scattering). During their chemotactic movement the cells elongate, and this changes their light-scattering properties. When during the rising phase of the wave many cells move in synchrony, this results in increased light-scattering waves, reflecting the rising phase of the cAMP signal. **b** Spiral optical density waves during the early aggregation phase, when the cells are still in a monolayer on agar. **c** Optical density waves in a streaming aggregate. In the body of the aggregate, multi-armed spiral waves rotate counterclockwise, throwing off individual wavefronts that propagate down the streams to the periphery of the aggregate. *White arrow* indicates the direction of wave propagation; *black arrow* indicates the direction of cell movement. **d** A slug migrating to the *right*, showing two dark optical density waves that travel from right to left (*white arrow*); cells move to the right following the tip (*black arrow*)

Recently, this method has been used to perform a high-throughput analysis of cAMP signalling mutants (Sawai, Guan et al. 2007). Initially the cells move towards the aggregation centre as individuals, but after 10–20 waves have passed they form bifurcating aggregation streams in which the cells make head-to-tail contacts via a calcium-independent adhesion molecule, contact site A, and side-to-side contacts via calcium-dependent cadherins (Wong, Yang et al. 2002; Harris, Ravandi et al. 2003). Stream formation is dependent on the localisation of ACA in the rear of the aggregating cells, resulting in polarised cAMP secretion from the back of the cells (Kriebel, Barr et al. 2003). cAMP wave propagation can be observed at the individual cell level by following the localised translocation of PIP3 at the leading edge of the cell (Dormann, Weijer et al. 2002; Dormann, Weijer et al. 2004). The number of cells in aggregation streams appears to be controlled by the local concentration of a secreted extracellular high molecular weight protein complex, a counting factor, which through modulation of movement and adhesion may control the numbers of cells that stably migrate in an aggregation stream (Jang and Gomer 2008)

Mound and Slug Formation

After the cells have aggregated, they form a hemispherical structure—the mound. Mounds are characterised by rotating waves of cAMP that direct the counterrotational periodic movement of the cells. Cells start to differentiate into prespore and prestalk cells during aggregation, based on physiological biases such as nutritional state and cell-cycle position at the time of starvation already present in the population before aggregation (Araki, Abe et al. 1997). As a result, there is little correlation between the time of arrival in the mound and differentiation fate. Therefore, initially the prestalk and prespore cell types display a salt-and-pepper distribution in the mound (see Fig. 5A, later in this chapter). A subpopulation of prestalk cells sort out to form the tip, and the slug tip guides the movement of all other cells, thus acting as an organiser (Weijer 2004). Use of a temperature-sensitive ACA mutant has shown that ACA activity is required for cells to be able to sort to the tip (Patel, Guo et al. 2000).The tip action as an organiser can be mimicked by the periodic injection of cAMP pulses of the right frequency and duration (Dormann and Weijer 2001), suggesting that the tip is a source of periodic cAMP waves, in agreement with the fact that prestalk cells express ACA and the extracellular cAMP phosphodiesterase pdeA (Verkerke-van Wijk, Fukuzawa et al. 2001; Weening, Wijk et al. 2003). It is not yet known which signals control tip cell fate (see below), but it is becoming clear that to proceed from the aggregate to the mound stage cell–cell adhesion and or contact start to play an important role. Mutants defective in the putative single-pass transmembrane contact molecules lagC, lagD cannot proceed beyond the aggregation stage and are defective in tip formation (Kibler, Svetz et al. 2003). There is evidence that *Dictyostelium* may possess several integrin-like adhesion molecules (Cornillon, Froquet et al. 2008), and it has been known that mutants in talin, paxillin, and a lim domain protein, which are thought to couple adhesion molecules to the actin cytoskeleton, are all defective in cell sorting (Chien, Chung et al. 2000; Tsujioka, Yoshida et al. 2004; Bukharova, Weijer et al. 2005). Sorting of prestalk cells towards the tip requires the invasive movement of prestalk cells through a tightly packed mass of other. Myosin II is absolutely required for progression beyond the mound stage, and it is known that prestalk cells express higher levels of myosin II (Eliott, Vardy et al. 1991; Springer, Patterson et al. 1994). For prestalk cells to sort, they need to assemble more myosin thick filaments than prespore cells (Dormann and Weijer, unpublished observations). Together all these observations suggest that tip formation is the result of cellular properties specific to tip-forming cells. Tip cells express high levels of ACA, resulting in increased signalling ability, therefore allowing them to set up a new independent signalling centre that can outcompete the aggregation centre organising the mound. They also assemble more myosin II thick filaments, critical to their ability to produce more force in response to a cAMP signal. This latter property allows them to push other cells aside and reaggregate within the mound to form the tip (Dormann and Weijer, in preparation).

In slugs, optical density waves can be seen to propagate from the middle of the prestalk zone to the back, reflecting the periodic movement of the cells forward

(Fig. 3). These optical waves are strictly dependent on the tip. Cells in the tip often rotate perpendicular to the direction of slug migration, especially when it is lifted from the substrate. In the back of the slug the cells move periodically forward, and all cells move on average with slug speed. It has been shown that the assumption of cAMP wave propagation and chemotaxis in response to these waves is, in principle, sufficient to explain morphogenesis from a single cell via aggregation and stream and mound formation to cell sorting and slug formation. The interactions between cell signalling and cell movement can be described by relatively simple mathematical models in a robust way, and it would appear that these process are sufficient to explain *Dictyostelium* morphogenesis (Fig. 4) (Vasiev and Weijer 2003; Umeda and Inouye 2004). However, the situation is almost certainly more

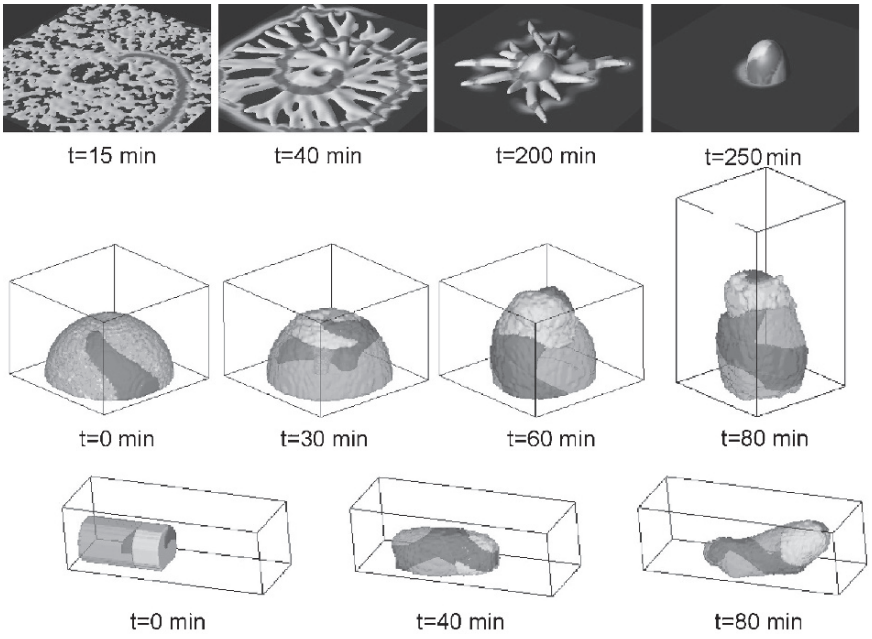

Fig. 4 Model calculation of wave propagation and cell movement from aggregation to slug migration using a hydrodynamic model. The *top row* depicts the aggregation up to the mound stage. The first image starts with the randomly distributed cells (*grey*), which are organised by a spiral wave of cAMP (*dark grey*). They form aggregation streams and finally a hemispherical mound (Vasiev, Siegert et al. 1997). The *middle row* shows cell sorting and the formation of a slug. The mound consists of two cells types: 20% light grey prestalk cells and 80% dark grey prespore cells. They are initially randomly mixed. The cAMP waves (*darkest grey*) organises the movement of the cells. In the model the assumption is that the prestalk cells are more excitable and develop more movement force in response to a cAMP wave. As a result of this, they move towards the centre of the mound and up to form the tip. The separation of the cells feeds back on the signal propagation, resulting in the formation of a twisted scroll wave; this leads to an intercalation of the cells and an upward extension of the slug (Vasiev and Weijer 1999). The *bottom row* shows that a slug organised by a scroll wave can move (Vasiev and Weijer 2003)

complex since strains lacking the aggregation-stage adenylylcyclase can still form slugs when they overexpress the catalytic subunit of protein kinase A, suggesting either that there either exists a ACA-independent mechanism to produce periodic cAMP signals, for instance, involving cAMP generation by other adenylylcyclases, ACB or ACG, and the recently discovered cAMP-stimulated cAMP phosphodiesterase (Meima, Weening et al. 2003), or that there exists altogether different mechanisms that can control cell movement such as contact following (Umeda and Inouye 2002). The latter mechanism does not, however, explain which signals direct the movement of the cells in the tip.

Differentiation

It is well established that *Dictyostelium* slugs can form as few as a few hundred cells and can contain up to several million cells, while the proportions between spore and stalk cells remain relatively constant (Rafols, Amagai et al. 2001; Maruo, Sakamoto et al. 2004). A major goal is to understand the relationship between cell movement and the signals that control differentiation. These signals must be able to maintain the correct proportioning of the prespore and prestalk cell types in an environment of extensive cell movement and changes in shape of the slug. In the slug the different cell types are arranged in a simple axial pattern: pstA cells in the tip, a band of pstO cells that form the upper and part of the lower cup of the fruiting body, prespore cells, precursors for spores, which are intermingled anterior-like cells, and rearguard cell precursors to the lower cup and basal disk in the back of the slug (Fig. 5A) (Williams 2006). It seems evident that this requires adaptive signalling dynamics, but the signals and the details of their regulation are not yet understood in detail (Fig. 5B). cAMP pulses control the expression of aggregation-stage genes necessary for cAMP relay and cell–cell contact, and cAMP is necessary for prespore gene expression in later development (Saran, Meima et al. 2002; Iranfar, Fuller et al. 2003). Prespore cells in turn produce DIF (differentiation-inducing factor, a small cholinated hexaphenone), which controls the differentiation of pstO cells (Kay and Thompson 2001; Maeda, Sakamoto et al. 2003; Thompson, Fu et al. 2004; Saito, Taylor et al. 2006). DIF spreads by simple diffusion from the prespore zone in adjacent regions where it controls the differentiation of prestalk O cells and possibly rear guard cells (Fukuzawa, Abe et al. 2003). Cells in the pstA zone express ACA, and studies investigating the cyclic AMP-dependent nuclear translocation of the transcription factor statA have shown that cAMP levels are high in the tip, while cAMP is lower elsewhere in the slug (Dormann, Abe et al. 2001; Verkerke-van Wijk, Fukuzawa et al. 2001), compatible with the idea that all cells in the tip relay the cAMP signal and only the anterior-like cells in the rest of the slug do so. However, the signals that control the expression of functionally important tip-enriched molecules such as ACA and myosin II still have to be identified. It also remains to be seen how accurate cell-type proportioning is achieved in slugs despite their vastly different sizes and dynamic changes in shape.

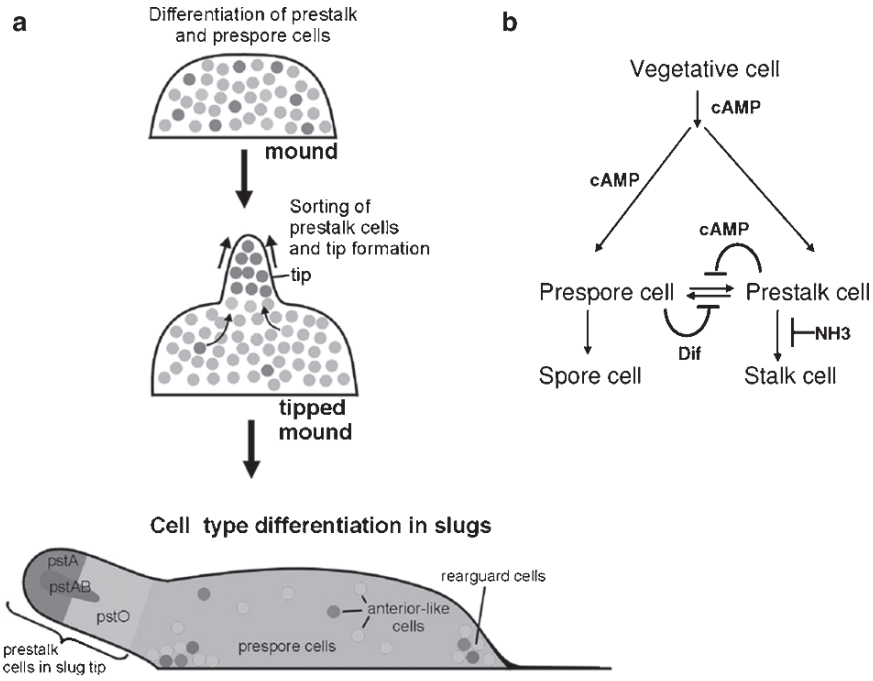

Fig. 5 Cell types and cell-type proportioning in *Dictyostelium*. **a** During aggregation, cells start to differentiate into prestalk cells (*dark grey*) and prespore cells (*light grey*). Because cells arrive in the mound in random order, they form a salt-and-pepper distribution of cell types. After a variable time of movement, the prestalk cells reaggregate to form the tip and the initial prestalk zone. The tip guides the movement of all the other cells, and the structure elongates to from a slug that topples over and migrates away. In the slugs, there are at least four cell types. The tip is made up of PstA (*dark grey*) cells, followed by a cohort of PstO (*light grey*) cells, which together form the prestalk zone. The prestalk zone is followed by the prespore zone in which mainly prespore cells are intermingled with anterior-like cells, cells of prestalk character that do not sort but express ACA and relay the cAMP signal. In the back of the slug, the rearguard cells are found. **b** Prespore and prestalk cells differentiate from vegetative-stage cells. The early differentiation in aggregation-stage cells requires cAMP pulses. The cells then differentiate into prestalk and prespore cells. Prestalk cells initiate cAMP waves, and extracellular cAMP is needed for prespore gene expression. Prespore cells make differentiation-inducing factor (*DIF*), which is necessary for PstO cell differentiation. Prestalk cells secrete DIF-ase that inactivates DIF. Prestalk cells differentiate into stalk cells, and prespore cells differentiate into spores. Stalk differentiation is inhibited by NH3. An open question is how cell-type proportioning works quantitatively, which is the subject of further modelling studies

The switch from migrating slugs to culmination appears to be controlled by a fall in ammonia concentration. The identification of a number of ammonia transporters, some of which are expressed in the very tip and when deleted show a slugger phenotype, supports the importance of ammonia as a morphogen (Kirsten, Xiong et al. 2005; Singleton, Kirsten et al. 2006). Ammonia most likely signals through the histidine kinase DhkC to the response regulator domain of the internal cAMP phosphodiesterase RegA, which is a major determinant in the control of

intracellular cAMP levels (Singleton, Zinda et al. 1998; Saran, Meima et al. 2002). High ammonia is expected to result in activation of regA and low internal cAMP levels. A drop in ammonia is expected to result in a rise of intracellular cAMP and stalk cell differentiation.

In conclusion, *Dictyostelium* is, besides being a system of choice to investigate the molecular mechanisms underlying cell polarity and chemotaxis, also an excellent model system to investigate the cellular principles that underlie multicellular tissue formation and morphogenesis.

Acknowledgments This work was supported by the BBSRC and the Wellcome Trust.

References

Andrew, N. and R. H. Insall (2007). Chemotaxis in shallow gradients is mediated independently of PtdIns 3-kinase by biased choices between random protrusions. Nat Cell Biol 9(2):193–200.

Araki, T., T. Abe, et al. (1997). Symmetry breaking in *Dictyostelium* morphogenesis: evidence that a combination of cell cycle stage and positional information dictates cell fate. Dev Biol 192(2):645–648.

Bosgraaf, L. and P. J. van Haastert (2006). The regulation of myosin II in *Dictyostelium*. Eur J Cell Biol 85:969–979.

Bretschneider, T., S. Diez, et al. (2004). Dynamic actin patterns and Arp2/3 assembly at the substrate-attached surface of motile cells. Curr Biol 14(1):1–10.

Bukharova, T., G. Weijer, et al. (2005). Paxillin is required for cell-substrate adhesion, cell sorting and slug migration during *Dictyostelium* development. J Cell Sci 118(pt 18):4295–4310.

Chen, L., M. Iijima, et al. (2007). PLA2 and PI3K/PTEN pathways act in parallel to mediate chemotaxis. Dev Cell 12(4):603–614.

Chien, S., C. Y. Chung, et al. (2000). The *Dictyostelium* LIM domain-containing protein LIM2 is essential for proper chemotaxis and morphogenesis. Mol Biol Cell 11(4):1275–1291.

Comer, F. I., C. K. Lippincott, et al. (2005). The PI3K-mediated activation of CRAC independently regulates adenylyl cyclase activation and chemotaxis. Curr Biol 15(2):134–139.

Cornillon, S., R. Froquet, et al. (2008). Involvement of Sib proteins in the regulation of cellular adhesion in *Dictyostelium discoideum*. Eukaryot Cell 7(9):1600–1605.

Dormann, D., T. Abe, et al. (2001). Inducible nuclear translocation of a STAT protein in *Dictyostelium* prespore cells: implications for morphogenesis and cell-type regulation. Development (Camb) 128(7):1081–1088.

Dormann, D. and C. J. Weijer (2001). Propagating chemoattractant waves coordinate periodic cell movement in *Dictyostelium* slugs. Development (Camb) 128(22):4535–4543.

Dormann, D. and C. J. Weijer (2003). Chemotactic cell movement during development. Curr Opin Genet Dev 13(4):358–364.

Dormann, D., G. Weijer, et al. (2002). Visualizing PI3 kinase-mediated cell-cell signaling during *Dictyostelium* development. Curr Biol 12(14):1178–1188.

Dormann, D., G. Weijer, et al. (2004). In vivo analysis of 3-phosphoinositide dynamics during *Dictyostelium* phagocytosis and chemotaxis. J Cell Sci 117(pt 26):6497–6509.

Eichinger, L., J. A. Pachebat, et al. (2005). The genome of the social amoeba *Dictyostelium discoideum*. Nature (Lond) 435(7038):43–57.

Eliott, S., P. H. Vardy, et al. (1991). The distribution of myosin-II in *Dictyostelium discoideum* slug cells. J Cell Biol 115:1267–1274.

Falk, D. L., D. Wessels, et al. (2003). Shared, unique and redundant functions of three members of the class I myosins (MyoA, MyoB and MyoF) in motility and chemotaxis in *Dictyostelium*. J Cell Sci 116(pt 19):3985–3999.

Franca-Koh, J., Y. Kamimura, et al. (2007). Leading-edge research: PtdIns(3,4,5)P3 and directed migration. Nat Cell Biol 9(1):15–17.

Fukuzawa, M., T. Abe, et al. (2003). The Dictyostelium prestalk cell inducer DIF regulates nuclear accumulation of a STAT protein by controlling its rate of export from the nucleus. Development (Camb) 130(4):797–804.

Goldberg, J. M., E. S. Wolpin, et al. (2006). Myosin light chain kinase A is activated by cGMP-dependent and cGMP-independent pathways. FEBS Lett 580(8):2059–2064.

Harris, T. J., A. Ravandi, et al. (2003). Cytoskeleton interactions involved in the assembly and function of glycoprotein-80 adhesion complexes in *Dictyostelium*. J Biol Chem 278(4):2614–2623.

Insall, R. and N. Andrew (2007). Chemotaxis in *Dictyostelium*: how to walk straight using parallel pathways. Curr Opin Microbiol 10(6):578–581.

Iranfar, N., D. Fuller, et al. (2003). Genome-wide expression analyses of gene regulation during early development of *Dictyostelium discoideum*. Eukaryot Cell 2(4):664–670.

Iwadate, Y. and S. Yumura (2008). Actin-based propulsive forces and myosin-II-based contractile forces in migrating *Dictyostelium* cells. J Cell Sci 121(pt 8):1314–1324.

Janetopoulos, C. and R. A. Firtel (2008). Directional sensing during chemotaxis. FEBS Lett 582:2075–2085.

Jang, W. and R. H. Gomer (2008). Combining experiments and modelling to understand size regulation in *Dictyostelium discoideum*. J R Soc Interface 6(5 suppl 1):S49–S58.

Kay, R. R. and C. R. Thompson (2001). Cross-induction of cell types in *Dictyostelium*: evidence that DIF-1 is made by prespore cells. Development (Camb) 128(24):4959–4966.

Kibler, K., J. Svetz, et al. (2003). A cell-adhesion pathway regulates intercellular communication during *Dictyostelium* development. Dev Biol 264(2):506–521.

Kirsten, J. H., Y. Xiong, et al. (2005). Ammonium transporter C of *Dictyostelium discoideum* is required for correct prestalk gene expression and for regulating the choice between slug migration and culmination. Dev Biol 287(1):146–156.

Kreppel, L., P. Fey, et al. (2004). dictyBase: a new *Dictyostelium discoideum* genome database. Nucleic Acids Res 32(database issue):D332–D333.

Kriebel, P. W., V. A. Barr, et al. (2003). Adenylyl cyclase localization regulates streaming during chemotaxis. Cell 112(4):549–560.

Maeda, M., H. Sakamoto, et al. (2003). Changing patterns of gene expression in dictyostelium prestalk cell subtypes recognized by in situ hybridization with genes from microarray analyses. Eukaryot Cell 2(3):627–637.

Mahadeo, D. C. and C. A. Parent (2006). Signal relay during the life cycle of *Dictyostelium*. Curr Top Dev Biol 73:115–140.

Maruo, T., H. Sakamoto, et al. (2004). Control of cell type proportioning in *Dictyostelium discoideum* by differentiation-inducing factor as determined by in situ hybridization. Eukaryot Cell 3(5):1241–1248.

Meima, M. E., K. E. Weening, et al. (2003). Characterization of a cAMP-stimulated cAMP phosphodiesterase in *Dictyostelium discoideum*. J Biol Chem 278(16):14356–14362.

Patel, H., K. D. Guo, et al. (2000). A temperature-sensitive adenylyl cyclase mutant of *Dictyostelium*. EMBO J 19(10):2247–2256.

Rafols, I., A. Amagai, et al. (2001). Cell type proportioning in *Dictyostelium* slugs: lack of regulation within a 2.5-fold tolerance range. Differentiation 67(4-5):107–116.

Saito, T., G. W. Taylor, et al. (2006). Identification of new differentiation inducing factors from *Dictyostelium discoideum*. Biochim Biophys Acta 1760(5):754–761.

Saran, S., M. E. Meima, et al. (2002). cAMP signaling in *Dictyostelium*. Complexity of cAMP synthesis, degradation and detection. J Muscle Res Cell Motil 23(7-8):793–802.

Sasaki, A. T., C. Janetopoulos, et al. (2007). G protein-independent Ras/PI3K/F-actin circuit regulates basic cell motility. J Cell Biol 178(2):185–191.

Sawai, S., X. J. Guan, et al. (2007). High-throughput analysis of spatio-temporal dynamics in *Dictyostelium*. Genome Biol 8(7):R144.
Singleton, C. K., J. H. Kirsten, et al. (2006). Function of ammonium transporter A in the initiation of culmination of development in *Dictyostelium discoideum*. Eukaryot Cell 5(7):991–996.
Singleton, C. K., M. J. Zinda, et al. (1998). The histidine kinase dhkC regulates the choice between migrating slugs and terminal differentiation in *Dictyostelium discoideum*. Dev Biol 203(2):345–357.
Soll, D. R., D. Wessels, et al. (2003). Computer-assisted reconstruction and motion analysis of the three-dimensional cell. Sci World J 3:827–841.
Springer, M. L., B. Patterson, et al. (1994). Stage-specific requirement for myosin II during *Dictyostelium* development. Development (Camb) 120:2651–2660.
Thompson, C. R., Q. Fu, et al. (2004). A bZIP/bRLZ transcription factor required for DIF signaling in *Dictyostelium*. Development (Camb) 131(3):513–523.
Tsujioka, M., K. Yoshida, et al. (2004). Talin B is required for force transmission in morphogenesis of *Dictyostelium*. EMBO J 23(11):2216–2225.
Uchida, K. S. and S. Yumura (2004). Dynamics of novel feet of *Dictyostelium* cells during migration. J Cell Sci 117(pt 8):1443–1455.
Umeda, T. and K. Inouye (2002). Possible role of contact following in the generation of coherent motion of *Dictyostelium* cells. J Theor Biol 219(3):301–308.
Umeda, T. and K. Inouye (2004). Cell sorting by differential cell motility: a model for pattern formation in *Dictyostelium*. J Theor Biol 226(2):215–224.
Vasiev, B., F. Siegert, et al. (1997). A hydrodynamic model for *Dictyostelium discoideum* mound formation. J Theor Biol 184(4):441.
Vasiev, B. and C. J. Weijer (1999). Modeling chemotactic cell sorting during *Dictyostelium discoideum* mound formation. Biophys J 76(2):595–605.
Vasiev, B. and C. J. Weijer (2003). Modelling of *Dictyostelium discoideum* slug migration. J Theor Biol 223(3):347–359.
Verkerke-van Wijk, I., M. Fukuzawa, et al. (2001). Adenylyl cyclase A expression is tip-specific in *Dictyostelium* slugs and directs StatA nuclear translocation and CudA gene expression. Dev Biol 234(1):151–160.
Weening, K. E., I. V. Wijk, et al. (2003). Contrasting activities of the aggregative and late PDSA promoters in *Dictyostelium* development. Dev Biol 255(2):373–382.
Weijer, C. J. (2004). *Dictyostelium* morphogenesis. Curr Opin Genet Dev 14(4):392–398.
Willard, S. S. and P. N. Devreotes (2006). Signaling pathways mediating chemotaxis in the social amoeba, *Dictyostelium discoideum*. Eur J Cell Biol 85(9-10):897–904.
Williams, J. G. (2006). Transcriptional regulation of Dictyostelium pattern formation. EMBO Rep 7(7):694–698.
Wong, E., C. Yang, et al. (2002). Disruption of the gene encoding the cell adhesion molecule DdCAD-1 leads to aberrant cell sorting and cell-type proportioning during *Dictyostelium* development. Development (Camb) 129(16):3839–3850.
Yumura, S., M. Yoshida, et al. (2005). Multiple myosin II heavy chain kinases: roles in filament assembly control and proper cytokinesis in *Dictyostelium*. Mol Biol Cell 16(9):4256–4266.
Zhang, H., P. J. Heid, et al. (2003). Constitutively active protein kinase A disrupts motility and chemotaxis in *Dictyostelium discoideum*. Eukaryot Cell 2(1):62–75.

Metabolic Information Highway: Interorgan Metabolic Communication Via the Autonomic Nervous System

Hideki Katagiri

Introduction

Our research goals are the development of therapeutic strategies for diabetes mellitus.

The incidence of obesity is rising at an alarming rate in much of the world [1]. Obesity, especially visceral obesity, is prone to be associated with hypertension, glucose intolerance, and dyslipidemia, collectively termed the metabolic syndrome. Independently of hypercholesterolemia, especially increased levels of oxidized low density lipoproteins [2], the metabolic syndrome increases the risk for atherosclerosis and cardiovascular morbidities [1]. To overcome obesity-related diabetes and the metabolic syndrome, it seems to be necessary to treat obesity itself. Therefore, we have attempted to unravel and manipulate the regulatory systems governing body weight as well as energy metabolism.

Leptin and Leptin Resistance

What endogenous mechanisms do we have for energy homeostasis?

Leptin, one of the adipokines, is a major contributor to energy homeostasis. Leptin is secreted mainly from adipocytes into the circulating blood, in proportion to fat stores, and binds to its receptor in the hypothalamus, leading to decreased expression of orexic neuropeptide (NPY) and increased expression of anorexic neuropeptide (POMC), resulting in suppression of food intake. Therefore, when energy storage is increased, leptin secretion is increased, leading to suppression of food intake and thus weight reduction. Conversely, decreased energy storage in adipose tissue decreases leptin secretion, resulting in weight gain. Through this mechanism, the leptin system contributes to fixing body weight within a certain range [3].

H. Katagiri
Division of Advanced Therapeutics for Metabolic Diseases, Center for Translational and Advanced Animal Research, Tohoku University Graduate School of Medicine, 2-1 Seiryo-machi, Aoba-ku, Sendai 980-8575, Japan

S. Nakanishi et al. (eds.), *Systems Biology*,
DOI:10.1007/978-4-431-87704-2_23,

However, this system is impaired in the obese state. According to obesity development, food intake amounts are gradually increased [4]. Thus, obesity itself further enhances food intake, forming a vicious cycle for further worsening obesity. Such obesity-enhanced food intake is explained by decreased hypothalamic sensitivity to leptin. In the obese state, circulating leptin concentrations are high, but the responses of hypothalamic cells to leptin are markedly impaired. This impairment of leptin responses is called leptin resistance. Therefore, hypothalamic leptin resistance is an important mechanism maintaining obesity and a potential target for fighting obesity.

Interorgan Metabolic Communication

Then, what endogenous mechanisms other than the leptin system do we have for energy homeostasis, especially energy expenditure?

Metabolism does not go on independently in different tissues and organs, but rather in a coordinated and regulated manner throughout the body. This coordinated metabolic regulation involving several organs/tissues requires interorgan communication systems. Because the human body is a multiorgan entity, I believe that the metabolic communication network among organs is essential for metabolic homeostasis.

Humoral factors, such as insulin and adipokines, are known to play important roles in this communication. However, using tissue-specific transgenic and knockout mice, unexpected metabolic phenotypes are reported in remote tissues other than the gene-disrupted tissue, which means the presence of as yet unknown systems for metabolic communication.

Therefore, our goal is to identify ways of (1) improving leptin sensitivity, as well as (2) other endogenous mechanisms maintaining energy homeostasis, via interorgan metabolic communication.

I looked for a strategy that would give us some insight into the mechanisms underlying metabolic crosstalk among organs and tissues. I suspected that, if metabolism could be acutely altered in just one organ, it would be much easier to analyze acute effects on metabolism in other remote tissues. Intervening in this step would give us an understanding of the mechanisms. In addition, the metabolic effects might be compensatory and thereby beneficial for systemic metabolism, possibly making it a potential therapeutic target. Therefore, the interorgan communication system could become a therapeutic target for the metabolic syndrome.

Therefore, we selected an adenoviral gene transfer system to express proteins that alter metabolism in a single tissue/organ of mice that had become obese and diabetic [5]. Using this strategy, in addition to well-known humoral signals, we have recently shown the importance of afferent neuronal signals for interorgan metabolic communication.

Metabolic Information Highways

Afferent Signals for Improving Hypothalamic Leptin Resistance from Visceral Adipose Tissue

As I already described, obesity induces leptin resistance. Therefore, I wondered what happens to hypothalamic leptin sensitivity when adipose tissue is acutely diminished in obese mice. As uncoupling protein (UCP)-1 is known to enhance cellular metabolism by blocking ATP synthesis in mitochondria, we expressed UCP1 in intraabdominal fat tissues of obese mice.

Direct injection of UCP1 adenovirus into the epididymal fat of mice with high fat diet-induced obesity resulted in very limited but significant expression of UCP1 in adipocytes, with no detectable expression in other tissues. Limited expression of UCP1 in intraabdominal fat suppressed overeating in mice with diet-induced obesity, suggesting improvement of leptin resistance in the hypothalamus. To examine whether leptin sensitivity truly had improved, we performed leptin tolerance testing. Administration of leptin markedly decreased food intake as compared with the control mice. In addition, although daily leptin administration did not decrease the body weight of control mice, because of leptin resistance, the body weight of UCP-1 mice did decrease quite a lot. Thus, leptin sensitivity was clearly shown to be improved by UCP1 expression in intraabdominal adipose tissues. Furthermore, UCP1 expression in visceral adipose tissue actually altered hypothalamic neuropeptide expression: NPY expression was decreased and POMC expression was increased. These results demonstrate that enhanced metabolism in intraabdominal fat tissue does indeed improve leptin sensitivity in the hypothalamus. Then, to elucidate the underlying mechanism, we attempted to intervene in intertissue communication.

Except for markedly decreased leptin levels, no adipokines were altered. Therefore, we hypothesized that neuronal signals are involved in this effect. So, we dissected nerve bundles innervating bilateral epididymal fat tissues. Ten days after nerve dissection, LacZ or UCP1 adenovirus was injected into epididymal fat tissues. Nerve dissection blocked the suppression of overeating seen in sham-operated mice. These findings suggest that neuronal signals from intraabdominal fat tissue are involved in regulating food intake [6].

Thus, visceral adipose tissue secretes leptin into the circulating blood and also regulates its own sensitivity in the hypothalamus via a neuronal pathway (Fig. 1). Food intake is likely to be precisely regulated by these dual signals from visceral adipose tissue. Our findings may provide evidence of a third key role of adipose tissue. The first one is energy storage, and the second one is adipokine secretion. This third adipose tissue role is to transmit afferent signals about energy status to the brain [7].

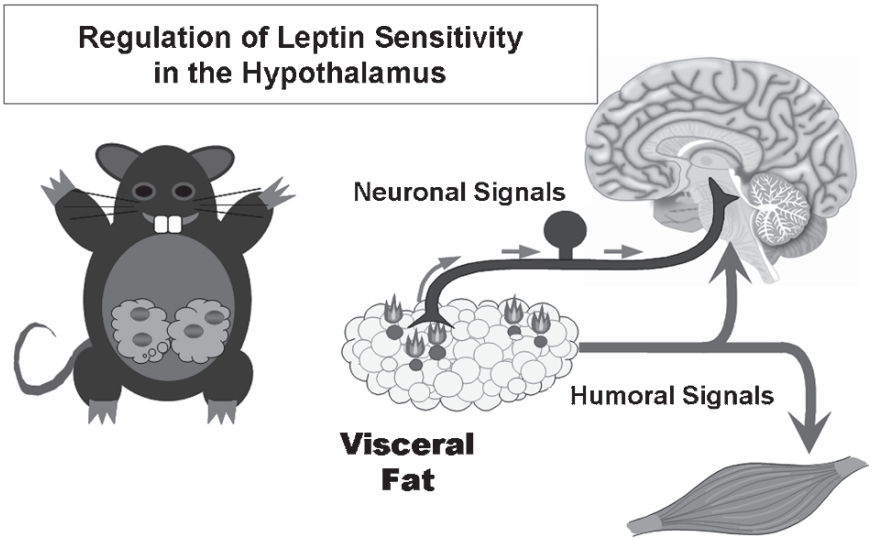

Fig. 1 Metabolic information highway from visceral adipose tissue. Neuronal signals from visceral adipose tissue regulate hypothalamic leptin sensitivity

Afferent Signals Enhancing Energy Expenditure from the Liver

We have another question: What happens when energy storage is increased in the liver?

To address this question, we attempted to express peroxisome proliferator-activated receptor-gamma (PPARγ) in the liver. PPARγ is a strong transcriptional factor that induces expression of genes involved in lipid synthesis and lipid uptake [8]. Although PPARγ expression in the liver is very low in the lean state, hepatic expression of PPARγ, especially PPARγ2, is functionally enhanced in a number of obesity models, including mice with genetically induced and high fat diet-induced obesity, as well as human obese subjects. Furthermore, liver-specific disruption of PPARγ in genetically obese mice reportedly prevents hepatic steatosis [9], suggesting PPARγ expression in the liver to play an important role in development of hepatic steatosis. Therefore, to enhance hepatic lipid accumulation, a recombinant adenovirus encoding PPARγ2 was intravenously administered. Systemic infusion of recombinant adenoviruses into mice through the tail vein resulted in PPARγ2 being expressed primarily in the liver, with no detectable expression in other tissues such as fat, muscle, or brain.

As expected, hepatic PPARγ2 expression induced severe steatosis in the liver. In contrast, intriguingly, in PPARγ2 mice, adipose tissues were remarkably diminished, by 50%, in just 1 week. Basal metabolic rates were increased, by

30%, in these mice, while food intakes were unchanged. As a result, high fat chow-induced weight gain was markedly suppressed. Surprisingly, despite marked hepatic steatosis, glucose tolerance and insulin sensitivity were markedly improved in PPARγ2 mice, as demonstrated by glucose tolerance and insulin tolerance testing.

The metabolic phenotypes associated with hepatic PPARγ2 expression are summarized here. In the liver, hepatic PPARγ2 expression induced abundant lipid accumulation. In contrast, in the periphery, fat accumulation was markedly decreased and insulin sensitivity was strikingly improved. In addition, systemic basal metabolic rates were significantly increased. As a result, systemic glucose tolerance was remarkably improved by hepatic PPARγ2 expression. These remote effects are very beneficial for fighting obesity and diabetes.

We obtained data suggesting the involvement of sympathetic nerve activation in increased lipolysis and energy expenditure. Therefore, the target of hepatic signals is not in the periphery, but rather the brain. At this time as well, we speculated about neuronal involvement. To determine whether the beneficial remote effects involve the vagal nerve, we dissected its hepatic branch.

Seven days after selective hepatic vagotomy, recombinant adenovirus was administered. In mice subjected to hepatic vagotomy, hepatic PPARγ2 expression increased liver weight and hepatic triglyceride content essentially as it had in sham-operated mice. Thus, the hepatic phenotypes are not affected by hepatic vagotomy.

In contrast, intriguingly, the decreases in brown adipocyte sizes and white adipose tissue weight as well as increases in serum free fatty acids (FFA) levels, which reflect increased lipolysis, and basal metabolic rates were completely blocked by selective hepatic vagotomy. In addition, pharmacological afferent blockade of the hepatic vagus similarly blocked these remote tissue effects.

Taken together, these observations show that hepatic PPARγ2 expression conveys metabolic information to the brain via the afferent vagus, resulting in efferent sympathetic activation, which enhances lipolysis and energy expenditure and improves obesity-related insulin resistance and diabetes. Hepatic PPARγ expression is physiologically induced when energy intake is excessive. Therefore, it may function as a feedback mechanism against excess energy intake, preventing the development of obesity by enhancing energy expenditure [10] (Fig. 2). This concept was introduced as the Metabolic Information Highway in “This Week” in *Science*, the issue in which our article was published. The autonomic nervous system is the pavement for this highway.

Let us compare this machinery with the leptin system. In the leptin system, adipose tissue recognizes excess energy accumulation and releases leptin to the brain via circulating blood. On the other hand, with this neuronal machinery, the liver senses energy storage and releases signals to the brain via the afferent vagus. While leptin mainly suppresses appetite, hepatic neuronal signals mainly enhance energy expenditure. Both inhibit weight gain. We are now working to identify which molecules activate the vagal nerve and what portions of the brain integrate peripheral metabolic signals.

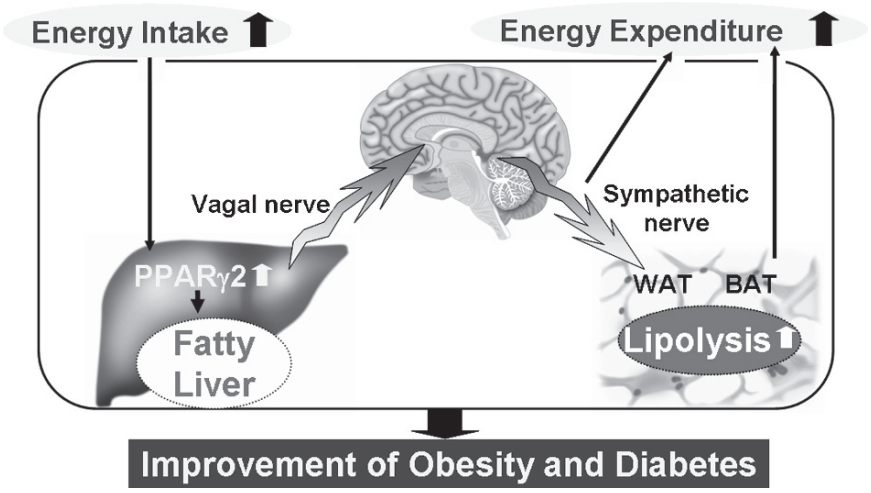

Fig. 2 Metabolic information highway from the liver. Neuronal signals from the liver regulate systemic energy metabolism to prevent the development of obesity by enhancing energy expenditure. *PPARγ,* peroxisome proliferator-activated receptor-gamma; *WAT*, white adipose tissue; *BAT,* brown adipose tissue

Conclusion

Two metabolic information highways via afferent neuronal pathways are presented: neuronal signals from adipose tissue affect hypothalamic leptin sensitization and neuronal signals from the liver regulate systemic energy expenditure. In addition to these two systems, we are now identifying another metabolic information highway from the liver to the pancreas [11]. Furthermore, the afferent signals originating in hepatic PPARγ2 expression appear to be involved in the development of obesity-related diseases (Uno K. and Katagiri H. et al., unpublished data). Thus, growing evidence has revealed the important roles of afferent neuronal signals in interorgan metabolic communication.

Collectively, the involvement of afferent neuronal signals highlights the importance of the central nervous system. The brain receives various forms of metabolic information from peripheral organs/tissues via two avenues, humoral factors and neuronal signals. These inputs from the periphery are probably integrated and processed in the brain, leading to the transmission of regulatory signals for appropriate systemic responses [1]. In addition, humoral and neuronal signals affect each other, as exemplified by the findings that adiponectin expressions are regulated by sympathetic activity [12]. Further elucidation of these regulatory systems may facilitate unraveling the mechanisms underlying metabolic homeostasis and development of the metabolic syndrome as a state of dysregulation. Moreover, targeting of the coordinated regulatory system is a potential therapeutic strategy for several types of diabetes as well as the metabolic syndrome [13].

Acknowledgments We thank Prof. Y. Oka and all other members of Division of Molecular Metabolism and Diabetes, Tohoku University Graduate School of Medicine. We also thank Ms. I. Sato and K. Kawamura for technical support. This work was supported by the Uehara Memorial Foundation.

References

1. Katagiri H, Yamada T, Oka Y. Adiposity and cardiovascular disorders: disturbance of the regulatory system consisting of humoral and neuronal signals. Circ Res 2007;101(1):27–39.
2. Ishigaki Y, Katagiri H, Gao J, Yamada T, Imai J, Uno K, Hasegawa Y, Kaneko K, Ogihara T, Ishihara H, Sato Y, Takikawa K, Nishimichi N, Matsuda H, Sawamura T, Oka Y. Impact of plasma oxidized low-density lipoprotein removal on atherosclerosis. Circulation 2008;118 (1):75–83.
3. Friedman JM, Halaas JL. Leptin and the regulation of body weight in mammals. Nature (Lond) 1998;395(6704):763–70.
4. Gao J, Katagiri H, Ishigaki Y, Yamada T, Ogihara T, Imai J, Uno K, Hasegawa Y, Kanzaki M, Yamamoto TT, Ishibashi S, Oka Y. Involvement of apolipoprotein E in excess fat accumulation and insulin resistance. Diabetes 2007;56(1):24–33.
5. Ishigaki Y, Katagiri H, Yamada T, Ogihara T, Imai J, Uno K, Hasegawa Y, Gao J, Ishihara H, Shimosegawa T, Sakoda H, Asano T, Oka Y. Dissipating excess energy stored in the liver is a potential treatment strategy for diabetes associated with obesity. Diabetes 2005;54(2):322–32.
6. Yamada T, Katagiri H, Ishigaki Y, Ogihara T, Imai J, Uno K, Hasegawa Y, Gao J, Ishihara H, Niijima A, Mano H, Aburatani H, Asano T, Oka Y. Signals from intra-abdominal fat modulate insulin and leptin sensitivity through different mechanisms: neuronal involvement in food-intake regulation. Cell Metab 2006;3(3):223–9.
7. Rosen ED, Spiegelman BM. Adipocytes as regulators of energy balance and glucose homeostasis. Nature (Lond) 2006;444(7121):847–53.
8. Desvergne B, Michalik L, Wahli W. Transcriptional regulation of metabolism. Physiol Rev 2006;86(2):465–514.
9. Matsusue K, Haluzik M, Lambert G, Yim SH, Gavrilova O, Ward JM, Brewer B Jr, Reitman ML, Gonzalez FJ. Liver-specific disruption of PPAR-gamma in leptin-deficient mice improves fatty liver but aggravates diabetic phenotypes. J Clin Invest 2003;111(5):737–47.
10. Uno K, Katagiri H, Yamada T, Ishigaki Y, Ogihara T, Imai J, Hasegawa Y, Gao J, Kaneko K, Iwasaki H, Ishihara H, Sasano H, Inukai K, Mizuguchi H, Asano T, Shiota M, Nakazato M, Oka Y. Neuronal pathway from the liver modulates energy expenditure and systemic insulin sensitivity. Science 2006;312(5780):1656–9.
11. Imai J, Katagiri H,Yamada Y, Ishigaki Y, Suzuki T, Kudo H, Uno K, Hasegawa Y, Gao J, Kaneko K, Ishihara H, Niijima A, Nakazato M, Asano T, Minokoshi Y, Oka Y. (2008) Regulation of Pancreatic β cell Mass by Neuronal Signals from the Liver. Science 2008;322 (5905): 1250–4.
12. Imai J, Katagiri H, Yamada T, Ishigaki Y, Ogihara T, Uno K, Hasegawa Y, Gao J, Ishihara H, Sasano H, Oka Y. Cold exposure suppresses serum adiponectin levels through sympathetic nerve activation in mice. Obesity (Silver Spring) 2006;14(7):1132–41.
13. Yamada T, Oka Y, Katagiri H. Inter-organ metabolic communication involved in energy homeostasis: potential therapeutic targets for obesity and metabolic syndrome. Pharmacol Ther 2008;117(1):188–98.

Involvement of the CCR4-NOT Deadenylase Complex in the Control of Cell Growth

Masahiro Morita, Kentaro Ito, Toru Suzuki, and Tadashi Yamamoto

Introduction

The Tob/BTG family comprises six proteins, Tob, Tob2, ANA, BTG1, BTG2/PC3/TIS21, and PC3B, which share a common amino-terminal domain (1). All these proteins, when overexpressed, suppress growth of NIH3T3 cells (2). There is evidence that the Tob/BTG family of proteins is involved in regulation not only of cell growth but also of differentiation and development. For instance, BTG1 is thought to be involved in myogenesis induced by triiodothyronine (3). Analysis of tob-deficient mice revealed that Tob is involved in bone development (4). Although they lack DNA-binding domains, the Tob/BTG proteins are generally viewed as transcriptional cofactors. For example, Tob interacts with Smad in BMP2 signaling (4) and in T-cell anergy (5). BTG2 enhances Hoxb9-mediated transcription (6). Both Tob and BTG2 reduce cyclin D1 expression (7,8), possibly by recruiting histone deacetylase to the cyclin D1 promoter (9), contributing to G_0/G_1 arrest. On the other hand, Tob/Btg family proteins are also implicated in translational regulation by regulating the deadenylase activity or by interacting with the polyA binding proteins (10).

The CCR4-NOT complex is a large (>1 MDa) multi-subunit protein complex and is conserved from yeast to humans (11). The mammalian CCR4-NOT complex consists of 10 Cnot proteins: Cnot1-Cnot4, Ccr4a/Cnot6, Ccr4b/Cnot6L, Caf1/Cnot7, Pop2/Cnot8, Caf40/Cnot9, and Caf130/Cnot10 (Table 1). Yeast CCR4-NOT has been considered to be a global transcription complex that regulates a variety of genes such as the nonfermentative gene either positively or negatively (11). Accumulating evidence also shows that the mammalian Cnot proteins interact with proteins in the transcription machinery. For example, Cnot1 and Cnot7 are reported to interact with estrogen receptor-α (12,13). Cnot7 is also shown to interact with retinoid X receptor-β (14). Another report showed that Cnot9 is associated with retinoic acid receptor-α (15). Therefore, the mammalian CCR4-NOT complex appears to be involved in various transcription events controlled by the nuclear

M. Morita, K. Ito, T. Suzuki, and T. Yamamoto
Division of Oncology, The Institute of Medical Science, The University of Tokyo, 4-6-1 Shirokane-dai, Minatok-ku, Tokyo 108-8639

S. Nakanishi et al. (eds.), *Systems Biology*,
DOI:10.1007/978-4-431-87704-2_24, © Springer 2009

Table 1 Function of core subunits of the CCR4-NOT complex

Human	Yeast	
CNOT1	Scaffold protein, interacts with Era	NOT1
CNOT2	Repressor for transcription?	NOT2
CNOT3	Helicase?	NOT3
CNOT4	Ubiquitin ligase	NOT4
		NOT5
CNOT6	Deadenylase	CCR4
CNOT6L	Deadenylase	
CNOT7	Deadenylase, associates with RXRb	Caf1
CNOT8	Deadenylase	
CNOT9	Associates with RAR	Caf40
CNOT10	?	Caf130

receptors. In addition the CCR4-NOT complex associates with components of general transcription factor TFIID complex (11). On the other hand, evidence is accumulating that the Cnot6 and Cnot7 encode major deadenylases, suggesting that this complex also plays a role in RNA degradation. Therefore, it appears that the CCR4-NOT complex has two functions in RNA metabolism: cytoplasmic function to regulate mRNA turnover and nuclear function to regulate mRNA synthesis. The mechanism by which these dual activities are coordinated remains largely elusive. It is worthy to mention that the CCR4-NOT complex is vitally important for the cells, because disruption of the complex results in induction of apoptosis (Ito et al., unpublished data).

Association of Tob with CCR4-NOT

Intracellular signaling is mediated by protein–protein interaction as well as multiprotein complexes, and mass spectrometric analysis is commonly used to identify components of protein complexes. We used a proteomics approach to identify Tob-interacting proteins.

To obtain sufficient quantities of Tob-interacting proteins, we produced Tob-Flag expressing HeLa S3 clones. Cells that stably expressed Tob-Flag grew more slowly than the original HeLa S3 cells, as was expected from the antiproliferative activity of Tob. After Tob-Flag-expressing HeLa S3 cells were cultured, their lysates were prepared and subjected to tandem-affinity purification of Tob-Flag with anti-Flag and anti-Tob monoclonal antibodies. The purified proteins were separated by gel electrophoresis and subjected to MALDI-TOF/TOF mass spectrometry analysis, which identified components of the CCR4-NOT complex, RNA helicases, RNA-binding proteins, and tankyrase-binding protein TAB182 as Tob-interacting proteins (16).

Because the yeast Not1 protein serves as a scaffold protein of the yeast CCR4-NOT complex (11), we assumed that human Cnot1 might also act as a scaffold. To substantiate the interaction between Tob and the CCR4-NOT complex, we examined

whether Cnot1 interacts with Tob. Co-immunoprecipitation assays of the lysates of COS7 cells transfected with plasmid carrying Flag-Cnot1 and Myc-Tob together showed that Myc-Tob interacted with Flag-Cnot1 either directly or indirectly. We further showed that other components of the complex, Cnot3 and Cnot6L, interact with Tob by using the lysates of the cells transfected with plasmids carrying Tob-myc and Flag-Cnot3 or Flag-Cnot6L (16).

Biological Function of Deadenylase Subunits of the CCR4-NOT Complex

In eukaryotes, the cap structure and the poly(A) tail protect functional mRNA from degradation by exonucleases. In the general turnover pathways, mRNA degradation is initiated by shortening of the poly(A) tail. Most often, deadenylation induces decapping of the target mRNA through a poorly known mechanism. This action triggers the rapid destruction of the mRNA in P-bodies by the 5'-to-3' exonuclease Xrn1. Alternatively, deadenylation is followed by the exosome-mediated degradation of the mRNA in the 3'-to-5' direction (17,18). Apparently, deadenylation is a critical step for mRNA turnover, as poly(A) shortening removes the targeted mRNA from the translatable pool and initiates the mRNA degradation process. However, little is known about how poly(A) tail shortening is initiated and regulated. Accumulating evidence shows that CCR4-NOT is a major deadenylase that triggers mRNA decay (18). In mammals, two orthologues of Ccr4, Cnot6 and Cnot6L, and two orthologues of Pop2, Cnot7 and Cnot8, have been identified. However, the respective contributions of these factors to mRNA deadenylation remain unclear. The mechanism by which the CCR4-NOT complex is recruited to the poly(A) sequence at the 3'-end of mRNA is not known, either.

Analysis of a Component of the CCR4-NOT Complex: Subcellular Localization and Activity of Cnot6L

Previous reports indicated that yeast Ccr4p is involved in two cellular functions: transcriptional regulation in the nucleus and deadenylation of mRNAs in the cytoplasm (11,19). To assess the possible function of the mammalian homologue of Ccr4, we examined the subcellular localization of Cnot6L protein in NIH 3T3 cells transfected with expression plasmid encoding GFP-Cnot6L. Immunofluorescence analysis revealed that GFP-Cnot6L was present predominantly in the cytoplasm. The results were confirmed by immunoblotting the biochemically prepared subcellular fraction with anti-Cnot6L antibodies. The majority of the Cnot7 proteins are present in the cytoplasm (20), although Cnot7 could also cooperate with nuclear transcription factors (14).

Yeast CCR4p is a catalytic component of the cytoplasmic deadenylase complex, and its C-terminal region is highly homologous to apurinic endonucleases (9). Putative catalytic residues present in the C-terminal region of Ccr4p were conserved in Cnot6 and Cnot6L. We examined whether Cnot6L was associated with deadenylase activity by an in vitro deadenylase assay using single-stranded poly(A) RNA as a substrate. The GST-tagged protein purified from GST-tagged Cnot6L-transfected HEK293T cells cleaved the poly(A) RNA substrate from the 3'-end (21). Introduction of mutation at the active sites of nuclease/phosphatase family proteins in Cnot6L, which is Glu195Ala (E195A), Glu239Ala (E239A), Asp410Ala (D410A), Asp489Ala (D489A), or His529Ala (H529A) substitution, destroyed the deadenylase activity (21).

Suppression of Cnot6L Impairs the Growth of NIH 3T3 Cells

To clarify the biological significance of Cnot6L, we generated a retrovirus-based vector expressing Cnot6L shRNAs under the control of the U6 promoter. The retroviral vector also expressed the puromycin phosphotransferase gene, which allowed selection of transduced cells with puromycin. By examining NIH 3T3 cells infected with the viruses, we found that *Cnot6L* mRNA expression was almost completely inhibited by Cnot6L-specific shRNA. We also found that the proliferation rate of Cnot6L-depleted cells was significantly lower than that of control shRNA-treated cells. Severe reduction of proliferation of Cnot6L-depleted cells was also observed in colony formation experiments. Flow cytometric analysis showed that the proportion of G_0/G_1 phase cells (83%) was elevated and that of S-phase cells (5%) was reduced by Cnot6L depletion in comparison with control cells (G_0/G_1, 57%; S, 16%) (Fig. 1a). These data suggested that Cnot6L depletion inhibited progression of the cell cycle from G_0/G_1 to S phase (21).

To examine the significance of the Cnot6L deadenylase activity in cell growth, we prepared retrovirus vectors expressing RNAi-refractory wild-type Cnot6L (rCnot6L-WT) and mutant Cnot6L (rCnot6L-E239A) that has no deadenylase activity in vitro. The expression levels of rCnot6L-WT and rCnot6L-E239A were similar in immunoblotting experiments. Ectopic expression of rCnot6L restored the proliferation of Cnot6L-depleted cells, confirming that the growth defect was not the result of off-target effects by Cnot6L shRNA. Importantly, ectopic expression of rCnot6L-E239A did not rescue the growth defect caused by Cnot6L depletion. The profile of expression of cell cycle-related genes (described below) in rCnot6L-expressing cells was similar to that in control cells. On the other hand, in the rCnot6L-E239A-expressing cells, $p27^{Kip1}$ and cyclin D1 expression and the phosphorylation state of the RB protein did not return to a level similar to that in control cells. These data suggested that the deadenylase activity of Cnot6L played an important part in cell growth regulation (21).

Table 2 Genes expressed differentially between control and Cnot6L RNAi cells

	Gene	Characteristics	Fold change
Increased in Cnot6L-depleted cells	*p27^{Kip}*	CDK inhibitor	2.1
Decreased in Cnot6L-depleted cells	Nr2fl	Nuclear factor	−3.2
	Ddit3	Transcription	−2.2
	F2f5	Transcription	−4.9
	Lig3	DNA replication	−2.0
	Pml	Transcription	−2.5

Alteration of p27^{Kip1} mRNA Expression in Cnot6L-Depleted Cells

To investigate the molecular mechanism that underlies G_0/G_1 arrest in Cnot6L-depleted cells, we examined the expression of cell cycle-related proteins, including cyclins, CDKs, and CDK inhibitors, by immunoblotting (Fig. 1b). We found that expression of p27^{Kip1} was increased significantly by Cnot6L depletion, whereas expression of p21^{Cip1}, CDK2, and CDK4 in the Cnot6L-depleted cells was similar to that in control cells. Levels of cyclin D1 and cyclin A were decreased in Cnot6L-depleted cells. Consistent with these results, the unphosphorylated form of RB became dominant in Cnot6L-depleted cells. Thus, increased expression of p27^{Kip1} in Cnot6L-depleted cells would contribute to G_0/G_1 arrest of the cell-cycle progression (21).

We next compared the expression profiles of the cellular genes between control and Cnot6L-depleted NIH 3T3 cells by DNA microarray analysis. Among 1508 cell cycle-related genes described in the analysis, the level of *p27^{Kip1}* mRNA was prominently increased in Cnot6L-depleted cells (Table 2). We further confirmed that the *p27^{Kip1}* mRNA level was increased in the absence of Cnot6L, whereas the *p21^{Cip1}* mRNA level was not affected. By examining the half-life of *p27^{Kip1}* mRNA using actinomycin D-treated cells, we found that the rate of decline in *p27^{Kip1}* transcript levels was lower in Cnot6L-depleted cells than in control cells. The half-lives of *p27^{Kip1}* mRNA were 1.8 h and 1.3 h in Cnot6L-depleted and control cells, respectively. The possibility that the *p27^{Kip1}* mRNA level was increased by transcriptional activation was ruled out by examining the promoter activity of the *p27^{Kip1}* gene in the absence or presence of Cnot6L.

We then performed PAT assays to show that the poly(A) tail of *p27^{Kip1}* mRNA, but not that of *p21^{Cip1}* mRNA, was significantly longer in Cnot6L-depleted cells than that in control cells. These data suggested that Cnot6L functions as a deadenylase for the poly(A) tail of *p27^{Kip1}* mRNA in vivo (21).

Mechanism of Cnot6L Action

To investigate the mechanism by which *p27^{Kip1}* mRNA stability is affected by Cnot6L deadenylase, we performed UTR (untranslated region) luciferase assays. The 5'-UTR and 3'-UTR of *p27^{Kip1}* mRNA were inserted upstream and downstream of the luciferase

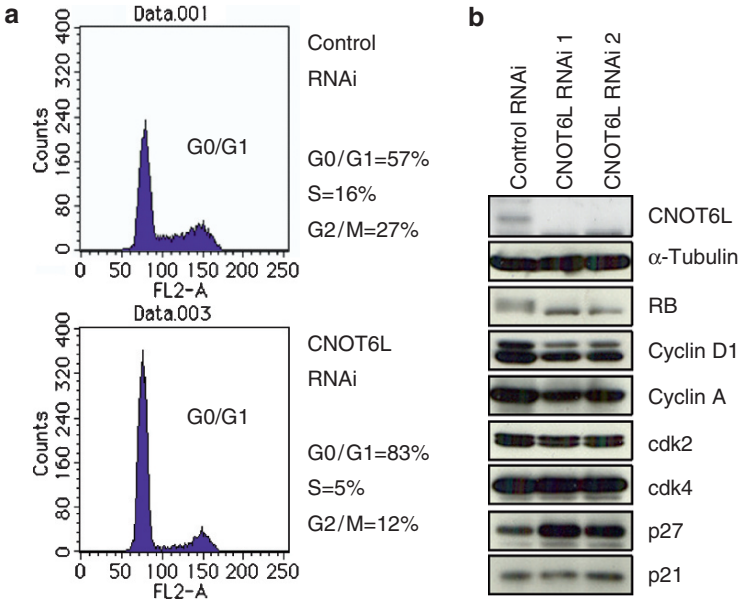

Fig. 1. Cnot6L RNAi inhibits the growth of NIH 3T3 cells. **a** The DNA contents of control and Cnot6L-depleted cells were determined by fluorescence-activated cell sorting. The percentages of cells in the G_0/G_1, S, and G_2/M phases of the cell cycle were quantified. **b** Expression levels of cell-cycle regulatory proteins were examined by Western blotting. The proteins were identified and quantified with anti-Cnot6L, anti-α-tubulin, anti-RB, anti-cyclin A, anti-cyclin D1, anti-cdk2, anti-cdk4, anti-$p27^{Kip1}$, and anti-$p21^{Cip1}$ antibodies. Detection of α-tubulin was performed as an internal control for protein loading

coding region, respectively. We transfected control or Cnot6L-depleted NIH 3T3 cells with luciferase constructs (control Luc, 5'-UTR plus Luc, and Luc plus 3'-UTR) and determined the luciferase activities in cell lysates. The results showed that the luciferase activity of 5'-UTR plus Luc was not significantly affected by the presence or absence of Cnot6L. In contrast, the luciferase activity of Luc plus 3'-UTR was decreased more than that of Luc only in the control cells. This result was most likely due to ARE (AU-rich element) sequences of *p27*^{Kip1} mRNA, which would promote rapid deadenylation-dependent mRNA degradation (22). Importantly, in the Cnot6L-depleted cells, the luciferase activities of Luc plus 3'-UTR were not decreased. These data suggested that Cnot6L contributes to the deadenylation and degradation of *p27*^{Kip1} mRNA through the 3'-UTR ARE-mediated mechanism in vivo.

Effects of Tob/Btg on Deadenylase Activity of CCR4-NOT

To address the biological significance of the interaction between Tob and the CCR4-NOT complex, we examined whether the deadenylase activity of the CCR4-NOT complex is affected by Tob using anti-Cnot6L immunoprecipitates. Cnot6L and associated

proteins were purified from HEK293T cells transfected with GFP-Cnot6L expression plasmid with or without pME-Flag-Tob. The deadenylase assay with purified proteins showed that cleavage of the poly(A) RNA substrate occurred. Importantly, anti-GFP immunoprecipitates from the pME-Flag-Tob cotransfected cells contained the Flag-Tob protein and deadenylated the poly(A) substrates less efficiently. The data suggested that the in vitro deadenylase activity of the CCR4-NOT complex was negatively regulated by Tob (16). Consistently, Cnot7 deadenylase assays with wild-type BTG2 revealed the suppressive role of BTG2 in the regulation of Cnot7 deadenylase activity. X-ray crystallography-based structural analysis as well as co-immunoprecipitation analysis revealed that Cnot7 directly interact with Tob and BTG2. BTG2-mediated suppression was hampered by introducing mutation that disrupts the interaction with Cnot7 (Yang et al., unpublished data).

Discussion

We provide evidence suggesting that Tob cooperates with the CCR4-NOT complex to regulate the length of the poly(A) tail of mRNAs and thereby their translation. Each mRNA has a distinct degradation rate. Although the precise mechanism of deadenylation remains to be established, the deadenylation rate of each mRNA would influence the mRNA degradation rate. Sequence elements that are responsible, at least in part, for mRNA turnover by promoting deadenylation have been identified in the c-Fos, interleukin 2, and tumor necrosis factor-alpha genes. One of the best-studied and most prevalent elements is the ARE, which is found in the 3'-UTR of mRNAs (22). AREs in the interleukin 2 mRNA and tumor necrosis factor-alpha mRNA promote rapid deadenylation-dependent mRNA decay. We also show here that the ARE in the 3'-UTR of *p27*^{Kip1} mRNA is involved in Cnot6L-mediated deadenylation. Probably Cnot6L and/or its associated molecules interact with the proteins binding to the ARE of *p27*^{Kip1} mRNA. Because the 3'-poly(A) tail can enhance translation, deadenylation influences the efficiency of translation. In fact, we detected increment of p27^{Kip1} in the Cnot6L-depleted cells, which induced cell growth suppression. Thus, deadenylases are crucial for gene expression and therefore are likely to be important for many biological processes.

A recent report shows that GW182 protein that is required for P-body integrity interacts with the CCR4-NOT deadenylases (23). GW182 also interacts with the AGO (argonaut) family proteins, micro-RNA effectors (24). These observations raise the possibility that the CCR4-NOT deadenylase utilizes the micro-RNA system to recognize the target mRNAs. In addition, target specificity would be also determined by the interaction of the CCR4-NOT complex with various AU-rich binding proteins. We previously showed that Tob interacts with poly(A)-binding proteins PABP and iPABP and is involved in translational control (10). Ezzeddine et al. recently reported that Tob interacts with PABPC1 and Cnot6/Cnot7 simultaneously and regulates deadenylation positively (25). Tob may help recruit the CCR4-NOT complex to the vicinity of the poly(A) sequence of mRNAs by binding

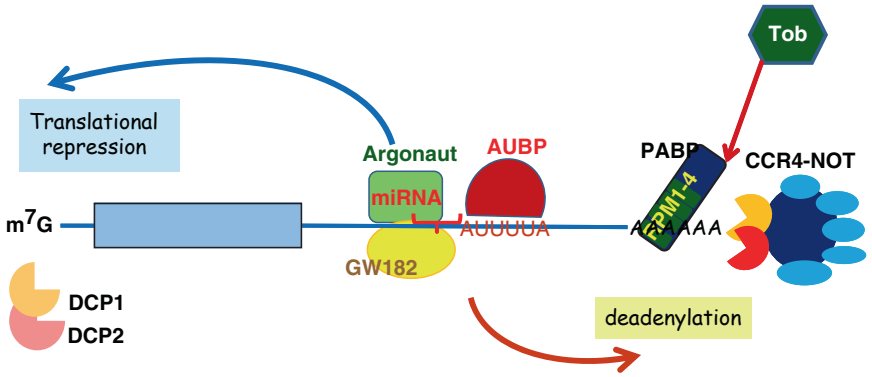

Fig. 2 Possible cooperation of micro-RNA and its partner Argonaut, ARE-binding protein, poly(A)-binding protrein, Tob, and the CCR4-NOT complex in the translational control. *miRNA*, micro-RNA; *AUBP*, AU-rich element-binding protein; *PABP*, poly(A)-binding protein

with the poly A-binding protein (26) (Fig. 2). The possible tripartite interaction of Tob, CCR4-NOT, and PABP/iPABP would destabilize target mRNAs, resulting in suppression of translation. However, the scenario could be more complicated because Tob is able to inhibit deadenylase activity in vitro (which leads to stabilization of mRNA and enhancement of translation). Further studies are needed to clarify how the deadenylase activity of the CCR4-NOT complex is regulated by Tob and/or PABP in vivo.

There are many unanswered questions. Is each deadenylase (Cnot6L, Cnot6, Cnot7, Cnot8) functionally redundant? Are the deadenylases cooperating to control mRNA stability? Does each deadenylase have preference in targeting mRNA? Do they have any activities other than the exonuclease activity? How does the CCR4-NOT complex differentially utilize the Tob family proteins? Further extensive studies are required to answer these interesting questions.

Acknowledgments Our work presented here were supported by grants from Uehara Memorial Foundation and the Ministry of Education, Science, Culture, Sports, and Technology, Japan.

References

1. Tirone F (2001) The gene *PC3* (*TIS21/BTG2*), prototype member of the *PC3/BTG TOB* family: regulator in control of cell growth, differentiation, and DNA repair? J Cell Physiol 187:155–165
2. Jia S, Meng A (2007) Tob genes in development and homeostasis. Dev Dyn 236:913–921
3. Rodier A et al. (1999) BTG1: a triiodothyronine target involved in the myogenic influence of the hormone. Exp Cell Res 249:337–348
4. Yoshida Y et al. (2000) Negative regulation of BMP/Smad signaling by Tob in osteoblasts. Cell 103:1085–1097

5. Tzachanis D et al. (2001) Tob is a negative regulator of activation that is expressed in anergic and quiescent T cells. Nat Immunol 2:1174–1182
6. Prevot D et al. (2000) The leukemia-associated protein Btg1 and the p53-regulated protein Btg2 interact with the homeoprotein Hoxb9 and enhance its transcriptional activation. J Biol Chem 275:147–153
7. Guardavaccaro D et al. (2000) Arrest of G(1)-S progression by the p53-inducible gene PC3 is Rb dependent and relies on the inhibition of cyclin D1 transcription. Mol Cell Biol 20:1797–1815
8. Suzuki T et al. (2002) Phosphorylation of three regulatory serines of Tob by Erk1 and Erk2 is required for Ras-mediated cell proliferation and transformation. Genes Dev 16:1356–1370
9. Yoshida Y et al. (2003) Mice lacking a transcriptional corepressor Tob are predisposed to cancer. Genes Dev 17:1201–1206
10. Okochi K et al. (2005) Interaction of anti-proliferative protein Tob with poly(A)-binding protein and inducible poly(A)-binding protein: implication of Tob in translational control. Genes Cells 10:151–163
11. Collart MA, Timmers HT (2004) The eukaryotic Ccr4-not complex: a regulatory platform integrating mRNA metabolism with cellular signaling pathways? Prog Nucleic Acid Res Mol Biol 77:289–322
12. Winkler GS et al. (2006) Human Ccr4-Not complex is a ligand-dependent repressor of nuclear receptor-mediated transcription. EMBO J 25:3089–3099
13. Prevot D et al. (2001) Relationships of the antiproliferative proteins BTG1 and BTG2 with CAF1, the human homolog of a component of the yeast CCR4 transcriptional complex: involvement in estrogen receptor alpha signaling pathway. J Biol Chem 276:9640–9648
14. Nakamura T et al. (2004) Oligo-astheno-teratozoospermia in mice lacking Cnot7, a regulator of retinoid X receptor β. Nat Genet 36:528–533
15. Hiroi N et al. (2002) Mammalian Rcd1 is a novel transcriptional cofactor that mediates retinoic acid-induced cell differentiation. EMBO J 21:5235–5244
16. Miyasaka et al. (2008) Interaction of antiproliferative protein Tob with the CCR4-NOT deadenylase complex. Cancer Sci 99:755–761
17. Meyer S et al. (2004) Messenger RNA turnover in eukaryotes: pathways and enzymes. Crit Rev Biochem Mol Biol 39:197–216
18. Garneau NL et al. (2007) The highways and byways of mRNA decay. Nat Rev Mol Cell Biol 8:113–126
19. Denis CL, Chen J (2003) The CCR4-NOT complex plays diverse roles in mRNA metabolism. Prog Nucleic Acids Res Mol Biol 73:221–250
20. Ikematsu N et al. (1999) Tob2, a novel anti-proliferative Tob/BTG1 family member, associates with a component of the CCR4 transcriptional regulatory complex capable of binding cyclin-dependent kinases. Oncogene 18:7432–7441
21. Morita M et al. (2007) Depletion of mammalian CCR4b deadenylasetriggers increment of the $p27^{Kip1}$ mRNA level and impaires cell growth. Mol Cell Biol 27:4980–4990
22. Chen CYA, and Shyu AB (1995) AU-rich elements: characterization and importance in mRNA degradation. Trends Biochem Sci 20:465–470
23. Behm-Ansmant I et al. (2006) mRNA degradation by microRNAs and GW182 requires both CCR4:NOT deadenylase and DCP1:DCP2 decapping complexes. Genes Dev 20:1885–1898
24. Ding L, Han M (2007) GW182 family proteins are crucial for microRNA-mediated gene silencing. Trends Cell Biol 17:411–416
25. Ezzeddine N et al. (2007) Human TOB, an antiproliferative transcription factor, is a poly(A)-binding protein-dependent positive regulator of cytoplasmic mRNA deadenylation. Mol Cell Biol 27:7791–7801
26. Funakoshi Y et al. (2007) Mechanism of mRNA deadenylation: evidence for a molecular interplay between translation termination factor eRF3 and mRNA deadenylases. Genes Dev 23:3135–3148

Reconstruction of Nuclear Reprogramming by Defined Factors

Shinya Yamanaka

Introduction

Embryonic stem (ES) cells are pluripotent stem cells derived from the inner cell mass of blastocyst. The generation of mouse ES cells (Evans et al., 1981; Martin, 1981) resulted in the "knockout mouse" technology (Hooper et al., 1987; Doetschman et al., 1987). The generation of ES cell lines from human blastocyst-stage embryos (Thomson et al., 1998) has opened up the possibility of using these cells in cell transplantation therapies for juvenile diabetes, Parkinson's disease, heart failure, and spinal cord injury. The usage of human embryos and tissue rejection, however, remain a concern for human ES cells. One strategy to overcome such issues is to reprogram the nuclei of differentiated cells to an ES cell-like, pluripotent state.

Reprogramming by Fusion with ES Cells

Miller and Ruddle demonstrated that thymocytes acquired pluripotency upon fusion with embryonal carcinoma (EC) cells (Miller and Ruddle, 1976), and similar results were later obtained by electrofusion with embryonic germ (EG) cells (Tada et al., 1997) and mouse ES cells (Tada et al., 2001). Transplantation of these cells into nude mice resulted in the formation of teratomas consisting of various tissues from all three germ layers, confirming the pluripotency of these cells. Reprogramming by fusion with human ES cells was also reported in 2005 (Cowan et al., 2005; Yu et al., 2006). These results suggest that ES cells contain factors that induce pluripotency in somatic cells (PIF, pluripotency-inducing factor).

S. Yamanaka
Center for iPS Cell Research & Application (CiRA) / Institute for Frontier Medical Sciences, Kyoto University, Kyoto 606-8507, Japan

S. Nakanishi et al. (eds.), *Systems Biology*,
DOI:10.1007/978-4-431-87704-2_25, © Springer 2009

Generation of Induced Pluripotent Stem (iPS) Cells

Fusion-induced reprogramming showed that ES cells contain PIF. These factors also play are likely play important roles in the maintenance of pluripotency in ES cells. Based on this hypothesis, we selected three groups of PIF candidates (Takahashi and Yamanaka, 2006). The first group consists of transcription factors specifically expressed in ES cells, including Nanog, Oct-3/4, Sox2, UTF1, Sall4, Sox15, and Rex1. The second group consists of growth- and tumor-related genes that play roles in ES cells, including c-Myc, Stat3, β-catenin, Grb2, KLF4, TCL1, and ERas. The third group consists of genes that are also specifically expressed in ES cells, but with less defined functions, including ECAT1, ESG1, Fbx15, DNMT3L, ECAT8, GDF3, ECAT15-1, ECAT15-2, Fthl17, and Stella.

To test these candidates, we developed a system in which the induction of pluripotency can be detected by marker gene expression. This system utilized Fbx15, which is specifically expressed in ES cells and early embryos but is dispensable for self-renewal of ES cells (Tokuzawa et al., 2003). The βgeo cassette (a fusion of β-galactocidase and the neomycin-resistant gene) was knocked into the mouse Fbx15 genes by homologous recombination. ES cells homozygous for βgeo knock-in ($Fbx15^{\beta geo/\beta geo}$) were resistant to a high concentration of G418 (up to 12 mg/ml), whereas somatic cells derived from $Fbx15^{\beta geo/\beta geo}$ mice were sensitive to the selection. Even a partial induction of pluripotency would make somatic cells resistant to a normal concentration of G418 (0.3 mg/ml).

We introduced the PIF candidate into $Fbx15^{\beta geo/\beta geo}$ mouse embryonic fibroblasts (MEF) by retrovirus-mediated transfection. No G418-resistance colonies were obtained with any single factor. However, by combining four factors (Oct3/4, Sox2, c-Myc, and Klf4), multiple G418-resistant colonies were obtained (Fig. 1). These cells showed morphology and proliferation similar to ES cells. Furthermore, when transplanted into nude mice, these ES-like cells produced teratomas containing various tissues of the three germ layers. We designated these cells iPS cells for induced pluripotent stem cells (Takahashi and Yamanaka, 2006).

Fbx15-selected iPS cells, however, were not able to contribute to adult chimeric mice when transplanted into blastocysts. DNA microarray analyses revealed significant difference in global gene expression patterns between Fbx15-selected iPS cells ES cells. In addition, the promoter regions of Oct-3/4 and Nanog remained methylated in Fbx15-selected iPS cells. These data demonstrated that reprogramming in Fbx15-selected iPS cells was not complete.

To obtain better iPS cells, three groups utilized Nanog as a selection maker (Wernig et al., 2007; Okita et al., 2007; Maherali et al., 2007). We expected that Nanog would serve as a better marker because it is more tightly associated with pluripotency than is Fbx15 (Pan and Thomson, 2007). All the three groups showed that Nanog-selected iPS cells are nearly indistinguishable from ES cells in gene

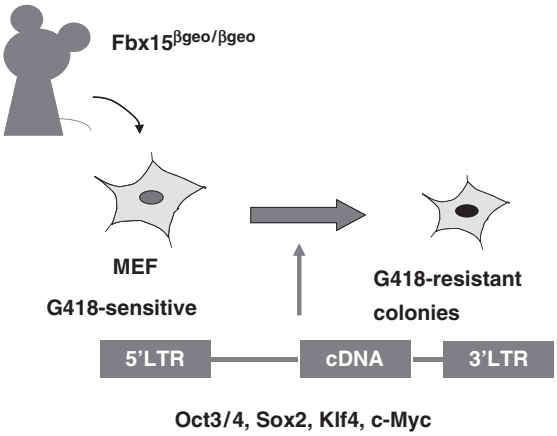

Fig. 1 The induction of iPS cells by Oct-3/4, Sox2, c-Myc, and KLF4. Retroviral transfection of *Oct-3/4, Sox2, c-Myc, and KLF4* into mouse fibroblasts results in the induction of pluripotent iPS cells

expression and epigenetic status. Furthermore, Nanog-selected iPS cells contributed to adult and germline-competent chimeras.

How Are iPS Cells Generated by the Four Factors?

ES cells are similar to tumor cells in that they are immortal and proliferate rapidly. Thus, generation of iPS cells from somatic cells should also require transformation, which might be achieved by the two tumor-related gene products, c-Myc and KLF4. The Myc protein induces transformation (Adhikary and Eilars, 2005). However, it also elicits p53-dependent apoptosis. KLF4 might be required to suppress p53- and c-Myc-induced apoptosis (Rowland and Peeper, 2006). KLF4, in contrast, activates p21 and suppresses proliferation. The Myc protein can alleviate this cytostatic effect of KLF4 by suppressing *p21*. The balance between c-Myc and KLF4 might be critical for transformation in iPS cells. In addition, Myc proteins probably loosen chromatins of somatic cells by binding to numerous sites throughout the genome and by recruiting multiple histone acetylases complexes (Knoepfler et al., 2006). Oct-3/4 and Sox2 are likely to direct cell fate from tumor cells to pluripotent cells during iPS cell generation. KLF4 may also function as a co-factor of Oct-3/4 and Sox2 (Nakatake et al., 2006).

The four factors, however, cannot explain every aspect of iPS cell induction. Among fibroblasts that express all the four transgenes, only a small portion (less than 1%) can become iPS cells. Future studies are required to determine the molecular mechanism for iPS cell generation by the four factors.

References

Adhikary S, Eilers M (2005) Transcriptional regulation and transformation by Myc proteins. Nat Rev Mol Cell Biol 6:635–645.

Cowan CA, Atienza J, Melton DA, Eggan K (2005) Nuclear reprogramming of somatic cells after fusion with human embryonic stem cells. Science 309:1369–1373.

Doetschman T, Gregg RG, Maeda N, Hooper ML, Melton DW, Thompson S, Smithies O (1987) Targetted correction of a mutant HPRT gene in mouse embryonic stem cells. Nature (Lond) 330:576–578.

Evans MJ, Kaufman MH (1981) Establishment in culture of pluripotential cells from mouse embryos. Nature (Lond) 292:154–156.

Hooper M, Hardy K, Handyside A, Hunter S, Monk M (1987) HPRT-deficient (Lesch-Nyhan) mouse embryos derived from germline colonization by cultured cells. Nature (Lond) 326:292–295.

Knoepfler PS, Zhang XY, Cheng PF, Gafken PR, McMahon SB, Eisenman RN (2006) Myc influences global chromatin structure. EMBO J 25:2723–2734.

Maherali N, Sridharan R, Xie W, Utikal J, Eminli S, Arnold K, Stadtfeld M, Yachechko R, Jaenisch JT, Plath K, Hochedlinger K (2007) Directly reprogrammed fibroblasts show global epigenetic remodelling and widespread tissue contribution. Cell Stem Cell 1:55–70.

Martin GR (1981) Isolation of a pluripotent cell line from early mouse embryos cultured in medium conditioned by teratocarcinoma stem cells. Proc Natl Acad Sci U S A 78: 7634–7638.

Miller RA, Ruddle FH (1976) Pluripotent teratocarcinoma-thymus somatic cell hybrids. Cell 9:45–55.

Nakatake Y, Fukui N, Iwamatsu Y, Masui S, Takahashi K, Yagi R, Yagi K, Miyazaki J, Matoba R, Ko MS, Niwa H (2006) Klf4 cooperates with Oct3/4 and Sox2 to activate the Lefty1 core promoter in embryonic stem cells. Mol Cell Biol 26:7772–7782.

Okita K, Ichisaka T, Yamanaka S (2007) Generation of germ-line competent induced pluripotent stem cells. Nature (Lond) 448:313–317.

Pan G, Thomson JA (2007) Nanog and transcriptional networks in embryonic stem cell pluripotency. Cell Res 17:42–49.

Rowland BD, Peeper DS (2006) KLF4, p21 and context-dependent opposing forces in cancer. Nat Rev Cancer 6:11–23.

Tada M, Tada T, Lefebvre L, Barton SC, Surani MA (1997) Embryonic germ cells induce epigenetic reprogramming of somatic nucleus in hybrid cells. EMBO J 16:6510–6520.

Tada M, Takahama Y, Abe K, Nakatsuji N, Tada T (2001) Nuclear reprogramming of somatic cells by in vitro hybridization with ES cells. Curr Biol 11:1553–1558.

Takahashi K, Yamanaka S (2006) Induction of pluripotent stem cells from mouse embryonic and adult fibroblast cultures by defined factors. Cell 126:663–676.

Thomson JA, Itskovitz-Eldor J, Shapiro SS, Waknitz MA, Swiergiel JJ, Marshall VS, Jones JM (1998) Embryonic stem cell lines derived from human blastocysts. Science 282:1145–1147.

Tokuzawa Y, Kaiho E, Maruyama M, Takahashi K, Mitsui K, Maeda M, Niwa H, Yamanaka S (2003) Fbx15 is a novel target of Oct3/4 but is dispensable for embryonic stem cell self-renewal and mouse development. Mol Cell Biol 23:2699–2708.

Wernig M, Meissner A, Foreman R, Brambrink T, Ku M, Hochedlinger K, Bernstein BE, Jaenisch R (2007) In vitro reprogramming of fibroblasts into a pluripotent ES cell-like state. Nature (Lond) 448:318–324.

Yu J, Vodyanik MA, He P, Slukvin, II, Thomson JA (2006) Human embryonic stem cells reprogram myeloid precursors following cell–cell fusion. Stem Cells 24:168–176.

Index